

# Preliminary design of a Very Light Business Jet

Group: 02

Antoni Alférez Balcells

Guillem Batlle i Capa

Sergi Company Aguilar

Nil Couto Ovejero

Anna Martínez Medina

Dani Regener Roig

Matyas Rosta

Jorge Salort Ortolà

Professor:

Martí Coma Company

Disseny d'Avions

Grau en Enginyeria en Vehicles Aeroespacials

Escola Superior d'Enginyeries Industrial, Aeroespacial i Audiovisual  
de Terrassa

Universitat Politècnica de Catalunya

December 2019



# Contents

<b>Contents</b>	<b>i</b>
<b>List of Figures</b>	<b>vii</b>
<b>List of Tables</b>	<b>xiii</b>
<b>Changes from 1st deliverable</b>	<b>xvii</b>
<b>Abstract</b>	<b>xxiii</b>
<b>Scope</b>	<b>xxv</b>
<b>Nomenclature</b>	<b>xxxiii</b>
<b>Acronyms</b>	<b>xxxv</b>
List of Abbreviations and Common Terms	xxxv
<b>1 Introduction</b>	<b>1</b>
1.1 Type of private jet election and differential value	1
1.2 Similar aircraft statistics	3
1.3 Design situation analysis	12
1.4 Mission and performance requirements	13
1.5 Conclusions	15
<b>2 General arrangement</b>	<b>17</b>
2.1 Geometry	17
2.1.1 Fuselage	17
2.1.2 Wing	19
2.1.3 Propulsion plant	24
2.1.4 Empennage	29
2.1.5 Landing gear	31

---

2.2	Materials	34
2.2.1	External materials	34
2.2.2	Internal materials	37
2.3	Conclusions	38
<b>3</b>	<b>Weight and centring</b>	<b>39</b>
3.1	Introduction	39
3.1.1	Definitions	40
3.2	Similar business jets analysis	41
3.3	Weight estimation	42
3.3.1	<i>MTOW</i> first approximation	42
3.3.2	Maximum Payload ( <i>MPL</i> ) calculation	43
3.3.3	<i>OEW</i> references	44
3.3.4	Fuel weight calculation	46
3.3.5	Operative Empty Weight calculation	51
3.3.6	Approximation methodology	51
3.3.7	Preliminary weight estimation results	51
3.4	Centring estimation	52
3.5	Conclusions	53
<b>4</b>	<b>Initial sizing</b>	<b>55</b>
4.1	Design point analysis	55
4.2	Wing sizing	64
4.3	Engine selection and configuration	65
4.4	Conclusions	66
<b>5</b>	<b>Mission performance</b>	<b>69</b>
5.1	Flight profile	69
5.2	Breguet equation resolution	70
5.2.1	Breguet equation treatment	71
5.2.2	Relative error in the Breguet equation calculation	73
5.3	Cruise conditions	76
5.4	Payload-range	76
5.5	Conclusions	78
<b>6</b>	<b>Fuselage design</b>	<b>81</b>

---

6.1	Introduction	81
6.2	Technical aspects on fuselage design	83
6.3	Inner design	84
6.3.1	Cabin sizing	85
6.3.2	Doors and emergency exits	89
6.3.3	Cockpit design	91
6.3.4	Fuel, cargo and systems compartments	92
6.4	Outer design	93
6.4.1	Drag estimation	95
6.5	Conclusions	96
<b>7</b>	<b>Wing design</b>	<b>99</b>
7.1	Initial aspect ratio determination	99
7.2	Airfoil definition	100
7.3	Wing modeling	101
7.3.1	Iterative design procedure	101
7.3.2	Numerical method definition	102
7.3.3	Wing modeling results	102
7.4	High-Lift Devices	108
7.4.1	General considerations	109
7.4.2	High-Lift Devices location along the span	111
7.4.3	Type of High-Lift Devices	111
7.4.4	High-Lift Devices chord ( $C_f$ ) [1]	114
7.4.5	High-Lift Devices span ( $b_f$ )	115
7.4.6	High-Lift Devices maximum deflection ( $\delta_{f_{max}}$ )	115
7.4.7	Flap Sizing Method	116
7.5	Conclusions	126
<b>8</b>	<b>Weight and balance</b>	<b>127</b>
8.1	Empennage design	127
8.1.1	Horizontal tail sizing	128
8.1.2	Vertical tailplane design	129
8.1.3	Horizontal empennage validation with fixed controls static stability	130
8.1.4	Aerodynamic CG limits	132

8.2	Loading CG limits . . . . .	132
8.2.1	Weight estimation of major inertial parts of the aircraft . . .	132
8.2.2	Fuel and Payload weight estimation . . . . .	134
8.2.3	Centre of Gravity position . . . . .	135
8.3	Conclusions . . . . .	136
<b>9</b>	<b>Landing gear design</b>	<b>139</b>
9.1	Landing gear disposition . . . . .	140
9.1.1	Angles of pitch and roll during takeoff and landing . . . .	140
9.1.2	Stability at touchdown . . . . .	141
9.1.3	Nose landing gear position . . . . .	141
9.1.4	Avoiding sideways turnover of the aircraft . . . . .	142
9.1.5	Final undercarriage disposition . . . . .	143
9.2	Number of wheels. LCN estimation . . . . .	145
9.2.1	Single wheel per leg . . . . .	146
9.2.2	Two wheels per leg . . . . .	147
9.3	Conclusions . . . . .	149
<b>10</b>	<b>Propulsion System Design</b>	<b>151</b>
10.1	Engine installation . . . . .	151
10.1.1	Thrust Reversal . . . . .	156
10.2	Conclusions . . . . .	159
<b>11</b>	<b>Aircraft airframe</b>	<b>161</b>
11.1	Structural elements . . . . .	161
11.2	Fuselage airframe . . . . .	162
11.3	Wing airframe . . . . .	164
11.4	Empennage airframe . . . . .	166
11.5	Conclusions . . . . .	167
<b>12</b>	<b>Flight envelope</b>	<b>169</b>
12.1	Flight envelope at sea level . . . . .	169
12.2	Flight envelope at cruise altitude . . . . .	171
12.3	Gust load factors . . . . .	172
12.4	Combined flight envelope . . . . .	174
12.5	Conclusions . . . . .	175

<b>13 Conclusions</b>	<b>177</b>
<b>Annexes</b>	<b>180</b>
<b>A Numerical methods equations</b>	<b>183</b>
A.1 Trapezoidal Rule . . . . .	183
A.2 Simpsons Rule . . . . .	184
<b>B Fuselage drawing</b>	<b>187</b>
<b>C Wing geometric iteration results</b>	<b>189</b>
C.1 Sweep and dihedral analysis . . . . .	189
C.2 Twist analysis . . . . .	192
<b>D Xflr5 software error analysis</b>	<b>193</b>
<b>E MATLAB Code</b>	<b>197</b>
E.1 Weight initial estimation . . . . .	197
E.2 Breguet Analysis . . . . .	203
E.2.1 Trapezoidal Rule function . . . . .	203
E.2.2 Simpson's Rule function . . . . .	203
E.2.3 Relative error script . . . . .	204
E.3 Payload-Range diagram . . . . .	206
E.4 Design Point matching graph . . . . .	209
E.5 Flap Sizing Method . . . . .	212
E.6 LG disposition loop . . . . .	216
E.7 Flight envelopes . . . . .	219
E.8 Plate 2D . . . . .	225
<b>Bibliography</b>	<b>235</b>



# List of Figures

1.1	Cessna 510 Citation Mustang. . . . .	4
1.2	Embraer Phenom 100. . . . .	5
1.3	Honda HA-420 HondaJet. . . . .	6
1.4	Eclipse Aviation EA500. . . . .	7
1.5	Syberjet SJ30. . . . .	8
1.6	Adam Aircraft A700. . . . .	9
1.7	Cessna CitationJet/M2 (CJ1). . . . .	10
1.8	Bombardier Learjet 24. . . . .	11
1.9	Evolution of sells in business jets year-by-year. [2] . . .	13
2.1	Geometric fuselage parameters [3]. . . . .	18
2.2	Airbus A400M, as a High-wing configuration example .	20
2.3	De Havilland Canada DHC-8 [4]. . . . .	21
2.4	Dassault Rafale, as an example of mid-wing configuration [5]. . . . .	22
2.5	Hamburger Flugzeugbau HFB 320 Hansa Jet. Sweep forward private jet with mid-wing configuration [5]. . .	23
2.6	Number of engines, thrust loading and Take-off length comparison [6]. . . . .	26
2.7	Probability of engine failure as function of the number of engines [6] . . . . .	27
2.8	Tailplane single fin configurations [6]. . . . .	29
2.9	Tailplane twin fin configurations [6]. . . . .	30
2.10	Cirrus Vision SF50 with V tail configuration [7]. . . . .	31
2.11	Taildragger or conventional gear undercarriage [8] . . .	32
2.12	Tricycle or nosewheel configuration [9] . . . . .	33
2.13	Reinforcing fibres commonly used in aerospace applications [10]. . . . .	35

2.14	Polymeric matrices commonly used in aerospace sector [11].	36
3.1	Chart to estimate the operative empty weight of transport and executive airplanes.	44
3.2	Mission profile for a commercial airplane.	47
4.1	Definition of FAR 25 Take-off Distance. Extracted from [3].	58
4.2	Take-Off Parameter (TOP) in front of take-off Field Length ( $s_{TOFL}$ ). Extracted from [12]	59
4.3	Take-off and Climb path. Extracted from [12]	61
4.4	Definition of FAR 25 Landing Distances. Extracted from [12]	62
4.5	Design point matching all sketches from performance equations.	63
4.6	Design point matching graph with possible adequate engines thrust-to-weight ratio.	65
5.1	Private jet flight profile.	70
5.2	Comparative between the Trapezoidal and Simpson's rule with $n=5000$ .	74
5.3	Comparative between the Trapezoidal and Simpson's relative error as function of the number of discretization.	75
5.4	Different aircraft weight configurations with range.	77
5.5	Payload-Range diagram.	78
6.1	Four generic fuselage configurations. (a) Large transport aircraft. (b) Fighter aircraft. (c) Light GA aircraft. (d) Glider. [1]	81
6.2	Drag coefficient of streamline bodies of revolution at low speeds. [6].	83
6.3	Typical definition for airplane's fuselage sizing [13]	84
6.4	Internal arrangement of a civil passenger low-wing aircraft. [1]	84
6.5	Typical values for the seats sizing [6].	86

---

6.6	Sizing for the cabin regarding commodity and duration of the flight. [6]. . . . .	87
6.7	Classification and sizing of emergency exits regarding CS 25.807. [6]. . . . .	90
6.8	Cockpit geometry for a transport aircraft. [1] . . . . .	92
6.9	Drag increment vs upsweep angle and afterbody drag of a fuselage tail, when added to a cylindrical shape part. [6]. . . . .	94
7.1	Initial tapered wing. . . . .	103
7.2	First iteration graphs for sweep and dihedral. . . . .	104
7.3	Second iteration graphs for twist modification. . . . .	105
7.4	Simulation results for the modified wing. . . . .	107
7.5	Design point for $S_W = 18.2m^2$ . . . . .	108
7.6	Lift curves with and without high-lift devices. Extracted from [6]. . . . .	110
7.7	Top view of right wing high-lift devices parameters. Extracted from [1]. . . . .	110
7.8	Trends in performance of trailing-edge flaps. Extracted from [6]. . . . .	112
7.9	Top view of high-lift devices located on the leading-edge. Extracted from [6] . . . . .	114
7.10	Side view of the inboard wing parameters with the flap deflected. Extracted from [1] . . . . .	116
7.11	Algorithm used in flap sizing method. Based on [14] and [15]. . . . .	117
7.12	Definition of flap surface ( $S_f$ ). Extracted from [16] . .	119
7.13	Effect of Thickness Ratio and Flap Chord Ratio on $C_{l_{\delta_f}}$ . Extracted from [3]. . . . .	120
7.14	Effect of Flap Chord Ratio and Flap Deflection on $K'$ . Extracted from [3]. . . . .	120
7.15	Effect of Flap Chord Ratio and Flap Type on $K$ . Extracted from [3]. . . . .	121
7.16	Geometrical parameters on Single Slotted Flap . . . . .	121

7.17	Section Lift Effectiveness Parameter for Single Slotted Flaps. Extracted from [3]. . . . .	122
7.18	Results for Plain Flap type. . . . .	123
7.19	Results for Single Slotted Flap type. . . . .	124
7.20	Results for Fowler Flap type. . . . .	125
8.1	Sketch of the horizontal empennage preliminary design. . . . .	129
8.2	Sketch of the vertical empennage preliminary design. . . . .	130
8.3	Results of the $C_m$ analysis with different positions of the CG and NACA0009 and NACA0012 profiles. . . . .	131
8.4	Position of the centre of gravity of major components . . . . .	134
8.5	Centre of gravity excursion diagram . . . . .	136
8.6	Permissible operating centre of gravity range . . . . .	137
8.7	Centre of gravity variation for different operating loading conditions compared with the neutral point position . . . . .	138
9.1	Scheme of distances for NLG boundaries calculation. . . . .	142
9.2	Limits of the undercarriage disposition based on stability considerations [6]. . . . .	143
9.3	Static deflection sensitivity on the LG parameters: height, track, and MLG and NLG positions. . . . .	145
9.4	Load Classification Number for various combinations of tire pressure and wheel load [6]. . . . .	147
9.5	$ESWL$ dependent on the thickness of pavement, for the dual wheel assembly, for different tire pressures ( $S_T = 30\text{ cm}$ ). . . . .	148
9.6	$ESWL$ dependent on the thickness of pavement, for the dual wheel assembly, for different distances between imprint centres ( $P = 11\text{ kg/cm}^2$ ). . . . .	148
10.1	Variation of fuel burn with fan diameter for podded and embedded systems. Extracted from [17]. . . . .	153
10.2	Inlet align of the nacelles mounted to the rear sides of the fuselage. Extracted from [6]. . . . .	155

---

10.3	Method for Mounting Jet Engines in Airframes. Extracted from [3].	156
10.4	Bucket Target Type Thrust Reverser System. Extracted from [18].	157
10.5	Clamshell Type Thrust Reverser System. Extracted from [18].	158
10.6	Cascade Type Reverser System (cold stream). Extracted from [18].	158
11.1	Stiffened panel. Extracted from [19]	163
11.2	Honeycomb sandwich panel. Extracted from [20]	163
11.3	Hat stiffened skin. Extracted from [21]	164
11.4	Crown panel. Extracted from [21]	164
11.5	Examples of basic types of wing structure. Extracted from [6]	165
11.6	T-tail parts. Ribs, spars and beaded skin on the empennage Extracted from	167
11.7	Honda Jet's fuselage structure. Extracted from [22]	168
12.1	Flight envelope at sea level and <i>MTOW</i> .	172
12.2	Flight envelope at cruise altitude of <i>43000 ft</i> and <i>MTOW</i> .	173
12.3	Gust load factors on the flight envelope at cruise altitude with <i>MTOW</i> .	175
12.4	Combined flight envelope considering gusts effects at the cruise altitude with <i>MTOW</i> .	176
A.1	Trapezoidal Rule representation [23]	183
A.2	Simpson's Rule representation [23].	184
D.1	Experimental and simulated polar curves ( $N_{crit} = 2$ ) for NACA 23012 [24]	194



# List of Tables

1	Changes from 1st deliverable. (1/6) . . . . .	xvii
2	Changes from 1st deliverable. (2/6) . . . . .	xviii
3	Changes from 1st deliverable. (3/6) . . . . .	xix
4	Changes from 1st deliverable. (4/6) . . . . .	xx
5	Changes from 1st deliverable. (5/6) . . . . .	xxi
6	Changes from 1st deliverable. (6/6) . . . . .	xxii
1.1	Cessna 510 Citation Mustang Specifications [25], [26], [27], [28]. . .	4
1.2	Embraer Phenom 100 Specifications [25], [29]. . . . .	5
1.3	Honda HA420 HondaJet Specifications [30], [25], [31]. . . . .	6
1.4	Eclipse Aviation EA500 Specifications [25], [32]. . . . .	7
1.5	Syberjet SJ30 Specifications [33]. . . . .	8
1.6	Adam Aircraft A700 Specifications [34], [25]. . . . .	9
1.7	Cessna CitationJet/M2 (CJ1) Specifications [25], [35], [36]. . . . .	10
1.8	Bombardier Learjet 24 Specifications [37], [38]. . . . .	11
1.9	Requirements comparison . . . . .	15
2.1	Comparison of internal structural materials. . . . .	37
3.1	Similar VLJ weight analysis. . . . .	42
3.2	Typical values of $C_j$ and $L/D$ for business jets during ascend phase [3] . . . . .	48
3.3	Typical values of $C_j$ and $L/D$ for business jets during cruise[3] . . .	49
3.4	Typical values of $C_j$ and $L/D$ for business jets during loiters[3] . . .	49
3.5	Typical values of $C_j$ and $L/D$ for business jets during flight to alternate and descent[3] . . . . .	50
3.6	Business jet preliminary estimated weights . . . . .	52
3.7	Centre of gravity position for different aircraft models . . . . .	52
3.8	Business jet preliminary estimated weights . . . . .	53

3.9	Business jet preliminary estimated weights ratios . . . . .	54
4.1	Connection between <i>MTOW</i> and wing area for similar VLJs [39]. . . . .	64
4.2	Suggested engines adequate for business jets with 2 engines. . . . .	65
4.3	JT-15D-1B Basic specifications . . . . .	66
6.1	Values for the preliminary sizing of the cabin. . . . .	91
6.2	Values for the preliminary sizing of the cabin. . . . .	96
7.1	Aspect ratio for similar jets. . . . .	100
7.2	Different values of sweep, dihedral and twist studied. . . . .	102
7.3	Numerical method constants. . . . .	102
7.4	Tapered Wing Geometry. . . . .	103
7.5	Final wing geometry. . . . .	106
7.6	Typical flap deflection at landing operation for different types of flap. Extracted from [14]. . . . .	116
7.7	Flap acceptable range of values [3]. . . . .	117
8.1	Tail volume coefficient values proposed by [40] . . . . .	128
8.2	Corrected tail volume coefficients. . . . .	128
8.3	Range of usual horizontal empennage geometric parameters . . . . .	129
8.4	Range of usual horizontal empennage geometric parameters . . . . .	130
8.5	Aerodynamic CG limits . . . . .	132
8.6	Participation of the main components in the Maximum Take Off Weight . . . . .	133
8.7	Main Components Weight Estimation . . . . .	133
8.8	Empennage geometric parameters . . . . .	137
8.9	Main Components Mass . . . . .	137
9.1	Static deflection sensitivity on landing gear main parameters. . . . .	145
9.2	Landing gear main parameters. . . . .	145
12.1	Design airspeeds for the flight envelope with <i>MTOW</i> at sea level and at cruise altitude. . . . .	173
12.2	Gust load factors at different design speeds for the cruise altitude of <i>43000 ft</i> . . . . .	174

13.1 Main parameters determined during the preliminary design stage of the Very Light Business Jet. . . . .	178
C.1 Maximum $C_L/C_D$ and optimal $C_L$ for $\Lambda[^\circ] = 5, 10, 15$ and $\Gamma[^\circ] = 2, 4, 6$	189
C.2 Maximum $C_L/C_D$ and optimal $C_L$ for $\Lambda[^\circ] = 5, 10, 15$ and $\Gamma[^\circ] = 2, 4, 6$	192
D.1 Experimental and simulation data for NACA23012 . . . . .	194



# Changes from 1st deliverable

TABLE 1: Changes from 1st deliverable. (1/6)

ID	Text
Sec.	The scope has been reorganized and redesigned.
Sec. 1.1	The very light jet (VLJ) (...) includes private jets that typically accommodate 6 to 7 to 6 passengers with an average range over 2000 km.
Sec. 2.2	<p>In conclusion, if the aim is to create a competitive private jet its materials must have the best properties, especially considering that private jets are in a luxurious sector.</p> <p>Following Fig. 2.13 and Fig. 2.14 and having as a reference the VLJ HondaJet [22], the selected materials will be:</p> <ul style="list-style-type: none"> <li>- Aluminum alloys for empennage and wings.</li> <li>- Composite: matrix of Cytec 5276 epoxy resin (which provides a high damage-tolerance) and reinforcement of TOHO G30-500 high-strength, intermediate-modulus fiber, for the hole fuselage.</li> </ul>
Sec. 2.2	<p>In conclusion, if the aim is to create a competitive private jet its materials must have the best properties, especially considering that private jets are in a luxurious sector. Following Fig. 2.13 and Fig. 2.14 the most suitable composite for the external materials would be an epoxy matrice with fiber reinforcement. For the fiber, glass and carbon will be considered due to its properties. In 11 it is discussed the type of configuration needed for each part of the aircraft and which composite would be the most appropriate.</p>
Sec. 2.3	<p>In Sec. 2.2 it has been defined the materials that</p>
Sec. 2.3	<ul style="list-style-type: none"> <li>- will be used when manufacturing the jet: it has been decided that wings and empennage</li> <li>- will be made of aluminum alloys while the fuselage will be built using a composite with a</li> <li>- matrix of Cytec 5276 epoxy resin and reinforcement of TOHO G30-500 high-strength. About</li> <li>- the inner materials, composites based on dual-cure toughened epoxy matrices, such as TC275-1</li> <li>- or TC275-1E, are chosen to be used as they give a good performance but entails less weight than</li> <li>- aluminum alloys. However, titanium alloys or steel might be used in critical parts such as the</li> <li>- landing gear. For the structural materials a more developed study will be carried out further in</li> <li>- the project.</li> </ul>
Sec. 2.3	<p>In Sec. 2.2 it has been defined the materials that will be used when manufacturing the jet: composites will be used on external materials due to the weight reduction and the improve of their properties. However, titanium alloys or steel might be used in critical parts such as the landing gear. For the structural materials a more developed study will be carried out further in the project.</p>
Tab. 4.3	<p>Specific Fuel Consumption 2.181 kg/(N*s) at cruise</p>
Tab. 4.3	<p>Specific Fuel Consumption 0.55 lb/(lbs·hr) at cruise</p>

TABLE 2: Changes from 1st deliverable. (2/6)

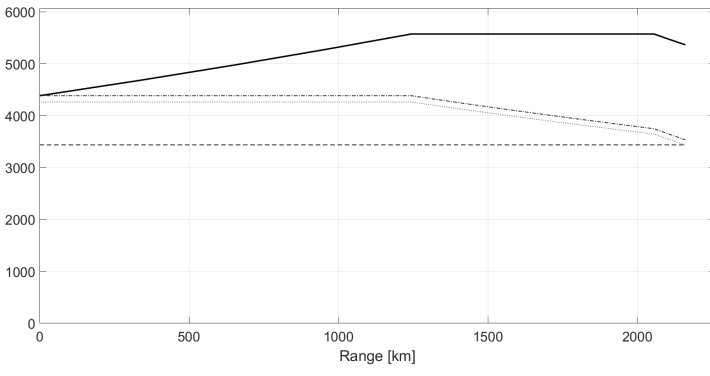
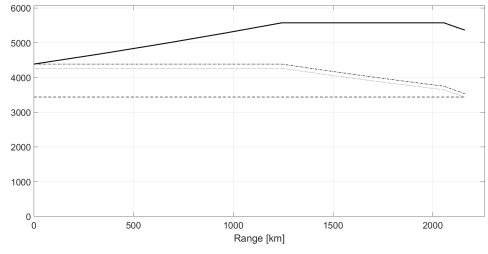
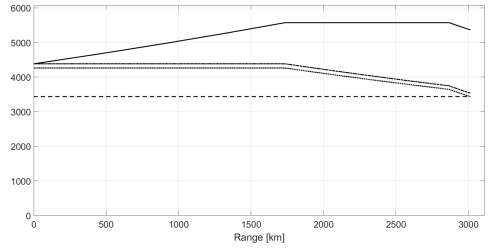
ID	Text
Fig. ??	<p>[Deleted]</p>  <p>A line graph showing Range [km] on the x-axis (0 to 2000) and Fuel Consumption [kg] on the y-axis (0 to 6000). There are three data series: a solid line, a dotted line, and a dashed line. The solid line starts at approximately 4500 kg at 0 km and rises to about 5700 kg at 1300 km, then remains flat until 2000 km. The dotted line starts at approximately 4500 kg at 0 km, rises to about 4500 kg at 1200 km, and then gradually decreases to about 3500 kg at 2000 km. The dashed line starts at approximately 3500 kg at 0 km and remains relatively flat until 2000 km.</p>
Sec. 5.4	<p><del>Cruise conditions for range calculations have been set using Mach and altitude values specified in Sec. 5.3. The specific fuel consumption has been set to 0.77 [lb/(lb h)] according to [1, 6] and as explained in Sec. 4.3.</del></p> <p>Cruise conditions for range calculations have been set using Mach and altitude values specified in Sec. 5.3. The specific fuel consumption has been set to 0.55 [lb/(lb h)] according to [1, 6] and as explained in Sec. 4.3.</p>
Fig. 5.4	<p>[Deleted]</p>   <p>Two line graphs showing Range [km] on the x-axis (0 to 2000 and 0 to 3000) and Fuel Consumption [kg] on the y-axis (0 to 6000). Both graphs show three data series: a solid line, a dotted line, and a dashed line. In the first graph (0-2000 km), the solid line rises to about 5700 kg at 1300 km and remains flat. The dotted line rises to about 4500 kg at 1200 km and then decreases. The dashed line remains flat at approximately 3500 kg. In the second graph (0-3000 km), the solid line rises to about 5700 kg at 1300 km and remains flat. The dotted line rises to about 4500 kg at 1200 km and then decreases. The dashed line remains flat at approximately 3500 kg.</p>

TABLE 3: Changes from 1st deliverable. (3/6)

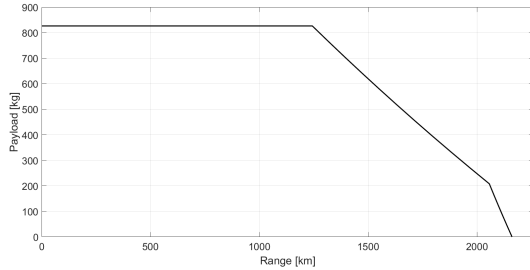
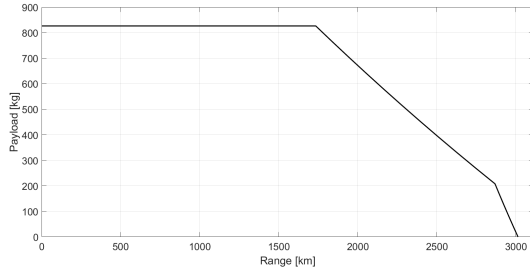
ID	Text
Fig. 5.5	<p>[Deleted]</p>  
Sec. 5.4	<p>On the one hand, Fig. 5.4 shows the range for different aircraft weight configurations, for example <i>MTOW</i> with <i>MPL</i>, giving a range of 1200 <i>km</i> approximately, or <i>MTOW</i> with <i>MFW</i>, resulting in slightly more than 2000 <i>km</i>.</p> <p>On the other hand, Fig. 5.5 shows the maximum payload for a specific range, or seen from another point of view, the maximum achievable range for a given payload. It can be seen that, according to the requirements detailed in Sec. 1.4, the 2000 <i>km</i> of range are achieved with approximately 2 people on the aircraft. After having analysed the range sensitivity on different parameters, it could be seen that the specific fuel consumption was determining, as reducing it by 0.1 [<i>lb/(lb f h)</i>], the range increases about 200 <i>km</i>. In order to achieve a greater PL for 2000 <i>km</i> and taking into account that the <i>MTOW</i> is close to the maximum allowed by regulations for Level 2 aircrafts (see [41]), future studies and iterations will try to attain the best Mach-Altitude combination that gives the optimum efficiency for a given reference of specific fuel consumption.</p> <p>On the one hand, Fig. 5.4 shows the range for different aircraft weight configurations, for example <i>MTOW</i> with <i>MPL</i>, giving a range of 1750 <i>km</i> approximately, or <i>MTOW</i> with <i>MFW</i>, resulting in slightly less than 2900 <i>km</i>.</p> <p>On the other hand, Fig. 5.5 shows the maximum payload for a specific range, or seen from another point of view, the maximum achievable range for a given payload. It can be seen that, according to the requirements detailed in Sec. 1.4, the 2000 <i>km</i> of range are achieved with almost all passengers with their own luggage, or all of them without any cargo. This result is acceptable and it is achieved due to the low SFC (<math>0.55 \text{ lb}/(\text{lb h})</math>) achieved with the JT15D-1B.</p>

TABLE 4: Changes from 1st deliverable. (4/6)

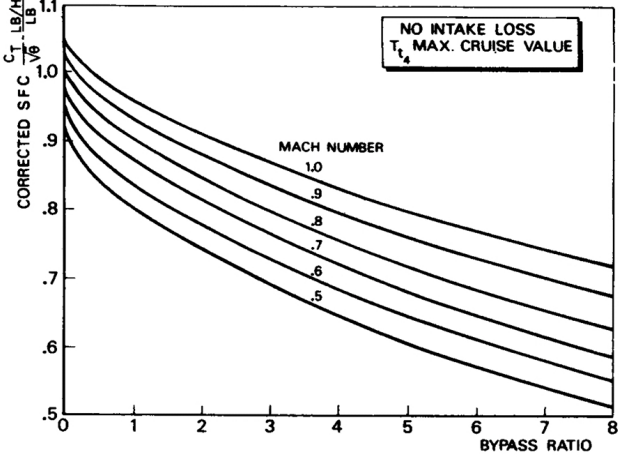
ID	Text
Sec. 5.5	<p>Finally, obtaining the Payload Range diagram it has been determined that the 2000 km range required can be achieved with a low percentage of the MPL, so future iterations, once aerodynamic studies have been done, will try to improve this fact by finding the best Mach-Altitude combination to reduce fuel consumption and achieve higher ranges for the same weight.</p> <p>Finally, obtaining the Payload-Range diagram it has been determined that the 2000 km range required can be achieved with a high percentage of the MPL due to the low SFC (0.55 <math>lb/(lb \cdot h)</math>) achieved with the JT15D-1B.</p>
Sec. 6.2	<p>Fig. 6.3 is a suitable illustration to use when defining fuselage and cabin sizes. So as to, this nomenclature will be followed among this paper. As this deliverable is preliminary, only the cabin sizing will be calculated and studied, taking into consideration both, comfort and regulations. One of the points to be discussed will be the possibility to install a lavatory, so as to it is a differential value when buying a business jet [42].</p> <p>Later on, when the preliminary design is intended to be completed, a more accurate analysis of the sizing, geometry and distribution of the fuselage and its elements will have been already done.</p> <p>Fig. 6.3 is a suitable illustration to use when defining fuselage and cabin sizes.</p> <p>So as to, this nomenclature will be followed among this paper.</p> <p>The cabin sizing will be calculated and studied, taking into consideration both, comfort and regulations. One of the points to be discussed will be the possibility to install a lavatory, so as to it is a differential value when buying a business jet [42].</p> <p>Later on, a more accurate analysis of the sizing, geometry and distribution, as well as the configuration for the cockpit will be developed.</p>
Chap. 6	This chapter was not totally completed in the partial delivery, so new content has been added.
Fig. ??	<p>[Deleted]</p> 
Sec. 4.3	except SFC. For this characteristic, statistical data is used, knowing the cruise Mach (0.7) and the Bypass Ratio (3.3):

TABLE 5: Changes from 1st deliverable. (5/6)

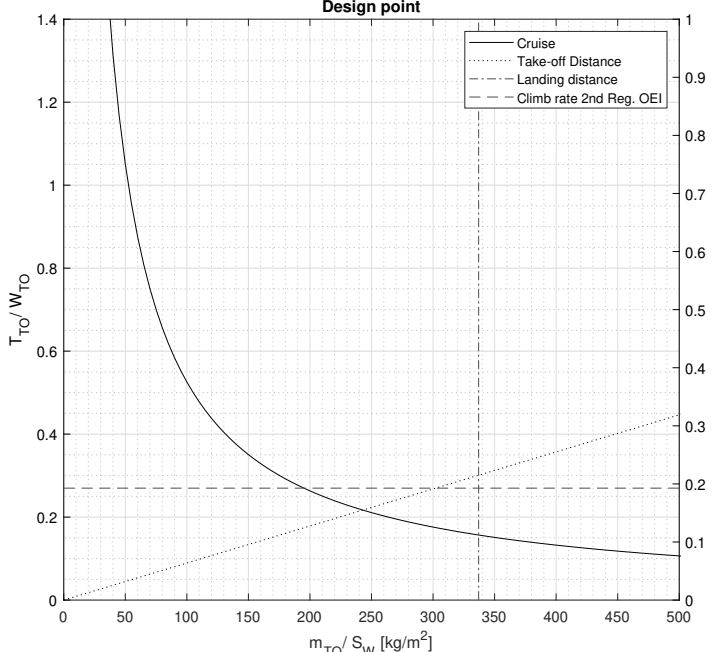
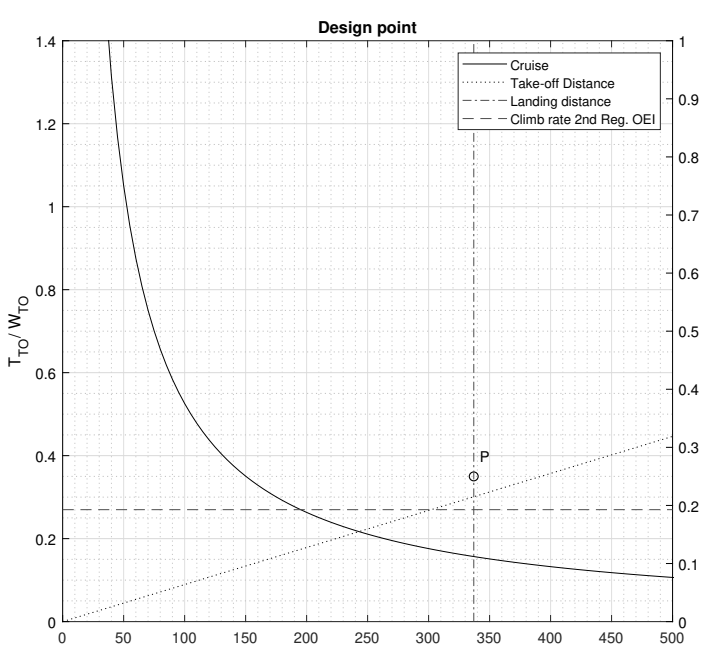
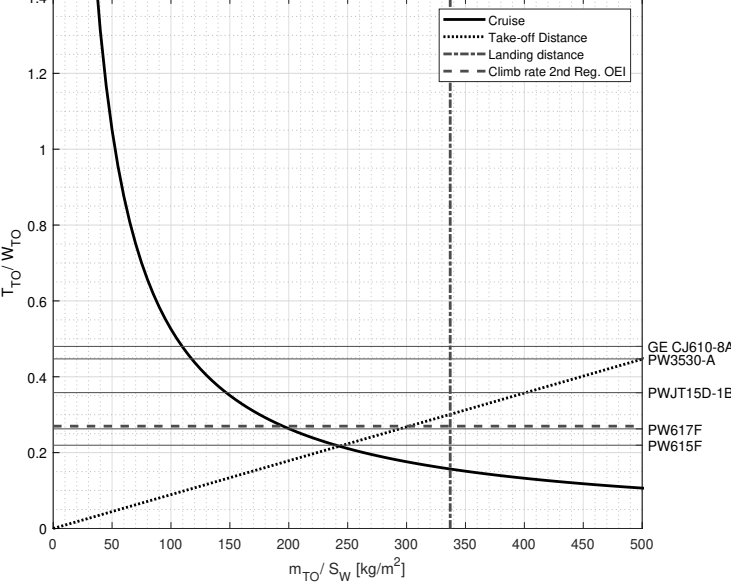
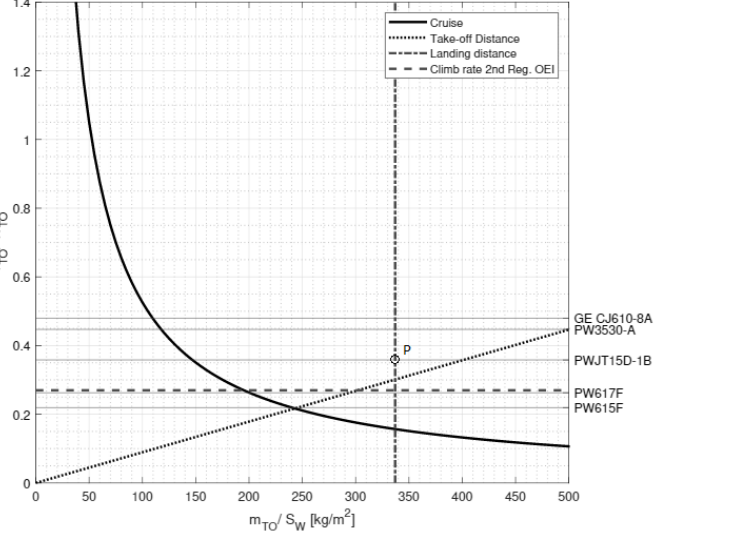
<i>ID</i>	<b>Text</b>
	<p>[Deleted]</p>  <p>Design point</p> <p>Y-axis: <math>T_{TO}/W_{TO}</math></p> <p>X-axis: <math>m_{TO}/S_W [\text{kg}/\text{m}^2]</math></p>  <p>Design point</p> <p>Y-axis: <math>T_{TO}/W_{TO}</math></p> <p>X-axis: <math>m_{TO}/S_W [\text{kg}/\text{m}^2]</math></p>

Fig. 4.5

TABLE 6: Changes from 1st deliverable. (6/6)

ID	Text
[Deleted]	 
Abstract	A new abstract is carried out.

# Abstract

The aim of this project is to design a private jet. In order to do so, some data has been taken from references of likewise aircrafts. Also, the given in-class materials have been used as a guide while the project development.

The first task has been the election of the type of aircraft, a Very Light Jet, based on the performance requirements and the business target.

Once the requirements had been defined, the design part was ready to begin. A state of the art of similar jets has been done in order to define the general configuration for the main parts of the aircraft -fuselage, wing, propulsion plant, empennage and landing gear-. A preliminary study of aeronautic materials has been carried out.

Next step has been the estimation of the aircraft's weight and CG as they were needed in order to design other parts of the plane. The design point has been analyzed so as to define the power plant and the the needed wing's surface. A performance study has been presented, showing the flight profile of the aircraft. Moreover, the Breguet equation has been solved. Additionally, cruise conditions and the relation between payload and range have been analyzed.

The fuselage has been conceptually design, focusing only in the cabin's sizing. Geometric characteristics of the wing have been defined and a study and analysis of high-lift devices has been developed. The empennage has also been designed in order to carry out the stability analysis and the weight centring of the jet. The main characteristics of the landing gear have also been defined. A further analysis of the propulsion system has been developed following the previous election of the

type of engine. Additionally, a research of the aircraft's airframe has been done for the fuselage, wing and empennage.

Finally, a study of the flight envelope based on CS-23 has been carried out.

# Scope

This project will consist of making a preliminary design of a Very Light Business Jet. The project will be completed by December, 2019. The report will include the description of the studied parts and the justification of the methods used, but taking into account it is just in a preliminary design stage.

Bibliographic resources will be used to obtain empiric data and recommended methods, whereas similar airplanes will help the project determine the conceptual shape and initial weight estimation of the plane. For the weight sizing, mission performance, centring, wing design, static stability analysis, landing gear sizing and flight envelope calculation, numerical methods will be implemented in Matlab. During the fuselage design, Solidworks will be used to help visualizing the shape and dimensions of the plane. The other contents, including the data for the fuselage design and the aircraft airframe will consider bibliographic references to determine its conclusions. Due to the project depth, the scope will be defined separately for relevant areas of study, taking into account the development methods mentioned above:

## General arrangement

- The general arrangement of the plane will be developed as an initial stage of the design. It will consider similar airplanes and also literature to perform decisions of the general arrangement. This general arrangement will consider the wing type, the tail shape, the landing gear composition and also the place where to install the engines.

- The weight estimation of the plane will be developed by using different methods: both bibliographic data and similar planes data will be used. An iterative process will be programmed in Matlab to, by fixing an initial payload, obtain the respective Maximum Take-Off Weight and the Operative Empty Weight.
- The Design Point will be studied by considering the performance of the plane, given by statistical literature data. The Design Point will determine the election of the engine and the initial wing surface.

## Fuselage

- The fuselage will start by considering what will this plane carry inside its cabin. So as to, the comfort given to its passenger will be the most important designing parameter. Analytical expressions will give the surface inside the cabin, to verify at the end that there is enough space for the passengers. Also, the inclusion of a lavatory will be considered as a differential value.
- The external shape of the fuselage will use bibliographical data and plots to design it by considering the drag as an important design parameter. None numerical approximation will be used to size the external shape of the fuselage.
- The afterbody of the fuselage will be designed by using empirical bibliographic data, but the nose of the fuselage will not be studied in this design stage.
- The cabin itself will only be sized regarding the surface inside it. Any furniture item, such as seats, compartments for baggage, etc. will not be considered in this report.
- The fuselage airframe will be defined.

## Engine installation

- The engine will be selected from the Design Point Analysis thrust taking into account all the performances that the aircraft must operate.

- The specifications of the engine selected will be specified.
- The number of engines, the location (wing/fuselage mounted) and installation (podded/embedded) will be selected.
- The nacelle, the attaching structure and the inlet of the engines will not be designed.
- The thrust reversal type will be selected.

## Wing

- The wing design will be based on the first approximation given by the Design Point Analysis which results in a estimated wing surface.
- An iterative process will be used to determine the wing geometry according to XFLR5 simulations with the objective to obtain optimal efficiency for cruise phase.
- A study of the similar jets geometry parameters will be used to determine the initial values for iteration.
- The airfoil selection will be based on observing the performance of the simulations of various airfoils. It will not be performed a more extensive study of the airfoil selection.
- The wing airframe will be selected.
- It will be carried out an state of the art study of Passive High-Lift Devices.
- It will be developed a analytical method for sizing the trailing-edge flaps (chord, span, and flap type).
- It will not be considered the leading-edge flaps for the sizing study and neither will be selected for this initial design.
- The control surfaces will not be designed in this preliminary study.

**Empennage**

- A study of the weight centering and static stability will be performed.
- The empennage will be dimensioned according the static stability study.
- The empennage airframe will be defined.

**Landing Gear**

- The landing gear type and disposition will be determined.
- The landing gear will be sized and the number of wheels estimated.
- A stability and manoeuvrability study will be carried out.

**Performance**

- A payload-range diagram will be plotted by considering the fuel-consumption of the plane given by Breguet's integral equation resolution. The specific fuel consumption will be the one established by the engine chosen.
- The flight envelope for the performance of the plane will be plotted by taking into account the regulations involved in CS-23.

Due to the fact that the aim of the project is to perform a preliminary design, any system will not even be defined. That means that anything related to avionics, electrical system, hydraulic system, flight control system, landing gear retraction, braking or anti-skid systems, among many others, will not be quoted in this report.

# Nomenclature

$\alpha_{\delta f}$	Section lift effectiveness parameter for single slotted flaps
$\bar{C}$	Mean geometric chord [m]
$\beta$	Compressibility effects factor
$\beta$	Fuselage upsweep angle [deg]
$\Delta C_{L_{max_L}}$	Maximum lift coefficient increase with landing configuration
$\Delta C_L$	Lift coefficient increase
$\Delta W_E(b_f, l_f, h_f)$	Torenbeek's correction for <i>OEW</i> depending on fuselage dimensions [kg]
$\delta$	Relative error
$\delta_f$	Flap deflection angle [rad or deg]
$\eta_i$	Inner point of the flap span
$\eta_o$	Outer point of the flap span
$\Gamma$	Dihedral angle [deg]
$\Lambda$	Sweep angle [deg]
$\lambda$	Wing taper ratio
$\lambda_h$	Horizontal tailplane taper ratio
$\lambda_v$	Vertical tailplane taper ratio
$\mu g$	Aeroplane mass ratio
$\phi$	Roll angle [deg]
$\phi_h$	Horizontal tailplane sweep
$\phi_v$	Vertical tailplane sweep
$\rho$	Density at certain altitude [kg/m <sup>3</sup> ]
$\rho_0$	Air density at Sea Level [kg/m <sup>3</sup> ]
$\rho_{baggage}$	Density for the baggage [kg/m <sup>3</sup> ]
$\rho_{mer}$	Density for the carried goods [kg/m <sup>3</sup> ]
$\sqrt{\theta}$	Correction factor of the speed of sound for a certain altitude

$\theta$	Temperature correction factor
$\theta_{LOF}$	Pitch angle during takeoff [deg]
$\theta_{TD}$	Pitch angle during touchdown [deg]
$\varphi$	Aerodynamic efficiency parameter
$A$	Aspect Ratio
$a_0$	Speed of sound at sea level [m/s]
$A_h$	Horizontal tailplane aspect ratio
$A_v$	Vertical tailplane aspect ratio
$b_f/b$	Flap span ratio
$b_c$	Cabin's Width [m]
$b_f$	Fuselage's Width [m]
$b_{if}/b$	flap span starting point ratio
$C_D$	Drag coefficient
$c_f/c$	Flap chord ratio
$C_h$	Horizontal tail volume coefficient
$C_N$	Normal force coefficient
$C_v$	Vertical tail volume coefficient
$C_{d_i}$	Induced drag coefficient
$C_{D_0}$	Zero lift drag coefficient
$C_j$	Specific fuel consumption for the engines [kg/N · s]
$C_{L\alpha}$	Wing lift curve slope [1/rad]
$C_{L_{min}}$	Minimum lift coefficient
$C_{L_{opt}}$	Lift coefficient for maximum efficiency
$C_{l_{\delta_f}}$	Airfoil lift coefficient depending on $\delta_f$ and $t/c$
$C_{L_{max \ clean}}$	Maximum lift coefficient of the wing with clean configuration
$C_{L_{max \ L}}$	Maximum lift coefficient of the wing at landing configuration
$C_{L_{max,TO}}$	Maximum lift coefficient of the wing at take-off configuration
$C_{L_{max}}$	Maximum lift coefficient of the wing with flaps retracted
$C_{m\alpha}$	Static stability in fixed controls index
$C_m$	Moments coefficient at the CG
$cg_{env}$	Range of CG possible positions with MTOW [m]
$cg_{for}$	Extreme forward position of the CG with MTOW [m]
$D$	Distance between the closest contact area edges of the main wheels [m]
$D$	Total drag [N]
$E$	Aerodynamic efficiency

---

$e$	Oswald's factor
$e_s$	Static deflection of the tire plus shock absorber [m]
$g_0$	Gravity constant [ $m/s^2$ ]
$h$	Altitude of flight [m]
$h_g$	Landing gear leg height [m]
$h_{cg}$	height of CG above the ground during taxiing [m]
$h_c$	Cabin's Height [m]
$h_f$	Fuselage's Height [m]
$i_h$	Horizontal tailplane geometrical incidence
$K$	Flap type correction parameter
$K'$	Flap chord ratio correction parameter
$k_{sg}$	Undercarriage stiffness parameter
$K_\Lambda$	Sweep angle correction in flaps down configuration
$K_{bd}$	Fulness coefficient for the cargo-bay
$k_l$	Statistic Landing constant
$K_{TF}$	Breguet Factor [m]
$k_{to}$	Statistic Take-off constant
$kg$	Gust alleviation factor
$L$	Total lift [N]
$L/D$	Aerodynamic lift-to-drag ratio, e.g aerodynamic efficiency
$l_h$	Horizontal tail distance to CG
$l_m$	Distance between the MLG and the most rearward CG position with MTOW [m]
$l_v$	Vertical tail distance to CG
$L_W$	Load per tire of the MLG [kg]
$l_c$	Cabin's Length [m]
$l_f$	Fuselage's Length [m]
$l_{n1}$	Distance between the aerodynamic centre and the NLG location for 8% of the load [m]
$l_{n2}$	Distance between the aerodynamic centre and the NLG location for 15% of the load [m]
$M$	Mach number
$M_{ff}$	Mission's overall weight ratio
$n$	Load factor
$n$	Number of discretization

$n_g$	Positive aeroplane gust load factor due to gust at $V_C$
$n_y$	Lateral load/weight
$n_{crew}$	Number of crew members
$n_{max}$	Maximum load factor
$n_{min}$	Minimum load factor
$n_{pax}$	Number of passengers
$p$	Inflation pressure of the main wheel [ $kg/m^2$ ]
$q$	Dynamic pressure [ $Pa$ ]
$R$	Ideal gas constant [ $J/kg\Delta K$ ]
$R$	Range [ $km$ ]
$R_4$	Range covered during ascend phase [ $km$ ]
$R_{cr}$	Range for the cruise [ $km$ ]
$S_h$	Horizontal tail wet surface
$S_T$	Distance between the imprint centers of the wheels in one leg [ $m$ ]
$S_v$	Vertical tail wet surface
$S_r$	Slenderness ratio
$STOFL$	Take-off Field Length [ $m$ ]
$S_W$	Wet surface [ $m^2$ ]
$T$	Total thrust [ $N$ ]
$t$	Landing gear track [ $m$ ]
$t/c$	Airfoil thickness ratio
$T_{11}$	Temperature at 11000 m [K]
$T_{alt}$	Thrust at certain altitude [N]
$T_{cr}$	Thrust at cruise [N]
$T_{SL}$	Thrust at Sea Level [N]
$T_{TO}$	Thrust at Take-off[N]
$TF_m$	Total fuel weight for the mission [ $kg$ ]
$TR$	Taper ratio
$U_{de}$	Gust velocity [ $m/s$ ] or $fps$ when specified
$V_A$	Design manoeuvring speed [ $m/s$ ]
$V_B$	Design speed for maximum gust intensity [ $m/s$ ]
$V_C$	Design cruising speed [ $m/s$ ]
$V_D$	Design dive speed [ $m/s$ ]
$V_F$	Maximum speed with limit load factor for flaps fully extended [ $m/s$ ]
$v_h$	Horizontal tailplane dihedral

---

$V_S$	Stalling speed with flaps retracted [m/s]
$V_{asc}$	Horizontal speed when ascending [m/s]
$V_{climb}$	Vertical speed when ascending [m/s]
$V_{STO}$	Stall Speed at Take-off [m/s]
$V_{SF}$	Stall speed with flaps fully extended [m/s]
$W$	Weight [kg]
$W_2$	Weight after taxi and before take-off [kg]
$W_{baggage}$	Weight for the baggage [kg]
$W_{cr}$	Average cruise weight [kg]
$W_C$	Crew weight [kg]
$W_{engine}$	Weight for the engines [kg]
$W_E$	Operative Empty Weight [kg]
$W_F$	Fuel weight [kg]
$W_L$	Landing weight [kg]
$W_{MZF}$	Maximum Zero Fuel weight [kg]
$W_{pax}$	Weight for each passenger [kg]
$W_{PL}$	Payload [kg]
$W_r$	Ramp Weight [kg]
$W_{tf}$	Weight of all trapped (e.g unusable) fuel and oil [kg]
$W_{TO}$	Tale-off weight [kg]
$W_u$	Useful Load [kg]
$x/d_{ab}$	Afterbody Fineness Ratio
$z_{11}$	Altitude of 11000 m [m]
$z_{fh}/c$	Flap downward displacement ratio
b	Wing span [m]



# Acronyms

<b>ASDR</b>	Accelerate-Stop Distance Required	<b>MZFL</b>	Maximum Zero Fuel Weight
<b>CG</b>	Center of gravity	<b>NLG</b>	Nose Landing Gear
<b>CW</b>	Crew Weight	<b>OEI</b>	One Engine Inoperative
<b>EW</b>	Empty Weight	<b>OEW</b>	Operative Empty Weight
<b>FW</b>	Fuel Weight	<b>PL</b>	Payload
<b>HLD</b>	High-Lift Devices	<b>RF</b>	Reserve Fuel
<b>LCN</b>	Load Classification Number	<b>SFC</b>	Specific Fuel Consumption
<b>LE</b>	Leading Edge	<b>SL</b>	Sea Level
<b>LG</b>	Landing Gear	<b>TE</b>	Trailing Edge
<b>MFL</b>	Maximum Fuel Weight	<b>TF</b>	Trip Fuel
<b>MLDW</b>	Maximum Landing Weight	<b>TODR</b>	Take-Off Distance Required
<b>MLG</b>	Main Landing Gear	<b>TOP</b>	Take-off Parameter
<b>MPL</b>	Maximum Payload	<b>TOW</b>	Take-off Weight
<b>MTOW</b>	Maximum Take-off Weight	<b>VLJ</b>	Very Light Jet



# Chapter 1

## Introduction

In this paper, the preliminary design of an aircraft is carried out. The initial decision made was to choose the type of aircraft to develop the project. After a brief discussion, a private jet was selected for some reasons: it is not a common type of aircraft used by the team members on their regular basis, so it could help everyone to widen its knowledge about private jets. Furthermore, some of the members expressed their interest in carrying out the cabin design: a private jet allows lots of ideas and possible configurations.

After the initial decision, there was a need to start the conceptual design. To carry out this process, the type of private jet as well as the value to differentiate the brand from others had to be selected. To better get to know some private jets, a research and analysis about what is offered by other brands was made.

At the end, all team members discussed about the mission and performance requirements of the private jet in order to set the initial parameters of the project.

### 1.1 Type of private jet election and differential value

Business jets can be categorized according to different parameters such as their size, autonomy or passengers capacity [43]:

### **Very light jets**

The very light jet (VLJ) is a classification initiated by the release of the Eclipse 500, on December 2006 [32]. It includes private jets that typically accommodate 4 to 6 passengers with an average range over 2000 km [44]. The most important advantage that VLJs offer is their suitability to land at short runways, what gives them a wider range of operational possibilities.

### **Light jets**

Light jets are the next category after very light jets. They are designed to take in up to 9 passengers. About their performance, their autonomy is usually between three and four hours [45]. Even if they can operate in short runways, they need longer runways than very light jets.

### **Midsize jets**

Midsize jets have a 3 to 5 hours autonomy and can accommodate up to 9 passengers [43]. Despite the fact that they show similar characteristics when talking about the number of passengers they can accommodate and their autonomy, they differ from the light jets for their size, which gives more space inside the cabin. However, this size increase entails some restrictions such as the need for longer runways and an increase of the costs for both the initial investment and operational issues.

### **Super midsize jets**

The category situated in the middle point between midsize and large jets is the super midsize jet, which gives many benefits that large jets offer as more cabin space, higher range, more autonomy –7 hours [43]– or more passengers capacity –from 8 to 12 passengers [43]–.

The disadvantages with respect to the lower category behind them are the costs and the runway length needed.

### **Large jets**

Large jets are the last category and as their own name say, they are the most large-sized jets. These jets offer a wide range of benefits: more cabin space, thus

more passengers accommodation –from 8 to 19 people–[43] or their capability for performing transatlantic flights. Even so, costs highly increase and they can only operate in large airports.

In order to determine which kind of jet is going to be designed, it was needed to carry out a global comparative between all the explained categories. In addition, the target of the project was an important point to focus on. Along these lines, it was decided to design a VLJ, offering the possibility to land in small airports, such as Sabadell one. The potential costumer profiles are companies that need to travel for business daily. By offering this type of plane, they economise the journeys and also the time to meet up with other companies. The possibility to land and take-off from small airports is a plus-value the aim of which is to reduce useless time spent in traffic jams.

## 1.2 Similar aircraft statistics

The aim of this section is to list the most leading VLJs nowadays and give a summary of their specifications and other relevant parameters, in order to find a shortage to be competitive or to use average values for initial estimations.

## Cessna 510 Citation Mustang

TABLE 1.1: Cessna 510 Citation Mustang Specifications [25], [26], [27], [28].

Cessna 510 Citation Mustang			
<b>Capacity</b>	4-5 pax + 2 pilots	<b>Mach Maximum Operating</b>	0.63
<b>Cabin observations</b>	Small lavatory	<b>Cruise speed</b>	175 m/s (340 ktas)
<b>Powerplant</b>	2x Pratt & Whitney Canada PW615F 6.49 kN each	<b>Range</b>	2160 km
<b>Undercarriage</b>	Retractable Tricycle	<b>Service Ceiling</b>	12500 m (41500 ft)
<b>Length</b>	12.37 m	<b>Rate of climb</b>	3010 fpm
<b>Wingspan</b>	13.16 m	<b>Thrust/Weight</b>	0.337
<b>Height</b>	4.09 m	<b>Take-off distance</b>	948 m
<b>Wing Area</b>	19.51 m <sup>2</sup>	<b>Landing distance</b>	729 m
<b>Empty Weight</b>	2540 kg	<b>Aspect Ratio</b>	8.89
<b>Fuel Weight</b>	1170 kg	<b>Materials</b>	Aluminium Alloy
<b>Payload</b>	528 kg	<b>Unit cost</b>	\$3.35 M USD
<b>MTOW</b>	3930 kg	<b>Others</b>	-



(A) Image by Juergen Lehle.



(B) Image by Juergen Lehle.

FIGURE 1.1: Cessna 510 Citation Mustang.

## Embraer Phenom 100

TABLE 1.2: Embraer Phenom 100 Specifications [25], [29].

Embraer Phenom 100			
<b>Capacity</b>	5-7 pax + 2 pilots	<b>Mach Maximum Operating</b>	0.7
<b>Cabin observations</b>	Cabin height 1.5 m	<b>Cruise speed</b>	208 m/s (400 ktas)
<b>Powerplant</b>	2x Pratt & Whitney Canada PW617F1E 7.7 kN each	<b>Range</b>	2182 km
<b>Undercarriage</b>	Retractable Tricycle	<b>Service Ceiling</b>	12500 m (41,000 ft)
<b>Length</b>	12.82 m	<b>Rate of climb</b>	3061 fpm
<b>Wingspan</b>	12.3 m	<b>Thrust/Weight</b>	0.337
<b>Height</b>	4.35 m	<b>Take-off distance</b>	975 m
<b>Wing Area</b>	14.86 m <sup>2</sup>	<b>Landing distance</b>	741 m
<b>Empty Weight</b>	3235 kg	<b>Aspect Ratio</b>	8.89
<b>Fuel Weight</b>	1279 kg	<b>Materials</b>	Aluminium Alloy
<b>Payload</b>	775 kg	<b>Unit cost</b>	\$3.35 M USD
<b>MTOW</b>	4799 kg	<b>Others</b>	-



(A) Image extracted from [46].



(B) Image extracted from [46].

FIGURE 1.2: Embraer Phenom 100.

## Honda HA420 HondaJet

TABLE 1.3: Honda HA420 HondaJet Specifications [30], [25], [31].

Honda HA-420 HondaJet			
<b>Capacity</b>	6 pax + 2 pilots	<b>Mach Maximum Operating</b>	0.73
<b>Cabin observations</b>	Small lavatory	<b>Cruise speed</b>	216 m/s (420 ktas)
<b>Powerplant</b>	2x GE Honda HF120 9.1 kN each	<b>Range</b>	2,661 km
<b>Undercarriage</b>	Retractable Tricycle	<b>Service Ceiling</b>	13100 m (43,000 ft)
<b>Length</b>	12.99 m	<b>Rate of climb</b>	3990 fpm
<b>Wingspan</b>	12.12 m	<b>Thrust/Weight</b>	-
<b>Height</b>	4.56 m	<b>Take-off distance</b>	975 m
<b>Wing Area</b>	16.4 m <sup>2</sup>	<b>Landing distance</b>	741 m
<b>Empty Weight</b>	3267 kg	<b>Aspect Ratio</b>	8.5
<b>Fuel Weight</b>	816.5 kg	<b>Materials</b>	Carbon Fiber/Epoxy Composite
<b>Payload</b>	635 kg	<b>Unit cost</b>	\$5.28 M USD
<b>MTOW</b>	4808 kg	<b>Others</b>	-



(A) Image by Michael Pereckas.



(B) Image by Michael Pereckas.

FIGURE 1.3: Honda HA-420 HondaJet.

## Eclipse Aviation EA500

TABLE 1.4: Eclipse Aviation EA500 Specifications [25], [32].

Eclipse Aviation EA500			
<b>Capacity</b>	4-5 pax + 2 pilots	<b>Mach Maximum Operating</b>	0.64
<b>Cabin observations</b>	NO lavatory	<b>Cruise speed</b>	190 m/s (370 ktas)
<b>Powerplant</b>	2x Pratt & Whitney Canada PW610F 4kN each	<b>Range</b>	2084 km
<b>Undercarriage</b>	Retractable Tricycle	<b>Service Ceiling</b>	12500 m (41,000 ft)
<b>Length</b>	10.1 m	<b>Rate of climb</b>	3424 fpm
<b>Wingspan</b>	11.4 m	<b>Thrust/Weight</b>	-
<b>Height</b>	3.4 m	<b>Take-off distance</b>	715 m
<b>Wing Area</b>	13.4 m <sup>2</sup>	<b>Landing distance</b>	686 m
<b>Empty Weight</b>	1740 kg	<b>Aspect Ratio</b>	9.69
<b>Fuel Weight</b>	539 kg	<b>Materials</b>	Composites and Aluminium
<b>Payload</b>	362 kg	<b>Unit cost</b>	\$2.5 M USD
<b>MTOW</b>	2722 kg	<b>Others</b>	-



(A) Image by Alan Radecki Akradecki.



(B) Image by Alan Radecki Akradecki.

FIGURE 1.4: Eclipse Aviation EA500.

## Syberjet SJ30

TABLE 1.5: Syberjet SJ30 Specifications [33].

Syberjet SJ30			
<b>Capacity</b>	4-5 pax + 2 pilots	<b>Mach Maximum Operating</b>	0.83
<b>Cabin observations</b>	Cabin height 1.3 m	<b>Cruise speed</b>	250 m/s (486 ktas)
<b>Powerplant</b>	2x Williams Int. FJ44-2A 10.23 kN each	<b>Range</b>	4600 km
<b>Undercarriage</b>	Retractable Tricycle	<b>Service Ceiling</b>	15000 m (49,000 ft)
<b>Length</b>	14.26 m	<b>Rate of climb</b>	3663 fpm
<b>Wingspan</b>	12.9 m	<b>Thrust/Weight</b>	-
<b>Height</b>	4.33 m	<b>Take-off distance</b>	1200 m
<b>Wing Area</b>	17.7 m <sup>2</sup>	<b>Landing distance</b>	778 m
<b>Empty Weight</b>	1646 kg	<b>Aspect Ratio</b>	-
<b>Fuel Weight</b>	2200 kg	<b>Materials</b>	Composites and Aluminium
<b>Payload</b>	362 kg	<b>Unit cost</b>	\$8.3 M USD
<b>MTOW</b>	6327 kg	<b>Others</b>	-



(A) Image by Sergey Ryabtsev.



(B) Image by Sergey Ryabtsev.

FIGURE 1.5: Syberjet SJ30.

## Adam Aircraft A700

TABLE 1.6: Adam Aircraft A700 Specifications [34], [25].

Adam Aircraft A700			
<b>Capacity</b>	4-6 pax + 2 pilots	<b>Mach Maximum Operating</b>	0.59
<b>Cabin observations</b>		<b>Cruise speed</b>	175 m/s (340 ktas)
<b>Powerplant</b>	2x Williams Int. FJ33-4A 6.0 kN each	<b>Range</b>	2222 km
<b>Undercarriage</b>	Retractable Tricycle	<b>Service Ceiling</b>	12500 m (41,000 ft)
<b>Length</b>	12.42 m	<b>Rate of climb</b>	2550 fpm
<b>Wingspan</b>	13.41 m	<b>Thrust/Weight</b>	-
<b>Height</b>	2.92 m	<b>Take-off distance</b>	900 m
<b>Wing Area</b>	15.8 m <sup>2</sup>	<b>Landing distance</b>	823 m
<b>Empty Weight</b>	2494 kg	<b>Aspect Ratio</b>	-
<b>Fuel Weight</b>	680 kg	<b>Materials</b>	Composites and Aluminium
<b>Payload</b>	885 kg	<b>Unit cost</b>	\$2.2 M USD
<b>MTOW</b>	3855 kg	<b>Others</b>	Twin tail booms



(A) Image extracted from [34].



(B) Image extracted from [34].

FIGURE 1.6: Adam Aircraft A700.

## Cessna CitationJet/M2 (CJ1)

TABLE 1.7: Cessna CitationJet/M2 (CJ1) Specifications [25], [35], [36].

Cessna CitationJet/M2 (CJ1)			
<b>Capacity</b>	7 max pax + 2 pilots	<b>Mach Maximum Operating</b>	0.7
<b>Cabin observations</b>	-	<b>Cruise speed</b>	208 m/s (404 ktas)
<b>Powerplant</b>	2x Williams Int. FJ44-1AP-21 8.74 kN each	<b>Range</b>	2871 km
<b>Undercarriage</b>	Retractable Tricycle	<b>Service Ceiling</b>	12500 m (41,000 ft)
<b>Length</b>	12.98 m	<b>Rate of climb</b>	3698 fpm
<b>Wingspan</b>	14.40 m	<b>Thrust/Weight</b>	-
<b>Height</b>	4.24 m	<b>Take-off distance</b>	978 m
<b>Wing Area</b>	22.3 m <sup>2</sup>	<b>Landing distance</b>	789 m
<b>Empty Weight</b>	3068 kg	<b>Aspect Ratio</b>	-
<b>Fuel Weight</b>	907 kg	<b>Materials</b>	Composites and Aluminium
<b>Payload</b>	640 kg	<b>Unit cost</b>	\$5.15 M USD
<b>MTOW</b>	4717 kg	<b>Others</b>	-



(A) Image extracted from [47].



(B) Image extracted from [47].

FIGURE 1.7: Cessna CitationJet/M2 (CJ1).

## Bombardier Learjet 24

TABLE 1.8: Bombardier Learjet 24 Specifications [37], [38].

Bombardier Learjet 24			
<b>Capacity</b>	6 max pax + 2 pilots	<b>Mach Maximum Operating</b>	0.86
<b>Cabin observations</b>	-	<b>Cruise speed</b>	215 m/s (418 ktas)
<b>Powerplant</b>	2 x General Electric CJ610-6 13.1 kN each	<b>Range</b>	2728 km
<b>Undercarriage</b>	Retractable Tricycle	<b>Service Ceiling</b>	14000 m (45,000 ft)
<b>Length</b>	13.18 m	<b>Rate of climb</b>	6800 fpm
<b>Wingspan</b>	10.85 m	<b>Thrust/Weight</b>	-
<b>Height</b>	3.73 m	<b>Take-off distance</b>	850 m
<b>Wing Area</b>	21.53 m <sup>2</sup>	<b>Landing distance</b>	750 m
<b>Empty Weight</b>	3551 kg	<b>Aspect Ratio</b>	5.01:1
<b>Fuel Weight</b>	1360 kg	<b>Materials</b>	Composites and Aluminium
<b>Payload</b>	1620 kg	<b>Unit cost</b>	\$1 M USD
<b>MTOW</b>	6123 kg	<b>Others</b>	-



(A) Image extracted from [37].



(B) Image extracted from [37].

FIGURE 1.8: Bombardier Learjet 24.

## 1.3 Design situation analysis

From available data in Sec. 1.2, it can be seen that critical and differentiating aspects are mainly price, range and payload capacity. It is also shown that the usual Take-off distance is around 1000 m, a target to beat for getting a differential value. Another important aspect is that most cabins height is around 1.5 m, so it can be supposed that increasing this aspect would be very welcome in the market. From the structural point of view, there is a crescent using of composite materials in contrast to aluminium alloys: decreasing the total weight lets to an important improvement in the performance. It can be seen that the cruise behaviour is also an important affair to consider, given that all aforementioned jets share high service ceilings and high Mach numbers. Finally, they all make use of retractable undercarriage.

In this design, the main target traveller will be a man between 40 and 60 years old, allocated in Europe and USA – note that the largest markets of VLJs are in this territories, really far from other zones [44]–. The later could mean an important correction to the estimated weight per traveller, and so, it has to properly be analyzed. The average weight of a north-American citizen in the range of age mentioned above can be considered as 91.13 kg [48], while the mean average weight of a West-European citizen can be set as 86.40 kg [49]. The first weight is the one that will be considered during the design and the weight estimation, so as to it is the more restrictive.

For the luggage, the average weight of an invoice case is 16.7 kg, while the average weight of the hand luggage per person is 6.5 kg [50]. For this design, the average luggage weight is chosen as 13 kg, because it is understood that the main of the trips will be for a short time (2-3 days maximum) standing.

From the sells point of view, it is shown in reports by General Aviation Manufacturers Association [2]<sup>1</sup> that the sells of all sizes business jets keep approximately constant in time: As can be seen in the references (Fig. 1.9), while the sells of older VLJ decrease with time, the demand goes to newer airplanes from indistinctly new (Cirrus or Honda for example) and traditional companies (Learjet or Cessna for

---

<sup>1</sup>Data was also found for the first two quarters of 2019, being sold 566 business jets in this period. [2]

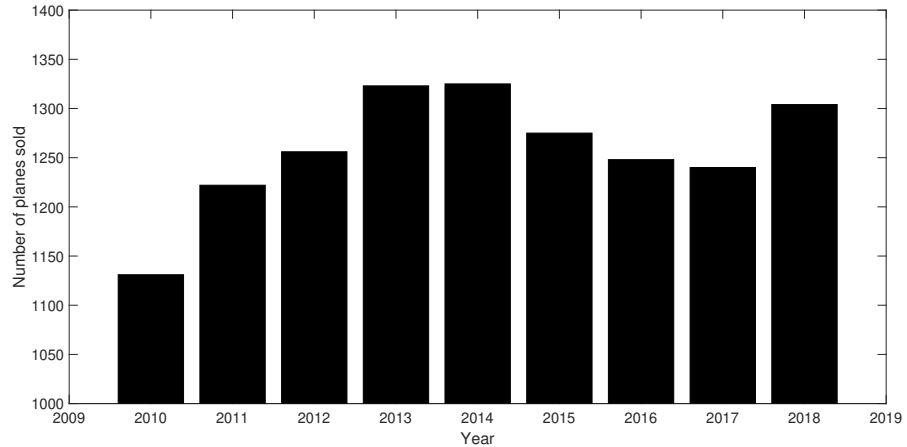


FIGURE 1.9: Evolution of sells in business jets year-by-year. [\[2\]](#)

example). This, combined with the relative invariability of the demand, can predict good acceptance of the product for the next five years for the less, but has to be something differential, to make a good introduction into the market.

## 1.4 Mission and performance requirements

Performance of the aircraft is crucial for its competitiveness and it has a great impact on almost every field of the design procedure. As explained in Sec. [1.1](#) the designed aircraft will be a VLJ that is able to operate to and from small airports with a limited runway length, in order to reach more destinations, so this way offering a more direct and comfortable journey to the passengers.

The operating range of the aircraft is determined taking into account the ability to cover short and mid-range flights, in order to make possible the operation in a regional and intracontinental scope. The VLJ will be able to cover the major part of the European Union, China, connect the most important cities in South-east Asia or in the United States (coast-to-coast flights are not considered), as an example.

The aircraft design and construction are based on the application of the most modern materials, such as composites. High efficiency propulsion systems, in order to improve performance and deliver the most efficient and economic private

jet in the market sector are also considered.

The performance requirements set for this aircraft, based on the above mentioned conditions and average values from Sec. [1.2](#) will be:

- Operating Range: approximately 2000 km (1080 nm) with MPL
- Cruising speed: 0.69 Mach
- Service Ceiling: 43000 [ft]
- Runway-length necessary for take-off and landing: 800 [m]
- Maximum passengers capacity: 6 passengers

These stipulations are in consonance to the technical requirements to be satisfied regarding CS-23 [\[41, 51\]](#). Furthermore, maximum take-off mas has to be lower than 8618 [kg], as specified by CS 23.2005 [\[41\]](#), whereas the maximum number of passengers is the maximum to classify this business jet into the *Level 2* category [\[41\]](#).

The above mentioned criteria and other qualitative requirements are important at the time of the aircraft design but they have different weights when a decision must be made. For this reason a list of some requirements has been created. The criteria are compared in pairs so that to establish relationships between them. In order to resolve conflicting situations: if a parameter depends on more than one variable, it must be determined keeping in mind the most important requirement and solve the situation changing it the least possible. These qualitative requirements for the aircraft are:

1. Fuel consumption reduction
2. Take-off and landing on small sized airports, with short runway-lengths
3. Good manoeuvrability
4. Assistance is not necessary at arrival and departure
5. Spacious, comfortable and silent cabin configuration

In order to establish interdependencies between these criteria the paired-comparison method has been used: evaluate in pairs the relative importance of each requirement. The more important one has a score of two or one (depending of its importance), and the not so important a score of zero. In case both criteria have the same importance, both will have a score of one and one. Summarizing the score each requirement obtained, a clear hierarchy can be made between them, as it is shown in Tab. 1.9.

No	1.	2.	3.	4.	5.	Total	RANK
1.	-	0	1	2	1	4	3.
2.	2	-	2	2	2	8	1.
3.	1	0	-	2	0	3	4.
4.	0	0	0	-	0	0	5.
5.	1	0	2	2	-	5	2.

TABLE 1.9: Requirements comparison

The final order of these requirements is:

1. Take-off and landing on small sized airports, with short runway-lengths
2. Spacious, comfortable and silent cabin configuration
3. Outstanding fuel efficiency
4. Good maneuverability
5. Assistance is not necessary at arrival and departure

## 1.5 Conclusions

After a comparison was made amongst the different categories of business jets, the VLJ came out as favorite. Its profile permit to develop an aircraft that is able to operate from airports where runway length is limited, and offer a huge variety of available destinations.

A statistical analysis has been also carried out in order to compare the existing

competitors in this target market and study their performance and other technical parameters. Improvement on cabin's comfort and total high inside the cabin came up as important design points.

The design situation was also studied to determine the actual state of the market and prognosticate the possible future changes and acceptance of the aircraft. It can be stated that the actual situation is promising, as the sector is keeping its interest in sales year by year. The target costumer will be 40 year old men based on Europe and USA. As a consequence, the design weight per passenger will be 91.13 kg, while for the baggage a value of 13 kg will be chosen.

The requirements of the aircraft's performance have been also established taking in mind several factors, such as efficiency and passengers preferences (operation from smaller airports). So that the following demands were stated: operating range of 2000 [km], 0,69 Mach cruising speed, service ceiling at 43000 [ft], 800 [m] runway length for take-off and landing and cabin's capacity for six passengers. The hierarchy of the technical requirements was also determined to facilitate decision making in future project stages, being the distance required for take-off and landing the most important criteria to achieve during the design.

# Chapter 2

## General arrangement

The aim of this chapter is to make a first approach to the general arrangement of the business jet, starting by using literature and taking the initial decisions about the chosen configurations. At the end of the chapter, a vague idea for the conceptual design of the business jet is going to be accomplished, regarding both geometry and materials to be used.

### 2.1 Geometry

The geometry of the plane is one of the most important facets to choose and study during the designing process. The geometry is directly related to the performance: it has a direct impact on the planes' aerodynamics and flight mechanics. Furthermore, as it is explained in Sec. 1.4, one of the requirements is to get an outstanding fuel efficiency, so that motors and their locations along the fuselage have to be also studied. The following sections will look through bibliography and similar business jets in order to get information about the general arrangement for the plane's geometry.

#### 2.1.1 Fuselage

The fuselage can be understood as the main and most important part of any aircraft, as it takes the payload from one place to another, which is the main goal

of any vehicle. For this reason this is one of the parts that are first designed. However, in this section only important parameters such as the slenderness ratio and the cross section will be discussed by analysing similar business jets. Fuselage diameters, length and internal layout, among others, will be further studied in Chap. 6.

Fig. 2.1 shows the typical geometric parameters of the fuselage for different types of aircrafts. As it can be seen, business jets' slenderness ratios go from 7 to 9.5. These values have been verified using the Cirrus Vision SF50 [7] and the Embraer Phenom 100EV [52] dimensions, resulting in 8.2 and 7.7, respectively.

Regarding the types of cross sections, these can be separated into rectangular and circular ones. Rectangular sections provide an easy construction although they present issues when the cabin is pressurized, as forces are not equally distributed and that leads to structural difficulties. Circular or near-circular cross sections provide structural robustness when there is an important pressure gradient. As it can be seen in Sec. 1.2, most of the business jets fly around 43000ft, and at this height a pressurized cabin is essential to guarantee passengers comfort and medical security [53]. Sometimes the fuselage bottom is flattened, mostly when no cargo or other loads need to be placed in the cargo hold or when the landing gear is located almost in the middle, as it happens on the A400M, for example. However, despite the fact that business jets are not expected to carry big luggage, the space under the seats will be considered to place some cargo and fuel tanks, although this will be further analysed in Chap. 6.

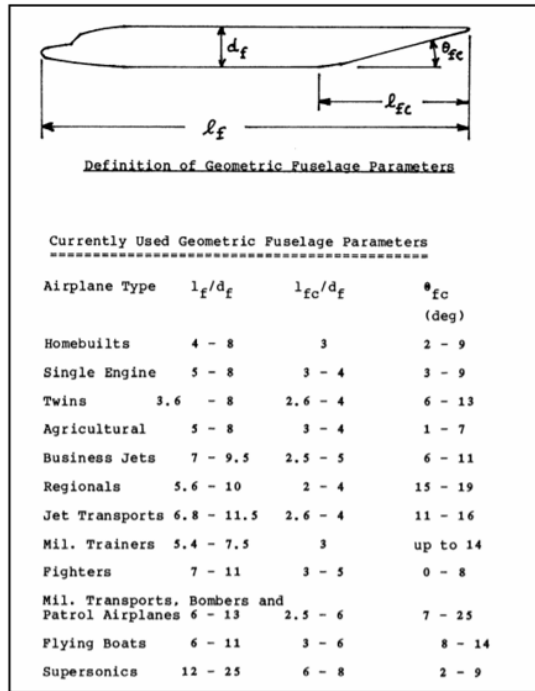


FIGURE 2.1: Geometric fuselage parameters [3].

## Decisions

Having seen the different fuselage main characteristics compared with similar jets, the slenderness ratio will be approximately 7.5, with a margin of 10%. The final value will be given after having designed the cabin in order to achieve an advantageous aerodynamic performance without compromising passengers comfort. The cross section will be near circular, without flattened bottom, allowing the cabin to be pressurized and some cargo to be placed under the seats.

### 2.1.2 Wing

This section discusses the general configuration of the wing and wing-fuselage position.

The wing location with respect to the fuselage depends on a series of aspects that have to be evaluated whether they are an advantage or a disadvantage for the technical and operational requirements which the aircraft is designed for. There are mainly three aircraft wing-fuselage configurations: High-wing, Mid-wing and Low-wing.

#### High-wing configuration

In High-wing configuration the wings are attached at the top of the fuselage and it is commonly used in military, cargo and STOL aircraft.

According to [6], the main advantages are the cargo hold proximity to the ground. This facilitate the unloading of the cargo through the nose or tail of the aircraft without the need for cargo lifts: the load can be unloaded through the ramp and ground vehicles can move under the wings for refuelling or carrying out maintenance tasks. Another point is the optimization of useful cargo volume due to spacious cargo hold. Moreover, in high-wing configuration engines are mounted

higher than usual and this fact keeps clear from dust and other objects that could be absorbed giving the capability to Take-off and land in non-asphalted runways.



FIGURE 2.2: Airbus A400M, as a High-wing configuration example

On the other hand, the main disadvantages are structural complexity due to wing joint and the increase of 20% of the vertical stabilizer because aerodynamics facts. Despite undercarriage is short (reducing structural strains), has to be folded in external protuberances at each side of the fuselage due to lack of space under the cargo hold and it makes that runways have to be wider. Another disadvantage is the difficulties related to operation and maintenance: the height of the engines complicates the technicians inspections or maintenance and the high wing complicates the refuelling due to the need of extra equipment. Moreover, high-wing in high speed is unfavourable due to aerodynamics despite of the high manoeuvrability that this configuration provide to the aircraft.

Some STOL (Short Take-off Landing) commercial aircrafts have high-wing configuration for example the *Evektor EV-55*, *Havilland Canada DHC-8* or the *ATR-42*. These aircrafts are designed for taking off and landing in short runways and for being powered by turboprop. This engines have to be mounted away from the ground, due to the propeller dimensions, so they force the high-wing configuration.



FIGURE 2.3: De Havilland Canada DHC-8 [4].

### Mid-wing configuration

In Mid-wing configuration the wings are attached at the mid position of the fuselage, crossing it. This configuration is mainly used in symmetrical-aerofoil aircrafts such as training, acrobatic aircrafts or fighters.

According to [6], there are many aerodynamic advantages in this configuration such as better rolling stability, capability to get lift in vertically reverse direction and reducing aerodynamic interference drag in the joint between wing and fuselage. In high speeds this configuration minimizes the drag. There are another advantages such as the capability to carry weapons under the wings.



FIGURE 2.4: Dassault Rafale, as an example of mid-wing configuration [5].

The disadvantages are important in commercial and cargo aircrafts. The most part of the fuselage is occupied by the wing because it crosses through the mid portion and it complicate the payload space use.

There are few examples of commercial jets with mid-wing configuration. One is the *HFB 320 Hansa* and it has the mid wing set into the back fuselage and forward sweep angle. The disadvantage of this plane is that small changes of payload should produce important variations in the gravity center affecting the stability. Also, the sweep-forward wings have aeroelasticity problems.



FIGURE 2.5: Hamburger Flugzeugbau HFB 320 Hansa Jet. Sweep forward private jet with mid-wing configuration [5].

### Low-wing configuration

In Low-wing configuration the wings are attached under the fuselage and it is commonly used in commercial planes.

According to [6], the principals advantages are the optimization of payload volume due to wings cross the fuselage at the lowest part of the fuselage. Also creates a cargo hold underneath the cabin floor used for folding the landing gear or for luggage cargo. The ground proximity of the wing make easier the operation and maintenance of the plane. Although impede ground vehicles of moving around the plane and under the wings, this configuration lets refuelling the plane or revising the engines without any lift or extra platform. Low-wing configuration also benefits the performance of the plane especially at Take-off and landing. First, low-wing lets the fuselage reduce in size at the tail zone and allows the plane to Take-off in higher rotation angle. The other benefit of the low-wing is the increase of the ground effect. The lower the wing is, less the tip vortex affect on the induced drag and this reduce the Take-off distance because the increase in lift. This generates a disadvantage when landing but is easily solved with aerodynamic breaks.

From the point of view of security the low-wing presents a disadvantage due to ground proximity in hard landings. Wings are where fuel is stored and in emergency or hard landings wings can impact the runway.

## Decision

Despite wing efficiency and drag reduction, for the optimization of the cabin space it is dismissed the mid-wing configuration. Moreover, it is dismissed the forwarded sweep wing due to its instability and structural difficulties.

The High-wing configuration is advantageous when it is desired to design cargo or STOL turboprop aircrafts. Since the fuselage will be narrow and with low cargo volume, the high-wing would reduce the space inside the cabin and would reduce the cabin height making the jet less comfortable. With low-wing configuration the wings would be joined at below the fuselage creating an extra underfloor cargo compartment. Another fact is that it is not a requirement to land in non-asphalted runways so engines can be mounted in lower position. Also is important the structural disadvantage that high-wing has: the joints to the fuselage are structurally complex. With low-wing, the undercarriage would be folded inside the wing and would not appear the necessity to create protuberances for folding it.

Ease for operation and maintenance is a priority because the operability in second-class airports where there are not enough equipment, high-wing configuration would be a disadvantage. From the point of view of aerodynamics, and since one operation requirement is the capability to land and Take-off in short runways, low-wing would be an advantage due to ground effect contribution to Take-off with a shorter distance.

For all the configurations aforementioned, a Low-wing configuration will be taken.

### 2.1.3 Propulsion plant

The aim of this section is to discuss the number of engines and their position on the aircraft, and justify the decided configuration in order to meet the design requirements.

Previously to the description of the design parameters, it must be pointed that during the documentation phase it has been observed how VLJ use turbofan technology (see Tab. 4.2) instead of turboprop or turbojet technology. For this reason

the comparative study between the three possible propulsion technologies has been dismissed and turbofan technology has been chosen as the one used.

### Engine location

In order to analyze the engine location (wing-mounted or rear-mounted) the following factors must be taken into account: Empty weight, engine maintenance, foreign object ingestion, systems, cargo loadability, flying qualities, noise and performance [6]. A brief description of the characteristics of each engine position according to the factors previously cited is presented below.

Regarding the wing-mounted configuration, its major advantage is the wing structure weight saving thanks to the mass relief effect that it has on the bending moment of the inner wing. Also, using wing-mounted engines makes it more accessible in terms of maintenance and simplifies the center of gravity travel. More underfloor cargo-hold behind the wing is achieved. On the other hand, engines mounted near the wing tip increase the landing impact associated stresses, and requires a larger vertical tailplane in order to compensate the roll moment.

The rear-mounted configuration allows having a clean wing, which increases the maximum lift and reduces the drag at high subsonic speeds due to the favorable aerodynamic interference [56]. However, some aircraft manufacturers –as Boeing– have disagreed on this fact claiming that in the clean wing the useful lift is reduced to ensure correct pitching behaviour at the stall [57]. In case of failure of an engine, the resulting yawing moment would be smaller than in a wing-mounted configuration, improving the tail design [6].

The main disadvantages of the rear-mounted configuration are the loss of cargo-hold at the tail, adding structural weight and requiring a larger fuselage to carry the same payload as one with wing-mounted configuration [53]. The position of the engines makes it less accessible for maintenance, and the center of gravity study requires to be catered as it presents more complex loading characteristics. In addition, this configuration is often combined with a T-tail, which can lead to the deep stall in the high incidence range [6, 53].

### Number of engines

The key parameter in order to compare the different number of engines is the Take-off runway length [6], as it can be seen in the Fig. 2.6

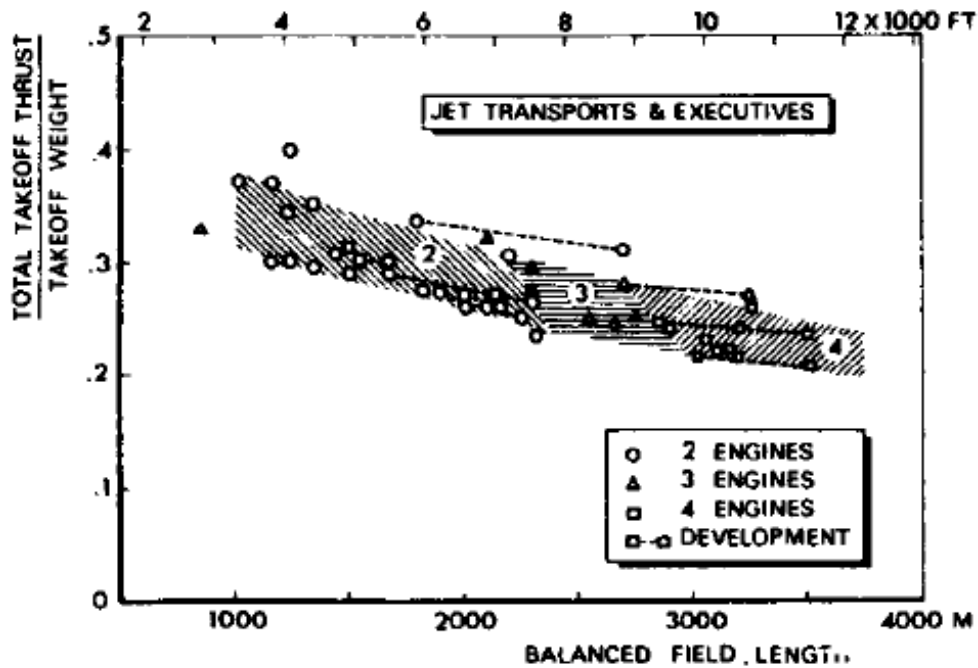


FIGURE 2.6: Number of engines, thrust loading and Take-off length comparison [6].

Even though the choice of the number of engines is not mandatory related to the Fig. 2.6, in the present document it will be adopted as the main reference to decide the number of engines. It should be pointed that the range of operation is also a key factor to take into account, and usually the short-haul aircraft use two engines and three or four engines for medium and large range of operation [6].

The two engines configuration requires relatively large fan diameters, forcing to use a high landing gear. In order to avoid this problem, it should be studied the use of either a rear-mounted configuration or a high wing.

The three engines configuration lead to a complex situation as the third engine has to be placed on the plane of symmetry, and generally it's located at the rear of the fuselage. The main problem of this configuration is the installation of the

third engine, as it leads to a greater structural weight and the requirement of using a longer and curved inlet [3]. In addition, if the engine is installed on top of the fuselage, the tail surface may be an obstruction for the outlet and aerodynamic interference would be a problem in the tail design.

The four engines configuration presents small in diameter engines, which allows more freedom sizing the landing gear. The lateral position of the engines has to be studied for each design case, and is directly related to the weight of the wing structure, the dimensions of the vertical tail and the location of the centre of gravity.

One key factor to take into account to determine the number of engines is the engine failure probability and the different scenarios where it could happen. If some engine malfunction occurred, it would lead to a considerable reduction of the thrust, as well as extra drag due to the asymmetrical conditions and yawing and rolling moments [56]. For this reason the safety range must be designed according the airworthiness regulation relating Take-off speeds and distances, climb performance, emergency manoeuvres, etc.[41, 51]. In order to compare in safety terms the different configurations, it's usually used the failure probability estimation showed in Fig. 2.7.

Failure of	Probability of engine failure (per flying hour)		
	1 engine	2 engines	3 engines
<b>twin-engine aircraft</b>	$2P$	$P^2$	-
<b>three-engine aircraft</b>	$3P$	$3P^2$	$P^3$
<b>four-engine aircraft</b>	$4P$	$6P^2$	$4P^3$

FIGURE 2.7: Probability of engine failure as function of the number of engines  
[6]

It can be observed how the probability of malfunction is the double in a four-engined aircraft than in the double-engined aircraft, and a two engines failure is

six times greater. As  $6P^2$  is not negligible, four-engined aircraft must be designed in order to meet with the regulation regarding performance with two engines inoperative during the cruise situation. In the two-engined aircraft the failure of both engines could lead to fatal consequences, but contemporary engines ensure such safety levels that a probability of  $P^2$  can be practically neglected during Take-off. In largest stages of the flight profiles the safety level of the actual engines is acceptable in order to perform non extended overwater flights.

## Decision

Regarding the engine location, a rear-mounted configuration has been selected. One of the key parameters that has been taken into account to select it is the safety improvement accomplished with the rear-mounted configuration, as in case of failure the rolling moments would be smaller in comparison with the wing-mounted configuration. Moreover, as the common cruise speed for VLJ is approximately  $M = 0.7$ , having a clean wing for high subsonic speeds will improve the aerodynamic characteristics and benefit other design parameters related to lift or drag as the fuel consumption. In terms of maintenance, as the dimensions of a private jet are very reduced in regard to a commercial aircraft, this factor does not have a big impact on the decision making criteria. In addition, as the capacity of the airplane is very reduced, losing cargo-hold capacity at the tail is not a critical situation as there is a relatively small volume of luggage to relocate.

As it has been previously said, the number of engines selection has been done according to Fig. 2.6. The parameters used in order to identify the region of the graph where the designed jet suites are:

- Total thrust: 24.44 kN (see Sec. 4.3)
- Take-off weight (using MTOW obtained at Tab. 3.6 ): 5572 kg
- Field length: 800 m

Introducing these values in Fig. 2.6 it can be observed how the VLJ designed fits in the top-left zone of the figure. For instance, the double-engined configuration has been selected. In addition, the probability of engine failure during the different

stages of the flight for a double-engined aircraft and the reliability of contemporary turbofan engines are acceptable for the ranges that the designed VLJ is intended to fly.

### 2.1.4 Empennage

This section will analyse the horizontal and vertical tails locations and positions from a study based on similar business jets. It must be noted that the tailplane configuration depends more on the general arrangement and the detail layout of the aircraft, given that its effectiveness is influenced by the wing and the operation of the engines (mostly on propellers). The main effects that influence it are: jet efflux effect, slipstream effects, engine failures (for rudder sizing mainly), and stability and control in the stall and post-stall condition. These effects will not be further studied in this preliminary design, although they are present in the empennage configuration decision.

Tailplane configurations can be divided depending on the number of fins: one fin, twin fins and butterfly tail.

#### Single fin

This is the most common current layout , where the stabiliser is mounted on the fuselage or on the fin (T-tail), as it can be seen in Fig. 2.8.

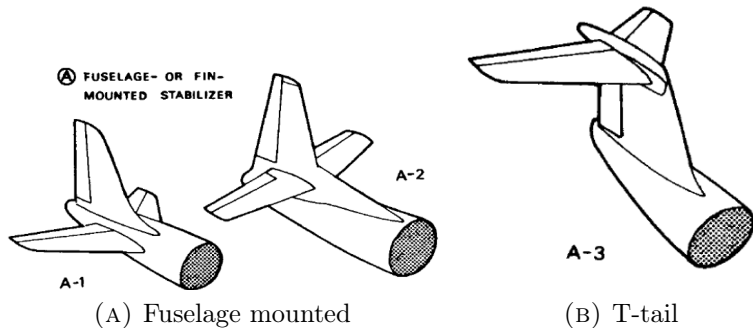


FIGURE 2.8: Tailplane single fin configurations [6].

This configuration is the simplest one in terms of structures and it guarantees the best stiffness, although the T-tail can be exposed to fluttering effects. The fuselage-mounted option is mostly used on airplanes with wing-mounted engines, where the tail is far enough from the engines so the jet efflux effect does not affect the tail's aerodynamic behaviour. On airplanes with rear-mounted engines, the T-tail is the commonly used configuration, considering that the horizontal stabiliser can be placed at a certain height where the jet efflux cone does not make any significant influence.

### Twin fins

Twin fins are used when a single fin would be so big that would create a considerable rolling moment when moving the rudder. This would be the case shown in Fig. 2.9a, where both fins are mounted at the horizontal stabiliser tips. The twin fins configuration can also be used in aircrafts with twin tail booms, usually seen in cargo or military aircrafts that need an easy and fast loading and unloading. This would be the case shown in Fig. 2.9b.

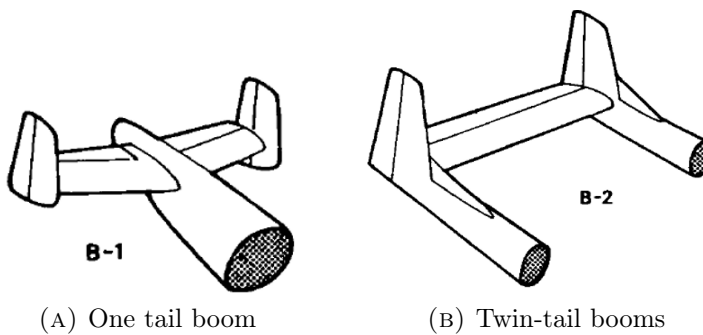


FIGURE 2.9: Tailplane twin fin configurations [6].

### V or butterfly tail

The V or butterfly tail is usually seen in sailplanes, preventing them from damaging the tail when landing on overgrown terrain. It can also be seen in powered aircrafts for avoiding the jet efflux, when a T-tail wants to be avoided or is not an option.

This is the case of the Cirrus Vision SF50 (see Fig. 2.10), which has a single rear-mounted engine located at the top of the fuselage and that means there should not be anything behind it, like the vertical tail.



FIGURE 2.10: Cirrus Vision SF50 with V tail configuration [7].

V tails have the disadvantage of a complicated control system design, given that the moving surfaces need to act as elevator and rudder at the same time. They are also the least efficient configuration, as there is always a component of the lift, perpendicular to the plane of symmetry, that is lost.

### VLJ tailplane configurations

Very-light jets (VLJ) normally use T-tails because of the engines position. As explained in Sec. 2.1.3, VLJ use to have 2 rear-mounted engines, limiting the possible configurations and positioning the T-tail as the best option due to its easy and stiff structure. Some examples are the HondaJet HA-420 (see Fig. 1.3) or the Cessna CitationJet M2 (see Fig. 1.1).

Having already decided that the business jet will be powered by two rear-mounted jets, the best tailplane configuration that will fit the jet design is the T-tail one. The horizontal stabiliser will have the height required for not being inside the jet efflux cone of 6 degrees.

#### 2.1.5 Landing gear

There are different types of landing gear configurations. In this section these configurations will be presented and compared with the purpose of deciding the best

option for the studied design.

The first decision that needs to be done is whether the landing gear is retractable or not. Retractable landing gears provide a more efficient performance as there is no presence of extra drag due to their presence. However, the resultant landing gear system will become more complex, not only for its installation but for its maintenance too. Despite its complexity, efficiency has been prioritized and the landing gear system has been decided to be retractable.

With the retractability issue resolved it is possible to begin the landing gear type election. Basically, there are two main configurations of landing gear [58]:

### Taildragger

The taildragger configuration was the primary configurations that was implemented in early aviation—which is why it is called conventional configuration too. Nowadays it is still used in some small-piston engine planes. In Fig. 2.11 the first configuration is shown. As it can be seen in the figure, this configurations displays two wheels in the front part of the aircraft and a single wheel positioned on the tail. The front wheels are located near the center of gravity and so they support the main weight of the plane. About the rear wheel, its function is to give support to the tail when the aircraft is moving on the ground so that the fuselage is not harmed. This rear wheel could be replaced by a skid if it ensured the fuselage integrity.



FIGURE 2.11: Taildragger or conventional gear undercarriage [8]

The main advantage of this configuration is that it reduces the runway longitude needed to Take-off as the wings inherently have a positive angle of attack. Additionally, for propeller user aircrafts the taildragger configuration increases

the operational security on ground as the distance between the propeller and the ground is increased.

The taildragger configuration presents some disadvantages: the pilot's visibility during taxi is reduced due to the inclination of the plane. Also, this configuration makes the aircraft become unstable as the center of gravity is positioned behind the front gear. Finally, the landing operation is more difficult to perform: if both front wheels do not touch the ground at the same time the aircraft may veer off damaging the wing on the side of the wheel that has touched the ground first or even the landing gear system itself [58].

### Tricycle configuration



FIGURE 2.12: Tricycle or nosewheel configuration [9]

Contrary to the taildragger configuration, the tricycle configuration positions one single wheel on the front part and two behind this one—see Fig. 2.12. This tricycle formation of the wheels is what gives this configuration its name. The system functions in an opposite way to the conventional configuration: the rear gear becomes the main part of the system while the front wheel takes an auxiliary role. Therefore, the rear

gear is responsible for supporting the aircraft's weight.

There are many advantages of this configuration: it provides much more stability as the center of gravity is positioned before the main gear and so the hazard of veering off while landing is avoided. Also, the pilot's visibility is increased as well as the aircraft's manoeuvrability during taxi.

The most significant drawback of the nose-wheel configuration is the drag during performance which is significantly increased[59]. For this reason many aircrafts

that use this configuration use also a retractable system.

It is important to notice that there are more landing gear configurations. However, the configurations that have not been explained are used for specific reasons such as landing on water –amphibian planes with special landing gears–, support very light aircrafts like sailplanes or gliders –for this planes a bicycle gear formed by two wheels positioned similarly to the conventional configuration but with only one front wheel– or ease the loading of cargo planes –quadricycle configuration, which allows to perform on a lower distance to the floor during ground operation–.

In conclusion, after what has been explained in this section it has been decided to adopt a tricycle configuration, as it gives more stability and manoeuvrability. Moreover, the drag increase due to the chosen configuration will be solved by using a retractable system as it has been also explained in the first part of this section.

## 2.2 Materials

Since the beginning of aerospace industry a lot of materials have been studied in order to increase the benefits and the mechanical properties of aircrafts. Metallic alloys have been the principal aerospace material, but for the last few years composites have become more popular because of their properties. In order to study which materials are optimum in a VLJ, they have been classified in "External materials" -skin and panels- and "Internal materials" -beams, spars, ribs...-.

### 2.2.1 External materials

Composites offer more advantages [11] than metallic materials. The most important are:

- Weight reduction
- High impact resistance
- High damage tolerance

- Fatigue and corrosion resistance
- Tailoring directional strength and stiffness

They also present some disadvantages [10], like the elevate cost of production and maintenance and the internal impact-damage that might go unnoticed. To select which is the best composite for the jet, it is important to choose the correct matrix and fibre. The matrix has to give shape to the structure and it helps to maintain the position and orientation of the reinforcement. On the other hand, the reinforcement –fibre- provides the strength and rigidity needed to support the structural load. Fig. 2.13 shows a list of polymeric matrices commonly used in aerospace sector and Fig. 2.14 shows typical reinforcing fibres.

Fibre	Density (g/cc)	Modulus (GPa)	Strength (GPa)	Application areas
<b>Glass</b>				
E-glass	2.55	65–75	2.2–2.6	Small passenger a/c parts, aircraft interiors, secondary parts; Radomes; rocket motor casings
S-glass	2.47	85–95	4.4–4.8	Highly loaded parts in small passenger a/c
<b>Aramid</b>				
Low modulus	1.44	80–85	2.7–2.8	Fairings; non-load bearing parts
Intermediate modulus	1.44	120–128	2.7–2.8	Radomes, some structural parts; rocket motor casings
High modulus	1.48	160–170	2.3–2.4	Highly loaded parts
<b>Carbon</b>				
Standard modulus (high strength)	1.77–1.80	220–240	3.0–3.5	Widely used for almost all types of parts in a/c, satellites, antenna dishes, missiles, etc
Intermediate modulus	1.77–1.81	270–300	5.4–5.7	Primary structural parts in high performance fighters
High modulus	1.77–1.80	390–450	2.8–3.0 4.0–4.5	Space structures, control surfaces in a/c
Ultra-high strength	1.80–1.82	290–310	7.0–7.5	Primary structural parts in high performance fighters, spacecraft

FIGURE 2.13: Reinforcing fibres commonly used in aerospace applications [10].

Thermosets					Thermoplastics
Forms cross-linked networks in polymerization curing by heating				No chemical change	
Epoxies	Phenolics	Polyester	Polyimides	PPS, PEEK	
<ul style="list-style-type: none"> <li>• Most popular</li> <li>• 80% of total composite usage</li> <li>• Moderately high temp.</li> <li>• Comparatively expensive</li> <li>• Low shrinkage (2-3%);</li> <li>• No release of volatile during curing</li> <li>• Can be polymerized in several ways giving varieties of structures, morphology and wide range of properties</li> <li>• Good storage stability to make prepgs</li> <li>• Absolute moisture (5-6%) causing swelling and degradation of high temp properties</li> <li>• Also ultra violet degradation in long term</li> </ul>	<ul style="list-style-type: none"> <li>• Cheaper</li> <li>• Lower viscosity</li> <li>• Easy to use</li> <li>• High temp usage</li> <li>• Difficult to get good quality composites</li> <li>• More shrinkage</li> <li>• Release of volatile during curing</li> <li>• Inherent stability for thermal oxidation.</li> <li>• Good fire and flame retardance</li> <li>• Brittle than epoxies</li> <li>• Less storage stability- difficult to prepg</li> <li>• Absorbs moisture but no significant effect of moisture in working service range</li> <li>• Density (g/cm<sup>3</sup>) 1.1-1.4</li> <li>• Tensile modulus 2.7-5.5 GPa</li> <li>• Tensile strength 40-85 MPa</li> </ul>	<ul style="list-style-type: none"> <li>• Cheap</li> <li>• Easy to use</li> <li>• Popular for general applications at room temp</li> <li>• High shrinkage (7-8%)</li> <li>• Good chemical resistance</li> <li>• Wide range of properties but lower than epoxies.</li> <li>• Brittle</li> <li>• Low <math>T_g</math></li> <li>• Difficult to prepg</li> <li>• Less sensitive to moisture than epoxies</li> <li>• Density (g/cm<sup>3</sup>) 1.1-1.4</li> <li>• Tensile modulus 2.7-4.1 GPa</li> <li>• Tensile strength 35-60 MPa</li> </ul>	<ul style="list-style-type: none"> <li>• High temp application 300°C</li> <li>• Difficult to process</li> <li>• Brittle</li> </ul>	<ul style="list-style-type: none"> <li>• Good damage tolerance</li> <li>• Difficult to process as high temp 300-400°C is required</li> <li>• Infinite storage life. But difficult to prepg</li> <li>• No moisture absorption</li> <li>• Density (g/cm<sup>3</sup>) 1.3-1.4</li> <li>• Tensile modulus 3.5-4.4 GPa</li> <li>• Tensile strength 100 MPa</li> </ul>	

FIGURE 2.14: Polymeric matrices commonly used in aerospace sector [11].

Epoxies are the most popular matrices in the aerospace industry due to its capability of giving different varieties of structures and having a wide range of properties. Its major inconvenience is the cost, which is expensive. Phenolic and polyester are different options to have in consideration since they are cheaper, but the quality of the final composites will not be the same.

Regarding the reinforcements [11], the most commons are:

- Glass: lightweight, strong and robust material. Strength properties and stiffness lower than carbon fibre, but it is less brittle and cheaper.
- Carbon: extremely strong and light fibre, but expensive.
- Aramid: heart-resistant and strong fibre. Typically used in ballistic composites and motor casings.

In conclusion, if the aim is to create a competitive private jet its materials must have the best properties, especially considering that private jets are in a luxurious sector. Following Fig. 2.13 and Fig. 2.14 the most suitable composite for the external materials would be an epoxy matrice with fiber reinforcement. For the fiber, glass and carbon will be considered due to its properties. In 11 it is discussed the type of configuration needed for each part of the aircraft and which composite would be the most appropriate.

### 2.2.2 Internal materials

For deciding the internal/structural materials, the same idea of external ones is followed: aluminium alloys and composites are compared. Aluminium alloys are chosen for the information in [60]. Composite materials are chosen for being the structural materials of Cirrus Vision SF50, the newest VLJ in the market. For further information of this materials the references in Tab. 2.1 can be consulted.

TABLE 2.1: Comparison of internal structural materials.

PROPERTY	ALUMINIUM 2090-T83	ALUMINIUM 8090	TC275-1	TC275 1E
Density [g/cm <sup>3</sup> ]	2.59	2.54	1.17	1.17
Tensile Strength [MPa]	550	450	1014	1060
Elastic Modulus [GPa]	76	77	148.2	67
Shear Strength [MPa]	320	270	103	130
Reference	[61]	[62]	[63]	[64]

As can be seen in Tab. 2.1, composites present less than 50% of density over the most advanced aluminium alloys, despite their properties strongly depend on the direction stressed. This fact is controlled in the structure of the aircraft, so it is not considered a deep problem for the time being. For representing around 50% saving in aircraft structure's weight, with the double of tensile strength, and for being a differential characteristic in VLJ, composite materials are chosen for the whole structure. Despite this, the most critical parts (like landing gear and wing main beams) can be done in Titanium alloys or Steel, that weight substantially more but present even more adequate parameters than composites for such strains.

## 2.3 Conclusions

After the explanations presented in this chapter, a summary of the decisions made will be given in this section.

A likewise aircraft analysis has provided an estimated slenderness ratio of 7,5 with a 10% margin for the fuselage. Also, the cross section of the fuselage has been decided to be designed in a near circular shape and without flattened bottom. In addition, it has been established that the cabin will be pressurized and that the seats will be designed so that some cargo can be placed under them.

About the wing, the low-wing configuration has been determined to be used in order to take advantage of the ground effect, which will allow the performance in shorter runways.

The power plant of the aircraft will have two turbofan engines that will be placed near the tail according to the rear-mounted configuration. This design gives a better performance when talking about structural loads and a safer performance in case of engine failure.

Related to the defined power plant, the empennage configuration has been determined so as to meet the requirements of the rear-mounted engines configuration: a T-tail configuration will be designed and it will be ensured that the horizontal stabiliser is not placed inside the 6 degree jet efflux cone.

In Sec. 2.2 it has been defined the materials that will be used when manufacturing the jet: composites will be used on external materials due to the weight reduction and the improve of their properties. However, titanium alloys or steel might be used in critical parts such as the landing gear. For the structural materials a more developed study will be carried out further in the project.

Finally, the landing gear will use the tricycle configuration, as it allows a more stable performance. Additionally, the landing gear will be retractable in order to reduce the drag –and so improving the efficiency– during performance.

# Chapter 3

## Initial weight and centring estimations

This chapter will make the initial weight estimation for the business jet's design process. The chapter will use many design references and also similar planes will be analysed. At the end, a tentative maximum take-off weight, as well as the operative empty weight and the fuel weight will be calculated. After that, the range for the position of the plane's center of gravity will be calculated by using similar business jets as a reference.

### 3.1 Introduction

One of the most important steps in the aircraft design process is the estimation of the weight of the plane. Several methods are explained by the literature to do so. Their accuracy depends on the stage of the design process. Therefore, the initial approximation methods can only be performed by gathering historical data and by assuming the class of the aircraft is known (see Chap. 2). Further approximations will be made for each iteration of the designing process by previously defining the initial sizing of the plane as well as the materials to be used for its construction (see Sec. 2.3).

### 3.1.1 Definitions

The following are standard definitions for weight used in the aircraft industry.

- **Operative Empty weight - OEW or  $W_E$ :** Weight of an aircraft without useful load. Includes oil, unusable fuel and hydraulic fluids. [3, 13].
- **Maximum take-off Weight - MTOW or  $W_{MTOW}$ :** The maximum take-off weight for the mission the airplane is designed for. It is also known as *Design Gross Weight* -  $W_0$ . [3, 13, 65].
- **Useful Load -  $W_u$ :** Useful load is defined as the difference between the *MTOW* and the *OEW*. It is the weight of everything the aircraft will carry besides its own weight. This typically includes occupants, fuel, cargo, etc. [13].
- **Payload - PL or  $W_{PL}$ :** The part of the useful load that yields revenue for the operator. Typically it is the passengers and cargo. [3, 13].
- **Crew Weight - CW or  $W_C$ :** Weight of occupants required to operate the aircraft. [13].
- **Fuel Weight - FW or  $W_f$ :** Weight of the fuel needed to complete the design mission. [3, 13].
- **Ramp Weight -  $W_R$ :** *MTOW* plus a small amount of fuel to accommodate warm-up and taxi into the take-off position. [13].
- **Maximum Landing Weight - MLDW:** Maximum weight at which the aircraft may land without compromising airframe strength. [13, 65].
- **Maximum Zero Fuel Weight - MZFW or  $W_{MZFW}$ :** Maximum weight the airplane can carry with no fuel on board. Note that the maximum zero fuel weight implies that all weight above *MZFW* must be fuel. [13, 65].
- **$W_{tfo}$ :** Is the weight of all trapped (e.g unusable) fuel and oil. [3].

### Mathematical expressions for weight definition

A convenient way to break down  $MTOW$  is as follows [3]:

$$MTOW = OEW + FW + PL \quad (3.1)$$

The operating empty weight ( $OEW$ ) is frequently written as follows [3]:

$$OEW = EW + WC + W_{tfo} \quad (3.2)$$

To simplify the calculations, both the fuel weight and the empty weight are expressed as fractions of the  $MTOW$  [1]:

$$W_{TO} = W_{PL} + W_C + \left( \frac{W_f}{W_{TO}} \right) W_{TO} + \left( \frac{W_E}{W_{TO}} \right) W_{TO} \quad (3.3)$$

Eq. (3.3) can be factored out for  $W_{TO}$  by using its definition (Eq. (3.1)):

$$W_{TO} \left[ 1 - \left( \frac{W_f}{W_{TO}} \right) - \left( \frac{W_E}{W_{TO}} \right) \right] = W_{PL} + W_C \quad (3.4)$$

Thus (3.4) results [1]:

$$W_{TO} = \frac{W_{PL} + W_C}{1 - \left( \frac{W_f}{W_{TO}} \right) - \left( \frac{W_E}{W_{TO}} \right)} \quad (3.5)$$

## 3.2 Similar business jets analysis

To begin with, similar business jets are analysed in Tab. 3.1. This table shows the  $MTOW$ ,  $OEW$  and  $FW$ <sup>1</sup> for the listed very light jets (VLJ). These values help to obtain the ratios  $\frac{OEW}{MTOW}$  and  $\frac{FW}{MTOW}$ , which are useful for the initial prediction of plane's maximum take-off weight [1, 6]. Moreover, Tab. 3.1 can also set up the initial ranges for these weight parameters.

---

<sup>1</sup> $FW$  value has been calculated by using  $MZFW$  definition:  $FW = MTOW - MZFW$ , in order to standardize all the values at the same references, and considering the data shown in the Type Certificate Data Sheet of each business jet.

TABLE 3.1: Similar VLJ weight analysis.

MANUFACTURER	MODEL	TYPE CERTIFICATE	MTOW [kg]	OEW [kg]	FW [kg]	$\frac{OEW}{MTOW}$	$\frac{FW}{MTOW}$	REFERENCES
Eclipse Aerospace Inc.	EA500	EASA IM.A.171	2722	1740	539	0.639	0.198	[25, 32]
ADAM Aircraft Inc.	A700	Not Certified	3855	2494	680	0.647	0.176	[25]
Textron Aviation Inc	Cessna Citation Mustang 525	EASA IM.A.502	3921	2517	860	0.642	0.219	[25, 26]
Bombardier	Learjet24	FAA A10CE	6123	3551	1360	0.579	0.222	[66]
Embraer	Phenom100	EASA IM.A.157	4799	3235	1279	0.674	0.266	[25, 29]
Honda Aircraft Company	HA-420	EASA IM.A.352	4808	3267	816.5	0.679	0.169	[25, 31]
<b>TOTAL</b>						<b>0.638</b>	<b>0.216</b>	

### 3.3 Weight estimation

The weight estimation is performed by using an iterative process, which will be explained along this section. The aim of this iteration is to verify the *OEW* of the plane by using different bibliography references, to proper adjust the value for plane's *MTOW*. The initial stage of this estimation is to gather together similar very light jets' data (see Tab. 3.1). The next stages are described along the following subsections:

#### 3.3.1 *MTOW* first approximation

First of all *MTOW* is calculated by using Eq. (3.4) [1, 13]. This value will be considered as the set-point of the iterative calculation process. To do so, payload and crew weight have to be estimated. Torenbeek [6] and Roskam [3] give the expression for these weights to be predicted:

$$W_{PL} = n_{pax}(W_{pax} + W_{baggage}) \quad (3.6)$$

Where  $n_{pax}$  is the number of passengers,  $W_{pax}$  is the weight for each passenger as described in Chap. 1 and  $W_{baggage}$  is the weight of the baggage for each passenger, fixed at 13 [kg] following the values range given by [6]. For the number of passengers ( $n_{pax}$ ), Sec. 2.3 has been taken into account. Regarding the crew, Eq. (3.7) shows the estimated crew weight:

$$W_C = n_{crew}(W_{crew} + W_{baggage}) \quad (3.7)$$

Where  $n_{crew}$  is the number of crew members,  $W_{crew}$  is the weight for each crew member, fixed at 77 [kg], value recommended by [3];  $W_{baggage}$  is the weight of the baggage for each crew, fixed also at 13 [kg] following the values range given by [6].

To avoid problems of excessive  $MTOW$ , two configurations can be used for the flight: 6 passengers and 1 crew member, or 5 passengers and 2 crew members, thus this is permitted by the regulations (see Sec. 6.3.3). Furthermore, it is a typical configuration for the business jets presented in Tab. 3.1, as most of them operate following *Commercial air transport* regulations, less restrictive than *Commercial operation*[67, 68].

After these initial calculations, fuel weight ratio and operative empty weight ratio have to be calculated from Tab. 3.1. With all these constraints known, Eq. (3.5) can be solved.

### 3.3.2 Maximum Payload ( $MPL$ ) calculation

The plane that is being designed it a business jet. It is not crucial to optimize the  $MPL$  to carry, but its calculation is useful for payload-range diagram Sec. 5.4. To compute the value for  $MPL$ , Torenbeek's equation is used [6]:

$$MPL = n_{pax}(W_{pax} + W_{baggage}) + \left[ k_{bd}V_b - \frac{n_{pax}W_{baggage}}{\rho_{baggage}} \right] \rho_{mer} \quad (3.8)$$

In Eq. (3.8)  $n_{pax}$  is the number of passengers,  $W_{baggage}$  is the weight for the baggage, considered to be 13 [kg] [6].  $K_{bd}$  is the fullness coefficient for the cargo-bay, established at 0.35 for the business jet, as it would not carry a big amount of goods [1].  $V_b$  is the usable volume of the cargo bay, which was calculated taking into account Chap. 6.  $\rho_{baggage}$  is computed by considering the typical dimensions of a trolley and the  $W_{baggage}$ . Finally  $\rho_{mer}$  is the density for the carried goods. As it is a business jet, it is difficult to identify the density of the carried goods because it will depend on the purpose of each operation. Water density has been fixed as an estimated value for  $\rho_{mer}$ .

### 3.3.3 OEW references

The literature offers many approximations for *OEW* calculation. Most of them use historical data to elaborate graphs or regression equations that are useful for validating the *OEW* calculated value.

#### Torenbeek's *OEW* approximation

Torenbeek *OEW* validation equation can be written as follows [6]:

$$W_E[\text{kg}] = 0.2W_{TO} + W_{engines} + 500 + \Delta W_E(b_f, l_f, h_f) \quad (3.9)$$

Where  $W_{engines}$  is the approximate weight for the engines (see Sec. 2.1.3) and  $\Delta W_E(b_f, l_f, h_f)$  is the correction of *OEW* depending on fuselage dimensions, being  $b_f$  the maximum width,  $l_f$  the maximum length and  $h_f$  the maximum height of the fuselage, all defined preliminary along Sec. 6.4. To find out the value for  $\Delta W_E$ , Fig. 3.1 shows a lineal regression of the relation between geometric dimensions of the fuselage and the value for  $\Delta W_E$ . To facilitate the programming process, this

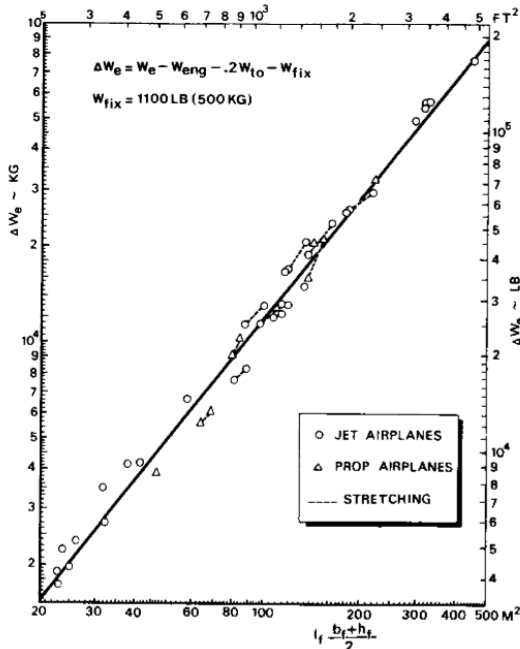


FIGURE 3.1: Chart to estimate the operative empty weight of transport and executive airplanes.

p.147[6].

regression can originate in an equation, by easily taking two points of reference:

$$\Delta W_E = 130.5 l_f \frac{(b_f + h_f)}{2} - 1110 \quad (3.10)$$

Finally, Eq. (3.9) is calculated by using *MTOW* as the variable for each iteration.

### Similar planes' *OEW* approximation

As *OEW* ratio is initially calculated from the comparative between similar business jets, *OEW* can be later evaluated by multiplying the *MTOW* found and the ratio between them. This approximation is also proposed by Gudmunson [13].

### Roskam's *OEW* approximation

Roskam proposes another approximation for *OEW* calculation. This time, a logarithmic regression is used, the coefficients of whom vary depending on the type of plane being analysed. Eq. (3.11) shows the relationship between *OEW* and *MTOW* by using statistical coefficients. Those are  $A = 0.2678$  and  $B = 0.9979$  for business jets (see p.47 [3]).

$$\log W_E = \frac{\log(W_{TO} - A)}{B} \quad (3.11)$$

This regression was calculated from statistical data but it is important to note that the materials used those days are not the same that are used nowadays. Aluminium and iron have been substituted by composite materials and, as it is explained along Sec. 2.2, new composites and lighter materials will be chosen to design this business jet. Roskam also offers a correction factor for this fact: the objective is to correct the calculated weights with the factor  $W_{comp}/W_{metal}$ , which expresses the relationship between the weights of the parts that compose the airframe [3].

### Gudmunsson's *OEW* approximation

Gudmunsson proposes a further approximation for *OEW* after having reached the value from the first iteration (Sec. 3.3.3). This new approach consists in using another logarithmic relationship, calculated from statistical values. Unfortunately, Gudmunsson's book [13] does not give any value for business jets, so that a similar reference has to be used. The list only shows general aircraft using twin turboprop as the one valid to compare with the business jet that is being designed. However, as it is explained in Sec. 2.1.3, the thrust generated by the engines comes from exhaustion of combustion gases and so, the turboprop cannot be considered as a valid reference. Notwithstanding this fact, the regression proposed by Gudmunsson is detailed below:

$$\frac{W_E}{W_{TO}} = 0.5371 + 0.066 \ln W_{TO} \quad (3.12)$$

### 3.3.4 Fuel weight calculation

The fuel weight calculation can be performed by using two different methodologies: From the one hand, Gudmundsson [13] proposes to use the fuel-to-weight ratio as the reference. From the other hand, Roskam [3] suggests imposing the *Flight Profile Methodology*. The first method is not enough accurate, although the design is still on its initial stage. So that, Roskam's approach will be analysed and discussed.

To start with, a preliminary flight profile has to be set up by taking both regulations and requirements (see Sec. 1.4) into account. Note that a more accurate flight profile will be conceived along Sec. 5.1. The initial approach for the flight profile will consider Roskam's one (see p. 55 [3] and Fig. 3.2). As it is detailed by regulations [41, 51], another loiter has to be also calculated in addition to the one already considered in Fig. 3.2. This second loiter has to be calculated at FL20, at 600 [MASL], for a duration of 45 minutes [41], and the amount of fuel consumed will be considered to be the reserve fuel *RF*.

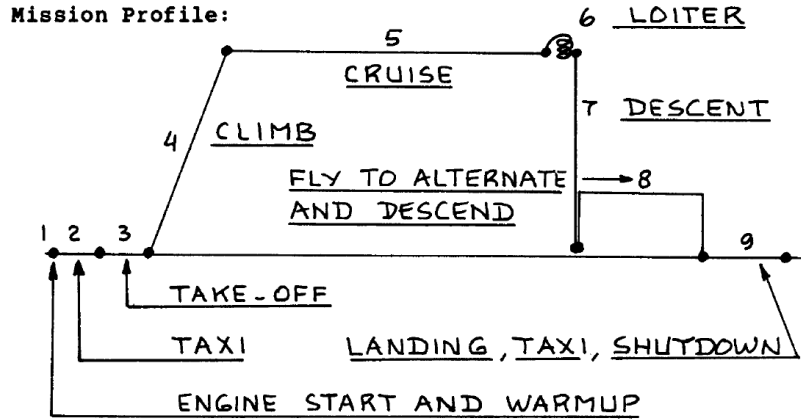


FIGURE 3.2: Mission profile for a commercial airplane.  
p.147[3].

With the flight profile known Fig. 3.2 the fuel weight can be estimated for each stage. Roskam offers the methodology to be followed in order to calculate the total fuel weight of the mission and gauge, later on, the operative empty weight for the plane[3]. The different mission stages and the fuel-weight ratio (see *Table 2.1* [3]) for each of them can be summarized as follows:

- **Phase 1: Engine Start and Warm-up .**

Begin weight is  $W_{TO}$  and end weight is  $W_1$ . Typical value of  $\frac{W_1}{W_{TO}}$  for business jet is 0.990.

- **Phase 2: Taxi.**

Begin weight is  $W_1$  and end weight is  $W_2$ . Typical value of  $\frac{W_2}{W_1}$  for the taxi of a business jet is 0.995.

- **Phase 3: Take-off.**

Begin weight is  $W_2$  and end weight is  $W_3$ . This phase is always calculated by statistical values, for example a value of  $\frac{W_3}{W_2}$  of 0.995 would be correct for business jets [3].

- **Phase 4: Climb to cruise altitude and accelerate to cruise speed.**

This phase can be either calculated by coefficients given by literature or by using Breguet's integration methodology. To obtain a more approximate value for the weight ratio of this stage, Breguet's equation will be solved. Sec. 5.2 widely explains how to solve Breguet's integral equation by using

a numerical solver. However, analytical equation can be easily solved for weight ratios, as detailed by Roskam [3]:

$$\frac{W_f}{W_i} = e^{-\frac{R}{C_j \frac{V_{asc}}{D}}} \quad (3.13)$$

Where  $W_f$  is the weight at the end of the stage,  $W_i$  is the weight before starting the stage,  $R$  is the range for the specific stage,  $V_{asc}$  is the calculated horizontal speed for the plane,  $C_j$  is the specific fuel consumption and  $\frac{L}{D}$  is the aerodynamic efficiency.  $C_j$  and  $\frac{L}{D}$  are statistically calculated and can be found in literature, such as [3, 6]. Otherwise,  $R$  can be sometimes a requirement, for example the range of the total mission (see Sec. 1.4), or calculated from other requirements, for instance the cruise-flight level. Furthermore,  $V$  is also reckoned by considering the design stipulations, being them the climbing rate and the average Mach number for the mission (see Sec. 1.4). To calculate the weight ratio of the climbing to cruise altitude and acceleration to cruise speed, Roskam gives a recommendation of the values to be considered [3], detailed in Tab. 3.2.

TABLE 3.2: Typical values of  $C_j$  and  $L/D$  for business jets during ascend phase [3]

$L/D$	11-13
$C_j [lb/lbs \cdot h]$	0.5-0.9

The range for this stage is calculated by considering that the plane will ascend up to 43000 [ft] with a climbing velocity equal to  $V_{climb} = 12.7$  [m/s] [13] and an equivalent horizontal velocity of  $V = 468$  [km/h], included in the values defined by [1]. With all this values, the ratios  $W_4 W_3$  can be estimated.

- **Phase 5: Cruise.**

This is the stage where the weight ratio is lower. The value can be found by using Breguet's equation, either by using a numerical methodology Sec. 5.2, either by solving it analytically. Analytical equation can be easily solved for weight ratios, as detailed by Roskam Eq. (3.13) [3]. In this case,  $R$  is the range for the cruise, defined as:  $R_{cr} = R_m - R_4$ , where  $R_m$  is the range for the mission and  $R_4$  is the range covered during ascend phase.

Roskam again gives typical values of  $L/D$  and  $C_j$  to be considered during cruise [3] (see Tab. 3.3).

TABLE 3.3: Typical values of  $C_j$  and  $L/D$  for business jets during cruise[3]

$L/D$	10-12
$C_j [lb/lbs \cdot h]$	0.5-0.9

For the cruise velocity  $V_{cr}$ , the cruise altitude and the Mach number have been taken into account, as defined in Sec. 1.4.

At the end of this stage  $w_5$  is calculated. The difference between  $w_5$  and  $w_4$  is the trip fuel  $TF$ , which will be later used along Sec. 5.4.

- **Phase 6: Loiter.**

Begin weight is  $W_5$  and end weight is  $W_6$ . The weight ratio can be estimated by using Breguet's endurance equation [1, 3]:

$$E_{ltr} = \left( \frac{1}{C_j} \right)_{ltr} \left( \frac{L}{D} \right)_{ltr} \ln \left( \frac{W_i}{W_f} \right) \quad (3.14)$$

In Eq. (3.14)  $E_{ltr}$  is the endurance time. Regulations specify that this loiter has to last at least 45 minutes [51], e.g. 0.75 [h] is used for computation. The others constants can be described as it was done before Eq. (3.13). Roskam gives the typical values to be considered during a loiter for a business jet p.14 [3], Tab. 3.4:

TABLE 3.4: Typical values of  $C_j$  and  $L/D$  for business jets during loiters[3]

$L/D$	12-14
$C_j [lb/lbs \cdot h]$	0.4-0.6

By solving Eq. (3.14) weight ratio  $W_6/W_5$  can be calculated in order to obtain the plane's weight after performing the loiter ( $W_6$ ).

- **Phase 7: Descent.**

It starts with  $W_6$  and finishes with  $W_7$ . No credit is taken for range. However, a penalty for fuel used during descents from high altitudes needs to be assessed. Typically the ratio  $W_7/W_6 = 0.990$  for business jets [3].

- **Phase 8: Fly to alternate and descend.**

Begin weight is  $W_7$  and end weight is  $W_8$ . The weight ratio can be calculated

from Eq. (3.13). This time, however, because of the short distance to fly to the alternate airport, it will not be possible to reach an economical cruise altitude. Roskam advises about the proper values to be considered for the flight to the alternate airport:

TABLE 3.5: Typical values of  $C_j$  and  $L/D$  for business jets during flight to alternate and descent[3]

$L/D$	10
$C_j [lb/lbs \cdot h]$	0.9

- **Phase *Extra*: Security Loiter.**

As it has already been mentioned, another loiter will be calculated, before landing in the alternate airport. The procedure to be followed will be the same as **Phase 6**, but considering that the aerodynamic efficiency will be approximately 20% lower, so as to this loiter is performed at FL20 [3]. The fuel consumption of this stage will be the reserve fuel  $RF$ . Note that this calculation depends on  $OEW$  and  $PL$ .

- **Phase 9: Landing, Taxi, Shutdown**

Initial weight is  $W_{Extra}$  and final weight is  $W_9$ . For a business jet the ratio of this stage can be assumed to be 0.992[3].

The overall weight ratio of the mission,  $M_{ff}$  can be calculated by Eq. (3.15):

$$M_{ff} = \left( \frac{W_9}{W_{Extra}} \frac{W_{Extra}}{W_8} \frac{W_8}{W_7} \frac{W_7}{W_6} \frac{W_6}{W_5} \frac{W_5}{W_4} \frac{W_4}{W_3} \frac{W_3}{W_2} \frac{W_2}{W_1} \frac{W_1}{W_{TOW}} \right) \quad (3.15)$$

As nominator and denominator equal values cancel each other, Eq. (3.15) results into:

$$M_{ff} = \frac{W_9}{W_{TO}} \quad (3.16)$$

And so, the total fuel weight for the mission ( $TF_m$ ) can be calculated from Eq. (3.16) as:

$$TF_m = W_{TO} - W_9 = W_{TO}(1 - M_{ff}) \quad (3.17)$$

### 3.3.5 Operative Empty Weight calculation

$OEW$  can be easily calculated by using Eq. (3.1), so as to  $MTOW$  is the initial value calculated and  $PL$  and  $FW$  have already been estimated.

### 3.3.6 Approximation methodology

With the aim to calculate a more reliable value for weights estimation, an iteration process has been programmed (see the code in Appendix E.1). Gauss-Seidel methodology has been followed in order to perform this script. This consists in supposing an initial value for  $MTOW$ , as explained in Sec. 3.3.1. After that,  $OEW$  allowed values are calculated following Sec. 3.3.3 [69]. Afterwards, total fuel weight is calculated by using the procedure in Sec. 3.3.4 and Eq. (3.17). Subsequently, estimated  $OEW$  value is computed by using Eq. (3.1). Following, this value is compared to those proposed by literature Sec. 3.3.3 and relative error is calculated. At the end,  $MTOW$  is recalculated and assigned to the initial value of the iteration  $MTOW_i = MTOW_c$ . If the relative error is lower than a fixed value (5% in this case), the iteration finishes. Finally,  $FW$  and  $OEW$  are again calculated by using the correct value of  $MTOW$ .

The relative error is calculated in this case by using Torenbeek's procedure for calculating  $OEW$  Sec. 3.3.3. Similars' methodology has been thrown out because of its simplicity, whereas Roskam's method has to be further studied in order to correct the given values for business jets made up of composite materials. Gudmunsson's estimation has been also discarded because it is only valid for turbo-propellers, not being the case for the current business jet being designed. All these values has been compared and analysed extensively in order to conclude the statements aforementioned.

### 3.3.7 Preliminary weight estimation results

The results calculated after running the script are shown in Tab. 3.6<sup>2</sup>. As it is yet an initial phase of the preliminary design of the business jet, a tolerance of about

---

<sup>2</sup>Note that  $FW$  is calculated using Roskam's reference [3] to perform a cruise of 2000 [km], as described along the requirements in Sec. 1.4.

$\pm 10\%$  would be considered correct, as justified by many references [1, 6].

TABLE 3.6: Business jet preliminary estimated weights

$MTOW [kg]$	$OEW [kg]$	$FW [kg]$	$PL [kg]$	$MPL [kg]$	$\frac{W_{OE}}{W_{MTOW}}$	$\frac{W_F}{W_{MTOW}}$
5572	3495	1362	625	827	0.63	0.24

### 3.4 Centring estimation

An important parameter related to weights is the centre of gravity position. This value will be of great importance further in the development of the project, specially for stability analysis.

An initial estimation for the center of gravity has been carried out by studying some likewise jets. Some references have allowed the designers to obtain a range of positions for the centre of gravity for similar aircrafts, which is represented in Tab. 3.7. The shown positions are the percentage of the centre of gravity limits at  $MTOW$  condition (measured from the nose pressure bulkhead) with respect to the fuselage length of the jet. This method was chosen so that a comparison between this data can be carried out, as some aircrafts CG positions were given as a percentage of the Main Aerodynamic Chord, and others as the distance from a given datum position (generally from the forward pressure bulkhead).

TABLE 3.7: Centre of gravity position for different aircraft models

Model	Fuselage length [m]	Forward CG position	Afterward CG position	Reference
Eclipse EA500	10,19	26,88	27,32	[70]
Cessna Citation Mustang	12,37	29,43	30,56	[71]
SJ 30i	14,26	28,28	29,89	[33]
Citation 525M2	12,98	29,35	30,28	[36]
Phenom 100	12,82	24,93	26,64	[72]

In order to obtain a first approximation of the center of gravity limits, an arithmetic mean has been calculated for the values shown in Tab. 3.7. It has been obtain that the forward position for the center of gravity is 27% of the fuselage length. Moreover, the afterward center of gravity position is 29% with respect to

the fuselage length, both measured from the nose pressure bulkhead.

It is important to comment that these values are an initial estimation of the centre of gravity position and that they may change during the project development. Additionally, a more accurate estimation could be performed if the mass and distance to a referent point for all parts of each aircraft studied were known.

A very important factor that has to be taken into account when studying the center of gravity of the jet is the power plant location. Along these lines, the references shown in Tab. 3.7 present rear-mounted double-engined configuration; so the power plant distribution has been considered in this approximation. In further developments the center of gravity position will be recalculated taking into consideration some variable weights such as the payload or the fuel weight but in the current state of the project does not make it possible to obtain a more accurate location for the CG.

### 3.5 Conclusions

After having carried out the initial weight and centring estimations for the design of the business jet, some conclusions can be summarized.

To start with, the weight regarding take-off, empty-weight and fuel capacity were calculated by using bibliography references and considering some likewise business jets in order to determine  $OEW/MTOW$  and  $FW/MTOW$  ratios, as an initial approximation. After that, an iterative calculation was performed in order to reduce the error of prediction. The results for  $MTOW$ ,  $OEW$  and  $FW$ <sup>3</sup> are recapitulated in Tab. 3.8 below.

TABLE 3.8: Business jet preliminary estimated weights

$MTOW$ [kg]	$OEW$ [kg]	$FW$ [kg]	$PL$ [kg]	$MPL$ [kg]
5572	3495	1362	625	827

<sup>3</sup> $FW$  is calculated using Roskam's reference [3] to perform a cruise of 2000 [km], as described along the requirements in Sec. 1.4.

As for Chap. 4 some weight coefficients are needed to plot the design chart (Fig. 4.5), their are presented Tab. 3.9 below, calculated along Sec. 3.3.4:

TABLE 3.9: Business jet preliminary estimated weights ratios

$\frac{W_{OE}}{W_{MTOW}}$	$\frac{W_F}{W_{MTOW}}$	$\frac{W_2}{W_{MTOW}}$	$\frac{W_{cr}}{W_{MTOW}}$	$\frac{W_L}{W_{MTOW}}$
0.63	0.84	0.98	0.89	0.76

Regarding the centring estimation, the following results were obtained, taking into consideration the average data for similar business jets: the forward position for the center of gravity is 27% of the fuselage length, while the afterward center of gravity position is 29% with respect to the fuselage length, both measured from the nose pressure bulkhead.

Centering estimation will be further developed because it is extremely important when thinking of airplane's stability analysis. Weights have to be properly distributed along the fuselage in order to facilitate the correct stability of the plane when thrust, lift and drag come into play [13].

# Chapter 4

## Initial sizing

After the weight parameters are determined in Sec. 3.3, in the preliminary design phase there is another crucial step to determine: definition of the Wing Area and Engine Sizing. For estimate those parameters previous analysis of the performance of the airplane have to be carried out. In this chapter it is made the Design point analysis which is a preliminary study for setting a starting point to make the sizing of the plane. Through this study it is possible to obtain a estimation of the wing load therefore the wing surface, and an estimation of the thrust-weight ratio and therefore the power plant needed for propelling the plane. For that, a sizing of the wing and the engine selection and configuration will be done.

### 4.1 Design point analysis

The objective of the Design point is to assess the dimensions of relevant parts of the plane (wing area and power plant) in order meet all performance requirements [6, 13]. This study is based on performance requirements, flight mechanics theories and is based on statistic parameters from similar aircrafts (lift and drag coefficients, aspect ratio, wing efficiency and among others) instead of calculating analytically due to the preliminary phase that the design is [1].

For obtain the wing area and the power plant needed for the airplane, graphs thrust-to-weight ( $T_{TO}/W_{TO}$ ) and wing loading ( $W_{TO}/S_W$ ) have to be made. For each aircraft performance requirement there is a relation between thrust-to-weight

ratio and wing loading and each requirement sketches a curve. For choosing the design point all the sketched curves have to be merged in one plot where it illustrates the variation of thrust-to-weight ratio with wing loading. The graphs will intersect with each other defining determined regions. From the point of minimizing costs and weights it is interesting to obtain for the determined performances, the minimum thrust-to-weight (smaller power plant, less expensive to acquire and operate and lighter [1]) and the major wing loading possible to support more force for area unit. The performances that have been sketched are:

- Cruise Performance
- Take-off Distance
- Climb Rate during Second Segment with Critical Engine Failure
- Landing distance

All of the equations are for jet powered airplanes:

## Cruise Performance

The following expression is used to determine  $T_{TO}/W_{TO}$  at Cruise Performance and is given by a cruise Altitude and a Cruise Speed:

$$\frac{T_{TO}}{W_{TO}} \geq \frac{T_{TO}}{T_{cr}} \frac{W_{cr}}{W_{TO}} \frac{q}{\frac{W_{TO}}{S_W} \frac{W_{cr}}{W_{TO}}} \left[ C_{D_0} + \frac{\left( \frac{W_{TO}}{S_W} \frac{W_{cr}}{W_{TO}} \right)^2}{q^2 \pi A \varphi} \right] \quad (4.1)$$

Where:

- $T_{TO}/T_{cr}$  is the relation between the thrust delivered by the jet engines at take-off and cruise regime. According to [13],  $\frac{T_{alt}}{T_{SL}} = \left( \frac{\rho}{\rho_0} \right)^n$  is the relation between thrust ratio and air density at each altitude.  $T_{alt}$  is the thrust at a determined altitude,  $T_{SL}$  the thrust at sea level and  $n$  varies between 0.7 at sea level and 1 at cruise conditions.

- Density at cruise level is calculated according to the service ceiling altitude given at Sec. 1.4 of 43000 ft (13100 m) with the following equation extracted from [56] (density calculation at stratosphere):

$$\rho = \rho_{11} e^{\frac{g_0}{RT_{11}}(z_{11}-z)}$$

- $\rho_{11}$  is the density at the tropopause (11000 m),  $z_{11}$  is the altitude of 11000 m and  $z$  is the service ceiling altitude in the case of study. The result of the density at 13100 m is  $\rho = 0.2732 \text{ [kg/m}^3]$ .
- The relation between density at sea level and ceiling is equal between  $T_{TO}$  and  $T_{cr}$  and it is equal to 4.484.
- $W_{cr}/W_{TO}$  is the relation between the weight at cruise segment and weight at take-off. It is extracted from previous calculations of Tab. 3.9 and it is 0.89.
- Dynamic pressure is  $q = \frac{1}{2}\rho V^2$ . Calculated with density at ceiling and velocity from statistic mean of similar business jets from Sec. 1.2 resulting 205 m/s. Dynamic pressure obtained is 5740 Pa.
- $C_{D_0}$  is determined by statistic data from similar business jets. According to [13],  $C_{D_0} = 0.02$ , according to [1]  $C_{D_0} = 0.015$  and according to [6]  $C_{D_0} = 0.017$ , whereby an average has been made. Statistic average  $C_{D_0}$  is 0.017.
- Aspect ratio ( $A$ ) has been estimated with statistic average with similar business jets from Sec. 1.2 and from the literature [1] and [13]. The aspect ratio estimated is  $A=9.2$ .
- Aerodynamic efficiency parameter ( $\varphi$ ) is determined with statistic according to [1] and it is a value of 0.85.

## Take-off Distance

Take-off Distance  $s_{TO_{FL}}$  is an important performance requirement factor in the determination of the thrust and wing loading. Take-off distance is defined as

the distance between the start of the running at the head of the runway to the position of an imaginary or real obstacle that the plane must clear. So taking off include a ground section plus airbone section [1]. The height of the obstacle ( $h_0$ ) is determined by FAR Part 25 (Passenger aircraft) airworthiness regulations and it is 35 ft (10.7 m) height above the runway ground.

The following expression is used to determine  $T_{TO}/W_{TO}$  at Take-off and is given by a the Take-off Distance and a determined configuration of the plane.

$$\frac{T_{TO}}{W_{TO}} \geq k_{to} \frac{\frac{W_{TO}}{S_W}}{\sigma C_{L,max_{TO}} s_{TO_{FL}}} \quad (4.2)$$

$s_{TO_{FL}}$  is the Take-off Field Length,  $k_{to}$  is the statistic take-off constant and is obtained by the relation  $k_{to} = \frac{s_{TO_{FL}}}{TOP}$ . Where  $TOP$  is the Take-off Parameter which it can be obtained from Fig. 4.2. In the case being studied the take-off condition is Balanced Field Take-Off. According to FAR Part 25, Balanced Field Take-Off is the condition that *Accelerate-Stop Distance Required (ASDR)* is the same to *Take-off Distance Required (TODR)* for the same aircraft, configuration and conditions. Looking at Fig. 4.1, *ASDR* is *Lift-Off Distance* plus *Stop Distance* and it is equal to *Take-Off Field Length (s<sub>TO<sub>FL</sub></sub>)* that is the distance where FAR Part 25 airworthiness regulations establishes ( $h_0$ ) and the aircraft designed has to accomplish. Therefore, the Balance Field Length is the shortest field length that Balance Field Take-Off complies with safety regulations [73].

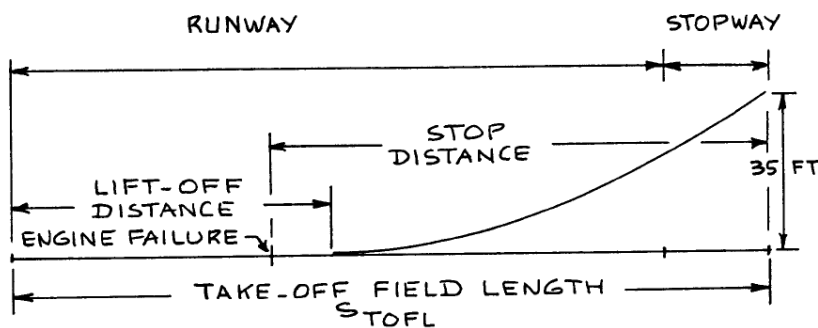


FIGURE 4.1: Definition of FAR 25 Take-off Distance. Extracted from [3].

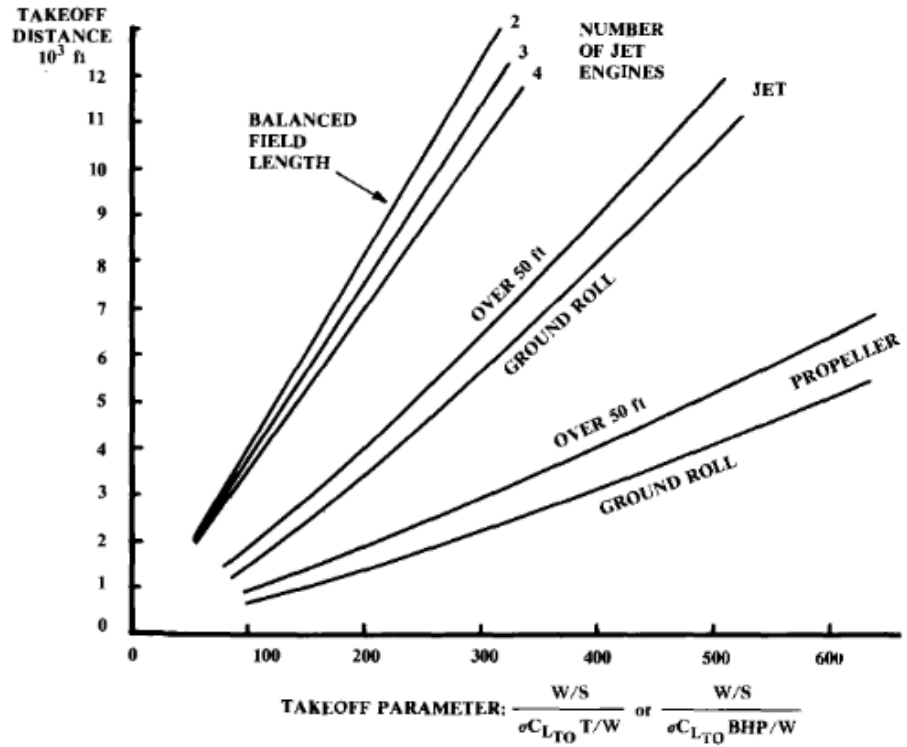


FIGURE 4.2: Take-Off Parameter (TOP) in front of take-off Field Length ( $s_{TO_{FL}}$ ). Extracted from [12]

According to Fig. 4.2 and taking into account that the number of jet engines that the plane has is  $N_e = 2$ , that the take-off condition is Balanced Field Take-off and the Take-off Distance established for technical requirements in Sec. 1.4 is 800 m (2624 ft), it is obtained the Take-Off Parameter of  $TOP = 60$ . Then,  $s_{TO_{FL}}$  dividing by  $TOP$  it is obtained the statistic parameter  $k_{to} = 13.3$ .

The parameter  $\sigma$  is the relation between the air density at take-off altitude and the air density at sea level. It is considered  $\sigma = 1$  because the difference is despicable.

$C_{L_{maxTO}}$  is the maximum lift coefficient at Take-off configuration. This includes the wing lift coefficient at take-off velocity and additionally the lift generated with hyper-sustaining surfaces such as flaps and slats. According to [1] and [3] a statistic maximum lift coefficient at Take-off configuration for several similar business jets is  $C_{L_{maxTO}} = 1.9$

## Climb rate during Second Segment with Critical Engine Failure

The Second Climb Rate (see Fig. 4.3) requirement demands a climb gradient with one engine inoperative of no less than 2.4% for two-engine airplanes [3]. The configuration of the plane in this segment, according to FAR 25.121 Climb Requirements is:

1. Take-off flaps configuration
2. Landing gear retracted
3. Remaining engines at take-off thrust or power
4. At  $V_2 = 1.2V_{STO}$
5. Out of ground effect
6. Ambient atmospheric conditions
7. At maximum take-off weight

The equation for sizing the plane, according to FAR 25 Climb Requirements with one engine inoperative (OEI) is:

$$\frac{T_{TO}}{W_{TO}} \geq \frac{N_e}{N_e - 1} \frac{T_{TO,1e}}{T_{2,1e}} \frac{W_2}{W_{TO}} \left[ \left( \frac{C_D}{C_L} \right)_2 + \gamma_2 \right] \quad (4.3)$$

Where:

- $N_e = 2$  is the number of engines (inoperative and operative)
- $\frac{T_{TO,1e}}{T_{2,1e}}$  is the relation of the thrust at take-off segment with one engine operative with the thrust at second segment with one engine operative. This relation is 1 due to FAR 25 requirement that the remaining engines must continue at take-off thrust.

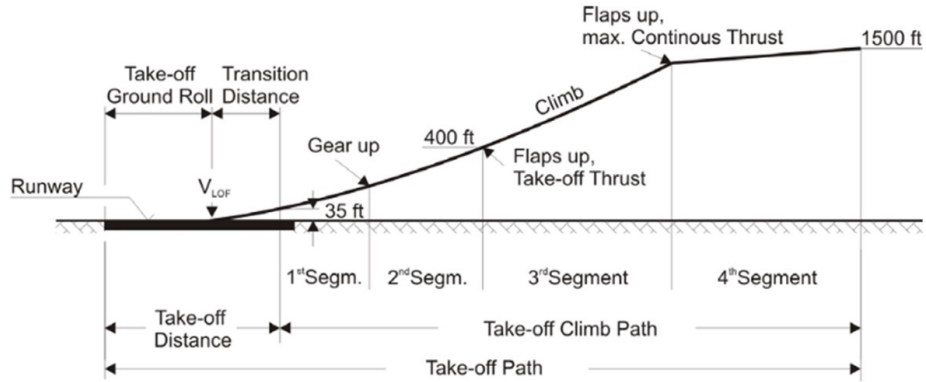


FIGURE 4.3: Take-off and Climb path. Extracted from [12]

- $\frac{W_2}{W_{TO}}$  is the relation between the weight at second segment and the weight at take-off. The value of this ratio, according to Tab. 3.9 is 0.98.
- $\frac{C_D}{C_L}$  is the inverse of maximum aerodynamic efficiency  $E$  at second range climb configuration (with take-off flaps configuration and landing gear retracted). The value is determined statistically according to [1] and it is  $E=8.8$ .
- Finally,  $\gamma_2$  is the climb gradient that is the same as climb path angle, determined by the FAR 25 Regulations and which must be 2.4%,  $\gamma_2 = 0.024$ .

## Landing Distance

The following expression is used to determine  $T_{TO}/W_{TO}$  at Landing and it depends basically on the Landing Distance and the maximum lift coefficient at landing configuration.

$$\frac{W_{TO}}{S_w} \leq k_l \frac{W_{TO}}{W_L} \sigma C_{L_{max_L}} s_{LFL} \quad (4.4)$$

- The factor  $W_{TO}/W_L$  is the relation between the weight at Take-off and the weight at Landing. According to Tab. 3.9, this relation is 1.316.
- $\sigma$  is considered 1 due to despicable difference between altitude at point of 50 ft (see Fig. 4.4) and the altitude at touchdown point.

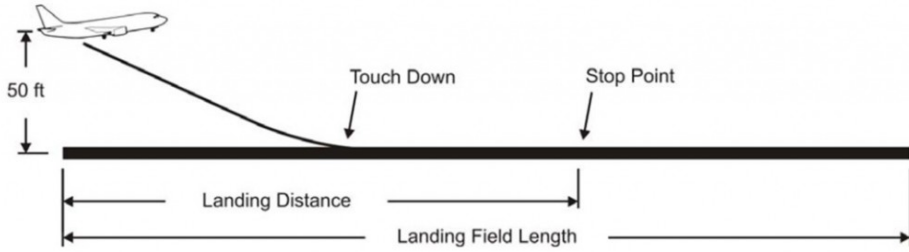


FIGURE 4.4: Definition of FAR 25 Landing Distances. Extracted from [12]

- $C_{L_{max,L}}$  is the maximum lift coefficient with aircraft configuration for Landing (flaps in landing position and landing gear). According to [3] and [1], the statistic value from various similar jets is 1.9
- The statistic landing factor is defined as  $k_l = \frac{1}{a} \frac{\rho_0}{g_0}$ . The parameter  $a$  comes from the following relations:

$$V_S = \frac{V_A}{1.3} = \frac{\sqrt{\frac{s_{L_{FL}}}{0.3}}}{1.3}$$

$$\frac{2W_{TO}/S_W}{\rho C_{L_{max,L}}} = V_S^2 = \frac{s_{L_{FL}}}{0.507} = \frac{s_{L_{FL}}}{a}$$

$V_A$  is the velocity which has the plane at the point over 50ft above the runway. The Landing Field Length  $s_{L_{FL}}$  is determined by the FAR 25 Regulation and include the landing distance which is from the point at the plane is flying over 50 ft until the stop point plus the rest of the runway that is not used. The value of  $k_l$  is 0.123 kg/m3.

## Design Point Matching graph

Once all the performance equations are analyzed they are merged in a single plot (see Fig. 4.5). Cruise, Take-off Distance, Landing Distance and Climb rate at second regime with One Engine Inoperative performances thrust-weight curves have been sketched in front of wing-loading. The code used to compute the equations and plotting it can be seen in Appendix E.4.

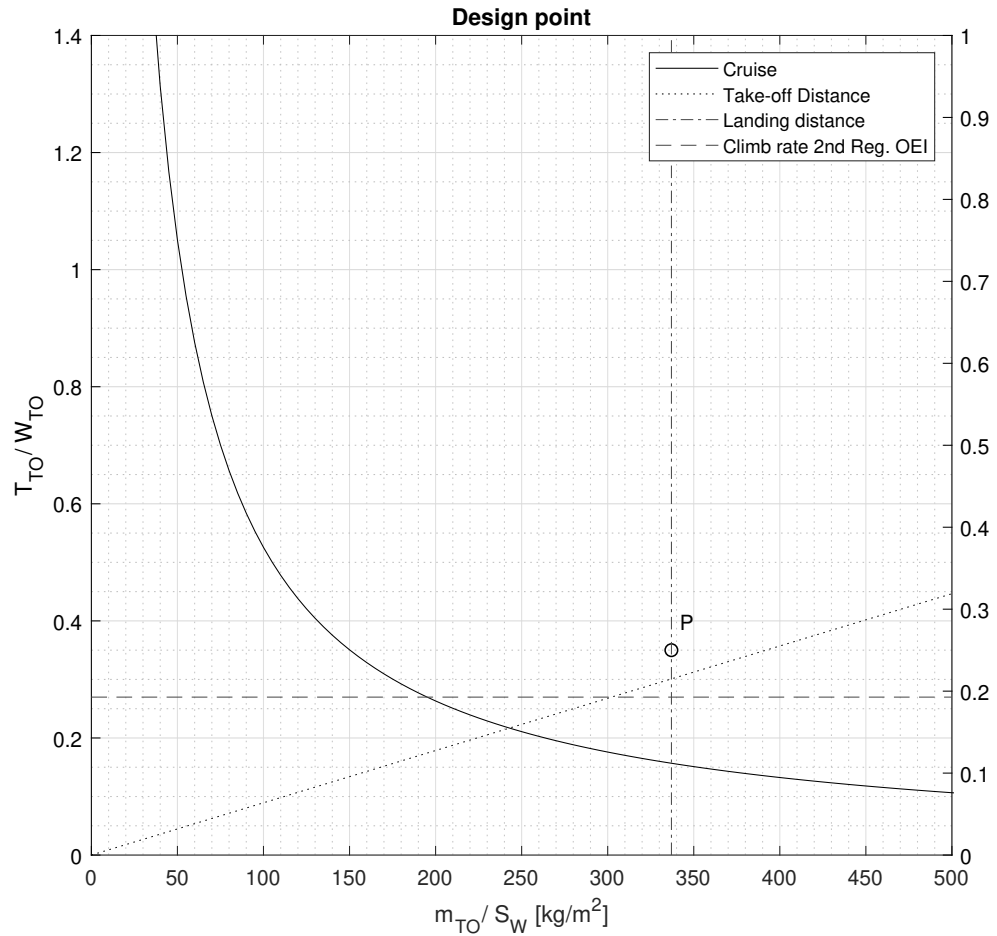


FIGURE 4.5: Design point matching all sketches from performance equations.

The acceptable region is the region that meets all aircraft performance requirements [1] and it is located above the Cruise, Take-off Distance and Climb rate at 2nd Regime curves and on the left of the Landing Distance. The best acceptable point is called the Design Point which is, where the minimum thrust is needed and where the maximum wing-loading is for accomplishing all the performance requirements. Design Point is desired to be as far to the right as possible in order to make smaller the wing surface. Also is desired to be as low as possible in order to install a less powerful power plant for reducing weight and operating costs.

## 4.2 Wing sizing

Once the design point has been obtained, one of the values that can be output is the wing area. Other wing parameters such as the aspect ratio or the main chord will be discussed in later aerodynamic studies.

Following the acceptable region shown in Fig. 4.5, the design point's wing load obtained is  $335 \text{ [kg/m}^2]$ . This value satisfies the range estimated for business jets from [3] (between 40-80 psf, which converted to mass against area means 195-390  $\text{kg/m}^2$ ); in fact it is a high value, what is always preferable. As shown in Tab. 3.6, the  $MTOW$  has been fixed to 5572 kg, giving a wing area of  $16.63 \text{ m}^2$  as indicated in Eq. (4.5).

$$\frac{MTOW}{S_w} = 335 \frac{\text{kg}}{\text{m}^2} \rightarrow S_w = 16,63 \text{ m}^2 \quad (4.5)$$

Tab. 4.1 compares the wing area,  $MTOW$  and wing load of similar VLJs.

Aircraft	$S_w \text{ [m}^2]$	$MTOW \text{ [kg]}$	$\frac{MTOW}{S_w} \text{ [kg/m}^2]$
Honda jet	13,63	4808	369,85
Phenom 100	14,86	4750	319,55
Citation Mustang	19,51	3921	200,97
Eclipse 550	15,1	3893	180,24
Spectrum 33	13,15	3391	257,87
Cirrus Vision SF50	15,5	2727	175,94

TABLE 4.1: Connection between  $MTOW$  and wing area for similar VLJs [39].

The wing area of this jets has a value between  $13.15 \text{ m}^2$  and  $19.51 \text{ m}^2$ , which matches the  $S_w$  obtained in the design point. It is also appreciated that the wing load obtained is similar to the Honda Jet and Phenom 100 ones, although their wing surface is lower than the one obtained in Eq. (4.5) given that both  $MTOW$ 's are smaller than 5572 kg.

### 4.3 Engine selection and configuration

The available engines are provided in Tab. 4.2.

TABLE 4.2: Suggested engines adequate for business jets with 2 engines.

Manufacturer	Model	Applications	Take-off thrust [kN]
Garret	TFE-731-20	Learjet 45	15.57
Ivchenko (Klimov)	AI-25	Yak-40	14.68
Bristol Siddeley (Rolls Royce)	Viper MK521	DH125-1A/-1B/-2	13.79
Williams/Rolls Royce	FJ44-3A	Citation CJ2+/CJ3	13.34
GE	CJ610-8A	Learjet 24E/F/25B/25C/25D/28/29	13.12
Pratt Whitney Canada	PW530-A	Citation Bravo	12.22
Pratt Whitney Canada	JT15D-1B	Citation I/ISP	9.79
Pratt Whitney Canada	PW617F	Embraer Phenom 100	7.18
Pratt Whitney Canada	PW615F	Cessna Citation Mustang	6

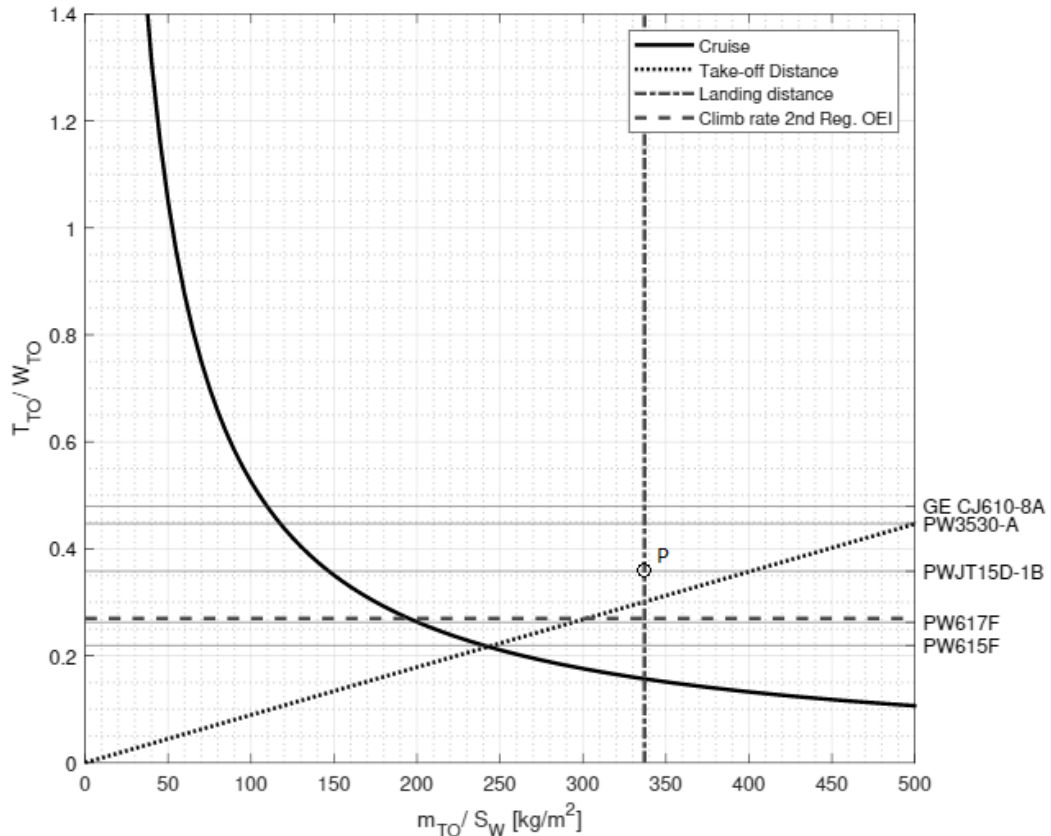


FIGURE 4.6: Design point matching graph with possible adequate engines thrust-to-weight ratio.

From the design point analysis plot Fig. 4.6, it is seen that PW615F and PW617F are below the design point, what requires a thrust of  $(0.3 * W_{TO})/N_e = 8.493kN$ , so these engines do not permit the expected performance of the plane, and they are not taken into account.

It can also be seen that in engines that provide a thrust more than  $8.493kN$  this power is not really needed because the different conditions that set the design point are accomplished. So, they are not taken into account as possible engines, supposing that this excess of power will be traduced in a fuel waste and mass that are not really needed for the correct performance of the plane. Conclusion is that the best available engine is JT-15D-1B, because it provides the minimum thrust above the design point:  $9.79kN$ .

TABLE 4.3: JT-15D-1B Basic specifications

<b>JT-15D-1B</b>	
Dry Weight	236 <i>kg</i>
Overall Length	1.5 <i>m</i>
Diameter	0.68 <i>m</i>
Bypass Ratio	3.3
Thrust	9.79 <i>kN</i>
Low Pressure Rotor max rpm	16540
High Pressure Rotor max rpm	31450
Specific Fuel Consumption	0.55 <i>lb/(lbs hr)</i> at cruise

Data extracted from TYPE Certificate EASA.IM.E.077 [74].

## 4.4 Conclusions

After studying the Take-off Distance, Landing Distance, Climb at 2nd Segment with *OEI* and Cruise performances with the compliance of the detailed requirements at Sec. 1.4, a matching of all sketches has been made at Fig. 4.5 and the design point has been found. This point is at  $T_{TO}/W_{TO} = 0.3$  and a wing-loading of  $335 \text{ kg/m}^2$ .

Next, with this information, the wing area has been calculated  $S_W = 16.63 \text{ m}^2$  and it has been verified with similar wing area from similar business jets.

In addition, thrust-to-weight ratio has allowed to know the minimum thrust needed for matching the Design Point. A minimum thrust of  $16.4 \text{ kN}$  is needed to accomplish the performance requirements. For that, the suitable engine selected has been *Pratt & Whitney Canada JT15D-1B* which develops a thrust of  $9.79 \text{ kN}$  each.



# Chapter 5

## Mission performance

This chapter will determinate the flight profile of a VLJ normal operation in order to identify the different stages of the flight that should be analysed. Moreover, a study on the Breguet equation will be carried out with the objective of obtaining an expression that relates the range with the Mach number and the altitude of flight to optimize the cruise conditions and reduce fuel consumption. Once the expression is obtained, two numerical resolution methods will be described and a study of the relative error of both will be analysed to justify the discretization used in further calculations. Finally, the Payload-range diagram will be obtained according to the hypothesis needed at this early stage of the project.

### 5.1 Flight profile

A flight profile is a graphic representation of the different stages that an aircraft will follow during its normal operation and it depends on the flight mission. In this project, it has been analyzed only the flight profile regarding a private jet. The flight profile of a Very Light Jet is very similar to the ones for short-haul commercial aircraft, and its graphical representation can be observed at Fig. 5.1.

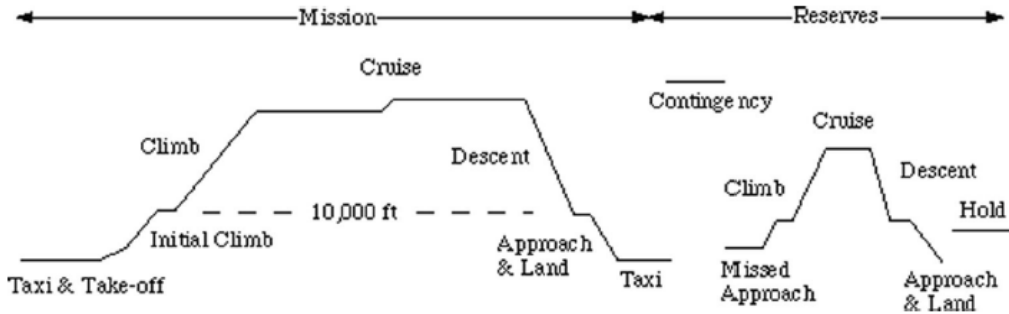


FIGURE 5.1: Private jet flight profile.

As it can be seen at Fig. 5.1, the flight profile can be classified into two parts: Mission and Reserves.

The mission part includes the simpler profile (Taxi/Take-off, Climb, Cruise, Descent, Approach/Land, Taxi). It can be observed how there is a cruise-climbing during the cruise phase, however due to the relatively short range fixed for the designed jet it has not been considered this manoeuvre in the following studies. In addition, the reference cruise altitude has been fixed at 43000 ft for the whole phase, as explained in Sec. 5.3.

It must be also contemplated the scenario where there is a failed attempt to land and the aircraft is forced to climb and perform a holding or fly to the destination alternate aerodrome, referred at Fig. 5.1 as the Reserves part. According to the airworthiness regulation for aeroplanes with turbine engines [75]: *"The fuel to fly for 30 minutes at constant speed at 1500 ft above aerodrome elevation in standard conditions calculated according the estimated mass on arrival at the destination alternate aerodrome, or the destination aerodrome when no destination alternate aerodrome is required"*.

## 5.2 Breguet equation resolution

The aim of this section is to specify how the Breguet equation as a function of the Mach number and the altitude of flight is obtained and present a brief comparison between the relative error obtained using a first and second order numerical method to solve the Breguet equation.

### 5.2.1 Breguet equation treatment

Breguet equation relates the range with different design parameters, allowing to obtain an initial approach of the range of the aircraft given that some of the parameters used have to be treated in greater detail in the subsequent studies. Depending on the type of powerplant used (turbofan or turboprop) some modifications should be introduced in the following explanation. According to the engine technology decided (See Sec. 2.1.3), the representation of the Breguet equation for turbofan propelled aircraft is:

$$\frac{dW}{dt} = -gc_j T \quad (5.1)$$

As this development is intended to obtain an expression for the range  $R$  as function of the weight  $W$ , the parameter  $dt$  can be represented as:

$$dt = \frac{dx}{V}$$

It must be pointed that the hypothesis of steady horizontal flight has been used for the entire Sec. 5.2, and as a result the thrust  $T$  is equal to the total drag  $D$  and the lift  $L$  is equal to the weight  $W$ . In order to introduce the aerodynamic efficiency  $E$ , Eq. (5.1) is multiplied both the numerator and denominator by the lift  $L$ . As aerodynamic analysis has not been carried out yet, the  $E$  at cruise configuration will be temporarily set at  $E = 11$  (see Tab. 3.3), an average value of the range specified in Tab. 3.3. The resulting equation applying all considerations mentioned is shown below.

$$dW = \frac{-gc_j W}{EV} dx \quad (5.2)$$

The flown distance can be expressed as a function of the weight as shown in Eq. (5.3), considering that all other parameters can be supposed as constants and redefining them with the Breguet Factor  $K_{TF}$  (Eq. (5.4)).

$$dx = K_{TF} \frac{dW}{W} \quad (5.3)$$

$$K_{TF} = \frac{-EV}{gc_j} \quad (5.4)$$

Even though at this stage of the project iterative structures are not needed, in following studies an iterative process will be performed in order to achieve the  $Ma$  and altitude values for the maximum  $E$ , resulting in another range value. For this reason, and with the aim of simplifying the scripts, it is interesting to express the Breguet equation as a function of Mach Number  $M$  and the altitude of flight  $h$ . To obtain this, relations presented in Eq. (5.5) and Eq. (5.6) have to be considered.

$$Ma = \frac{V}{a_0 \sqrt{\theta}} \quad (5.5)$$

$$\frac{c_j}{c_{jref}} = \left( \frac{M}{M_{ref}} \right)^\beta \quad (5.6)$$

Note that the altitude of flight is implicit into the temperature correction factor  $\theta$ , and for this reason Breguet equation is function of  $h$  too.  $\beta$  represents the compressibility effects on the consumption (as the engines use turbofan technology,  $\beta = 0.5$  [76]). In addition, the reference Mach number is set at  $M = 0.69$  [3] and the reference thrust-specific fuel consumption at  $c_{jref} = 0.77 \text{ lb}/(\text{lbf} \cdot \text{h})$  (See Tab. 3.3)

Replacing  $c_j$  and  $V$  using the expressions Eq. (5.5) and Eq. (5.6) into Eq. (5.4), the Breguet Factor can be represented as:

$$K_{TF} = \frac{-Ea_0 \sqrt{\theta} M_{ref}^\beta}{gc_{jref}} M^{1-\beta} \quad (5.7)$$

Finally, replacing Eq. (5.7) into the expression Eq. (5.3), the final expression for Breguet equation as a function of Mach number and height is obtained <sup>1</sup>:

$$dx = \frac{-Ea_0 \sqrt{\theta} M_{ref}^\beta}{gc_{jref}} M^{1-\beta} \frac{dW}{W} \quad (5.8)$$

Eq. (5.8) has been resolved by using both Trapezoidal Rule –as a first order resolution– and Simpsons' Rule –as a second order resolution– methods, as explained along Appendix A. The performed code to solve the latter can be found in Appendix E.2.

---

<sup>1</sup>Aerodynamic efficiency will be also sensitive to Mach and altitude values. Future aerodynamic analysis will define this.

### 5.2.2 Relative error in the Breguet equation calculation

In order to perform a proper analysis of the behaviour of the range as a function of the Mach number and the flight altitude, it is necessary to analyse the relative error involved in the results because of the use of numerical methods for the Breguet equation resolution. The selected numerical methods are the Trapezoidal Rule for a first order approximation and the Simpsons' Rule for the second order approximation (see Appendix [E.2](#)).

As a numerical method is based on sectioning the analyzed domain of a given function, a discretization error appears as the result will be an approximation of the area under the function curve. With the objective to select a discretization number  $n$  depending on the acceptable relative error, a previous analysis should be done to observe for which  $n$  value the relative error converges for both methods. It has to be pointed that calculations have been carried out with an initial mass of  $m_i = 5572 \text{ kg}$  which considers *MTOW* and *MPL* conditions and a final mass of  $m_f = 4210 \text{ kg}$ , considering that all fuel has been consumed (see Tab. [3.8](#)). It is important to notice that these weights are an initial approximation of the weight values defined in order to analyze the Breguet equation to determine the  $n$  parameter. A proper range analysis based on different weight configurations is shown in Sec. [5.4](#). In addition, only the cruise stage is considered, as take-off and landing operations are not contemplated.

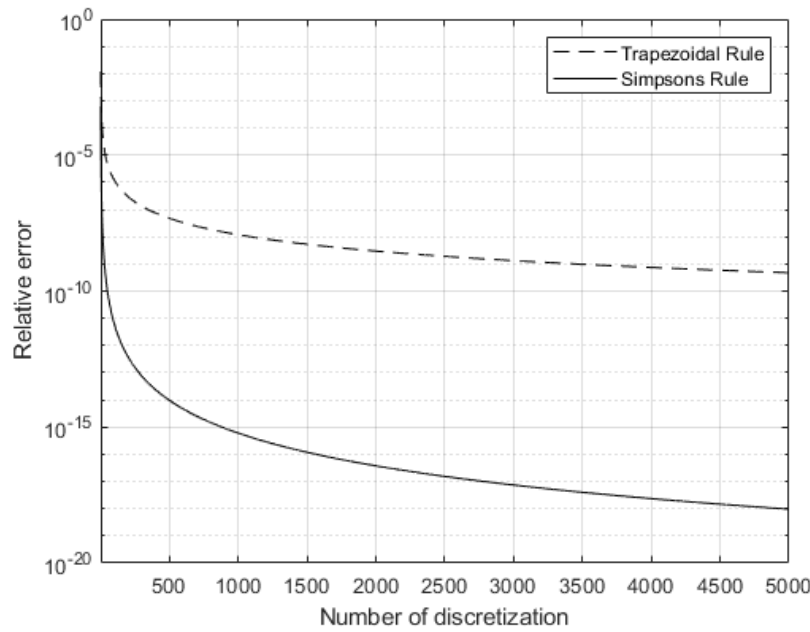


FIGURE 5.2: Comparative between the Trapezoidal and Simpson's rule with  $n=5000$ .

According to the Appendix A, the absolute error has been calculated, but a reference parameter must be introduced to obtain the relative error. As it can be seen at Fig. 5.2, it could be considered that both the relative error related to the Simpson's Rule and the Trapezoidal Rule has converged for  $n=5000$ . For this reason, and as an empirical value of the range cannot be obtained, it has been considered that the range obtained for a  $n = 5000$  is a good approach of the real value and it has been used as a reference for the relative error calculation.

Following the convergence analysis, a comparison between the two numerical methods is presented below.

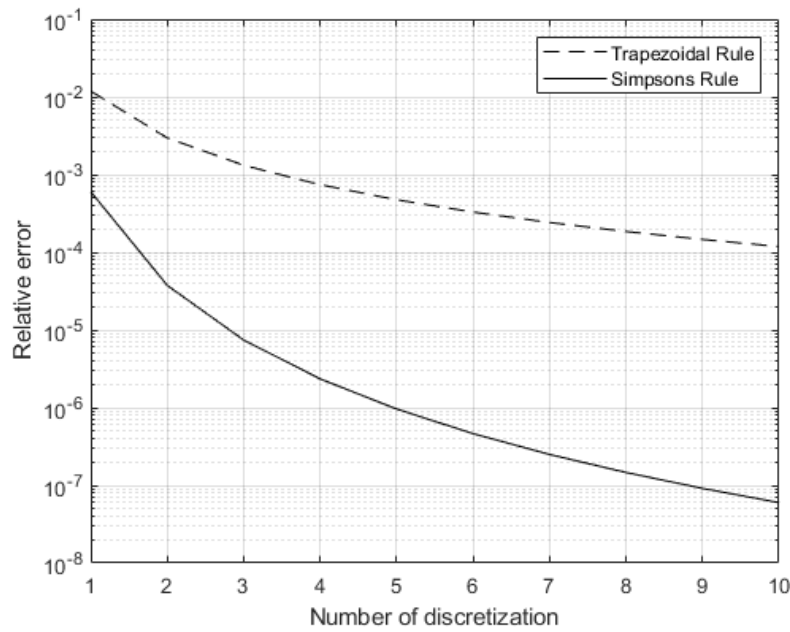


FIGURE 5.3: Comparative between the Trapezoidal and Simpson's relative error as function of the number of discretization.

According to Fig. 5.3, it can be seen how using a second order numerical method like the Simpson's Rule positively affects the relative error. For example, for  $n = 1$  the difference between the Trapezoidal and Simpson's Rule is approximately one order of magnitude, and for  $n = 5$  the difference drops to approximately three orders of magnitude.

By observing the relative error comparison and selecting the Simpson's Rule as the reference numerical method, the number of discretization that guarantees an error suitable for the order of magnitude of the range is selected. For instance, if the Breguet equation is solved using the Simpson's Rule for  $n = 2$  a range of  $R = 1543$  km is achieved. As Fig. 5.3 points, the relative error for  $n = 2$  is  $\delta = 3.749 \cdot 10^{-5}$ , meaning that the uncertainty of the range would be of the order of  $R = 1543 \pm 0.058\text{km}$ . As it can be seen, for  $n = 2$  the relative error is small enough to consider this order of discretization as acceptable.

### 5.3 Cruise conditions

The cruise performance is an essential study inside the flight envelope definition, and it must be accompanied or influenced by the airline or company mission. Cruise conditions can be optimised to reduce the fuel consumption or to achieve the maximum cruise-speed in case flight time wants to be reduced to its maximum, for example. In the case defined in this study, according to the mission of maximum efficiency and thus minimum fuel consumption, as explained in Sec. 1.4, variables such as Mach number and cruise altitude need to be further analysed to come to the optimum combination, giving the best possible aerodynamic efficiency. SFC becomes an implicit variable when giving its dependency on the Mach number, as seen in Eq. (5.6).

However, due to the early stage of the project in which cruise conditions need to be defined, Ma and altitude values for cruise phases of similar jets have been taken as a first approach, although it is expected to perform an optimisation of cruise conditions once an aerodynamic analysis has been done.

Sec. 1.2 has shown similar jets specifications and Sec. 1.4 gathers cruise performances and gives the average values of Mach and altitude for this phase:

- $M = 0.69$
- Altitude = 43000  $/ft$

### 5.4 Payload-range

This section shows the payload-range diagram for the cruise conditions defined in Sec. 5.3. The following hypothesis have been considered to obtain the diagram:

- The range has been computed considering only the cruise phase. Landing and descending distances have been neglected as explained in Sec. 3.3.4, given that they represent less than 10% and this uncertainty or difference is acceptable at this project stage.

- Reserve fuel changes with  $PL$ ; other weights influencing its value are constant (see Sec. 3.3.4).
- Aerodynamic efficiency has been set to 11 according to similar jet values for cruise phase (see Tab. 3.3).
- $MFW$  has been defined as the difference between the  $MTOW$  and the  $OEW$  plus 208 kg, the latter estimated as the weight of one passenger with his luggage and a pilot (see Sec. 3.3.1 for individual weights), the minimum logical PL weight. This value has resulted in  $MFW = 1868$  [kg].
- Cruise conditions for range calculations have been set using Mach and altitude values specified in Sec. 5.3. The specific fuel consumption has been set to 0.55 [lb/(lb h)] according to [1, 6] and as explained in Sec. 4.3.
- The range has been obtained using Simpsons rule and 2 phase divisions ( $n = 2$ ), as stated in Sec. 5.2 conclusions.

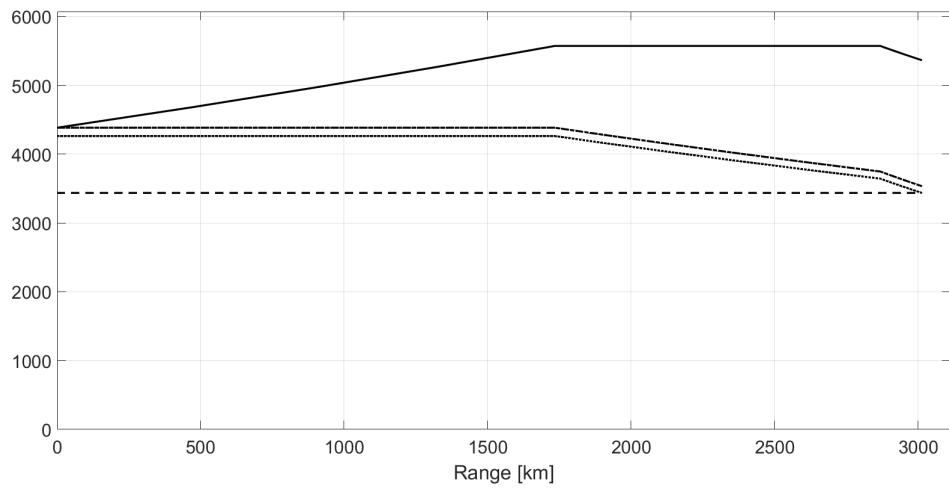


FIGURE 5.4: Different aircraft weight configurations with range.

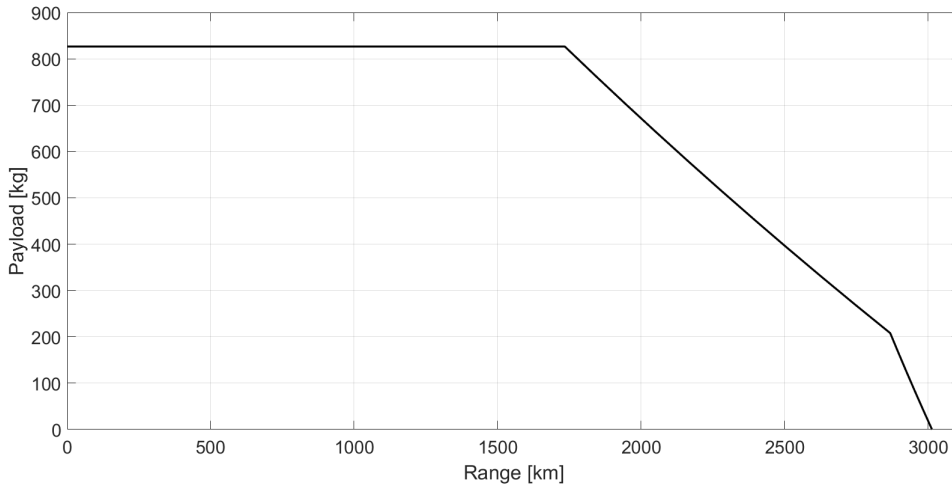


FIGURE 5.5: Payload-Range diagram.

On the one hand, Fig. 5.4 shows the range for different aircraft weight configurations, for example *MTOW* with *MPL*, giving a range of 1750 *km* approximately, or *MTOW* with *MFW*, resulting in slightly less than 2900 *km*.

On the other hand, Fig. 5.5 shows the maximum payload for a specific range, or seen from another point of view, the maximum achievable range for a given payload. It can be seen that, according to the requirements detailed in Sec. 1.4, the 2000 *km* of range are achieved with almost all passengers with their own luggage, or all of them without any cargo. This result is acceptable and it is achieved due to the low SFC ( $0.55 \text{ [lb}/(\text{lb h})]$ ) achieved with the JT15D-1B.

Fig. 5.4 and Fig. 5.5 have been obtained from a MATLAB code of own creation. This can be found in Appendix E.3.

## 5.5 Conclusions

Regarding the flight profile study, it has been determined that not only the mission profile should be studied, but also the reserves profile due to the possibility of a landing denial, which would suppose a holding situation or a cruise phase to the alternate aerodrome. In addition, it has been decided that no cruise-climbing maneuvers would be considered during the cruise phase because of its short length.

With respect to Sec. 5.2, the Simpson's Rule has been chosen as the numerical method used as it presents a lower relative error than the Trapezoidal Rule for the same number of discretization. In addition, the number of discretization has been set at  $n = 2$  with a relative error of  $\delta = 3.749 \cdot 10^{-5}$ .

Due to the early stage of the project, cruise conditions have not been further analyzed, and the reference Mach number and altitude of flight have been determined according to similar jets specifications, obtaining  $M = 0.69$  and an altitude of 43000 *ft*.

Finally, obtaining the Payload-Range diagram it has been determined that the 2000 *km* range required can be achieved with a high percentage of the MPL due to the low SFC (0.55 *lb/(lb h)*) achieved with the JT15D-1B.



# Chapter 6

## Fuselage design

This chapter will explain the decisions made for the fuselage design: starting by designing the cabin, adding the cockpit and finally studying the best geometry for the cone. Fuselage design is extremely important as it has a great impact on the aerodynamic resistance. A diameter 10% bigger than strictly necessary increases the total drag between 1.5 and 3% [1]. Sometimes its design is limited by external factors such as loading easiness. However, the latter is not relevant when talking about business jets, so in this case the best aerodynamic design is expected on the fuselage in order to increase the aircraft's efficiency.

This chapter will firstly design the interior of the cabin because it is plus-value for the potential costumer. After that, the sizing for the exterior of the fuselage will be determined.

### 6.1 Introduction

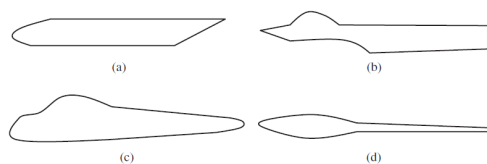


FIGURE 6.1: Four generic fuselage configurations. (a) Large transport aircraft. (b) Fighter aircraft. (c) Light GA aircraft. (d) Glider. [1]

The fuselage structure must allow components such as lifting surfaces, engines and landing gear to be mounted and offer adequate load paths to react the large loads these generate. As the business jet transports people, sufficient internal space must be given to each person. Also ample space should be offered for the passengers and cabin crew to move around (for instance, to go to the lavatory or exit in case of an emergency)[13]. Moreover, the fuselage should be designed with compartments intended to carry baggage and freight that are easily accessible. The fuselage must provide structure to allow baggage to be tied down so it will not shift in flight, possibly altering the center's of gravity position[13, 53].

Many authors recommend some important aspects to consider when conceptually designing the fuselage [1, 6]:

- The fuselage must be as small and compact as possible.
- The arrangement may be symmetric from the top view as far as possible.
- There must be sufficient space to accommodate all of the items.
- Usable loads such as fuel must be close to the aircraft center of gravity.
- The pilot cockpit must be allocated the most forward location of the fuselage, to ensure the pilot to view the runway during take-off and landing.
- Arrangements must be such that the aircraft center of gravity is close to the wing/fuselage aerodynamic center.

The initial point for the design of the fuselage is to consider what it will carry, thus it will define the generic fuselage configuration: the volume and external shape of the fuselage are functions of what is desired to be stored inside (see Fig. 6.1) [1]. For instance, Airbus Beluga hauls parts of other planes in process of construction. So as to, its fuselage is huge and wider enough to let these parts accommodate inside it. In this case, the plane's designing process started by considering the aim it was intended for [77].

Following this principle, the fuselage design for the business jet will start by reflecting on the number of passengers and also the comfort they will feature related

to the amount of free space inside the cabin. Another important issue to consider, as has already been mentioned (see Sec. 2.1.1), is the slenderness of the fuselage Eq. (6.1)[6]. As the slenderness is directly related to the generated aerodynamic resistance [3], the aim of the design process is to find the accurate relation between them to satisfy both, aerodynamic resistance reduction and interior fuselage volume needs [1]. Fig. 2.1 shows typical slenderness values for business jets: high slenderness present structural bending problems, while small ones increase the aerodynamic resistance [6], as it will be explained afterwards.

$$S_r = \frac{l_f}{a_f} \quad (6.1)$$

## 6.2 Technical aspects on fuselage design

To start with, technical aspects that has directly effect on the plane's performance have to be analyzed. The cross-section of the fuselage depends on the pressurization of the cabin and also on the volume needed. As explained along Sec. 2.1.1, by considering these technical aspects, the fuselage-cross section will be circular or near-circular. The drag is linked to the slenderness ratio as can be seen in Fig. 6.2. This chart helps to conclude that the slenderness (see Eq. (6.1)) has to be higher than 5 and lower than 10, in order to avoid aerodynamic decrease in performance due to the dimensions of the fuselage. Fig. 2.1 shows that business jets are commonly designed with a  $S_r$  between 7 and 9.5. So as to, for the business jet being designed along this paper, a slenderness ratio of  $S_r = 7.5$  will be considered to be correct, despite further studies shall be carried out in a more accurate step of the designing process.

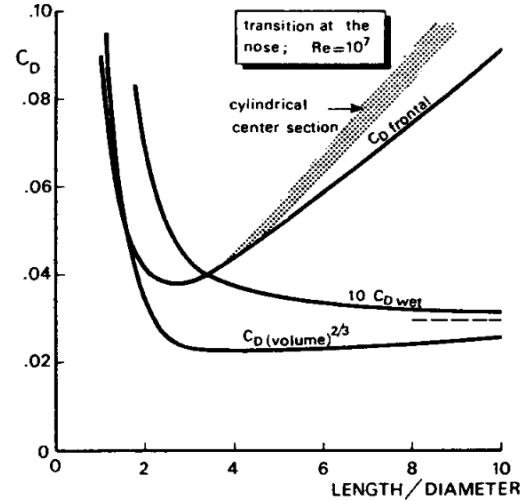


FIGURE 6.2: Drag coefficient of streamline bodies of revolution at low speeds. [6].

Fig. 6.3 is a suitable illustration to use when defining fuselage and cabin sizes. So as to, this nomenclature will be followed among this paper. The cabin sizing will be calculated and studied, taking into consideration both, comfort and regulations. One of the points to be discussed will be the possibility to install a lavatory, so as to it is a differential value when buying a business jet [42]. Later on, a more accurate analysis of the sizing, geometry and distribution, as well as the configuration for the cockpit will be developed.

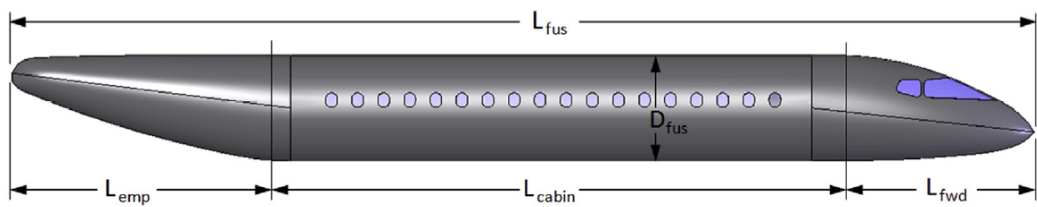


FIGURE 6.3: Typical definition for airplane's fuselage sizing [13]

### 6.3 Inner design

Fig. 6.4 shows the internal arrangement of a civil passenger low-wing aircraft (similar to the business jet being design, as it is explained along Sec. 2.1.2). As it can be seen, the biggest space to consider in the inner design is the passengers cabin, but space for fuel tanks, cargo and systems are also important. This paper will start by sizing the useful space inside the cabin as the initial design value. The remaining amount of free space below the cabin will be analyzed afterwards.

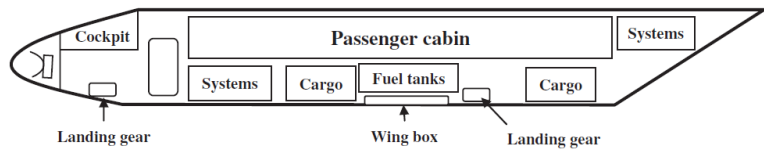


FIGURE 6.4: Internal arrangement of a civil passenger low-wing aircraft. [1]

The inner design has to mull over the amount of useful surface inside the cabin, seats distribution and other service to be offered to the passengers, such as a lavatory. Other space has to be contemplated in order to store small luggage.

After those, the cockpit has to be also sized. Both designs, however, strongly depend and regulations and technical specs to be satisfied in order to certify the plane.

### 6.3.1 Cabin sizing

The cabin is the place where people and small luggage travel. As the aim of this project is to make the preliminary design of a private jet, some considerations have to be taken into account before deciding its design: number of passengers, regulations to be considered, comfortableness, among others. Further design of the cabin should be performed later on as part of the detailed study of the plane design, which is out of the scope of this report.

To start with, the cabin will be designed taking into account the following requirements, which differ from some others business jets, specially when referring to the height inside the cabin (see Chap. 1):

- Enough space to carry six passengers comfortably (according to the initial requirements Sec. 1.4 and Fig. 6.6).
- 1.80 [m] height between the floor of the aisle and the ceiling.

The designing process of the cabin gave through to two different stages: firstly the surface needed inside the cabin was calculated by considering both aisle and seats surfaces. A free space surface was also contemplated in order to increase passengers comfort, as well as a surface to include a lavatory. After that, the diameter needed for the fuselage was calculated by using circumference formula Eq. (6.2)[78], the second restriction specified above and the minimum amplitude of the cross section of the fuselage to accommodate two passengers side-by-side and also the aisle. By considering the useful surface inside the cabin previously calculated, the total length for the cabin could be approximated.

$$(x - x_0)^2 + (y - y_0)^2 = r^2 \quad (6.2)$$

At the end, a preliminary CAD design was performed for the purpose of visualizing the calculated results and verifying they were correctly estimated. A more

accurate CAD design was later on developed with the aim to satisfy a proper seats distribution inside the cabin and to decide whether or not to install a lavatory.

Regulations and technical specs requirements involving this initial sizing process will be explained in the sections below.

### Cabin's surface calculation

As the plane being designed is a business jet, the most important part of the payload will be composed by passengers. As it has been already mentioned, the comfort inside the cabin is a cornerstone for its design. Private aircraft generally have no aisle between the seats and it is not so much the seat width as the cabin width which matters [1]. Following this principle, the minimum width for a single tandem arrangement will be [61 cm], whereas for side-by-side seating the minimum width will be 117 [cm]. This calculation takes into account the average shoulder width of an occupant (51 [cm]) and also a free space (5 [cm]) [6]. The later should be analyzed in a more detailed design phase. As it is only a preliminary design and sizing for the cabin, an aisle of 40 [cm] width –to easily carry a trolley inside the cabin– will be considered, as well as a side-by-side seating configuration.

Regulations are not clear enough when taking about the minimum space to size the seats for a business jet. However, the typical and regulated dimensions for *De Luxe* seats for commercial airplanes will be considered (see Fig. 6.5).

		SEAT CLASSIFICATION		
SYMBOL <sup>•</sup>	UNIT	DE LUXE	NORMAL	ECONOMY
a	inch	20(18½-21)	17(16½-17½)	16,5(16-17)
	cm	50(47-53)	43,5(42,5-45)	42(40,5-43,5)
b <sub>2</sub>	inch	47(46-48½)	40(39-41)	39(38-40)
	cm	120(117-123)	102(100-105)	99(97-102)
b <sub>3</sub>	inch	—	60(59-63)	57
	cm	—	152(150-160)	145
l	inch	2½	2½	2
	cm	7	5,5	5
h	inch	42(41-44)	42(41-44)	39(36-41)
	cm	107(104-112)	107(104-112)	99(92-104)
k	inch	17	17½	17½
	cm	43	45	45
m	inch	7½	8½	8½
	cm	20	22	22
n	inch	32	(24-34)	
	cm	usually 81	(61-86)	
p/p <sub>max</sub>	inch	28/40	27/37½	26/35½
	cm	71/102	69/95	66/90
$\alpha/\alpha_{max}$	deg	15/45	15/38	15/38

FIGURE 6.5: Typical values for the seats sizing [6].

As it can be seen in Fig. 6.5, the typical seat's width for *De Luxe* configuration in Commercial Airplanes is between 57 to 53 [cm]. A free space about 7 [cm] is left between seats for the arm-rest. The total width of two seats placed side-by-side is about 120 [cm]. So that, it can be stated that the minimum width dimensions for a business jet seats configuration are very similar to those involving typical seats design for *De Luxe* category of commercial aviation.

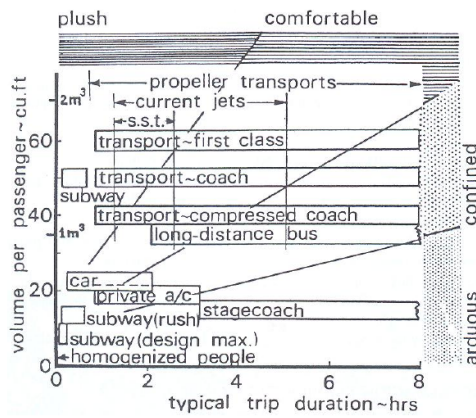


FIGURE 6.6: Sizing for the cabin regarding commodity and duration of the flight. [6].

ing of the fuselage, and delighting passengers with a very comfortable trip experience.

The initial sizing for the cabin design was performed by using dynamic tables in Microsoft Excel. The input values are detailed below, but all of them were taken by considering the bibliography mentioned above. In addition, for the initial sizing of the cabin, as it is aforementioned, a lavatory was also cogitated.

- Number of seats: 6 seats
- Seats width: 68 [cm]
- Seats length: 120 [cm]
- Aisle width: 40 [cm]
- Ratio length-to-width for the cabin ( $l_c/b_c$ ): 3.5-5.5<sup>1</sup>

<sup>1</sup>This value is calculated from statistical references and other planes [36, 53].

- Free space ratio 0.7<sup>2</sup>

From those points below, the calculations could began. Firstly total seats surface is calculated by considering both width and length for six seats inside the cabin. After that, the area for the lavatory is computed. Its dimensions are factorized from those involving seats configuration. For the lavatory: width is multiplied by 2.0, whereas length is multiplied by 1.3. This results to a lavatory of about 1.44 [ $m^2$ ], considered to be valid from Sadraey's reference [1].

Both Roskam and Sadraey's advises to consider other useful elements inside the cabin: a galley and a wardrobe. Their dimensions depend on the number of passengers [1, 3]. By adding the amount of free space inside the cabin, the total surface resulted about 10.87 [ $m^2$ ]. This value can easily be recalculated for the length and width needed inside the cabin: as the length-to-width ratio for the cabin is about 5, both length and width can be calculated as a function for the cabin's area –by supposing it has a rectangular shape–, being  $l_c = 5 \cdot b_c$  as follows:

$$l_c = \sqrt{\frac{S_c}{l_c/b_c}} \quad (6.3)$$

Eq. (6.3) gives a value of  $l_c \simeq 7.37[m]$ , which means cabin's width will be five times smaller:  $b_c = 1.47[m]$ . These calculations do not consider the seats distribution inside the cabin, meaning that the configuration of two side-by-side seats plus an aisle will be quite wider.

Regarding the diameter of the fuselage, it can be calculated from the later results and by fixing the restriction of a minimum height of 1.80 [m] between the aisle and the ceiling of the cabin. To do so, Eq. (6.2) is used: coordinates' origin is attached vertically to aisle's surface, whereas the horizontally axis is centered in the medium of the cabin's width. The initial calculation for the fuselage internal diameter gives a value of about 1.92 [m], for a cabin capacity of six passengers.

---

<sup>2</sup>It is a design parameter that will be directly related to passengers comfort. It considers the amount of surface inside the cabin that will be free, e.g. not occupied by seats, lavatory or furniture.

### Cabin's design optimization

After the initial calculations, further development was made with a CAD design program (SolidWorks specifically). There, the diameter was drawn as the initial sketch, fixing the restrictions aforementioned. The width was also an initial restriction in this case, being the sum of two seats side-by-side (68 [cm] each), and a 40 [cm] width aisle.

These restrictions automatically gave-way to an oversized diameter, because all of the restrictions were fixed in the same surface, e.g. in the aisle surface. To avoid such problems, a consideration was made: the aisle could be allocated 25 [cm] below the seats lower surface, in order to satisfy the proposed requirements but notwithstanding a non oversized cabin: to avoid aerodynamic drag problems. After that, an average diameter of 2.10 [m] was obtained. To optimize the relation  $l_c/b_c$ , the circular shape was substituted by an elliptical one (being now a near-circular cross-section), as it is also an acceptable shape when thinking of pressurizing the cabin [1, 3]. After those, the width resulted to be 1.90 [m], whereas the height was about 2.00 [m], for the interior design of the cabin.

Later, the cross-section of the cabin was extrude, with a total length of about 7 [m]. After that, both the lavatory and the seats were prefixed in their allocations, considering the aforementioned dimensions for them. The lavatory was installed in the back of the cabin, taking up the total width of the cabin. Six seats were set up in order to verify the calculation were correct.

#### 6.3.2 Doors and emergency exits

The access door to enter the business jet's cabin was also pre-designed with Solidworks software, with the aim to satisfy enough space for the passengers to come in and safely come out of the aeroplane. Regulations are extremely important when thinking of designing the emergency exits. CS 25.807 classifies the emergency exits for aeroplanes in four different categories, as shown in Fig. 6.7. Although the business jet being designed has to satisfy CS 23 regulations, this reference can be useful to choose the proper emergency exit. For an aeroplane carrying between

one and ten passengers, CS 23 specifies that: "*the emergency exit has to be a rectangular opening of not less than 48 [cm] wide by 66 [cm] high, with a corner radii not greater than one-third the width of the exit, located over the wing, with a step-up inside the aeroplane of not more than 74 [cm] and a step down outside the aeroplane of not more than 92 [cm]*" [41, 51].

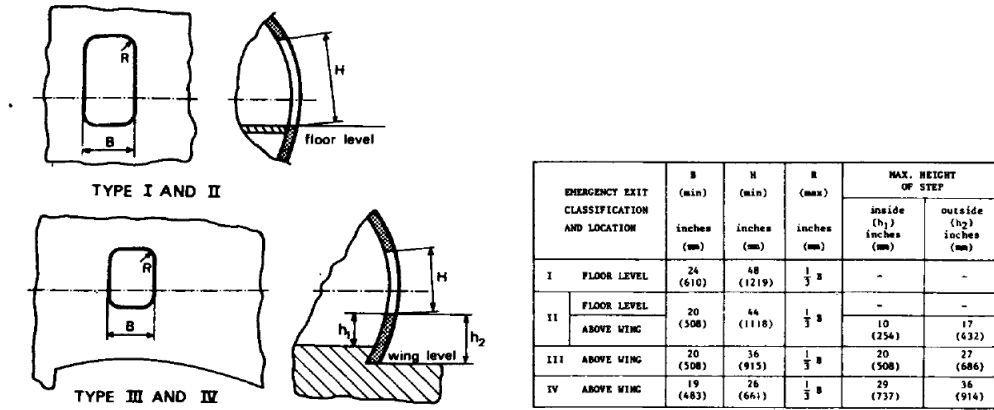


FIGURE 6.7: Classification and sizing of emergency exits regarding CS 25.807. [6].

As the required emergency exit for the business jet regarding regulations has to be allocated above the wing, the access door cannot be used in detriment of the emergency exit. So as to, the door will continue with the dimensions of the pre-design: 90 [cm] width and 154 [cm] high (see Appendix B), but at this stage of the design will not be considered to be an emergency exit. The emergency exit will be allocated above the wing, as it is specified by the regulations aforementioned.

### Cabin's preliminary sizes

After calculating the sizes for the cabin during Sec. 6.3.1, they can be summarized in Tab. 6.1.

TABLE 6.1: Values for the preliminary sizing of the cabin.

Item	[mm]
Average cabin's diameter	1950
Cabin's length	7000
Seats width	680
Seats length	1200
Aisle width	400
Aisle-ceiling height	1800

### 6.3.3 Cockpit design

Cockpit design has to consider strict regulations, involving pilots' angle of vision, easiness when managing the plane and disposition of avionics inside the cockpit [6]. This section will mull over all the aspects to be considered in order to, at the end, give the preliminary dimensions of the cockpit.

#### Number of pilots

The first point to be decided is related to the number of seats that will be inside the cockpit. Many airplanes can be flown by only one pilot: Commercial Air Transport regulations let planes to be operated with only one pilot, as long as it is not part of a Commercial Operation [67]. However, in order to widen the market share for this plane, it was decided to design the cockpit for two people: a pilot and a copilot. As mentioned before (see Chap. 3), the operative designing configurations for this business jet include, as maximum, the following: two pilots and five passengers, or one pilot and six passengers.

#### Cockpit geometry

A safe and comfortable flight by a pilot requires several items of personal equipment [1]. Depending upon the type of aircraft, pilot mission, flight duration and flight environment, the equipment needed is different: from seat and seat-belt to suit, google, helmet, parachute and pressure system [13]. For a business

jet, the pilot and the copilot must have a comfortable seat and enough space to carry out their tasks. When sitting, the main part of the body weight is transferred to the seat. Where the weight is transferred is key to a good seat design because, if not, pain and fatigue can occur to the pilots and the flight safety could be compromised [1]. This paper will only focus on the initial sizing of the cockpit, but any system or instrumental equipment will be determined.

Fig. 6.8 shows the typical geometry for a passenger transport aircraft. As it can be seen, the total length of the cockpit including the seat, free space for the pilot to operate and the instrument panel is about 130 [cm]. Moreover, Gudmunsson give a recommended value for the wide of the cockpit for several planes: for medium size planes operated by two people the cockpit wide goes from 140 to 160 [cm] [13]. To verify if the fuselage is wide enough to include a cockpit of these dimensions, the fuselage cross-section diameter has to be evaluated. As it is stated in Tab. 6.1, this diameter is about 195 [cm], which helps to conclude that there is enough space for the cockpit.

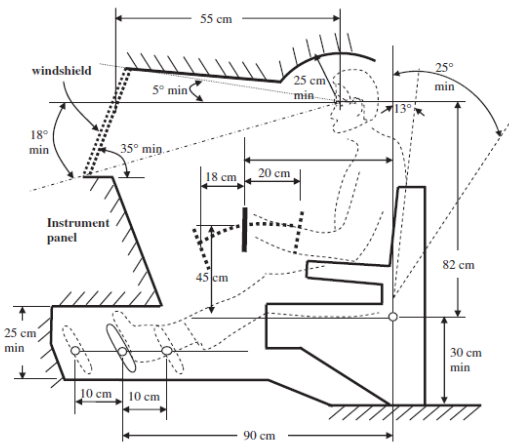


FIGURE 6.8: Cockpit geometry for a transport aircraft. [1]

### 6.3.4 Fuel, cargo and systems compartments

As it is aforementioned, also systems, cargo and fuel compartments should be considered when designing the fuselage (see Fig. 6.4). As can be seen in Appendix B, there is enough empty space below the cabin to allocate cargo, systems and fuel compartments. In this paper, systems and its allocation along the fuselage will not be considered because it is still a preliminary design.

#### Fuel compartment

The needed maximum amount of fuel is calculated along Sec. 5.4 ( $MFW = 1868kg$ ), which results to a required volume to store it. The first place where

to store the fuel is with tanks inside the wings (see Sec. 4.2), because it is recommended to try to keep the fuel out of the fuselage for sake of flight attendants, since it may leak or catch fire in an emergency situation [1]. When the amount of free volume inside the wings was calculated (see Sec. 8.2.2), it was obvious that there was not enough space. So that, another tank may be installed inside the fuselage. As it is aforementioned, this tank must be placed close to the aircraft center of gravity [1]. Appendix B shows that below the cabin exists enough space to store this amount of fuel.

### Cargo compartments

Along Sec. 3.3.2 the amount of cargo that will be able to carry the plane has been discussed. As this design is still in a preliminary stage, the volume needed to store the goods and cargo of the passengers has not been calculated. However, Appendix B shows that there is enough space below the cabin to allocate a cargo compartment, as well as a fuel one and still allowing the systems to be placed in.

## 6.4 Outer design

For the outer design, regulations and easiness when assisting the plane have to be considered. It is important to satisfy a quickly on-ground assistance, so as to not having the plane inoperative [6]. However, as it is a business jet, unless it operates many times per day, the assistance time is not much important, as aforementioned (see the abstract for Chap. 6). As part of a more detailed design, the ground handling should be evaluated in order to allocate the ground services in the most efficient way possible. This section will only evaluate the external shape and dimensions of the fuselage by using bibliography's formulae.

### Fuselage external diameter

The fuselage external diameter is an important parameter when approximating the drag generated by the fuselage. By using Saedray's formula [1] the external

diameter will be calculated, depending on the dimensions aforementioned:

$$\Delta d = d_{F,O} - d_{F,I} = 0.084 \text{ [m]} + 0.045 \cdot d_{F,I} \quad (6.4)$$

From the values in Tab. 6.1 and Eq. (6.4), the outer diameter can be calculated. The result gives an average value of 2.2 [m] for the outer diameter.

### Rear fuselage upsweep angle

Along Sec. 9.1.1 the rear fuselage upsweep angle has been analyzed. The aircraft may land or takeoff with some roll and pitch angles so that, the fuselage may consider a guard angle to prevent that any part of the aircraft contacts with the ground. As it has been already mentioned, in this stage of the design the guard angle is considered to be the same as the pitch angle for liftoff (see Sec. 9.1.1). By using Eq. (9.1) the angle of guard was established at 8°.

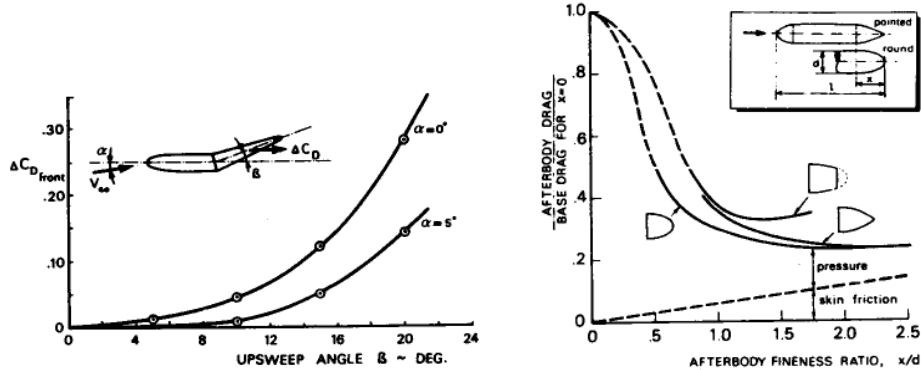


FIGURE 6.9: Drag increment vs upsweep angle and afterbody drag of a fuselage tail, when added to a cylindrical shape part. [6].

Fig. 6.9 shows the effect of the fuselage's rear part in the drag contribution. This phenomena is directly related to the vortex shedding due to the geometry of the fuselage [6, 13]. The higher value of  $\beta$ , the higher  $\Delta C_{D,front}$  increases. This plot helps to verify that the guard angle calculated above (in this case it is indicated by  $\Theta$  instead of  $\beta$ )  $\Theta = 8^\circ$  is valid from the point of view of the generated drag: the generated drag increment still tends to 0 when the guard angle is 8°.

With the guard angle established, the afterbody fineness ratio  $x/d_{ab}$  should be also evaluated. As it can be seen in Fig. 6.9, the higher is the fineness ratio, the lower is the afterbody generated drag. So that –keeping in mind that this design is still at a preliminary stage–, an afterbody fineness ratio  $x/d_{ab}$  of about 1.8 could be considered to be correct, from the point of view of this plot [6].

As the diameter of the fuselage was already calculated (see Sec. 6.4),  $d_f = 2.2$  [m], the  $x$  dimension –taking into account the fineness ratio of  $x/d_{ab} = 1.8$ – results to  $x = 3.96$ .

As part of the design and in order to use the empty space below the cabin, a preliminary form for the airplane hold was also designed. All this considerations and also the initial sizing for the business jet’s cabin and fuselage can be found in Appendix B.

### 6.4.1 Drag estimation

The final step to design the fuselage is to estimate the generated drag, although this is an important design parameter that has been taken into account along all this chapter. Sadraey’s gives some formulae to easily approximate the generated  $C_{D_{0f}}$  [1], but it shall be used in a more accurate design phase. For the current one, the graphs that have been used along this paper can be summarized in order to preliminary estimate the generated drag for the fuselage.

Fig. 6.2 shows the drag coefficient of streamline bodies of revolution at low speeds, depending on the slenderness ratio of the fuselage. By using the latter as a reference, and by knowing that  $S_r = 7.5$  is an initial design parameter, the  $C_{D_{wet}} = 0.03$ ,  $C_{D_{frontal}} = 0.06$  and  $C_{D_{volume}} = 0.02$  for the fuselage.

Furthermore, regarding the drag of the afterbody, Fig. 6.9 shows the relation between the afterbody geometry, the fineness ratio and the afterbody drag in relation to the base drag of the fuselage for  $x = 0$ . For a ratio  $x/d_{ab} = 1.8$ , the non-dimension drag is about 0.3.

Due to the upsweep angle of the fuselage another drag increment should be

considered. As it is shown in Fig. 6.9, for an upsweep angle of  $\theta = 8^\circ$ , the  $\Delta C_{D_{front}} = 0.04$ .

To sum up, the drag caused by the fuselage is directly related to its geometry and, unfortunately, it could generate an undesirable effect on the performance of the plane. So as to, when designing the fuselage, it is really important to be aware of the importance that the fuselage has when generating drag.

## 6.5 Conclusions

As a conclusion, it can be stated that a preliminary sizing design for the business jet's cabin was performed. This design considered a capacity for six people, the inclusion of a lavatory inside the cabin and an aisle 40 [cm] width. A width of 68 [cm] and a length of 120 [cm] were contemplated to size the seats. Furthermore, the cockpit has also been preliminary sized, considering a length of 130 [cm] and a width between 140-160 [cm]. For the afterbody, a  $\theta = 8^\circ$  angle has been chosen and a total length of 396 [cm]. Moreover, emergency exits has been evaluated regarding Certificate Specifications and allocated above the wings. The fuselage has been designed also to carry fuel, cargo and systems below the cabin. The results obtained after all the analysis can be summarized as follows:

TABLE 6.2: Values for the preliminary sizing of the cabin.

Item	[mm]
Average cabin's diameter	1950
Cabin's length	7000
Seats width	680
Seats length	1200
Aisle width	400
Total cabin's width	1760
Aisle-ceiling height	1800
Average outer fuselage diameter	2200
Cockpit's length	1300
Cockpit's width	1500
Afterbody length	3960

By adding the corresponding values summarized in Tab. 6.2, the total length of the fuselage can be calculated as follows, by using Fig. 6.3 reference. Eq. (6.5) gives a value of  $l_{fus} = 12.46 [m]$ . This value still does not consider the nose of the fuselage, which may be calculated in another design phase.

$$l_{fus} = l_{fwd} + l_{emp} + l_{cabin} \quad (6.5)$$



# Chapter 7

## Wing design

The wing is the most important part of the airplane as it is the element that provides lift that allows the aircraft to fly. In this chapter, the wing will be designed. First, an estimation of the aspect ratio will be performed. This aspect ratio will be the starting point, together with the airfoil that will also be defined, of the wing design and will make it possible to model the wing in XLF5 software. Later on, twist, sweep and dihedral will be introduced in order to obtain a wing that gives the best performance. These parameters will be fixed at the minimum value that gives the best performance of the wing. Once the final wing is obtained, the new design point will be determined to ensure that the defined wing fulfils the design point limitations. Finally, high-lift devices that allow the aircraft to perform different manoeuvres will be determined.

### 7.1 Initial aspect ratio determination

The first parameter that has been determined is the aspect ratio  $A$ . This parameter will allow a first sizing of a rectangular wing that will be modified afterwards in order to improve its performance by introducing geometrical variations such as sweep or dihedral.

Some methods have been developed to determine  $A$ . However, due to the preliminary stage of the design it has been decided to define an initial aspect ratio

taking similar jets as reference. Along these lines, in Tab. 7.1 the aspect ratio for different jets is shown. In order to obtain  $A$ , Eq. (7.1) has been applied introducing the wing span and wing area shown in Tab. 7.1.

$$A = \frac{b^2}{S} \quad (7.1)$$

Model	Wing span [m]	Wing area [ $m^2$ ]	A	Reference <sup>1</sup>
Cessna 510 Citation Mustang	13,16	19,51	8,88	[28]
Embraer Phenom 100	12,3	16,86	10,18	[29]
Honda HA420 Hondajet	12,12	16,4	8,96	[31]
Eclipse Aviation EA500	11,4	13,4	9,70	[32]
Syberjet SJ30	12,9	17,7	9,41	[33]
Adam aircraft A700	13,41	15,8	11,38	[34]

TABLE 7.1: Aspect ratio for similar jets.

Finally, an arithmetic mean has been applied to the  $A$  values shown in Tab. 7.1 and an initial aspect ratio of 9,5 has been determined.

## 7.2 Airfoil definition

Regarding the airfoil decision, it was firstly decided to determine it by looking at similar aircrafts. However, it has not been possible to obtain the airfoil used by the similar jets studied and so a different method had to be used. Along these lines, NACA 23012 was studied during the wing modeling phase –see Sec. 7.3 – and it was observed that it gave a good performance. Finally, as no information about the airfoil used by similar jets has been found, and taking into account the preliminary stage of the project, it has been decided that the airfoil used is the NACA 23012 as it gives a good performance for the jet.

---

<sup>1</sup>References used to extract the wing span and wing area.

## 7.3 Wing modeling

Once the aspect ratio is determined, the wing is simulated using XFLR5 with the objective to obtain the total aerodynamic efficiency and both lift and drag coefficients for the maximum efficiency case. As the optimal wing is designed for the cruise phase, the  $C_L$  required to maintain the equilibrium between lift and weight of the aircraft has been used as an indicator of the suitability of each wing model.

### 7.3.1 Iterative design procedure

Previously to the iterative method application, taper ratio has been fixed at a constant value that won't change for the subsequent geometric modifications. It has been estimated taking into account its influence on lift distribution (large taper ratios can improve tip stall) [16], and has been fixed on TR=0.75.

The use of an iterative procedure in order to obtain an optimal wing for the cruise phase has two main objectives: The first one is to simplify the decision making regarding sweep, dihedral and twist values, as their influence can be easily compared if the same sequence of analysis is carried out. The second one is to minimize manufacturing costs, as the minimum ones are achieved with rectangular wings. For these reasons, the sequence followed on the iterative process is:

1. Sweep
2. Dihedral

Once the best fitting sweep and dihedral values are obtained, twist iteration is carried out for the optimal wing. The reason why it's not included on the first iterative analysis is because twist manufacturing costs are greater than the related to sweep and dihedral. As a result, if a wing without twist complies with the minimum  $C_L$  required, twist addition will be dismissed.

For each parameter mentioned, 4 different values presented at Tab. 7.2 have been studied based on similar aircraft:

TABLE 7.2: Different values of sweep, dihedral and twist studied.

Sweep [°]	Dihedral [°]	Twist [°]
0	0	0
5	2	2
10	4	4
15	6	6

### 7.3.2 Numerical method definition

The numerical method used to simulate the wing's 3D model is the Ring Vortex method, which is a commonly used computational fluid dynamics method in the early stages of an aircraft design. In addition, all the simulations have been developed at constant cruise velocity. The analysis constants are presented in Tab. 7.3

TABLE 7.3: Numerical method constants.

Density	0.28 $kg/m^3$
Viscosity	4,82e-05 $m^2/s$
Velocity	199.27 m/s
$\beta$	0°
Plane mass	5572.00 kg
NCrit	2
$X_{CoG}$	0.00 m
$X_{CoG}$	0.00 m
$\Delta\alpha$	0.25°
Reynolds Number range	$4 \cdot 10^6 - 6 \cdot 10^6$

### 7.3.3 Wing modeling results

According to Sec. 7.3.1, the analysis begins with the basic tapered wing (*Wing\_tapered\_s0\_d0\_t0*) presented in Fig. 7.1. Its geometry is summarized in Tab. 7.4.

TABLE 7.4: Tapered Wing Geometry.

Wing span	12 m
Wing area	16.8 m <sup>2</sup>
Aspect Ratio	8.57
Taper Ratio	1.33
Root chord	1.6 m
Tip chord	1.2 m
MAC	1.41 m

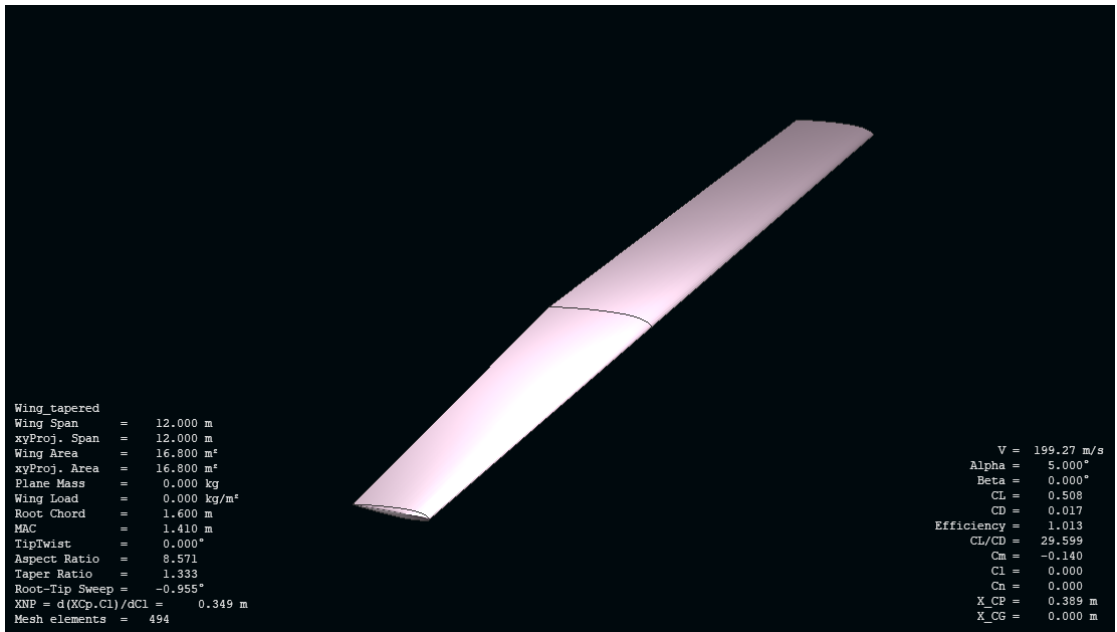


FIGURE 7.1: Initial tapered wing.

It must be pointed that Aspect Ratio differs from the one determined at Sec. 7.1. This is because  $A = 9.5$  has been used to design the rectangular wing, but by modifying the tip chord the Aspect Ratio was reduced. Nevertheless, the new Aspect Ratio still guarantees similarity according to Tab. 7.1, and its suitability will be assessed after the iterative study.

## Sweep and dihedral

After the iteration process for sweep and dihedral values cited at Tab. 7.2, the following results have been obtained:

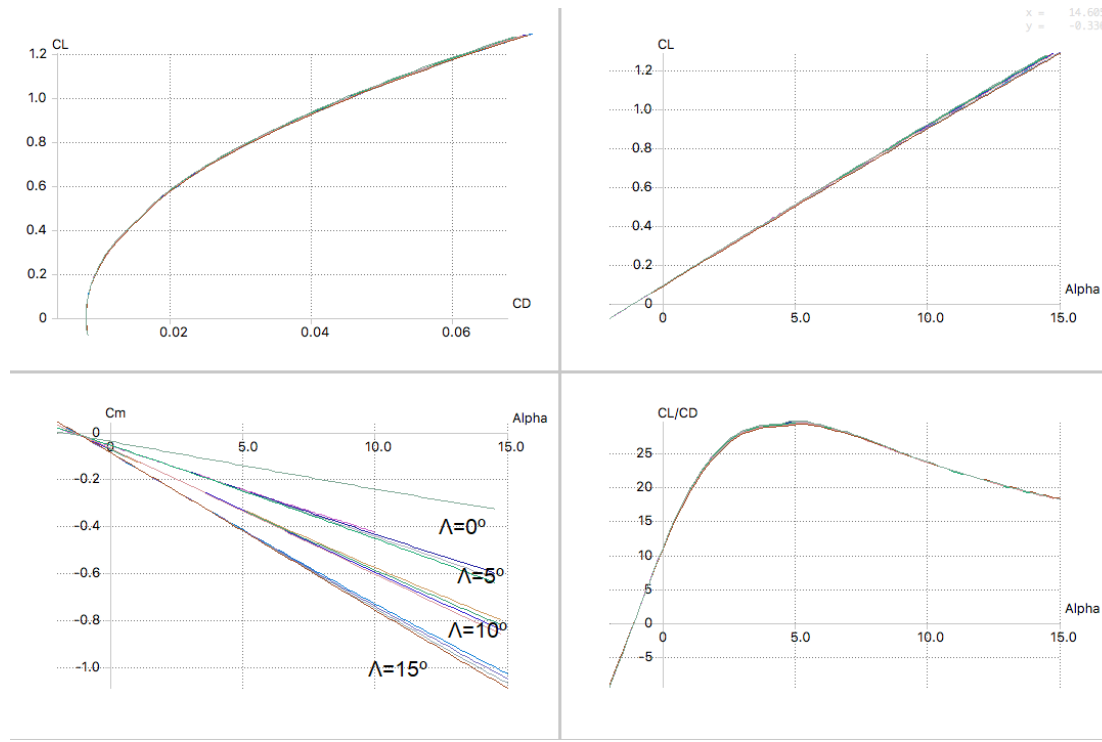


FIGURE 7.2: First iteration graphs for sweep and dihedral.

To simplify the justification of sweep and dihedral values, the maximum aerodynamic efficiency  $C_L/CD$  and the optimum  $C_L$  for each geometry studied are presented in Appendix C.1. Regarding Fig. 7.2, it can be observed how stall is not represented in the  $C_L$  VS  $\alpha$  graph. This is due to the numerical method selected, as VLM is a linear method and stall is a non-linear effect caused by viscosity [79]. As a result, the final point of each simulation's  $C_L$  VS  $\alpha$  indicates when a tip panel has achieved stalling conditions [80]. For this reason, these  $C_L$  values have been considered as  $C_{Lmax}$ .

Observing Tab. C.1 it can be seen how the  $C_L/CD$  remain fluctuating between  $C_L/CD=29$  and  $C_L/CD=29.5$  approximately. On the other hand, lift coefficient also remains at approximately at  $C_L=0.5$ . As a result, sweep and dihedral has been minimized (according to Sec. 7.3.1) , being fixed at:

- $\Lambda=5^\circ$
- $\Gamma=2^\circ$

It must be pointed that, even if the maximum aerodynamic efficiency and optimum lift coefficient are very similar for the wing selected and the wing without

dihedral and sweep, future studies has been considered as the differential value. Regarding dihedral, and based on similar aircraft, small angles are introduced to improve the stability in subsequent analysis [16]. On the other hand, sweep angle has been introduced to retard the critical Mach number (as it is also considered in similar aircraft) [81]. However, the study of this Mach number has been considered outside of the scope. As a result, sweep modifications should be introduced in a detailed analysis as the value presented is just a first approximation.

## Twist

After the iterative process for twist values cited at Tab. C.2 in Appendix C.2, the following results have been obtained:

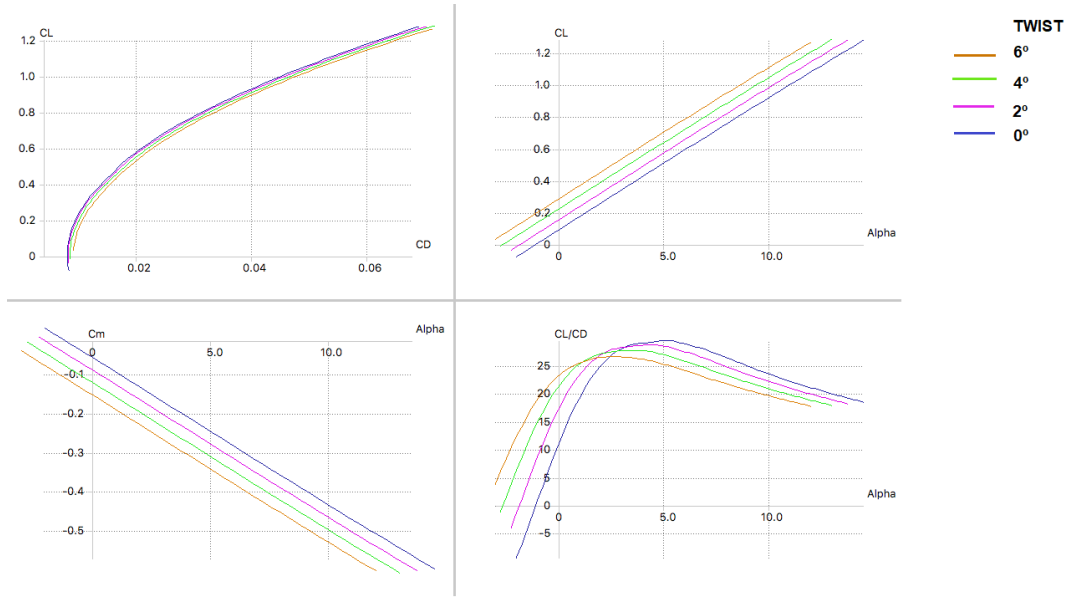


FIGURE 7.3: Second iteration graphs for twist modification.

In Fig. 7.3, it can be observed how the addition of twist produces a slight descent of the maximum aerodynamic efficiency, even though the optimum  $C_L$  remains constant for each twist value at approximately  $C_L = 0.5$ . However, the minimum  $C_L$  needed to equal the aircraft's weight and the total lift is  $C_L = 0.58$ . As a consequence, each wing obtained presents non-favorable cruise conditions. For this reason, some modifications on the wing geometry must be introduced in order to reduce the minimum  $C_L$  required and to increase the optimum  $C_L$  of the wing.

It should be assessed the introduction of twist to improve stalling characteristics of the wing. Notice that the introduction of sweep can lead to a tendency to wing tip stalling at lower cruise velocities, which requires twist introduction to compensate its effect by modifying the lift distribution along the span [6]. As there's no information provided by VLJ manufacturers regarding wing twist values, the first approximation of  $4^\circ$  has been selected [82], even though this value should be treated in the detailed analysis with a complete CFD study.

## Final geometry modification

As it has been previously commented, the geometry of the wing must be modified with the aim of obtaining an optimum  $C_L$  higher than the minimum  $C_L$  required for the cruise stage. For this reason the span is modified and, as a consequence, wing surface. In order to estimate the increment on the wing surface, it has been changed the Aspect Ratio to approximately equal with the previously obtained at Sec. 7.1. Notice that the previous study of the Aspect Ration intended to minimize the total drag, which has a big impact on the present study as the optimum  $C_L$  must be increased. The proposed geometry is presented in Tab. 7.5:

TABLE 7.5: Final wing geometry.

Wing span	13 m
Wing area	18.2 $m^2$
Aspect Ratio	9.29
Taper Ratio	0.75
Root chord	1.6 m
Tip chord	1.2 m
MAC	1.41 m
Sweep	$4.66^\circ$
Dihedral	$2^\circ$
Twist	$4^\circ$

The modification on Sweep angle from  $\Lambda = 5^\circ$  to  $\Lambda = 4.66^\circ$  in Tab. 7.5 is due to the XFLR5 sweep definition, as the input is in m rather than degrees. By modifying the wing span, the sweep angle for a constant offset (0.63m in our case) will also

change. However, as the new sweep angle is according with the range of sweep values studied,  $\Lambda = 4.66^\circ$  has been accepted. The simulation results obtained for the presented geometry are:

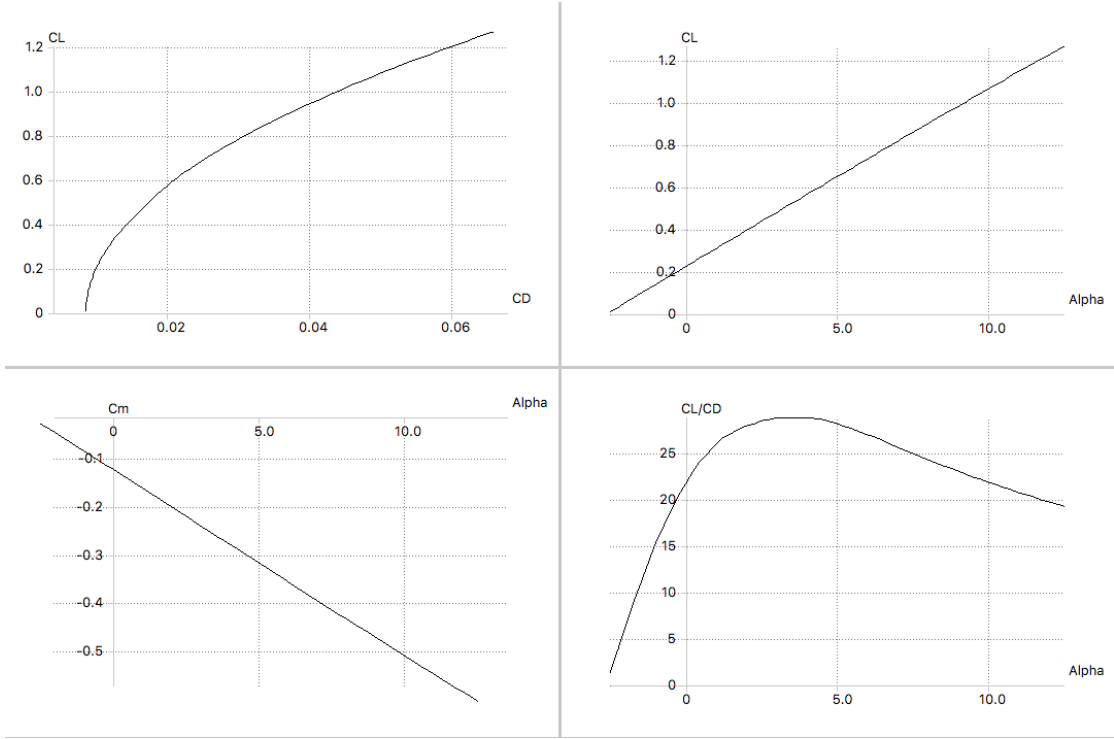
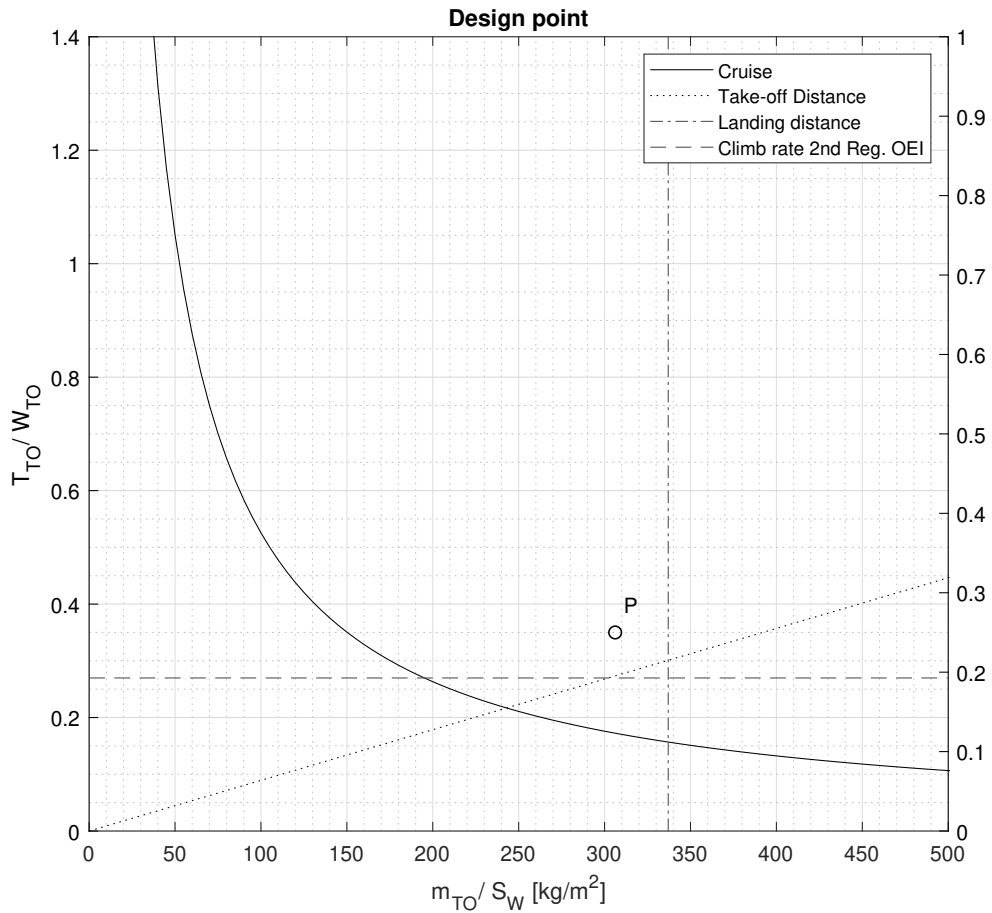


FIGURE 7.4: Simulation results for the modified wing.

By enlarging the wing surface, the required  $C_L$  has been reduced, being now  $C_{Lmin}=0.53$ . In addition, the actual optimum lift coefficient is  $C_{Lopt}=0.52$  (for  $\alpha = 3.5^\circ$ ). For this reason, the new configuration enables to fly at an angle of attack near the optimum one, and the minimum angle of attack required would be approximately  $\alpha = 4^\circ$ . With  $\alpha = 4^\circ$ , drag coefficient is  $C_D = 0.02$ , and total wing drag is approximately  $D=2$  kN. Taking into account the engine selection at Sec. 4.3, and knowing that each *Pratt Whitney Canada JT15D-1B* engine produces 9.79 kN each, the total drag of the wing is acceptable. However, the addition of fuselage and wing would contribute in total airplane drag, and an assembled simulation should be carried out to verify that total drag is smaller than thrust.

In addition, the suitability of the wing should be analysed with the design point, as the surface has been modified.

FIGURE 7.5: Design point for  $S_W = 18.2 m^2$ 

In Fig. 7.5 it can be seen how the design point has moved to the left, as a lower wing loading is obtained. Nevertheless, the designed configuration complies with design point limitations. As a result, this configuration has been accepted as a correct first approximation, defining the final wing of the aircraft.

## 7.4 High-Lift Devices

The design of an aircraft is based on the cruising performance considering that occupies the largest time of the flight. It is designed to optimize the fuel consumption, therefore for optimize the range. When the aircraft is carrying out some type of manoeuvres, such as take-off and landing, the velocity required for this

performance is below to the stall velocity for the designed wing. For that reason, devices such as flaps or slats are used to achieve extra lift to the airplane.

In take-off or landing operations these devices are crucial for reducing the field length required. For that, it is an important part for the design of the VLJ according to the operational requirements where the capability to land and take-off in runways of 800 m length is a must.

In this section it is reviewed the state-of-the-art of these devices and a sizing method it is carried out.

#### 7.4.1 General considerations

There are two types of High-Lift Devices: Active and Passive. Active Devices control the boundary layer resulting from improved pressure distributions, reenergizing or removing low energy boundary layers [6]. Passive Devices refers to leading-edge flaps (slats) or trailing-edge flaps which both modify airfoil geometry and the flow around it, changing the characteristic curves. Only Passive Devices are taken into account for the development of this study.

There are two types of passive devices: Trailing-edge and leading-edge flaps. As it can be observed in Fig. 7.6, trailing-edge flaps increase the camber and improve the flow at the trailing edge, but tend to promote leading edge stall on this sections and may cause a reduction in the stalling angle of attack. Leading-edge high-lift devices postpone or eliminate leading edge stall and little increase airfoil camber [6].

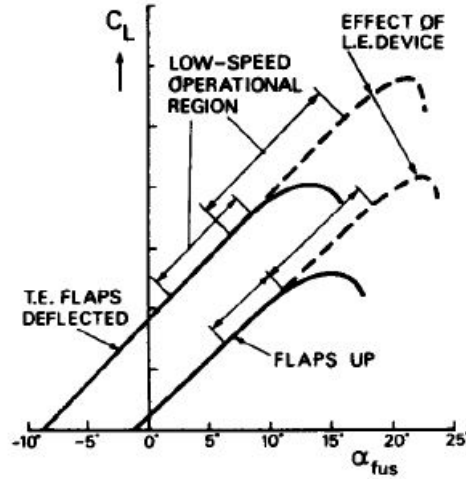


FIGURE 7.6: Lift curves with and without high-lift devices. Extracted from [6].

Even though the High-Lift Devices actuation mechanism should not be underestimate due to its complexity, in this preliminary design it will only be taken into account aerodynamic aspects. These parameters are presented in the sections below and are location along the span, type of HLD, chord, span and deflection. Fig. 7.7 shows the parameters in the right semi-wing span.

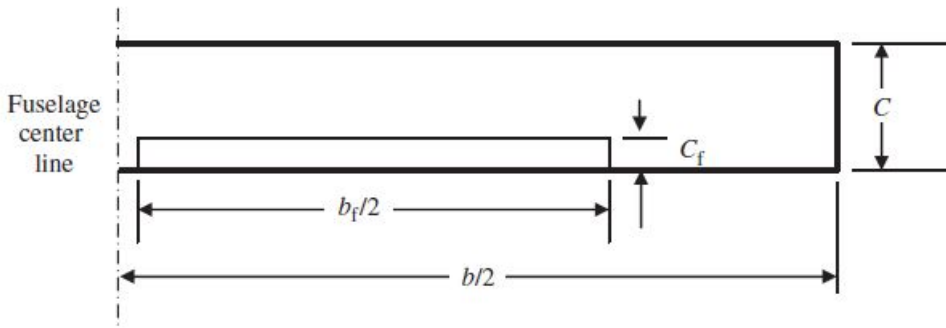


FIGURE 7.7: Top view of right wing high-lift devices parameters. Extracted from [1].

Even though the High-Lift Devices (HLD) actuation mechanism should not be underestimate due to its complexity, in this preliminary design it will only be taken into account aerodynamic aspects. These parameters are presented below and are location along the span, type of HLD, chord, span and deflection.

### 7.4.2 High-Lift Devices location along the span

HLD are usually located inboard portion of both semi-wing sections, near the fuselage. When these devices are applied simultaneously and symmetrically on right and left wing sections prevent appearing of rolling moment on the aircraft, which would have to be laterally trimmed. The location of HLD are mainly influenced by two reasons [1]:

The first fact which makes that flaps and slats in this position is for structural reasons. The actuation mechanism which permit to retract and extend these surfaces and the surfaces itself are heavy and occupies an important portion of the wing volume. If the design of the wing consider a tapered wing, at the root there will be more space than at the tip of the wing. Moreover, the more proximity to the fuselage is installed less bending moment is suffered by the root at the cast. These makes the structure of the wing lighter and causes less fatigue because it has not to support much weight at the tips.

The second reason is for allowing the ailerons or control surfaces to have larger arm to control rolling moment. As is known, moment is the product of force and distance. With large arm the force required for developing the same moment is reduced, hence the surface of aileron will be decreased. The further the position of the aileron is, more lateral control the aircraft have and faster roll is able to perform.

In conclusion, the position of flaps and slats in this preliminary design will be near the wing root as much as possible.

### 7.4.3 Type of High-Lift Devices

The final decision of the type of HLD is the outcome of a compromise among aerodynamics requirements and mechanical complexity (weight, safety, control requirements, manufacturing limitations). A simple HLD requires a simpler mechanism to operate but achieves lower  $\Delta C_L$ . On the contrary, complex HLD that needs a heaviest and an expensive complex mechanism, however, requires smaller wing area, results in a slower stall speed (more safety), and achieve a higher  $\Delta C_L$  allowing the aircraft to take-off and land in shorter runways [1].

## Trailing-Edge Flaps

Trailing-edge flaps operating in the linear-lift range change the lift of the basic airfoil by changing the effective airfoil angle of attack [83]. Moreover increase the camber and improve the flow at the trailing edge [6]. In Fig. 7.8, it can be seen the performance of the different types of trailing-edge flaps in relation to the aerodynamic effectiveness and mechanical complexity. The best type of flap in relation of aerodynamics is the one that provide the maximum lift increase lift with the minimum drag. Nevertheless, as the effectiveness increases, the more complex is the actuation mechanism of the device, implicating more weight, volume and design complexity.

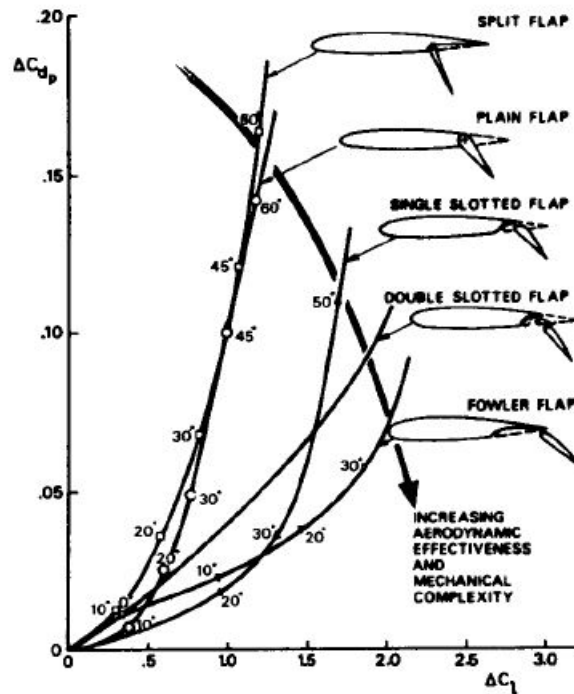


FIGURE 7.8: Trends in performance of trailing-edge flaps. Extracted from [6].

The different types of flaps, disposed in order from the less effectiveness to the most, are the following [1]:

- Split flap: consist of deflecting downward a stiffened plate on the lower surface of the airfoil without any change at the upper surface [13]. It is deflected by the rotation of a piano hinge just aft of the rear spar. It is very simple mechanically but the drag due to flap deflections is large, particularly in small

deflections [6]. The deflection of the split flap causes a wide wake to appear behind the airfoil. This large separation region prevents the realization of the full increase in circulation. The rate of lift is lower compared with other types and continuously is decreasing with increasing flap deflection because the wake widens as the flap deflection is increased [83].

- Plain flap: is an airfoil shape that is hinged at the trailing-edge of the wing such it can be rotated downward and upward (only is considered downward) without translation. Is the cheapest and easiest HLD to design and manufacture.
- Single slotted flap: similar configuration to the plain flap but with a slot that connects the intrados and the extrados. The leading-edge of a single-slotted modifies the boundary layer over the top surface of the wing, creating a new boundary layer over the flap which allow the flow to remain attached in high angle deflections. Moreover, slotted flap increase the effective chord of the wing.
- Double slotted flap: similar to the single slotted flap except that is divided in two segments instead of one. The second segment add another boundary layer permitting to deflect more the flap.
- Triple slotted flap: a third segment is added in the double slotted flap. It results in a high powerful HLD but requires a more complex mechanism. This type is used in heavyweight transport aircrafts
- Fowler flap: deflects downward and it translate the trailing-edge backwards, increasing the wing area. It generates the least amount of drag in comparison with the other flaps. Can be combined with slotted flaps. Double-slotted or triple-slotted fowler flaps give the best performance of all flaps, but are commonly used just in large aircrafts due to their complexity and weight.

### Leading-Edge Flaps

Leading-edge devices are beneficial to postpone the leading edge stall, but they are not commonly used on light aircrafts and small propeller transports due its complexity.

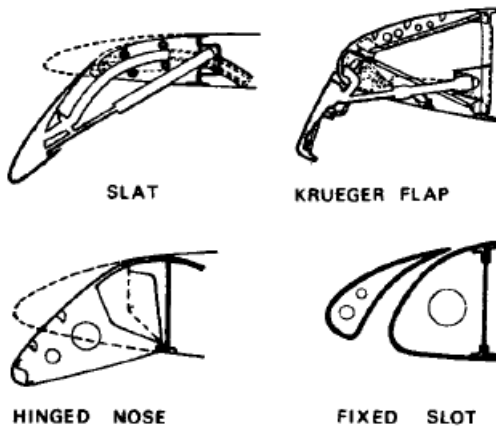


FIGURE 7.9: Top view of high-lift devices located on the leading-edge. Extracted from [6]

Following it is presented the different types of leading-edge flaps [1], [6].:

- Fixed slot: It has a slot that connects the intrados and the extrados, thus it controls the boundary layer in a similar way than the slotted flap. The air that goes through the slot prevents the detachment of the boundary layer near the LE.
- Slat: highly cambered airfoil forward the LE that modifies the speed field around the LE, decreasing the suction peak and delaying the detachment of the boundary layer.
- Krueger flaps: similar than the slat but thinner and more suitable for installation on thin wings. Usually it is located on the in-board part of wing with outboard slats to achieve longitudinal stability in the stall.
- Leading-edge flaps: less effective than slats. These flaps are suitable for thin airfoil sections.

#### 7.4.4 High-Lift Devices chord ( $C_f$ ) [1]

As it can be seen in Fig. 7.7, the chord of the HLD is determined as the ratio between the chord of the flap and wing chord ( $c_f/c$ ). During take-off and landing, the least amount of wing chord must be intended for HLD. Therefore, it is an

equilibrium process between balance drag and lift. The HLD chord must not be so high that the drag increment because due to its deflection nullifies its advantages. Also must have a minimum chord to achieve the necessary lift increment for the manoeuvres that this devices are designed for.

Moreover, HLD chord is a parameter related to the span and they can be interchanged to some extent. If design needs are to set a bigger aileron (reduction of HLD span), for maintaining HLD surface the chord can be increased. In tapered wings, HLD have to be tapered as well and does not have a constant chord along the span.

An usual value for initial sizing, is to allocate HLD 20% of the wing chord.

#### 7.4.5 High-Lift Devices span ( $b_f$ )

As it can be seen in Fig. 7.7, the span of HLD is the length of the total semi-wing span which the device is occupying. Generally these length is the maximum in order to leverage the useful surface and the outer limit of the flap is where the aileron surface begins. Therefore, the HLD span depends on the aircraft lateral controllability requirements. For low-speed general aviation aircraft utilize about 30% of the total semispan for ailerons [1].

HLD span is usually expressed as the ratio between flap span and net wing span,  $b_f/b$ .

#### 7.4.6 High-Lift Devices maximum deflection ( $\delta_{f_{max}}$ )

The deflection of the HDL is the angle that the flap is deflected respect the chord line of the airfoil (see Fig. 7.10). The amount of deflection affects directly on the amount of incremental flap lift.

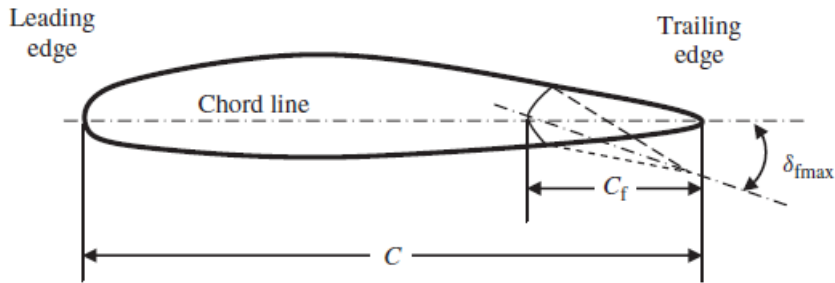


FIGURE 7.10: Side view of the inboard wing parameters with the flap deflected.

Extracted from [1]

The usual values of deflection in landing operation for the different types of flaps is presented in Tab. 7.6.

Flap type	$\delta_{f_{max}}$ [°]
Plain flap	60
Slotted flap	40
Fowler flap	40
Double slotted flap	50
Triple slotted flap	40

TABLE 7.6: Typical flap deflection at landing operation for different types of flap. Extracted from [14].

### 7.4.7 Flap Sizing Method

In this section it is developed a method which permits to size the aerodynamic HLD parameters (location, type, chord, span and deflection) according to the methods described in [14], [3] and [15] considering only trailing-edge flaps sizing in landing manoeuvre as operational condition, because it is the determining configuration where more lift increase is required.

#### Methodology

For this sizing method is used the algorithm showed in Fig. 7.11. It is an iterative process assuming various initial parameters ( $V_c$ ,  $V_{mo}$ ,  $V_s$ ,  $MTOW$ ,  $MLW$ ) and the

wing geometry (chord, span and  $C_{L, clean}$ ) is determined. The later is determined in previous sections and the results are used to develop the flap sizing.

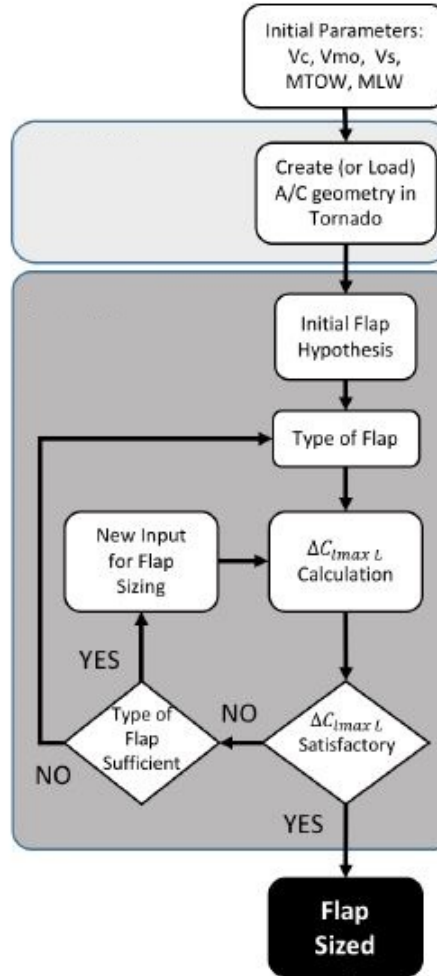


FIGURE 7.11: Algorithm used in flap sizing method. Based on [14] and [15].

The flap sizing process iterates within acceptable range of values of Span Ratio and Chord Ratio, shown in Tab. 7.7. The maximum deflection angle for each type of flap is presented in Tab. 7.6 and will not vary during the process. It is selected the maximum deflection at each type because it is the condition when is developed the maximum lift required for the landing operation.

Flap Parameter	Acceptable interval
Span Ratio, $\frac{b_f}{b}$	0.55 - 0.85
Chord Ratio, $\frac{c_f}{c}$	0.15 - 0.45

TABLE 7.7: Flap acceptable range of values [3].

The span-wise position ratio,  $b_{if}/b$  (i.e. the ratio between the distance from the  $x_{body}$  axis to the starting point of the flap and the wing span) will be determined according to the diameter of the fuselage obtained in Sec. 6.

The types of flaps considered for the iterative process will be Plain, Single Slotted and Fowler. The process start with the Plain flap and iterates with the flap span and chord ratio until  $\Delta C_{L_{max,L}}$  is satisfactory to accomplish with the  $C_{L_{max,L}}$  required for landing. If it is not satisfactory the the flap span and chord ratio increase until the maximum value is achieved. If the type of flap is not sufficient to reach the maximum lift coefficient for landing, it is changed to the Single Slotted, according to the performance of trailing-edge flaps in Fig. 7.8. Finally, if the Single Slotted is not sufficient, it is sized with the Fowler flap.

## Method

At landing operation the aircraft must have extra lift for land at low velocities. Apart from the lift generated by the clean wing it is required the lift by the HLD.

$$C_{L_{max,L}} = C_{L_{max,clean}} + 0.95\Delta C_{L_{max,L}} \quad (7.2)$$

The maximum lift coefficient at landing operation,  $C_{L_{max,L}}$ , is the maximum wing lift coefficient at clean configuration (landing gear and flaps retracted),  $C_{L_{max,clean}}$ , plus the increase of HLD in landing configuration,  $\Delta C_{L_{max,L}}$ .  $C_{L_{max,L}}$  is the lift coefficient required to sustain the aircraft at the velocity required to land,  $V_s$ , and it can be calculated with Eq. (7.3).

$$C_{L_{max,L}} = \frac{2W_L}{\rho_0 V s^2 S_W} \quad (7.3)$$

Where the landing weight obtained at Sec. 3.3,  $W_L$  is considered. Also air density at sea level, stall speed at landing,  $V_s$ , and the surface of the wing,  $S_W$  are used.  $V_s$  is obtained as FAR-23 Regulations set in landing operation and it is calculated as  $V_s = \sqrt{\frac{s_L}{0.5136}}$ , where  $s_L$  is the landing field length.

$C_{L_{max,clean}}$  is determined with the simulations of the wing obtained in Sec. 7.3.3.  $\Delta C_{L_{max,L}}$  is determined with Eq. (7.4) which relate the wing lift coefficient increase

with the airfoil lift coefficient. A factor of 0.95 is taken into account for the trim penalty introduced for the use of flaps [14].

$$\Delta C_{L_{max_L}} = \Delta C_{l_{max_L}} K_{\Lambda} \frac{S_f}{S_W} \quad (7.4)$$

According to [3],  $K_{\Lambda}$  is a factor that accounts the effect of the sweep angle in the flaps down case and it is computed as  $K_{\Lambda} = (1 - 0.08\cos^2(\Lambda_{c/4}))\cos^{3/4}(\Lambda_{c/4})$ . The last element,  $S_f/S_W$  is the ratio between flap usable surface and wing surface for straight tapered wings, as it can be seen in Fig. 7.12.

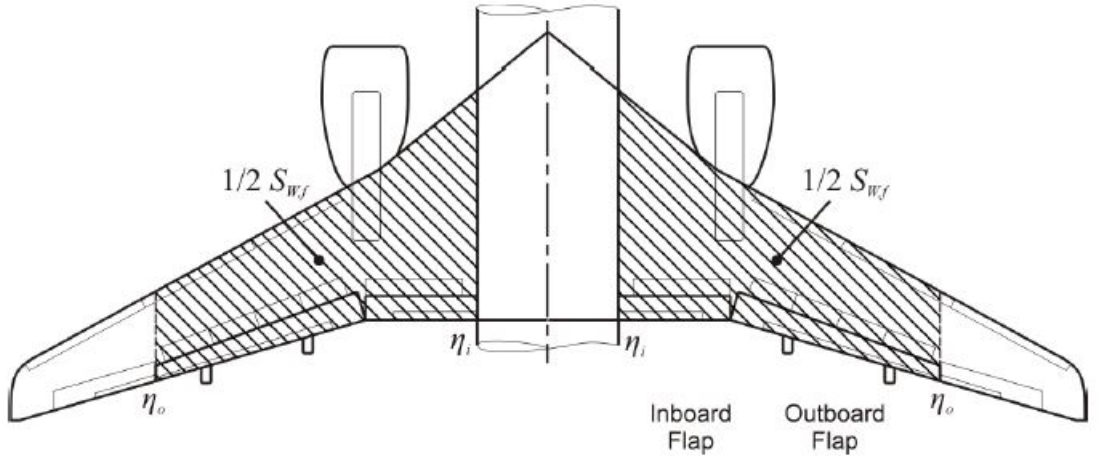


FIGURE 7.12: Definition of flap surface ( $S_f$ ). Extracted from [16]

According to [3], it can be calculated as Eq. (7.5).

$$\frac{S_f}{S_W} = \frac{(\eta_o - \eta_i)(2 - (1 - \lambda)(\eta_i + \eta_o))}{(1 + \lambda)} \quad (7.5)$$

$\eta_i$  is the inner point of the flap span and  $\eta_o$  the outer.  $\Delta C_{l_{max_L}}$  depends on the type of flap used. For Plain flaps:

$$\Delta C_{l_{max_L}} = C_{l_{\delta_f}} \delta_f K' K \quad (7.6)$$

, where  $C_{l_{\delta_f}}$  is the airfoil lift coefficient depending to the flap deflection and the thickness ratio. It can be obtained with Fig. 7.13.

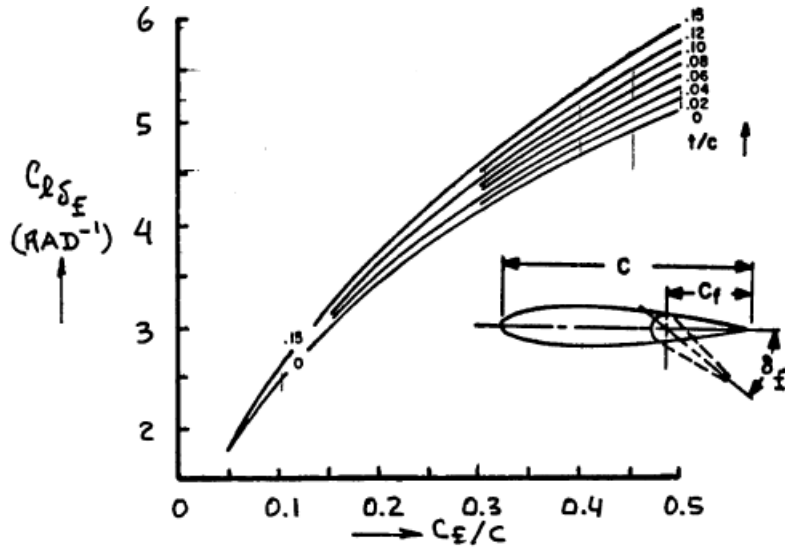


FIGURE 7.13: Effect of Thickness Ratio and Flap Chord Ratio on  $C_{l\delta_f}$ . Extracted from [3].

$\delta_f$  is the flap deflection angle. The value change for the different types of flap and it can be found in Tab. 7.6. The parameter  $K'$  is a correction which depend on the flap chord ratio and the deflection angle and it can be obtained from Fig. 7.14.

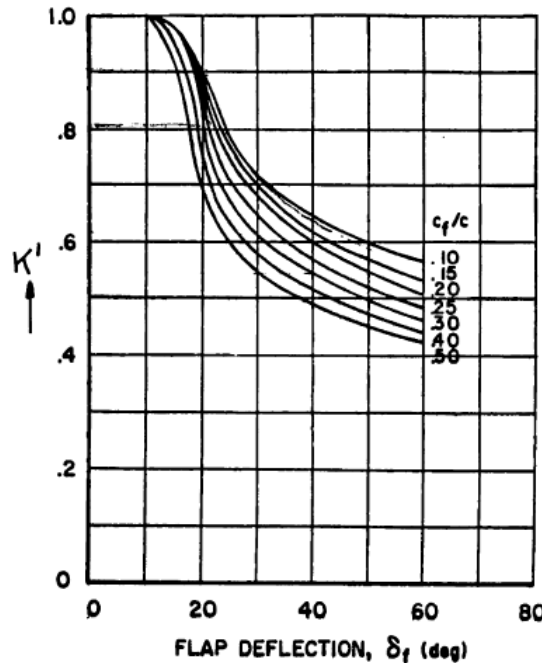


FIGURE 7.14: Effect of Flap Chord Ratio and Flap Deflection on  $K'$ . Extracted from [3].

$K$  is the semi-empirical parameter which is the ratio between  $\Delta C_{l_{max}}$  and  $\Delta C_l$  and depends on the type of flap and the flap chord ratio. It can be obtained from

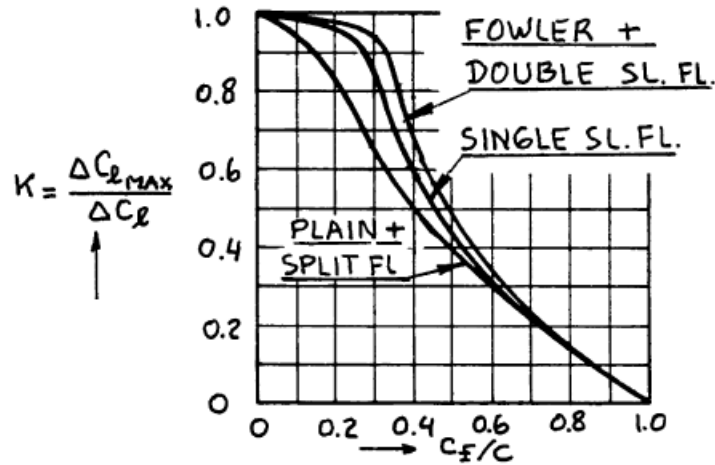


FIGURE 7.15: Effect of Flap Chord Ratio and Flap Type on  $K$ . Extracted from [3].

For Single Slotted Flap:

$$\Delta C_{l_{max,L}} = C_{l_{\alpha_f}} \alpha_{\delta_f} \delta_f K = 1.8\pi \left( 1 + 0.8 \frac{t}{c} \right) \left( 1 + 2 \left( \frac{z_{fh}}{c} \right) \tan \left( \frac{\delta_f}{2} \right) \right) \alpha_{\delta_f} \delta_f K \quad (7.7)$$

, where  $\frac{z_{fh}}{c}$  is the geometrical parameter represented in Fig. 7.16. And the  $\alpha_{\delta_f}$  coefficient is the Section Lift Effectiveness Parameter for Single Slotted Flaps depending on the flap deflection angle and it is obtained from Fig. 7.17.

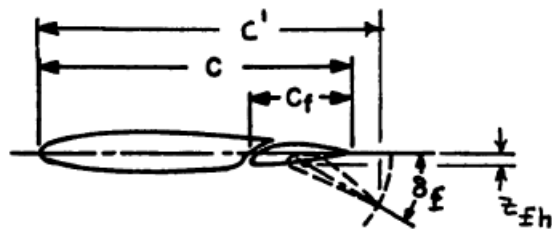


FIGURE 7.16: Geometrical parameters on Single Slotted Flap

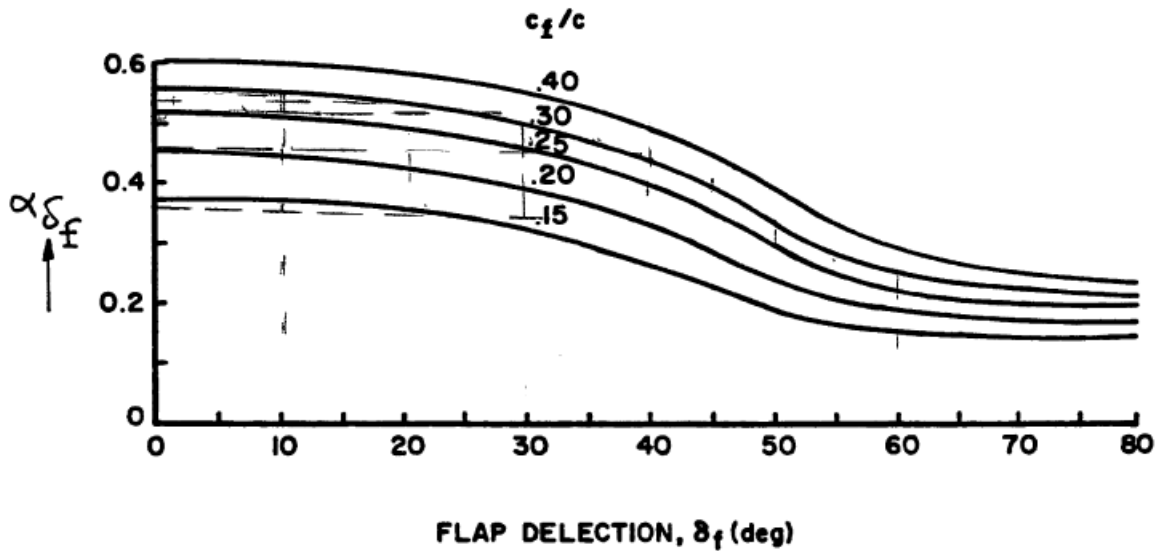


FIGURE 7.17: Section Lift Effectiveness Parameter for Single Slotted Flaps.  
Extracted from [3].

And for Fowler flaps:

$$\Delta C_{l_{max_L}} = C_{l_{\alpha_f}} \alpha_{\delta_f} \delta_f K = 1.8\pi \left(1 + 0.8 \frac{t}{c}\right) \left(1 + \frac{c_f}{c}\right) \alpha_{\delta_f} \delta_f K \quad (7.8)$$

If the calculated  $\Delta C_{l_{max_L}}$  satisfies the required value obtained from Eq. (7.3), the flap is sized. If not, an iterative process is afterwards carried out in all three levels (top to bottom): flap chord ratio, span chord ratio and flap type, until a final configuration with the parameters within the acceptable range defined in Tab. 7.7 is reached [14].

## Results

After the methodology is explained, a MATLAB ®code is carried out. The script is available on Appendix E.5 and the results are presented below:

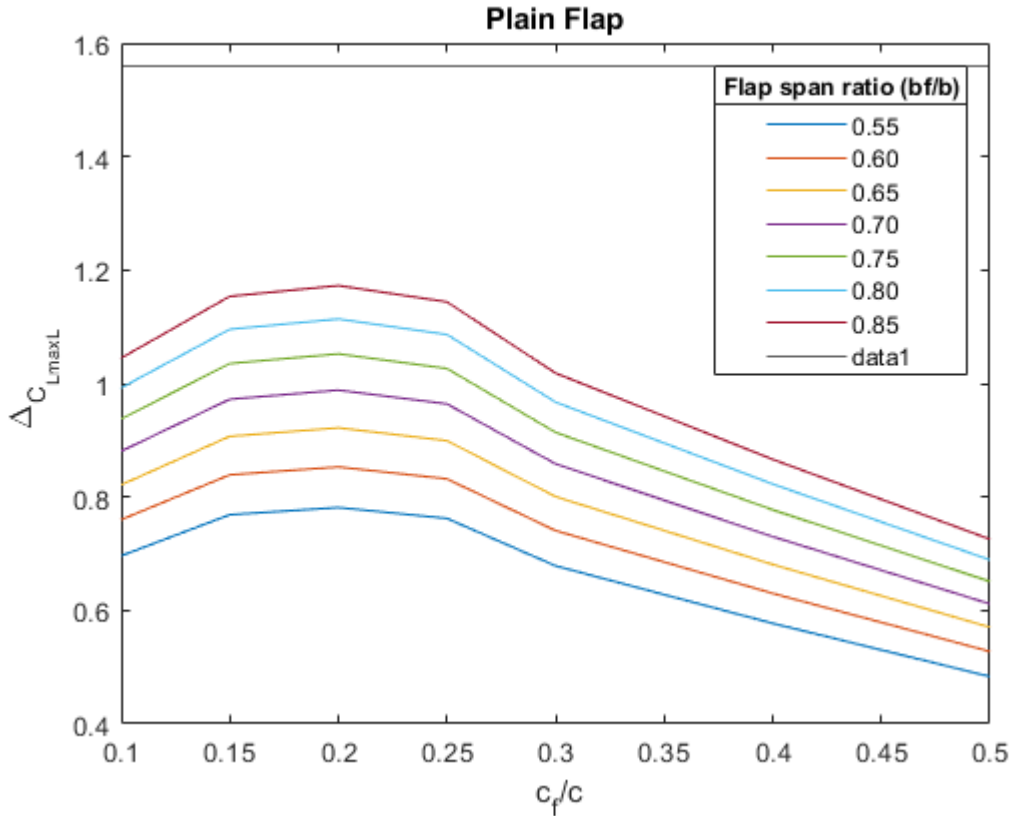


FIGURE 7.18: Results for Plain Flap type.

Fig. 7.18 shows the results of  $\Delta C_{L_{maxL}}$  for Plain Flap type for different flap span and chord ratio. The maximum value is achieved with a flap span ratio of 0.85 and with a flap chord ratio of 0.2. Any configuration of span or chord is able to reach the desired value of  $\Delta C_{L_{maxL}} = 1.56$  resulting from the equation Eq. (7.3) so this type of flap is discarded.

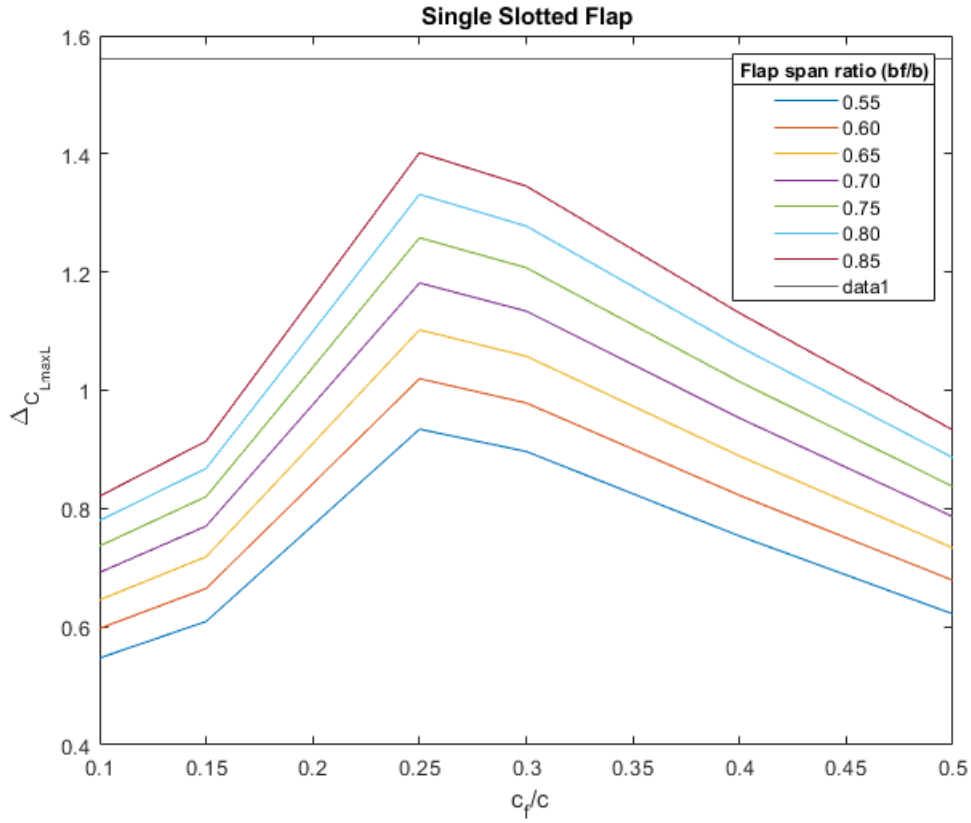


FIGURE 7.19: Results for Single Slotted Flap type.

Fig. 7.19 shows the results of  $\Delta C_{L_{maxL}}$  for Single Slotted Flap type for different flap span and chord ratio. The maximum value is achieved with a flap span ratio of 0.85 and with a flap chord ratio of 0.25. Any configuration of span or chord is able to reach the desired value of  $\Delta C_{L_{maxL}} = 1.56$  resulting from the equation Eq. (7.3) so this type of flap is discarded.

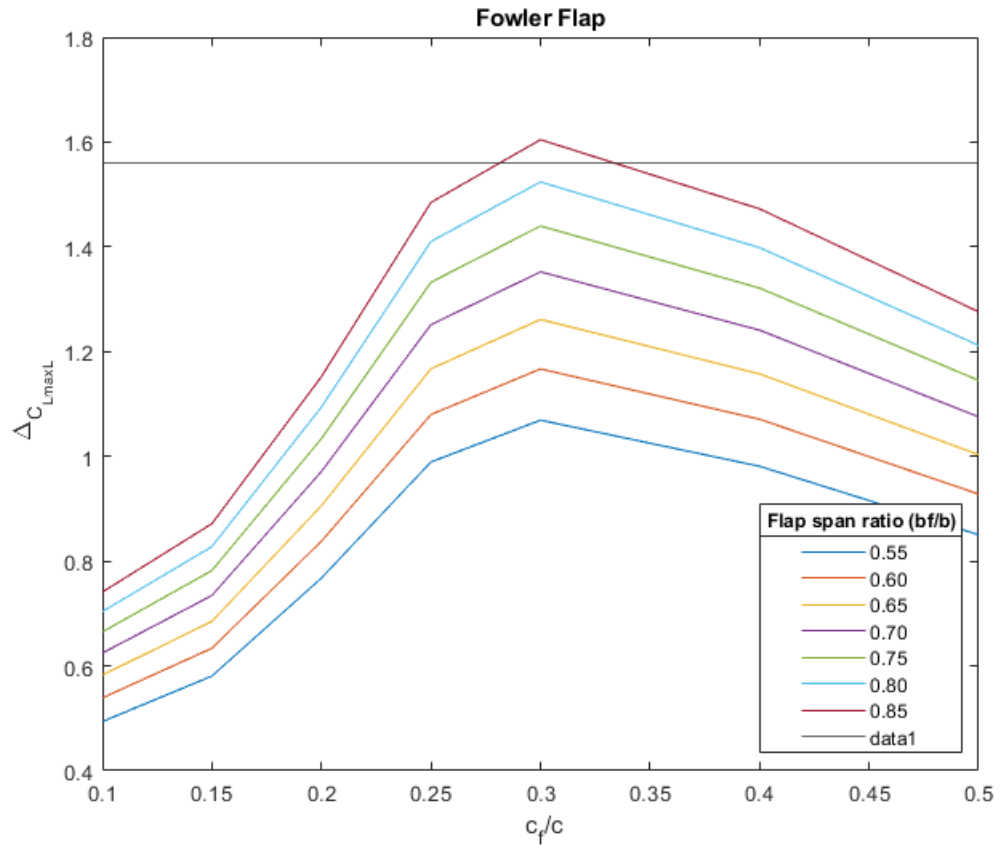


FIGURE 7.20: Results for Fowler Flap type.

Fig. 7.20 shows the results of  $\Delta C_{L_{maxL}}$  for Fowler Flap type for different flap span and chord ratio. The maximum value is achieved with a flap span ratio of 0.85 and with a flap chord ratio of 0.3. With this configuration of span or chord is able to reach the desired value of  $\Delta C_{L_{maxL}} = 1.56$  resulting from the equation Eq. (7.3) so this type of flap is valid.

Once the results are presented it can be seen that the the flap span ratio is bigger than the span usually utilized for aircrafts which is 70%, mentioned in Sec. 7.4.5. Seeing that with the sizing method applied only is possible to reach the  $\Delta C_{L_{maxL}}$  required for Fowler flaps at 85% of the span, it is proposed various solutions. The first one is the use of leading-edge devices, also called slats for increasing the lift coefficient required to land. With this solution it would be possible to reduce the trailing-edge flaps span, but it is out of scope. The other solution is to implement powerful trailing-edge devices such as Double or Triple Slotted Flap, or Double or Triple Slotted Fowler Flap. Using the later the aerodynamic

effectiveness would be increased but also the mechanical complexity. Since prevail the safety, efficiency and competitiveness against the complexity and costs of the project it is interesting to use more complex mechanisms for achieve a more quality and competitive aircraft relative to the market.

## 7.5 Conclusions

The final geometry consist on a 13m span single tapered wing, with a Taper Ratio is 0.75 to improve tip stall behaviour. The Aspect Ratio of 9.29 is close to the optimal Aspect Ratio previously studied. After the iterative process, sweep has been fixed at  $4.66^\circ$ , dihedral at  $2^\circ$  and twist at  $4^\circ$  for a surface of  $18.2m^2$ . These results aim to minimize the manufacturing costs and must be understood as a first approximation. Due to the numerical method used and software limitations, some hypothesis has been taken during the present section affecting the overall results. The geometric modifications of the wing introduced comply with the design point restrictions, reducing  $m_{TO}/S_W$  ratio. The final wing enables to fly in cruise conditions close to the optimal ones, even though different stages of the flight profile should be studied in a more detailed analysis.

Regarding the High-Lift Devices, the minimum type of flap required to accomplish the increase of lift for landing is a Fowler flap with span ratio of 0.85 and a chord ratio of 0.3. Above that it can be implemented a more complex and powerful type of flaps in order to be efficient and competitive in the market in more advanced stages of the design.

# Chapter 8

## Weight and balance

In this section the aerodynamic static stability and the weight centring of the aircraft will be done. Previously to the stability analysis the definition of the size and location of the horizontal and vertical tail plane will be done in Sec. [8.1](#) using similar airplanes method [\[84\]](#). The results will be validated calculating the stick fixed stability in straight flight in Sec. [8.1.3](#), using the results for presenting the limits of the CG based on this stability calculated, in Sec. [8.1.4](#). Once the empennage surfaces are known, the neutral point position will be determined, such as the weight estimation of the aircraft by main component groups. Using this method, the weight distribution and centring of the aircraft can be established. The maximum forward and aft position of the centre of gravity will be estimated and represented in a chart, as a function of the weight. Analysing the centre of gravity position, the stability margin of the model will be calculated.

### 8.1 Empennage design

The aim of the empennage is to create a force that acts upon a lever arm, consequently creating a moment (a pitch moment in case of the horizontal tailplane, and a yawing moment for the vertical tailplane. The objective of regulating this moments is to ensure trim, stability and control.

- **Trim** the moment created by the empennage balances out moments occurring on the aircraft for another reason. For example, the horizontal tailplane balances the wing moment.
- **Stability** refers to the capacity of the aircraft to return the original flying position after a disturbance.
- **Control** An aircraft must be sufficiently controllable in all critical flight states. the control forces should not be too extreme.

### 8.1.1 Horizontal tail sizing

Because the difficulty of calculating the conditions mentioned at the actual stage of the design, the first approximation to the design of the horizontal tailplane will be done using the volume coefficient [76]. This coefficient is defined in Eq. (8.1).

$$C_h = \frac{S_h l_h}{S_w c_{MAC}} \quad (8.1)$$

Being  $S_w$  and  $c_{MAC}$  dependent on the wing, for now it's needed an approximation of  $l_h$ . [40] proposes an average of 45...50% of the fuselage length for  $l_h$ , and a reduction factor of 5% for being the case of a T-tail. Finally, the conventional volume coefficients for transport jets are shown in Tab. 8.1.

TABLE 8.1: Tail volume coefficient values proposed by [40]

$C_h$	1
$C_h$	0.08

So, according to the correction of -5%, the resulting coefficients can be seen in Tab. 8.2.

TABLE 8.2: Corrected tail volume coefficients.

$C_h$	0.95
$C_v$	0.076

And, for this first calculations and the reasons explained,  $l_h$  is set to 8.78[m], considering the high rank of the average in order to reduce  $S_h$ .

For the other parameters of the horizontal tail, the conventional parameters proposed by [3] are shown in Tab. 8.3.

TABLE 8.3: Range of usual horizontal empennage geometric parameters

Dihedral	-4...9
Geometrical incidence	-3.5 [°]
Aspect ratio	3.2...6.3
Sweep	0...35 [deg]
Taper ratio	0.32...0.57

For selecting the parameters in the ranks known,  $A_h$  is set to the approximately the half of  $A_w$ , so  $A_h = 4$ , approximating to 4 trying to reduce this value in order to reduce the cost of building the horizontal empennage. The sweep angle can be 5 degrees less than  $\phi_W$ , so  $\phi_h = 10^\circ$  [84]. It is set  $\lambda_H = 0.45$ , in the margins proposed. Finally, NACA0009 and NACA0012 can be chosen as airfoils for the horizontal tailplane [85]. The dihedral angle of the horizontal empennage is set to  $v_h = 0$  for now. This parameter is used for preventing the horizontal be affected by the jet efflux, but for the T-tail this is not the case, and the affect in stability of this parameter can be neglected in front of the wing one [84].

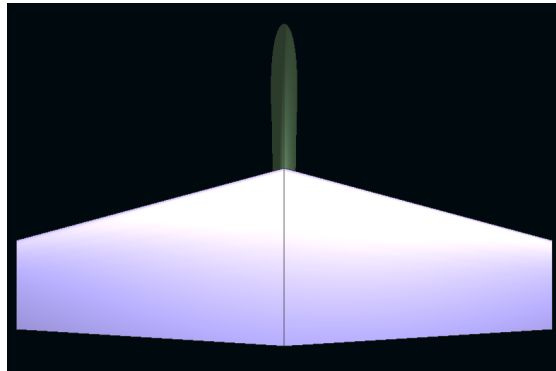


FIGURE 8.1: Sketch of the horizontal empennage preliminary design.

### 8.1.2 Vertical tailplane design

It can be designed following the same procedure and same references explained in Chap. 8.1.1. So, now the volume coefficient is defined as:

$$C_v = \frac{S_v l_v}{S_W b} \quad (8.2)$$

And the usual ranks of the parameters of the vertical tailplane are:

TABLE 8.4: Range of usual horizontal empennage geometric parameters

<b>Aspect ratio</b>	0.8...1.6
<b>Sweep</b>	28...55 [°]
<b>Taper ratio</b>	0.3...0.74

T-tails have smaller vertical tailplane aspect ratio than conventional tails, so for now  $A_v = 1$ . Considering the high speeds of the flight, the sweep angle of the vertical empennage can be  $\phi_v = 35^\circ$ , for preventing the transonic effects. Considering the rank explained, taper ratio will be considered as  $\lambda_v = 0.8$ . For symmetry in the  $xz$  plane reasons, a symmetrical airfoil has to be chosen for the vertical empennage. NACA 0009 and NACA 0012 will be considered [85].

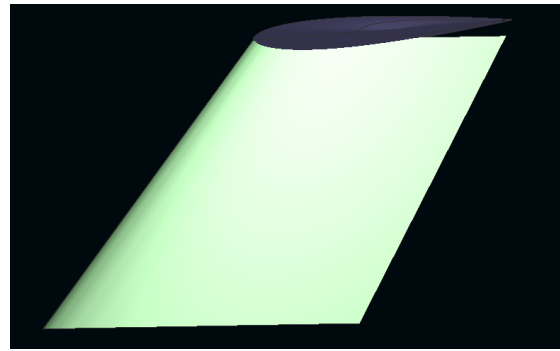


FIGURE 8.2: Sketch of the vertical empennage preliminary design.

### 8.1.3 Horizontal empennage validation with fixed controls static stability

To be sure that this similar airplanes approximation is valid for the VLJ being designed at the actual stage of the design, it is calculated the aerodynamic performance of the wing-empennage combination using ring vortex method. If the horizontal empennage is suitable for the design, the condition of fixed controls static stability should be accomplished for an acceptable range of rear CG limit position:

$$C_{m\alpha} < 0; \quad (8.3)$$

So, for the rear CG limit,  $C_{m\alpha} = 0$  and the vehicle is indifferent in fixed controls static stability. Ring vortex method provides the  $C_m$  of the solid studied, then some CG positions were tested in order to find the limitation position explained.

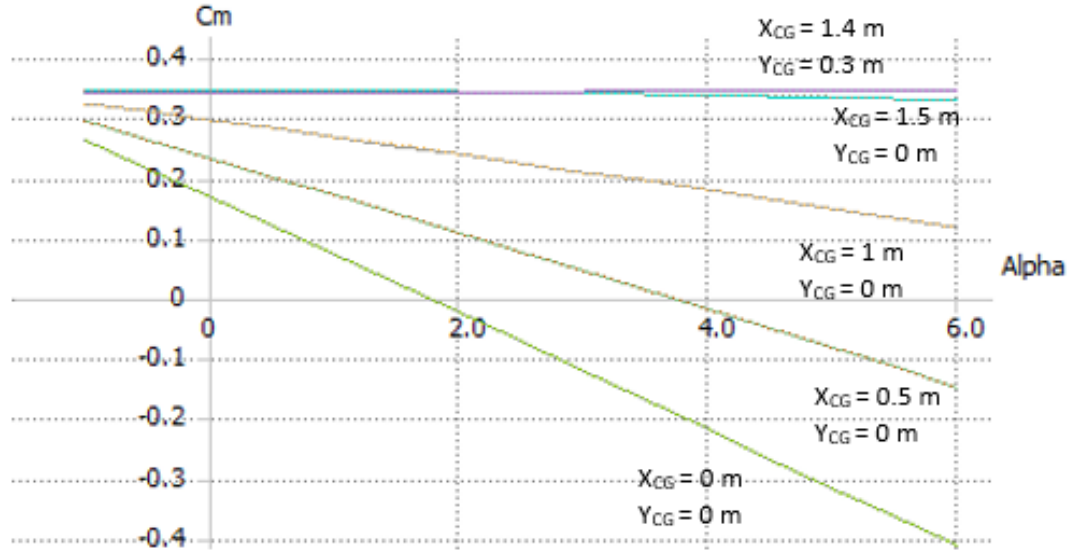


FIGURE 8.3: Results of the  $C_m$  analysis with different positions of the CG and NACA0009 and NACA0012 profiles.

In Fig. 8.3 can be seen that the behaviour of the two profiles tested is extremely similar. For this, NACA0012 is selected as profile for the empennage, for the major thickness. With this, is expected to reduce the building cost comparing to NACA009. After this fact, it is observed that the  $C_m(\alpha)$  graph is practically horizontal for an  $x_{CG} = 1.4$ . With this position, it is also tested the height of the CG, getting a maximum value of 0.3 m. So, this simulation gives two facts: The most rear and high position possible for the CG of the airplane, and the verification of the fact that the actual design of the empennage is a good first approximation for the design. As commented in Chap. 7, this approximation has to be improved on later stages of the design, when doing CFD simulations, the study and simulation of the static and dynamic stability under other conditions, structural restrictions...

### 8.1.4 Aerodynamic CG limits

As explained in Sec. 8.1.3, the aerodynamic CG limits considered for the preliminary design are:

TABLE 8.5: Aerodynamic CG limits

$x_{CG}$	1.4 m
$z_{CG}$	0.3 m

The  $y$  position of the CG has been taken as obvious for the fact that has to be the most similar to 0 possible, otherwise it would be needed to deflect the vertical stabilizer to keep the flight trimmed flying with  $\beta = 0$ , causing also a torque on the  $x$  axis, needed to be compensated with spoilers, as explained in [86], complicating a lot the flight mechanics.

The forward limits of the CG has not been contemplated in this study, because as it can be seen in [3], they depend on other conditions of static stability, as Stick Fixed Maneuver Stability.

## 8.2 Loading CG limits

The purpose of this section is the preliminary centre of gravity estimation of the aircraft. For this reason, a first class weight and balance method was used, as explained in [3].

### 8.2.1 Weight estimation of major inertial parts of the aircraft

For a better approximation of the centre of mass, the weight and position of each major component should be known. The applied method uses a weight breakdown estimation based on historical data of similar very light business jets. The weight of the main components of the aircraft is calculated for the following major groups: the fuselage group, the wing group, the empennage group, main equipment, landing gear, crew, passengers, baggage, cargo and fuel. The sum of the weight of the

fuselage, the wing, the empennage, equipment, landing gear, crew and reserved fuel must give the Operating Empty Weight.

In [3], [87] and [57] similar aircraft data was found to estimate the weight of the parts of a business jet as percents of the Maximum Take-off Weight, with a margin of 10 % approximately, see Tab. 8.6. The *MTOW* of the aircraft was found in

Parts	Wing	Fuselage	Empennage	LG	Engine	Equipment
% MTOW	9,8	10,5	2,4	3,9	8,2	16,6

TABLE 8.6: Participation of the main components in the Maximum Take Off Weight

previous sections Sec. 3.3.1, so from the above presented values the preliminary weight of each main group can be easily calculated, as represented in Tab. 8.7. The estimated Empty Weight of the aircraft after applying the 1.1 correction fac-

Parts	Wing	Fuselage	Empen.	LG	Engine	Equipment
Mass (kg)	546	585	134	218	456	925
Corr. Mass (kg)	600	644	147	240	502	1018

TABLE 8.7: Main Components Weight Estimation

tor results 3151 kg, which goes up to the previously estimated Operating Empty Weight of 3495 kg after adding the estimated crew and reserve fuel weight.

The above mentioned components were divided into smaller parts in order to estimate their weights as punctual masses. As the aircraft was considered perfectly symmetrical, the Y coordinate of the mass positions were taken as 0. For extended structures such as fuselage, wing and empennage stabilizers the centre of mass was estimated as proposed Roskam [3], shown in Fig. 8.4. The centre of gravity of the wing was placed at 40% of the Mean Aerodynamic Chord (MAC), as it is an intermediate value of the CG range that proposes Roskam. The centre of mass for the horizontal and vertical tail plane was considered as 30% of the MAC of each component. The shape of the fuselage has a huge influence on the CG [3]. The designed very light jet has a cabin type fuselage which centre of mass position can be considered as 39-40% of the total fuselage length. Other components weight, such as Landing Gear (LG), Engine and Equipment was estimated using [3] and [87], placing the main landing gear in an rearward position near the wing, and the nose LG under the cockpit. The engine location is rear-mounted, explained in Sec. 2.1.3, considering that its centre of mass is placed almost in the middle of

the engine, where it has its major cross section diameter. As the vast majority of the equipment is placed in the forward part of the aircraft - cockpit, at the beginning of the fuselage under the passenger's cabin, its mass centre was found at approximately 33% of the fuselage length. Using the obtained data, the centre

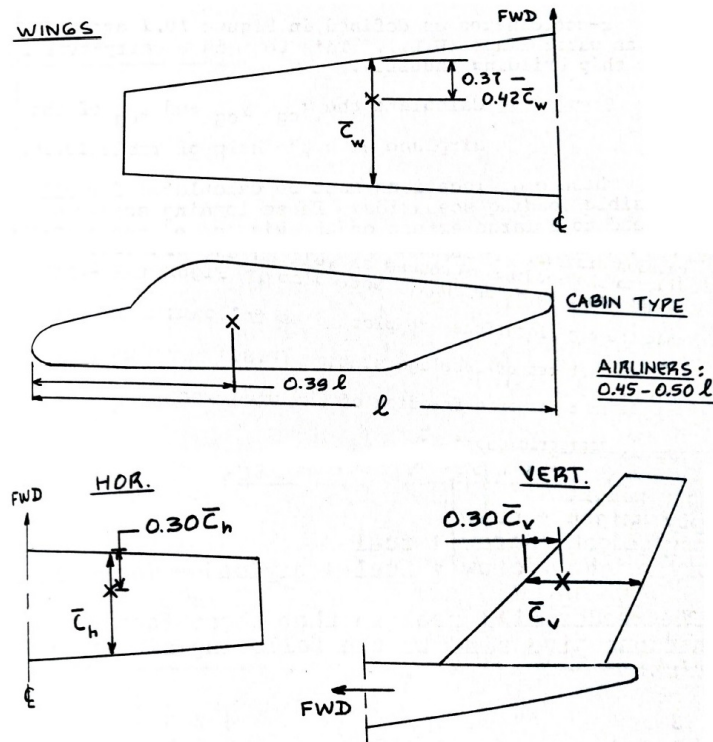


FIGURE 8.4: Position of the centre of gravity of major components

of gravity of the whole aircraft can be estimated for Empty Weight.

### 8.2.2 Fuel and Payload weight estimation

After the Empty Weight was calculated, it is necessary to estimate the weight of the fuel and payload. The payload weight has been determined previously in Tab. 3.8. As stated, the Maximum Payload Weight will be 827 kg, the weight of the passengers has been considered as 91,13 kg and of their baggage as 13 kg. The seating for the passengers can be seen in Appendix B, when cargo compartments are placed before and after the wing under the passenger's cabin or before and after the fuselage fuel tank if there is any, as suggested in Sec. 6.1. The maximum fuel weight was also determined in Sec. 3.3.4 as 1868 kg. The reserve fuel weight depends highly on the mission of the aircraft, for this reason its value was not

specified, but its maximum value was considered, as 122 kg. The usable maximum fuel result 1746 kg, which will be placed in the torque box of the aircraft's wing or in case it results insufficient, in the fuselage in separate tanks, see Sec. 6.3.4. The wing and empennage fuel volume must be estimated in order to determine if there is enough place to carry the required fuel.

### Wing and Empennage Fuel Volume Calculations

After the parameters of the wing are known (see Sec. 4.2), the usable volume can be estimated, as stated in [3]:

$$V_{WF} = 0,54 \cdot (S^2/b) \cdot (t/c)_r \left[ (1 + \lambda_w \tau_w^{0,5} + \lambda_w^2 \tau_w) / (1 + \lambda_w)^2 \right] \quad (8.4)$$

Eq. (8.4) is based on statistical data, and the given results have an error of approximately 10 %, which is acceptable in a preliminary design. This estimation gives the volume of the wet wing, space between the front and the rear spar, and takes into account lightning prevention as well: there is no fuel placed beyond 0,85 times the wingspan. In the previous equation  $\tau_w$  means the fraction of the profile thickness ratio of the tip and the root profile,  $\frac{(t/c)_t}{(t/c)_r}$ . The resulting fuel volume gives a result of  $1,247 \text{ m}^3$ . The weight of Jet A-1 that the wing can accommodate is around 1050 kg, as the equation may have an error of 10% only 945 kg is considered - so an other 800 kg must be placed in the fuselage. For this reason a  $1 \text{ m}^3$  tank will be placed under the cabin, near the centre of gravity of the aircraft. For checking the available empennage fuel volume, it will be also calculated using Eq. (8.4). The estimation gives a fuel volume of  $0,166 \text{ m}^3$ , which means 139 kg of fuel, which is higher than the previously determined maximum reserve fuel quantity.

#### 8.2.3 Centre of Gravity position

At this point of the design all the major weights and their positions have been estimated so the centre of gravity of the whole aircraft can be calculated. As a first step, the weight excursion diagram, see Fig. 8.5 was elaborated for five different loading conditions: for Operating Empty Weight (OEW), OEW and

Maximum Fuel Weight, OEW and Maximum Payload Weight, Maximum Take-Off Weight (MTOW) with Maximum Fuel Weight, and finally, MTOW with Maximum Payload Weight. The resulted most forward and most aft position of the mass

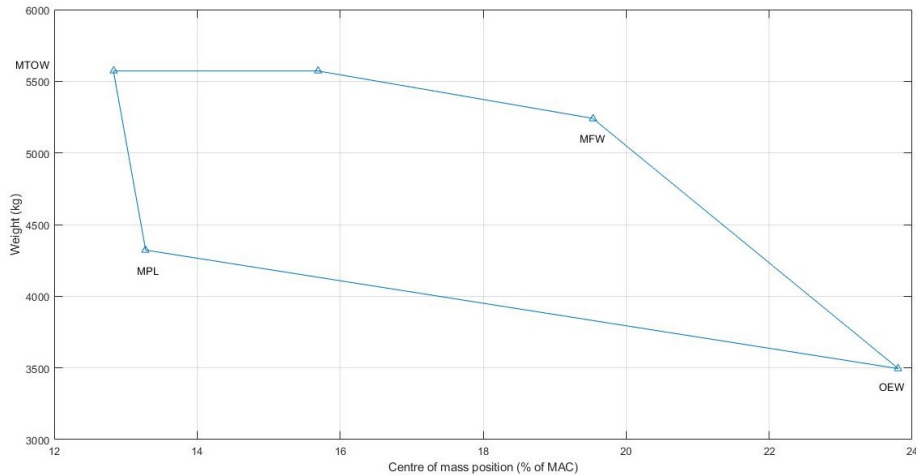


FIGURE 8.5: Centre of gravity excursion diagram

centre of the very light jet aircraft were found at 12,8 % and 23,8% of the Mean Aerodynamic Chord. This result was used to elaborate the permissible centre of gravity range diagram for any operating condition, as represented in Fig. 8.6. Comparing the obtained centre of mass positions with the neutral point position estimated in the longitudinal static stability analysis, the stability of the aircraft can be demonstrated. The maximum aft position of the CG is found at 23,8 % of the MAC, while the neutral point at 1,4 metres after the leading edge of the wing root airfoil, which is 81,42 % expressed as percentage of the MAC. As the neutral point is located in an afterward position respect to the CG, the aircraft is found stable for all operating loading conditions.

### 8.3 Conclusions

Resuming the obtained results, first the horizontal and the vertical tail plane sizing was elaborated, based on the volume coefficient of each one. The calculated parameters of the horizontal tail plane are represented in Sec. 8.1.1, and the geometric parameters of the vertical tail are calculated in Sec. 8.1.2, and summarized in the following table:

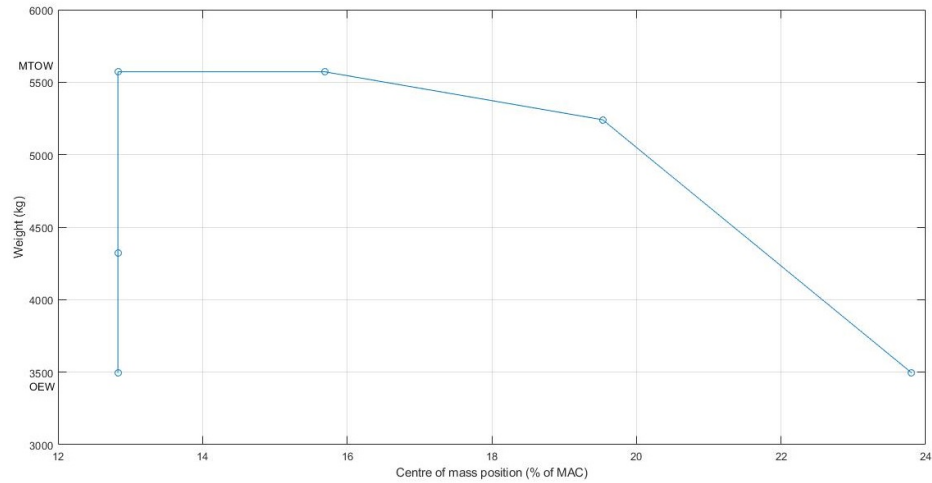


FIGURE 8.6: Permissible operating centre of gravity range

TABLE 8.8: Empennage geometric parameters

	Horizontal tail	Vertical tail
<b>Dihedral</b>	0	-
<b>Geometrical incidence</b>	-3.5 [°]	0
<b>Aspect ratio</b>	4	1
<b>Sweep</b>	10 [°]	35 [°]
<b>Taper ratio</b>	0.45	0.8

In Sec. 8.1.3, horizontal empennage has been validated for the static stability point with fixed stick using the calculations of XFLR5 Vortex Method, obtaining a margin of 1.4[m] after the leading edge of the wing in the root, and in the  $x$  direction. A maximum height for this limit of 0.3[m], as presented in Tab. 8.5. It can be noticed that this is a large range for the CG limits, so in later steps of the project the empennage has to be validated calculating stability under other conditions, and study if it can be reduced for saving weight and drag keeping good margins for the CH position.

After the fixed control longitudinal static stability analysis, the weight estimation of each main component group was carried out, see results in Tab. 8.9. Using

Parts	Wing	Fuselage	Empen.	LG	Engine	Equipment
Mass (kg)	600	644	147	240	502	1018

TABLE 8.9: Main Components Mass

Roskam's [3] component centre of mass estimation method and calculating the distribution of the fuel and payload weights - based on the previously determined maximum fuel and payload weights - the centring of the whole aircraft was elaborated. The centre of gravity range of the very light jet aircraft was represented as percents of the Mean Aerodynamic Chord. Its value varies between 12,8 and 23,8 %. Comparing this interval with the neutral point of the static analysis, it can be stated that the designed aircraft is statically stable - as the neutral point is found in a rearward position (81,42% of MAC) respect to the mass for any operating conditions. The difference between the centre of gravity and the neutral point is the static margin, represented in Fig. 8.7.

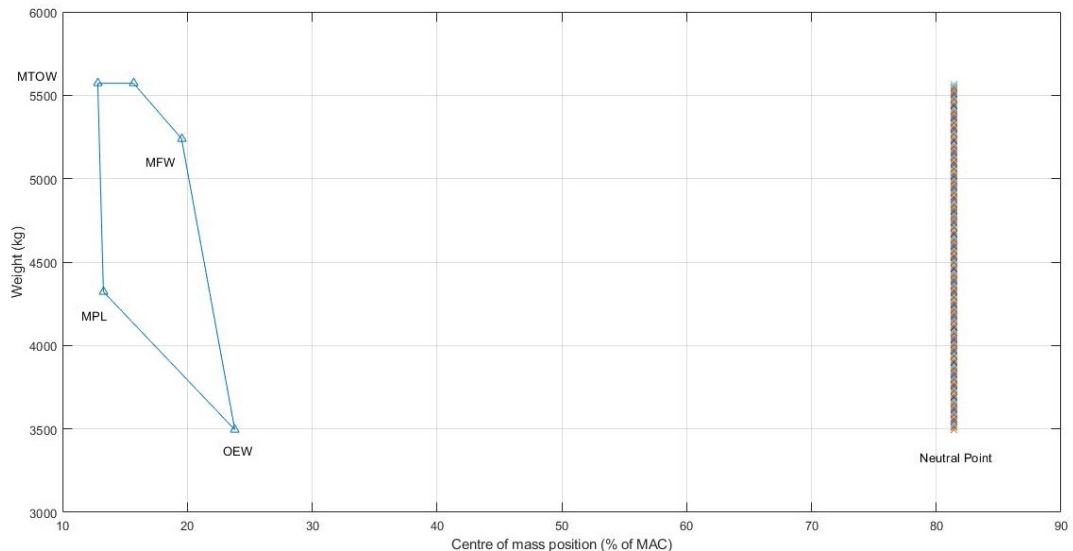


FIGURE 8.7: Centre of gravity variation for different operating loading conditions compared with the neutral point position

# Chapter 9

## Landing gear design

The undercarriage must be designed in order to absorb a certain amount of energy, to ensure that any part of the aircraft does not touch the ground during taxiing, lift-off and touchdown, and to avoid instabilities during extreme operations, such as maximum braking effort, crosswind landings and high-speed taxiing. Moreover, the undercarriage characteristics must consider the loads that it will transmit to airfields, as that will limit the airports in which it will be able to operate. This chapter will study an initial approach to the undercarriage layout, starting from the configuration decided in Sec. 2.1.5, but without getting inside the design of its structure. Other systems related to landing gears, such as the retraction system or the braking/anti-skid system, will not be studied as they are out of the scope of this preliminary design.

Sec. 9.1 explains how the different landing gear legs locations have been established from the boundaries based on stability, manoeuvrability and security conditions during taxiing, lift-off and touchdown. Sec. 9.1 also shows how the static deflection of the main landing gear can affect the different parameters that define its layout, given that this variable is not known yet and will not be analysed in this preliminary design. Once the main parameters of the undercarriage are known, Sec. 9.2 will discuss the placing of one or two wheels per leg, as well as the different variables that determine the *LCN* of the aircraft and how they affect on this value.

## 9.1 Landing gear disposition

The disposition of the wheels for a tricycle undercarriage can be determined from different conditions:

- Angles of pitch and roll during takeoff and landing
- Stability at touchdown and during taxiing

### 9.1.1 Angles of pitch and roll during takeoff and landing

The aircraft may land or takeoff with some roll and pitch angles, so *LG* legs must be high enough to guarantee that any part of the aircraft will come into contact with the ground.

As a first approach, Torenbeek [6] explains that the pitch angle for liftoff (considered to be the same as the guard angle at this stage of the project), assuming that slats are not present, can be obtained from Eq. (9.1).

$$\theta_{LOF} = 7\left(1 + \frac{3}{A}\right) \quad (deg.) \quad (9.1)$$

Once the  $\theta_{LOF}$  is calculated, taking into account that the roll angle the aircraft can assume is  $8^\circ$  for transport ones, the first relation between the track and the *LG* height is obtained in Eq. (9.2). This equation is obtained when imposing that the wing tip touches the ground on a touchdown maneuver (it has been assumed that the downward movement of the wing tip can be neglected due to the small wingspan).

$$\tan\phi = \tan\Gamma + \frac{2h_g}{b - t} - \tan\theta \tan\Lambda \quad (9.2)$$

Given that there is not enough information yet, Torenbeek [6] suggests that the pitch angle on touchdown may be assumed equal to the liftoff one ( $\theta_{TD} = \theta_{LOF}$ ), and so this value can be used in Eq. (9.2).

### 9.1.2 Stability at touchdown

When taking the first contact on the ground with the highest possible pitch angle and the centre of gravity in its most rearward and highest location (which can be seen in Sec. 8.1.4 and Sec. 8.2.3), the projection of the centre of gravity cannot be behind the main landing gear, otherwise all forces acting in that instant would cause a moment driving the tail to touch the ground. This condition restricts the horizontal distance between the most rearward *CG* and *MLG* positions, as it can be seen in Fig. 9.2. Eq. (9.3) shows how to calculate this distance.

$$l_m \geq (h_{cg} + e_s) \tan \theta_{TD} \quad (9.3)$$

For this preliminary design, a 10% of margin has been applied to the  $l_m$  obtained taking Eq. (9.3) as an equality.

### 9.1.3 Nose landing gear position

For the *NLG* location, Torenbeek [6] explains: "When the load on the nosewheel is less than about 8% of the *MTOW*, controllability on the ground and stability during taxiing will suffer, particularly in crosswind conditions. When the static load on the nosewheel exceeds about 15% of the *MTOW*, the load during heavy braking may become excessive, braking may be less efficient, and too much effort may be required for steering". It must be noticed that these limits depend on the *CG* location, so each boundary has to be obtained using the most limiting condition and so giving the smallest possible range for the *NLG* location: the 8% condition will be obtained from the most rearward *CG* location, and the 15% from the most forward *CG* position; this data can be extracted from Sec. 8.2.3, resulting in 12.83% and 23.81% of the *MAC* (backwards the aerodynamic centre). Taking these premises and with the support of Fig. 9.1, the two boundaries can be obtained from a balance of forces and moments. The resulting equations are Eq. (9.4) and Eq. (9.5).

$$l_{n1} = (l_m + cg_{env}) \frac{0.92}{0.08} - cg_{for} \quad (9.4)$$

$$l_{n2} = l_m \frac{0.85}{0.15} - cg_{for} - cg_{env} \quad (9.5)$$

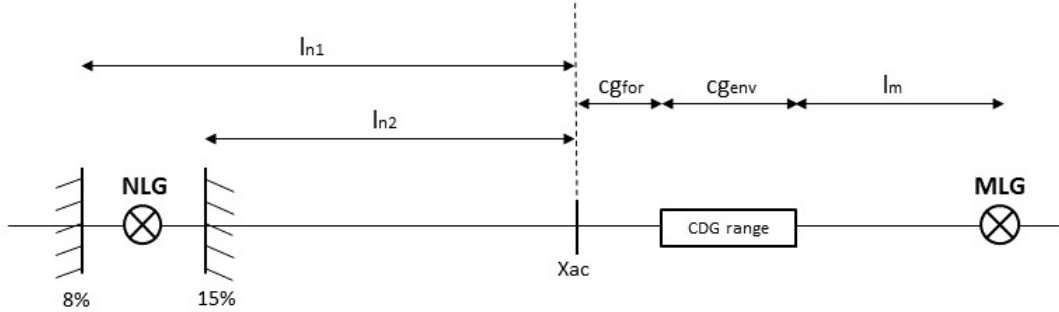


FIGURE 9.1: Scheme of distances for NLG boundaries calculation.

Once the boundaries for the NLG have been obtained, the wheel can be located in the middle as a first approach. Future studies, out of a preliminary design, would have to get a proper result, as structural considerations may be conclusive in deciding where to place the nose gear.

#### 9.1.4 Avoiding sideways turnover of the aircraft

As explained for the case in which the *CG* could not be behind the *MLG* in the worst scenario, the same can be applied when the aircraft has a certain bank angle, where the vertical projection of the *CG* cannot lie outside the triangle formed by the *MLG* and the *NLG*. This condition determines the *MLG* track.

For drawing the triangle, and so getting the track, it is first necessary to study the worst case for the *CG* position, which drives to the highest minimum track. This situation happens when the *CG* is located in the extreme forward and lateral position, what means an asymmetrical loading. From Fig. 9.2 it can be seen how the radius  $r$  is limiting the track by drawing a tangent line that crosses the *NLG*. This circle derives from the possible area in which the lateral load can drive the resultant force. The radius of the circle is given by Eq. (9.6).

$$r = n_y \ h_{cg} \left( 1 + 4k_{sg} \frac{e_s}{t} \frac{h_{cg}}{t} \right) \quad (9.6)$$

The lateral load/weight  $n_y$  value has been obtained in the most unfavorable case: a dry hard surface when the adhesion forces between the tire and the ground will be maximum. Torenbeek [6] suggests a value of  $n_y = 0.5$  for this scenario. Regarding the factor  $k_{sg}$ , the same author gives a typical range of values for a strut with hydraulic shock absorbers, which go from  $k_{sg} = 1/3$  to  $1/2$ . Given that there is not more information about the shock absorption system that will be used, the most restrictive value has been chosen, thus  $k_{sg} = 1/2$ .

By using basic trigonometry based on Fig. 9.2, and neglecting the lateral deviation of the  $CG$ <sup>1</sup>, the track can be calculated as shown in Eq. (9.7).

$$t = 2\tan\alpha (l_n + l_m) \quad (9.7)$$

, where  $\alpha = \arcsin(r/(l_n - cg_{env}))$ . It is important to notice that the distance  $l_n$  does not follow the same definition as in Sec. 9.1.3.

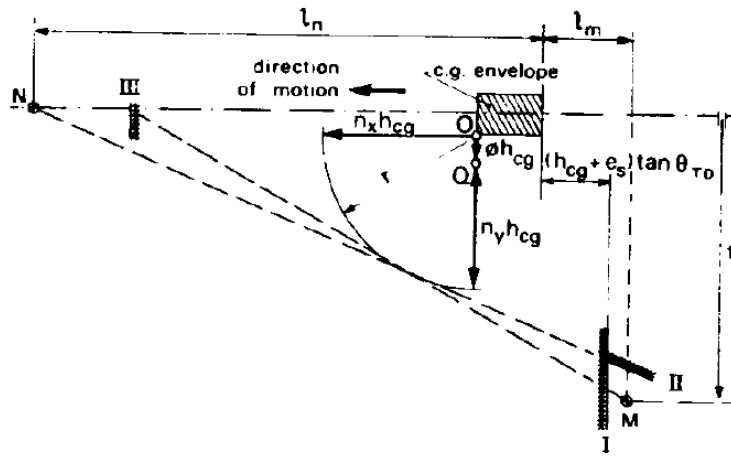


FIGURE 9.2: Limits of the undercarriage disposition based on stability considerations [6].

### 9.1.5 Final undercarriage disposition

After having analysed the different conditions that need to be met by the *MLG* and *NLG* positions so as to ensure a proper stability and manoeuvrability, the

<sup>1</sup>A factor of 20%, which is not considered in Eq. (9.7), will be applied to the final value of the track to compensate this hypothesis.

final results are presented in this subsection.

As it has been seen in all equations from this section, the wheel track and base values are related to each other, and any equation, but Eq. (9.1), cannot be fully calculated without making a first assumption of one parameter. That means that there must be a loop that supposes a first value of one parameter, and then, after having calculated all equations, the same parameter is calculated and compared to its first suggestion. For the purpose of this project, the value that has been supposed first is the track  $t$ , so first of all the leg's height can be obtained from Eq. (9.2), and finally the track is calculated from Eq. (9.7) and compared to the suggested value of the loop. A MATLAB function has been coded to perform this operation (see Appendix E.6), and it could be seen that only 10 iterations were needed to come to the solution with 1 cm of tolerance between the suggested value and the calculated one.

All parameters needed to perform the loop from Eq. (9.2) to Eq. (9.7) were known or could be estimated, except for the static deflection  $e_s$ , affecting Eq. (9.3) and Eq. (9.6). As this value could not be known until a study of the shock absorber and the tire properties is done (out of the scope of this preliminary design), the overall loop was performed for different values of  $e_s$  in order to know its sensitivity on the different undercarriage main parameters: wheel base, track, and height. These parameters were plotted against a range of static deflections from 0 to 25 cm, assuming that for LG heights of 67 cm approximately, the deflection would not be greater than 40%. Fig. 9.3 shows this sensitivity on the LG height, wheel track, and both *MLG* and *NLG* positions. On the one hand, it can be seen how an increase of 25 cm of static deflection does hardly affect the LG height by 1 cm, whereas the same increase of the static deflection separates the two legs of the *MLG* by almost 20 cm. On the other hand, an increase of 25 cm of the static deflection moves the *NLG* more than 30 cm forwards, and the *MLG* less than 5 cm backwards.

As seen in Fig. 9.3, a linear behaviour can be assumed on the static deflection sensitivity, so the sensitivity values shown in Tab. 9.1 are given for a proper understanding of its magnitude for the different LG parameters.

According to Fig. 9.3 and supposing a static deflection of 15 cm, the main parameters results are shown in Tab. 9.2 as a first approach of the undercarriage layout of

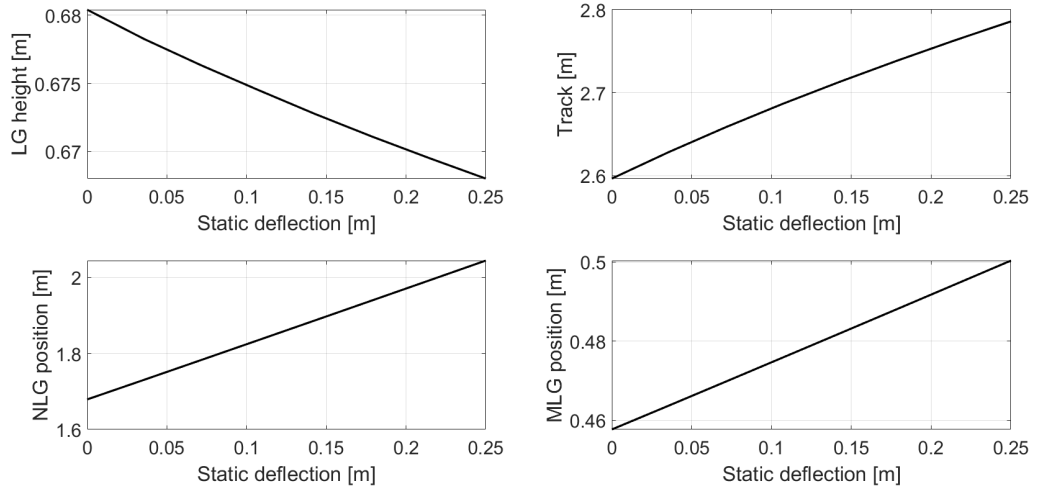


FIGURE 9.3: Static deflection sensitivity on the LG parameters: height, track, and MLG and NLG positions.

TABLE 9.1: Static deflection sensitivity on landing gear main parameters.

$\frac{h_g}{e_s}$	$\frac{t}{e_s}$	$\frac{NLG_x}{e_s}$	$\frac{MLG_x}{e_s}$
-0.05	0.82	1.47	0.17

the business jet, although from the same figure, better results should be get once some properties of the shock absorber are known. Both *MLG* and *NLG* distances have been calculated from the aerodynamic centre of the wing, with the positive direction pointing to the nose of the aircraft.

TABLE 9.2: Landing gear main parameters.

LG height [m]	MLG track [m]	MLG position [m]	NLG position [m]
0.67	2.70	-0.48	1.90

## 9.2 Number of wheels per leg. LCN estimation

Once the *MLG* and *NLG* are placed according to stability, manoeuvrability and security conditions, the number of wheels to place in each leg could be the next step to determine the undercarriage layout. One condition could be the load supported by one leg; in case it is too high, 2 wheels would be needed to carry such. In a business jet, where *MTOW* is usually lower than 10000 kg, the load in the *MLG*

is not high enough to be determining in the choice of the number of wheels. In this case, the airports in which the aircraft is intended to operate are decisive, as the *LCN* associated to the aircraft must be adequate to allow it run in the required runways. Sec. 1.4 tells the minimum railway length as a requirement for the aircraft, giving, in such a way, the airports in which the jet would be allowed to operate.

In order to obtain the *LCN* of the aircraft and see if it fits with the airport, it would be necessary to know the thickness of the pavement of the railway and the LCG provided by the airport. As this data is not known and its research is out of the scope of this preliminary design, two configurations will be analysed in this section: one with 2 wheels per leg, and another one with a single wheel per leg. The decision of presenting both configurations has been made from the fact that there are similar business jets using one or the other, and a proper study of the operating airports should be made as it has been stated as a design requirement. Furthermore, both configurations have important advantages and disadvantages: on the one hand, a single wheel per leg decreases the drag generated by the undercarriage, as well as it reduces its weight; but on the other hand, a 2 wheels configuration is safer given that a failure in one wheel can be assumed without endangering the whole aircraft.

### 9.2.1 Single wheel per leg

With the *NLG* located at the mid point between the ones of 8% and 15% of load, as seen in Fig. 9.1, the *MLG* supports 88.5% of the aircraft's weight. This *MLG* load, divided by the two legs, gives a wheel load of 2465 kg when being on ground with *MTOW*. From Fig. 9.4 it can be seen that the Single Wheel Load is so low that it is not shown, and according to the inflation pressure of tires, even if we suppose it is the maximum one, it is acceptable to think that the maximum *LCN* that the aircraft can reach is  $LCN = 15$ . Gudmundsson [13] states that business jets use to have the highest inflation pressures, what can be checked from the Cessna 650 Citation VII, which has a tire pressure of 168 *lb/sq.in* [1]. A high inflation pressure allows the undercarriage to have smaller and lighter tires, which reduces aerodynamic drag and the stowing volume, and business jets, given that

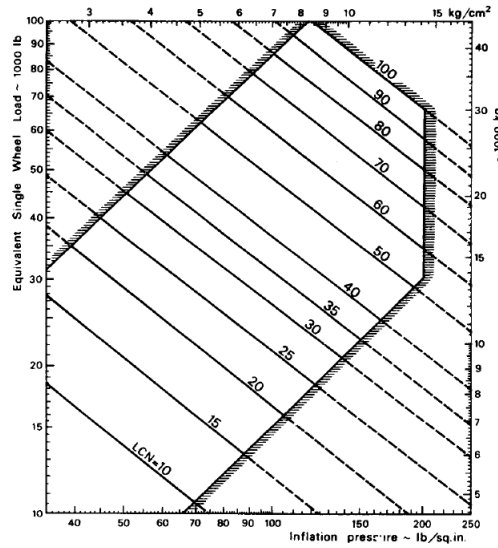


FIGURE 9.4: Load Classification Number for various combinations of tire pressure and wheel load [6].

they have lower wheel loads, can afford a higher pressure without compromising the *LCN*.

### 9.2.2 Two wheels per leg

From the one wheel per leg combination and Fig. 9.4, it has been seen that the maximum assumable *LCN* would be 15, as high as the pressure might be. But in case this value wants to be even lower once a proper analysis of the operating airports is made, 2 wheels per leg are studied in this subsection.

By adding a second wheel, the Equivalent Single Wheel Load (*ESWL*) can be reduced from  $0.885 \cdot MTOW/2 = 2465 \text{ kg}$ , the value for one wheel, to  $0.885 \cdot MTOW/4 = 1232 \text{ kg}$ , the load per leg distributed on its 2 wheels, reducing then the *LCN*.

In order to draw the graphic to determine the *ESWL* for a given thickness of pavement, it is necessary to know the distance between centres of tires ( $S_T$ ), and the distance between the closest contact area edges of the wheels ( $D$ ). Although there is not an equation for the  $S_T$  variable, Torenbeek [6] gives an approximation of the minimum distance between contact areas  $D$  based on the  $S_T$ , which is shown in Eq. (9.8).

$$\frac{D}{2} = \frac{S_T}{2} - \sqrt{\frac{L_W}{1.4\pi p}} \quad (9.8)$$

Given that it is hard to estimate the distance  $S_T$  in a preliminary design, and neither the tire pressure, the *ESWL vs. thickness of pavement* graphic has been done for different values of pressure for a fixed distance ( $S_T = 30 \text{ cm}$ ), and different values of  $S_T$  for a fixed pressure ( $P = 11 \text{ kg/cm}^2$ ), which can be seen in Fig. 9.5 and Fig. 9.6, respectively.

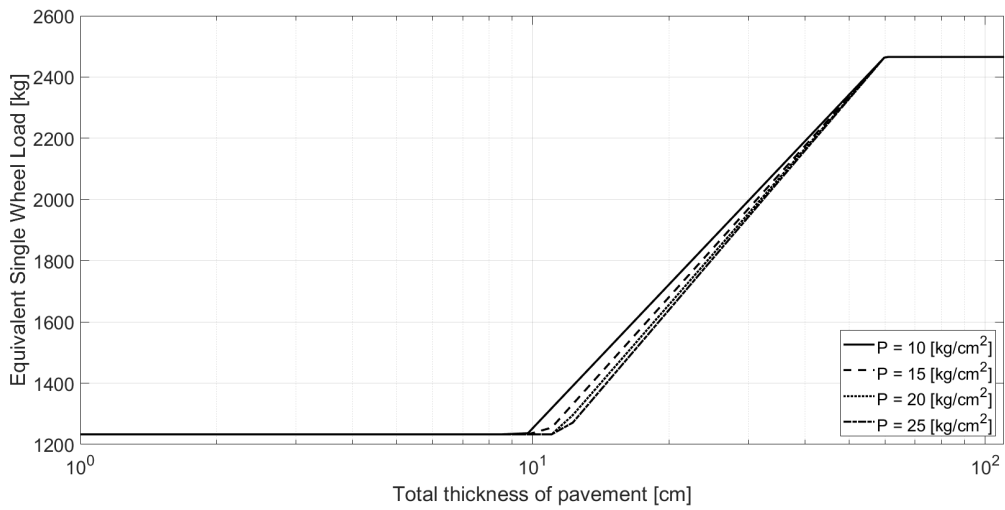


FIGURE 9.5: *ESWL* dependent on the thickness of pavement, for the dual wheel assembly, for different tire pressures ( $S_T = 30 \text{ cm}$ ).

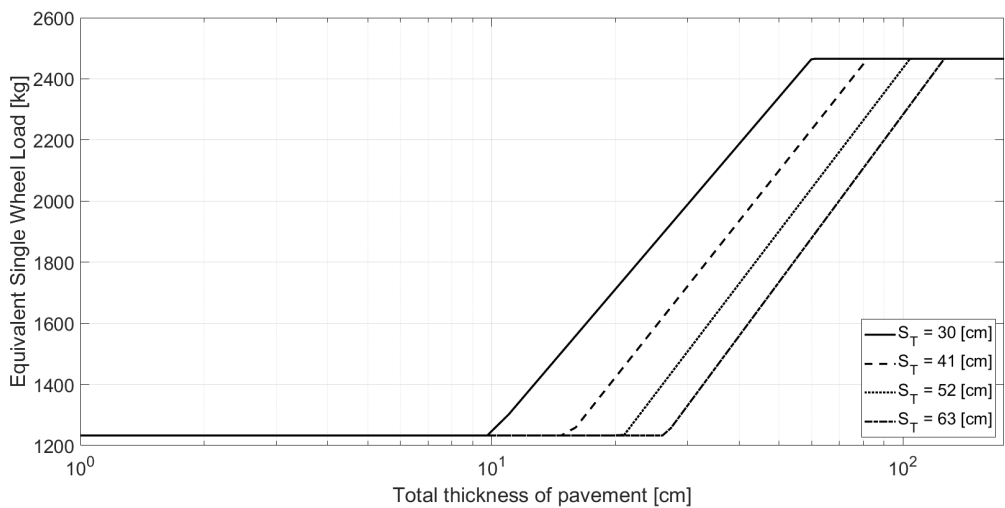


FIGURE 9.6: *ESWL* dependent on the thickness of pavement, for the dual wheel assembly, for different distances between imprint centres ( $P = 11 \text{ kg/cm}^2$ ).

Fig. 9.5 shows that the sensitivity of the inflation pressure on  $D$  is quite low, and so there is not a perceptible difference on the  $ESWL$  for a given thickness of pavement. Furthermore, Fig. 9.6 does show how the distance between centres of tires can affect the  $ESWL$  and so change the  $LCN$ . For example, for a thickness of pavement of 60 cm, if  $S_T$  is increased from 30 cm to twice its value, 60 cm, the  $ESWL$  difference between both is of 700 kg approximately, and from Fig. 9.4 it can be seen that such a difference in the  $ESWL$  can be translated into an increase of almost 5 in the  $LCN$ , if the tire pressure is maintained in both cases.

## 9.3 Conclusions

From the conditions of angles of pitch and roll during takeoff and landing and the stability at touchdown and during taxiing, the main characteristics of the landing gear have been obtained, resulting in a landing gear height of 67 cm, a wheel track of 2.70 m, and the *MLG* located 48 cm backwards the aerodynamic center of the wing and the *NLG* 1.90 m forwards the same point. These values have been obtained for a static deflection of the landing gear of 15 cm, although the sensitivity of this parameter can be seen in Tab. 9.1, as a more accurate value of these results should be obtained after analysing the required shock absorber and tire properties.

Regarding the number of wheels to install in each leg of the main landing gear, it has been seen that a single wheel per leg would have a load of 2465 kg, which could be translated into an  $LCN$  between 10 and 15, independently on the tire pressure, although business jets use to have the highest tire pressures (between 8 and 15  $kg/cm^2$ ) in order to reduce its size and so the aerodynamic drag. On the other hand, by installing 2 wheels per leg, the Equivalent Single Wheel Load can be reduced to 1232 kg for lower values of thickness of pavement, allowing a lower value of the  $LCN$  than the one obtained for a single wheel. This relation between the  $ESWL$  and the thickness of the pavement, which is then used to determine the  $LCN$ , has been plotted for different inflation pressures for a fixed distance between centres of tires, and then for different distances between centres of tires with a fixed pressure. This analysis has shown that the pressure hardly affects the  $ESWL$  value, although the distance between centres of tires,  $S_T$ , can decrease the  $LCN$ .

by almost 5, as 30 *cm* of difference in the  $S_T$  can increase the *ESWL* by 700 *kg* for the same thickness of pavement.

# Chapter 10

## Propulsion System Design

The propulsion system permits to the aircraft to be impulsed during the different performances of the flight. In previous chapters it is selected the type of engine, the model according to its thrust and the rear mounted position. In this chapter is concrete a more accurate position of the engine, it is decided the type of installation (podded/buried) and the thrust reversal system is selected.

### 10.1 Engine installation

In Sec. [2.1.3](#) has been discussed about the location and the number of engines that the business jet will have. The number of engines will be 2 for safety reasons and will be in a rear-mounted configuration for stability advantages and benefits of a clean wing in high Mach speed.

Since the payload has a small volume compared to the general volume and enough space is available at the end of the fuselage, will be studied the viability to attach the engines on the rear part of the fuselage.

The factors which affects the engine location are: flight safety, cost, drag, frontal area, inlet design, exit nozzle, stability, structural considerations, maintainability, operational requirements, aircraft center of gravity, engine maintenance, cabin noise, foreign object ingestion, stall, longitudinal equilibrium, engine-out control, aerodynamic interferences, heat exchange, among others [\[1\]](#). The main locations

to be mounted on the rear fuselage are buried inside rear fuselage or beside the rear section of the fuselage (on a pylon).

### **Podded vs. buried installation**

A buried engine is to insert the engine inside a part of the aircraft such as the wing or the fuselage. In this design, as exposed before, since the engines are rear-mounted appears some disadvantages. Considering that the fuselage will be much longer than the length of the engine, a more complex inlet duct design would be carried out. According to [1] there two solutions at this problem: designing a straight inlet duct from the nose of the plane to the engine. The disadvantage in this case is that the air conditions will not be the optimum for the efficiency of the engine because the length of the inlet. The second option is to have a short inlet and turn the flow placing the inlet beside the fuselage. However this option is easier to design, the short intake and exhaust ducts enable the engine to operate at its best conditions.

Nevertheless a buried engine is lighter than a podded one, the first one would occupy useful volume for the payload. Furthermore, with a podded engine there is more freedom to locate it in the best position for optimal air conditions and it is not required a considerable inlet design.

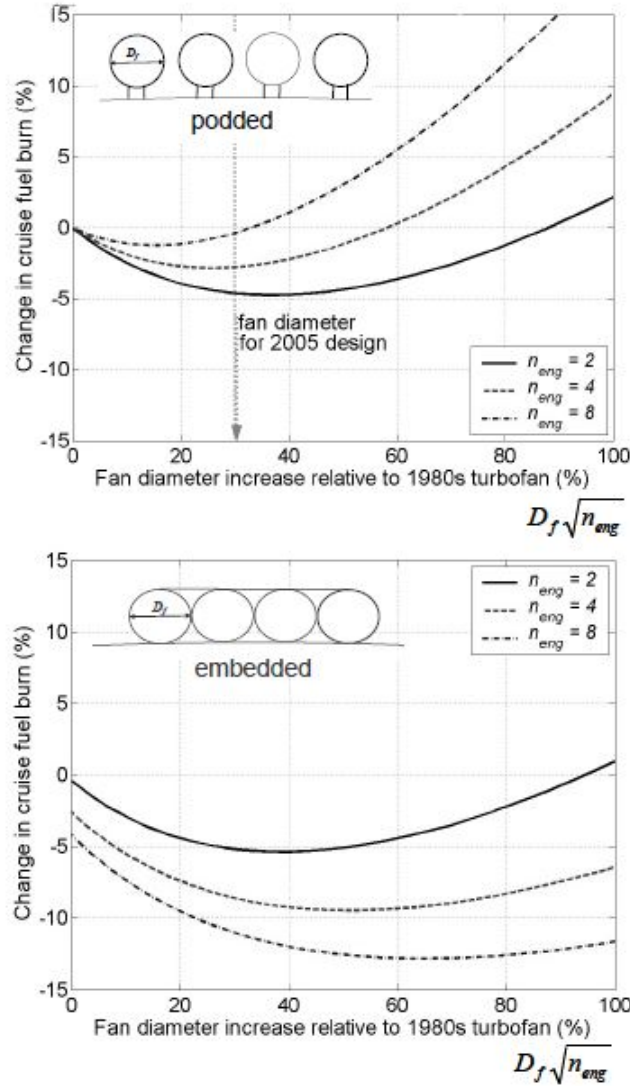


FIGURE 10.1: Variation of fuel burn with fan diameter for podded and embedded systems. Extracted from [17].

Regarding Fig. 10.1, it can be seen the change in cruise fuel burn related to fan diameter increase for different number of engines for podded and buried configurations. For large number of engines, buried or embedded installation benefits the fuel consumption due to the reduction of the wetted area related to the drag. However, for two engines installation the relation fan diameter-fuel burn between podded and buried is insignificant.

In conclusion, as the latter does not affect on the fuel consumption, more importance is given at volume and design complexity for the engine installation decision.

So, the engines will be mounted on the rear fuselage podded with pylons.

### Engine location and installation

Now, the location of the engine will be discussed. Firstly, the location of the engine nacelles mounted to the rear sides of the fuselage is an important parameter to take into account due to aerodynamic and stability facts.

Regarding stability, according to [1], the engines in a civil aircraft must be located such that the aircraft center of gravity is a small percentage of the wing aerodynamic center in front of the aircraft neutral point. Taking in account the latter, the aircraft will be longitudinally statically stable. The longitudinal position of the engines affect greatly in the aircraft center of gravity so is an important aspect to be considered. Another stability consideration is the engines proximity to longitudinal axis that permit the reduction of the yawing moment created in the event of engine failure. According to [6], the distance between the centerline of the nacelle and the local fuselage contour has to be around 75-80 percent of the maximum nacelle diameter.

From the point of view of aerodynamics, the installation of the engines have to avoid fuselage boundary layer and wake ingestion at large angles of attack, the inlet opening has to be raised sufficiently above the fuselage. Moreover, the engine should be located such that the hot gases exiting the nozzle does not impinge on any aircraft structure because hot surface will decrease efficiency.

According to [6], in fuselage-mounted podded engines placing it at the sides of the aft fuselage may produce, in high speeds, shock waves due to the drag generated in the convergent-divergent channel formed by the nacelle, the pylon and the adjacent fuselage wall. In addition, at large angles of attack when the boundary layer is separated, the wake created by the nacelles plus the pylons may affect on the horizontal tail-plane effectiveness. For that reason, engines have to be placed in such resulting in the least negative aerodynamic interference with the wing and tails.

Furthermore, the opening of the inlet must be located sufficiently ahead of the wing leading edge to minimize the negative effects of the inlet flow and wing flow.

The duct must supply the required air flow at different velocities, angles of attack and sideslip angles or an engine shutdown may occur [1].

In order to take advantage of the favorable effects and to minimize the negative effects on aerodynamics of the interference wing/fuselage with the inlet airflow, the inlet airflow has to be aligned. According to [1] and [6], the optimum nose-up pitch of about  $2\text{-}5^\circ$  and nose-outward angle of about  $1\text{-}3^\circ$  are recommended for rear-fuselage mounted engines.

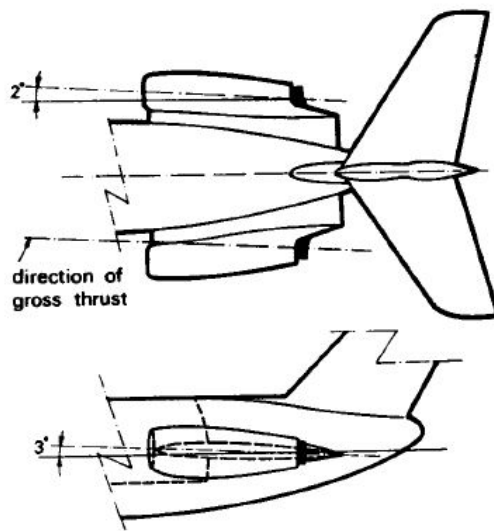


FIGURE 10.2: Inlet align of the nacelles mounted to the rear sides of the fuselage.  
Extracted from [6].

In Fig. 10.2 it can be seen a sketch of the recommended angles for inlet airflow align. Taking into account this inlets orientations the interference wing/fuselage drag can be reduced to 10-20 percent.

Another considerations that have to take in account are the stains of the engine couplings and security. Pylons of fuselage-mounted engine pods are more heavily loaded as a consequence of bending and contain heavy forgings in order to ensure favorable working conditions for the engine the air should reach the compressor with a minimum of pressure losses and fluctuations. In terms of security, fire in engine must not create fire in fuel tanks and it has to reduce possibility to ingestion of foreign objects during take-off.

To transmit thrust forces into the airframe it is necessary to establish a certain number of hard points (see Fig. 10.3 where the engine is physically attached to the

airframe. In a jet engine there are usually two or three attachment points which must support thermal expansion and weight loads [3].

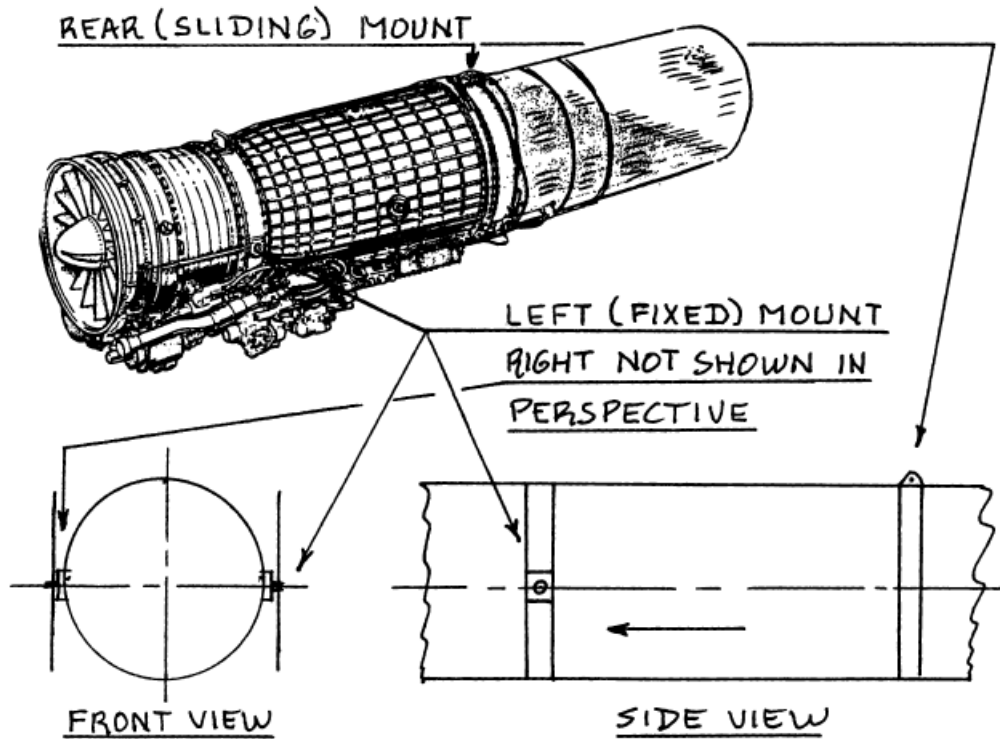


FIGURE 10.3: Method for Mounting Jet Engines in Airframes. Extracted from [3].

The engine attachment points cannot easily be changed due to the engine manufacturer normally determines their location.

### 10.1.1 Thrust Reversal

Since one of the design performance requirement is the capability to land in very short runways (800 m), it is necessary to install some devices to decelerate the aircraft rapidly after touching down due to high speeds in approximation such as wheel brakes, spoilers and thrust reversers. Thrust reverse is the mechanism which permits to divert momentarily the angle of hot exhaust gases towards the front of the airplane. The thrust will act against the motion of travel being a mean of deceleration [88].

Apart of providing an opposite thrust necessary for landing in short runways, reversal is used during day-to-day landing in order to alleviate the stress and reduce the wear on the brakes [6] or it is used to provide additional stopping force on wet, slushy and icy runways, for refused take-offs and for pushback [18].

There are three types of thrust reversals [18]:

- Bucket Target System (hot gases): is a hydraulic system which use bucket-type doors to redirect the hot gases stream forward. When the system is stowed two doors extended with a hydraulic actuator, form a convergent shape at the rear part of the engine nozzle. Is the most efficient system because uses the total amount of thrust which is coming out from the jet to be reversed. Moreover, it is used in engines with a low bypass ratio because this system does not occupy nacelle space [18].

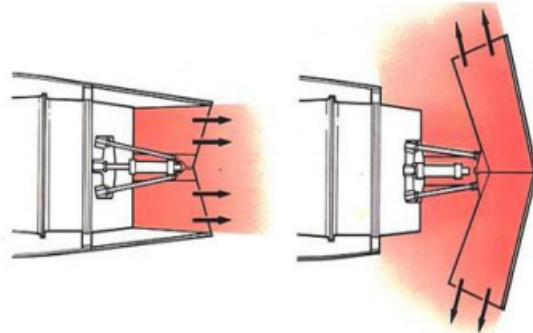


FIGURE 10.4: Bucket Target Type Thrust Reverser System. Extracted from [18].

- Clamshell type: is a pneumatic system which use rotating doors installed after turbine but before nozzle. The doors uncover the forward ducts and close the normal gas stream exit. It is used in mid and low bypass ratio and has the disadvantage that operates at temperatures of up to 600°C [18]. Moreover, it is required space inside the nacelle for the installation.

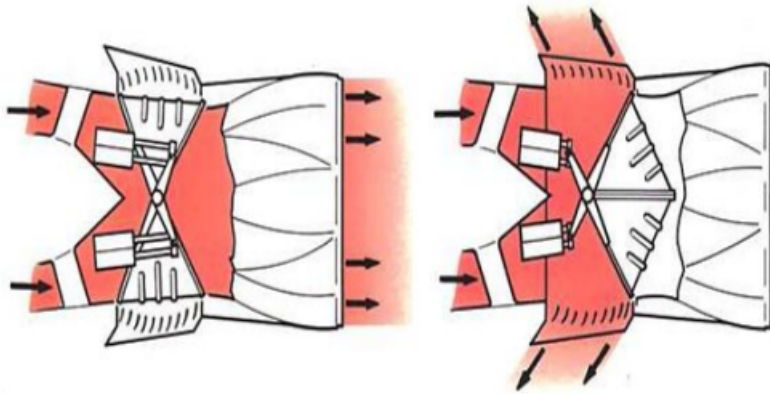


FIGURE 10.5: Clamshell Type Thrust Reverser System. Extracted from [18].

- Cascade Type Reverser system (cold stream): is a hydraulic system which moves an internal blocker door. When thrust reverse is selected this door is translated cowl rearwards blocking the cold stream final nozzle. Thus diverts the airflow through the cascade vanes situated around the nacelle perimeter [18]. It is used in high bypass turbofan engines. The disadvantages are the important weight and the difficulty to integrate inside small nacelles.

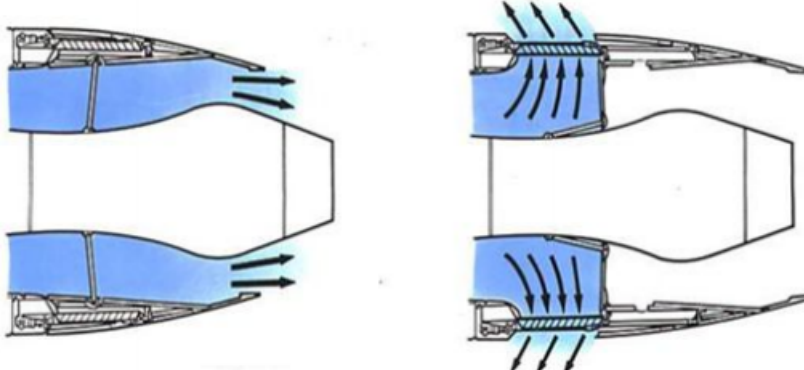


FIGURE 10.6: Cascade Type Reverser System (cold stream). Extracted from [18].

For the decision it is taken into account the weight, simplicity, effectiveness, the integration space and suitability to reduced nacelles. The cascade type is the most effectiveness in high bypass ratio and also has no structural problems due to the hot temperatures. Since the nacelle used has a low bypass ratio of 3.3, this type is discarded. Between the bucket and clamshell it is selected the bucket. The system in a bucket type is lighter, simple and effective for small nacelles. The doors are placed after the nozzle forming part of the nacelle structure without reducing the internal volume.

## 10.2 Conclusions

After a comparative study it can be concluded that the engines will be rear fuselage mounted and with a podded configuration using pylons. Moreover, they will be located vertically between the wing and the empennage in order to avoid the wing wake and to avoid the impinging of hot gases to the empennage control surfaces efficiency, respectively. Moreover, the nacelles will be placed with a nose-up pitch of  $3^\circ$  and nose-outward angle of about  $2^\circ$  for boundary layer ingestion of wing and fuselage.

Regarding thrust reversal, the bucket target type is selected due to its simplicity, low weight and suitability with small nacelles.



# Chapter 11

## Aircraft airframe

The airframe is the mechanical structure of an aircraft. It must resist all the internal and external loads that interfere with the aircraft.

In order to study the different airframe configurations, the Jet will be divided in 3 architectural parts: the fuselage Sec. [11.2](#), the wings Sec. [11.3](#) and the empennage Sec. [11.4](#).

An introduction to the most usual structural elements will be given in Sec. [11.1](#) in order fully understand the different airframe configurations.

### 11.1 Structural elements

The most common structural elements found on an aircraft's airframe are [\[76\]](#):

- Cladding: On the fuselage, it absorbs shear stresses due to torsion and supports pressure loads and other cross forces. It requires elements to stabilize it. On the wings and empennage it also receives the aerodynamics loads and transmit them to the ribs.
- Longerons: they prevent global instability due to bending.
- Stringers: they prevent local instability due to buckling.

- Frames: they provide cross stiffness, shape and they prevent stringers' instability.
- Bulkhead pressure: it distributes pressure forces.
- Ribs: they are found on the wings and the empennage and give shape to their airfoil. They prevent instability on stringers reducing their length. They also distribute the shear loads into the crossbeams.
- Torque box: on wings and on the empennage it is the space that contains the ribs, strings and crossbeams.

## 11.2 Fuselage airframe

The fuselage structure must be able to support bending and torsion forces just as axial loads [76]. Due to the need of a pressurized chamber, the structure will be formed by a single tube with thin walls. It will also have in consideration inertial loads stem from the movement inside the fuselage [76].

The traditional metallic structures [89] are the monocoque and semimonocoque. In a monocoque structure almost all imposed loads are supported by a stressed skin and it does not incorporate a load-carrying internal frame. Its construction mainly consists of the skin -cladding-, formers, and bulkheads. Its major inconvenience is keeping the weight within allowable limits in order to maintain enough strength to keep the fuselage rigid. On the other hand, semi-monocoque structures combine a tensile stressed skin with a compressing structure formed by longerons and ribs or frames.

As seen in Sec. 2.2, composite materials are commonly used in aircraft structures due to their weight reduction and mechanical properties. Unibody constructions -a type of semi-monocoque configuration- combine the body and frame of the fuselage in a single structure -panel- improving the stiffness and reducing the weight. The key to optimize these properties is strictly related to the manufacturing and configuration of the panel. Some examples of composite panels are:

- Stiffened panels [19]: composed of a longitudinal stiffener with its attached plating. The plating is usually designed to fail locally before the overall

failure of the stiffened panel. Plates are also capable of retaining their capacity load even though a portion of the plate has buckled. One way to reduce the panel's weight and cost is cocuring integrally the panel in an autoclave, as studied by Honda [90] .

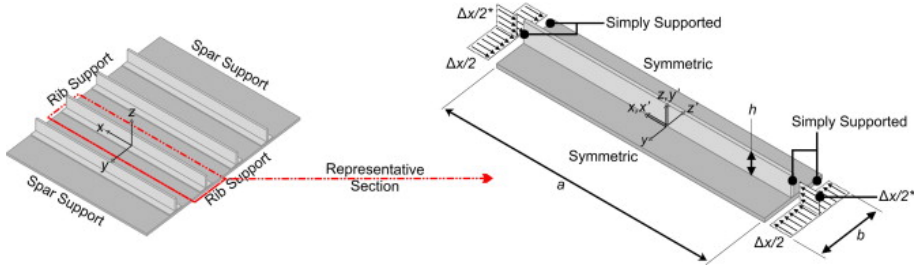


FIGURE 11.1: Stiffened panel. Extracted from [19]

- Sandwich panels [20]: structure made of a low-density core and a thin skin-layer bonded to each side of the core. Usually the core material has a low strength but higher thickness, which provides a high bending stiffness and low density to the panel. Fiber laminates such as carbon or glass with a thermoplastic matrix composites are commonly used as skin materials. To reduce the amount of used material, honeycomb cores are widely used in sandwich panels. It is important to take into account the interface between the core and the skin since the adhesive bond must support some degree of shear force.

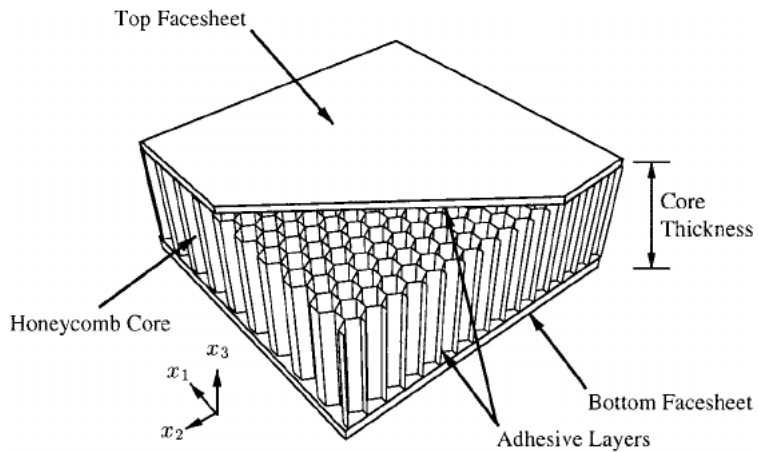


FIGURE 11.2: Honeycomb sandwich panel. Extracted from [20]

- Crown panels: precured frames cobonded to a skin panel that is stiffened with cocured hat stringers [11.3]. Several manufacturing processes have been studied in order to reduce the costs and weights of this panels. One of

the most important manufacturing techniques was developed by NASA and Boeing .[\[21\]](#)

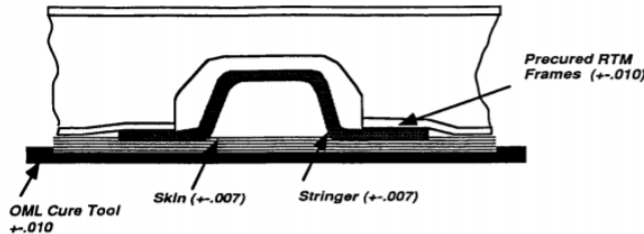


FIGURE 11.3: Hat stiffened skin. Extracted from [\[21\]](#)

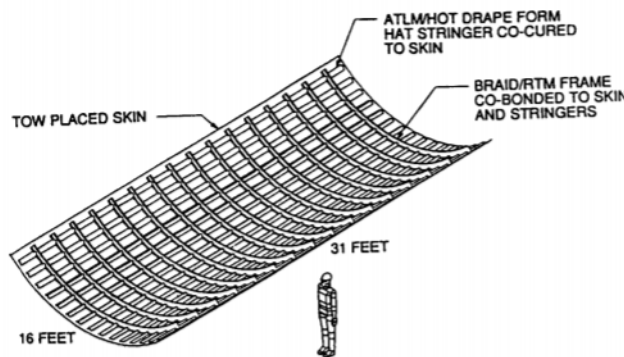


FIGURE 11.4: Crown panel. Extracted from [\[21\]](#)

### 11.3 Wing airframe

The main loads on the wing are [\[76\]](#):

- Aerodynamic loads, with special consideration on the lift.
- Gathered loads, mainly on the landing gear -if it is located on the wings-.
- Leading-edge and trailing-edge loads.
- Pressure loads: dynamic and static loads due to the fuel.

Having these loads in consideration, there are three basic types of wing structure [\[6\]](#) :

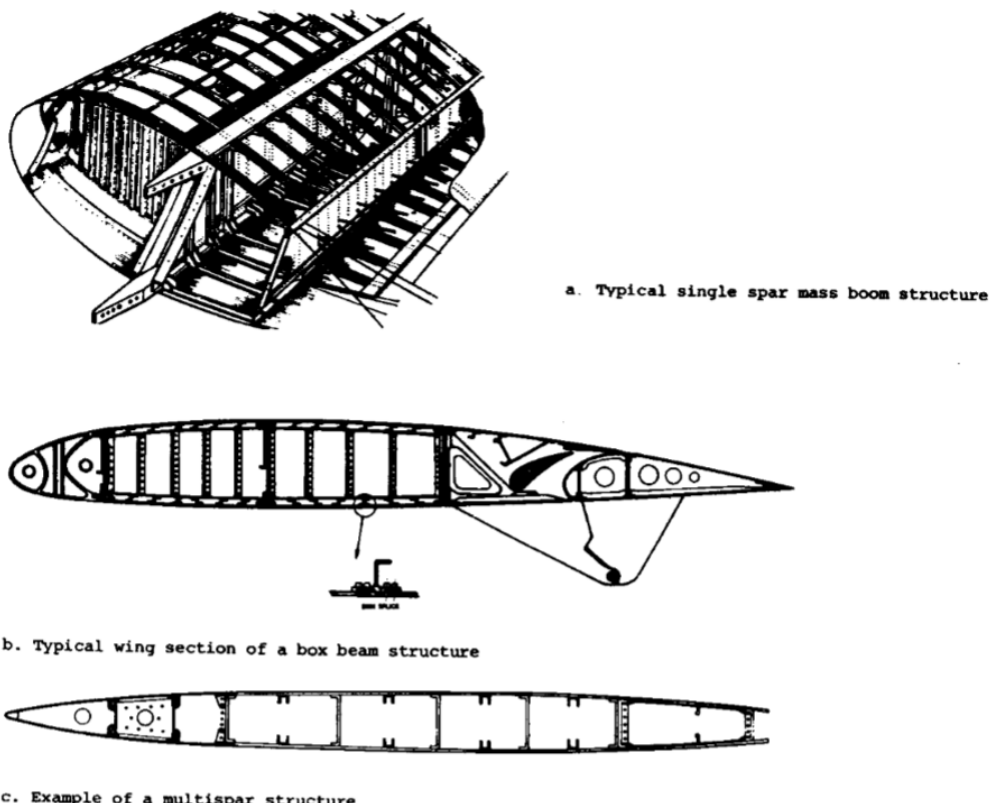


FIGURE 11.5: Examples of basic types of wing structure. Extracted from [6]

- Mass boom : the normal forces resulting from bending are carried by the flanges of one or two spars, while the torsional load is taken by the shear-spars and skin- or the spar webs. This structure is commonly used on slow aircrafts with thick wings. Advantages of this configuration:
  - Easy production and adaptation to the local stress level desired of the tapered booms.
  - Closely spaced ribs stringers dispense the shear forces on the skin, simplifying the manufacturing of the ribs.
  - Simple attachment to the fuselage using two main frames.
  - Lower openings and inspection doors' weight.

The important disadvantages that must be taken into account are:

- Failure of a spar boom is catastrophic, reason why the mass boom structure is no longer used.

- Large deflections under bending loads due to the high stresses in the spar.
  - The skin does not absorb the bending moment.
  - When a two-spar configuration is used, the airfoil thickness is higher than the spar height, thus the forces in the spar booms increase and more material is required.
  - To stabilize the spar booms it is needed to have many ribs.
  - If there are not stringers, the skin will buckle when loaded.
- Box beam: This structure uses skin panels to take shear forces. There are different configurations of the box beam, such as the three-spar/two-spar box beam with or without a stiffened nose section. Its main advantages are:
    - Better fail-safe design than the mass boom structure due to the stressed skin arrangement.
    - Suitable when skin thickness is required to obtain sufficient torsional rigidity on wing designed for high speed and/or thin, high aspect ratio wing.
    - Low stress levels in the upper skin for lightly loaded wings, avoiding buckling.
  - Multi-spar structure: Structure used on very thin wings. Its main disadvantage is the limited viability to install the required cutouts -for the landing gear, inspections etc-.

## 11.4 Empennage airframe

The main loads [76] that affect the empennage are the aerodynamics - with a lower lift impact than in the wing- and the gathered found in the joint of mobile surfaces.

Since it is a T-tail configuration, it is important to have an stiffness horizontal stabilizer due to aerelasticity problems. The fin must have heavy-gauge skin [22]

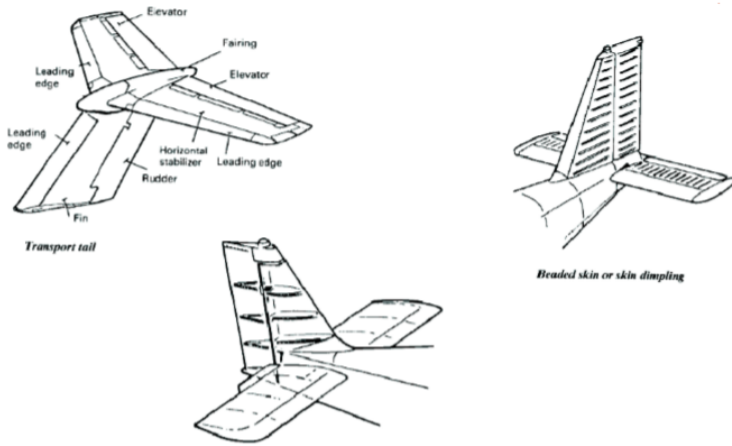


FIGURE 11.6: T-tail parts. Ribs, spars and beaded skin on the empennage  
Extracted from

to provide the adequate torsional stiffness, which is critical for the T-tail flutter mode.

As in the wing, spars and ribs are found in the torque box and are used to give shape to the tail, absorb inertial forces and support the main loads. On small aircrafts it is usual to find beaded skin [76], which provides local inertia and prevents the buckling.

## 11.5 Conclusions

As seen in Sec. 2.2, composites will be used to reduce weight and improve the mechanical properties of the structure. To do so, a unibody semi-monocoque configuration will be used. Further studies should be done in order to select the final type of panel, and most importantly its manufacturing process. Following the criteria used by Honda Jet [22], the proposed fuselage configuration is formed by the combination of stiffened and sandwich panels, as shown in Fig. 11.7. The cockpit and the tail section will be a honeycomb sandwich construction to maintain the compound curves, which interfere with the laminar-flow nose. In order to gain more cabin space, the constant cross-section of the fuselage will be made integrally of stiffened panels. Due to its stiffness and properties seen in Sec. 2.2, a carbon fiber composite is one of the best options to consider for the panels.

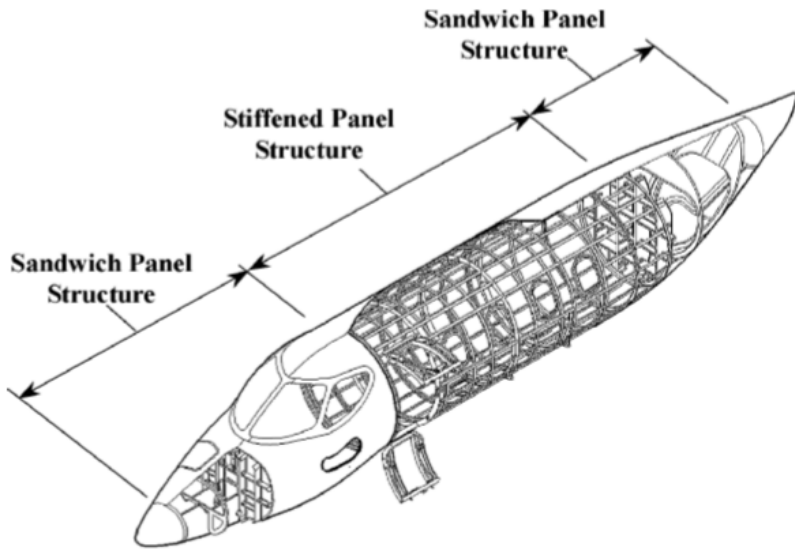


FIGURE 11.7: Honda Jet's fuselage structure. Extracted from [22]

A box beam configuration for the wing is the most suitable for the very light jet. To chose the number of spars and the stiffened nose section a further structural analysis should be done. A rigid composite material such as carbon or glass fiber will be used for the skin. The spars are a more critical element on the wing, so a metallic element like aluminium will be more efficient. The wing parts submitted to high bending forces, generally the joints, will be reinforced or integrally made of glass fiber composite due to its elastic modulus.

A carbon fiber composite beaded skin will be used on the empennage to provide the highest stiffness possible and prevent the buckling. As with the wing, further structural studies should be done to decide the number of spars and ribs that form the torque box.

# Chapter 12

## Flight envelope

This chapter will study the flight envelope of the business jet. The flight envelope represents the envelope of the flight loading conditions specified by the manoeuvring and gust criteria of the corresponding Certification Specifications document, the CS-23 [41] in the case of a business jets. There is an envelope diagram for each flight altitude and aircraft mass.

Sec. 12.1 will show the premises and the required calculations to obtain the flight envelope at sea level and  $MTOW$ , whereas Sec. 12.2 will do the same but at the cruise altitude of  $43000\text{ ft}$ , as specified in Sec. 5.3. Once the flight envelope for both flight levels has been obtained, gust load factors will be studied at the cruise altitude of  $43000\text{ ft}$  in Sec. 12.3. Finally, the combined diagram of the flight envelope considering gust loads will be presented at  $43000\text{ ft}$  in Sec. 12.4. Conclusions of this chapter will be exposed in Sec. 12.5

### 12.1 Flight envelope at sea level

The flight envelope can be drawn according to the following premises specified in CS 23.333 (b) [41]:

*Manoeuvring envelope. Except where limited by maximum lift coefficients, the*

*aeroplane is assumed to be subjected to symmetrical manoeuvres resulting in the following limit load factors:*

1. *The positive manoeuvring load factor specified in CS 23.337 at speeds up to  $V_D$ ;*
2. *The negative manoeuvring load factor specified in CS 23.337 at  $V_C$ ; and*
3. *Factors varying linearly with speed from the specified value at  $V_C$  to 0.0 at  $V_D$  for normal and commuter category.*

Together with this requirements, it needs to be known how to connect or draw the diagram from  $V = 0$  to  $V_D$  for positive manoeuvring load factors and to  $V_C$  for negative manoeuvring load factors: there is a first part, in both positive and negative load factors, defined by a parabola, which is determined by the maximum lift coefficient<sup>1</sup>. The positive parabola starts at  $V = 0$  and finishes at  $V_A$ , where the maximum positive load factor is achieved. The curve remains constant with this load factor value until  $V_D$ . The negative parabola follows the same criteria, with the reduced and negative lift coefficient, until the minimum load factor is achieved. Then it remains a flat line until  $V_C$ .

As detailed in CS 23.337, the limit manoeuvring load factors for the designed business jet are:

- $n_{max} = 3.8$
- $n_{min} = -0.4n_{max} = -0.4 \cdot 3.8 = -1.52$

Once the load factors are known, just like the premises explained in CS 23.333 and how to draw the entire diagram, the only thing to be determined before obtaining the flight envelope are the design airspeeds:

- *Design cruising speed,  $V_C$ :* is the cruise airspeed for which the aircraft is being designed. According to Sec. 5.3, with  $Ma = 0.69$  at sea level, the resulting cruise speed is  $V_C = 237 \text{ m/s}$ .

---

<sup>1</sup>The negative part of the parabola has been calculated using the 80% of the maximum positive lift coefficient, but with a negative sign  $C_{L-1} = -0.8C_{Lmax} = 1.016$ .

- *Design dive speed,  $V_D$* : according to CS 23.335 (b), and with a wing load of  $W/S = 335 \text{ kg/m}^2 \equiv 68 \text{ lb/ft}^2$  (see Sec. 4.2), the design dive speed results in  $V_D = 1.37V_C = 324 \text{ m/s}$ .
- *Design manoeuvring speed,  $V_A$* : it is defined as the minimum speed for which the aircraft achieves the limit manoeuvring load factor with the maximum lift coefficient and flaps retracted. Using Eq. (12.1) with  $n = 3.8$ ,  $C_N = 1.3$  as seen in Sec. 7.3.3, and considering  $MTOW$ , the resulting design manoeuvring speed is  $V_A = 120 \text{ m/s}$ . Note that  $V_A$  can also be obtained as  $V_A = V_S\sqrt{n}$ , where  $V_S$  is the computed stalling speed with flaps retracted at the design weight<sup>2</sup>.

$$nW = 1/2\rho V^2 S_W C_N \quad (12.1)$$

There is also a flight envelope for the flaps extended configuration, determined by the *Design flaps speed,  $V_F$* , and the positive limit load factor for this configuration, which is  $n = 2$  as detailed in CS 23.345 (a).  $V_F$  is defined as the maximum speed for which the aircraft is safe to operate with flaps fully extended with the limit load factor, and it is obtained as the greater of  $1.4V_S$  or  $1.8V_{SF}$ , as explained in CS 23.345 (b), where  $V_S$  is the computed stalling speed with flaps retracted at the design weight, and  $V_{SF}$  the computed stalling speed with flaps fully extended at the design weight. The first one can be obtained using Eq. (12.1) with the maximum lift coefficient  $C_{Lmax} = 1.3$ , whereas in the second one the maximum lift coefficient is  $C_{Lmax} = 2.75$  as explained in Sec. 7.4.

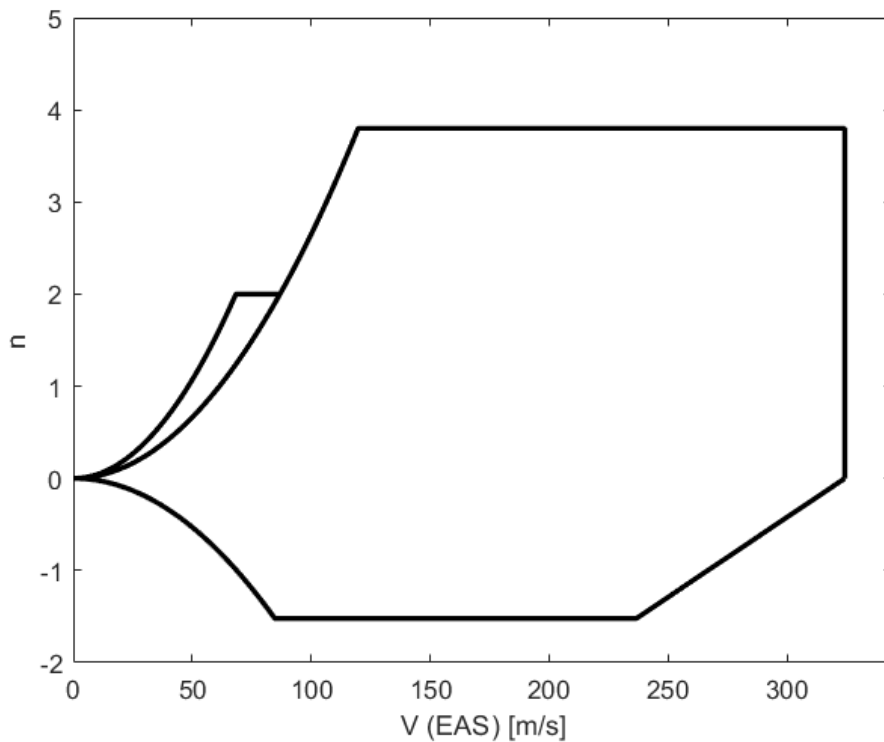
After having calculated all design airspeeds for both flaps configurations, which have been summarised in Tab. 12.1, and knowing the restrictions of the CS 23.333 for business jets, the flight envelope diagram at sea level with  $MTOW$  has been obtained. This can be seen in Fig. 12.1.

## 12.2 Flight envelope at cruise altitude

The flight envelope at a certain flight altitude is obtained in the same way as explained in Sec. 12.1, but if Mach number wants to be kept, the design cruise

---

<sup>2</sup>Remember that stalling implies  $n = 1$ , so Eq. (12.1) can also be used to obtain  $V_S$ .

FIGURE 12.1: Flight envelope at sea level and *MTOW*.

speed will decrease, as will the design dive speed  $V_D$ . For the cruise altitude of *43000 ft*, the resulting airspeeds are:

- $V_C = Ma a_0 \sqrt{\theta} = 0.69 \cdot 340[m/s] \cdot 0.867 = 205 [m/s]$ <sup>3</sup>
- $V_D = 1.37V_C = 281 [m/s]$

A comparison between design airspeeds at sea level and at the cruise altitude of *43000 ft* can be seen in Tab. 12.1, and the resulting flight envelope for such flight altitude is shown in Fig. 12.2.

### 12.3 Gust load factors

Gusts introduce or modify the load factor that the aircraft is experiencing at that moment, so their effect needs to be taken into account in the flight envelope, as it

<sup>3</sup> $\sqrt{\theta}$  is the correction factor of the speed of the sound for a certain altitude, which according to Torenbeek [6], it has a value of  $\sqrt{\theta} = 0.867$  for *43000 ft*.

TABLE 12.1: Design airspeeds for the flight envelope with  $MTOW$  at sea level and at cruise altitude.

	$V_C$ [m/s]	$V_D$ [m/s]	$V_A$ [m/s]	$V_F$ [m/s]	$V_S$ [m/s]
$h=0$ ft (SL)	237	324	120	86	62
$h=43000$ ft	205	281	120	86	62

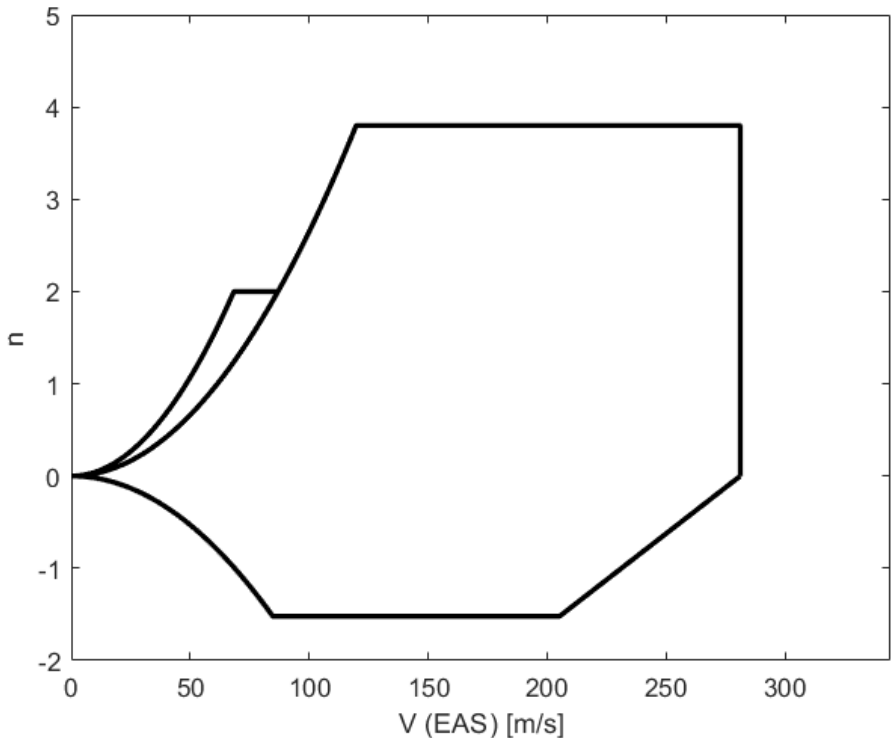


FIGURE 12.2: Flight envelope at cruise altitude of  $43000$  ft and  $MTOW$ .

will be modified to a more restrictive envelope. CS 23.333 (c) specifies the value of the symmetrical vertical gusts depending on the airspeed ( $V_C$ ,  $V_D$  or  $V_B$ ) and flight altitudes considered.  $V_B$  is the *Design speed for maximum gust intensity*, defined as the suggested speed to fly in a turbulent environment, and, according to CS 23.335 (d), it has to be lower than  $V_C$  and than  $V_S\sqrt{n_g}$ , where  $n_g$  is the positive aeroplane gust load factor due to gust at  $V_C$ . The value obtained for  $V_B$  has been  $V_B = 95$  [m/s].

The final results of gusts for  $43000$  ft, and following the CS 23.333 (c), have been:

- $U_{de} = 16 \text{ } fps$  at  $V_D$
- $U_{de} = 31 \text{ } fps$  at  $V_C$
- $U_{de} = 45 \text{ } fps$  at  $V_B$

The affected value of the load factor considering gusts can be computed using Eq. (12.2), as explained in CS 23.341 (c).

$$n = 1 \pm \frac{kg \rho_0 U_{de} V C_{L\alpha}}{2(W/S_w)} \quad (12.2)$$

where -

$$kg = \frac{0.88\mu g}{5.3 + \mu g} \quad (12.3)$$

$$\mu g = \frac{2(W/S_w)}{\rho \bar{C} C_{L\alpha} g} \quad (12.4)$$

Tab. 12.2 shows the resulting gust load factors for  $V_C$ ,  $V_D$  and  $V_B$  at cruise altitude using Eq. (12.2). Sea level has not been studied due to the fact that it made more sense to have gusts at a high enough flight level, not at sea level where gusts may not have such intensity. That also explains why the flaps fully extended configuration has not been analysed in this study.

Finally, the limit gust envelope has been plotted for the cruise altitude in Fig. 12.3.

TABLE 12.2: Gust load factors at different design speeds for the cruise altitude of 43000 ft.

	$V_C$	$V_D$	$V_B$
$n (+gust)$	2.41	1.99	1.95
$n (-gust)$	-0.41	0.01	0.05

## 12.4 Combined flight envelope

A final flight envelope is represented in Fig. 12.4<sup>4</sup> for the cruise altitude of 43000 ft combining the flight envelope obtained in Sec. 12.2 together with the effects of gusts on the load factors for the different design speeds  $V_C$ ,  $V_D$  and  $V_B$ . Fig. 12.4

<sup>4</sup>The combined flight envelope, as well as the other 3 figures presented in this chapter, have been obtained using a MATLAB code that can be found in Appendix E.7.

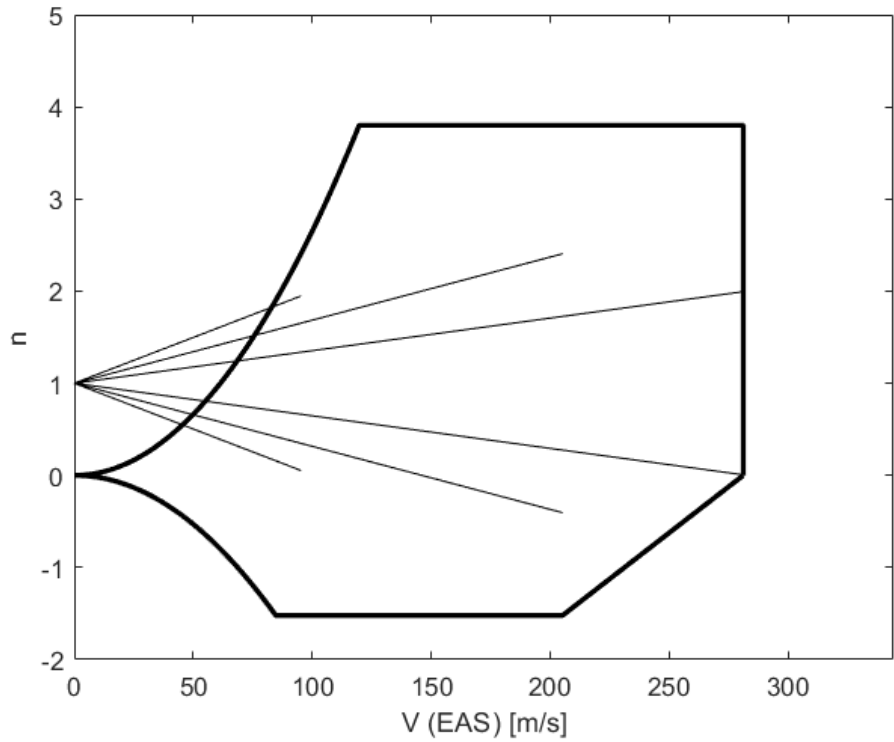


FIGURE 12.3: Gust load factors on the flight envelope at cruise altitude with *MTOW*.

shows the extreme manoeuvres that the aircraft can assume in a turbulent environment. To give an example, in the scenario of a turbulent atmosphere at the cruise altitude of *43000 ft*, from Fig. 12.4 it can be stated that the extreme manoeuvre it can be performed is the one implying a load factor of 2.41 at the design cruise speed of *205 [m/s]*, where a vertical gust could increase the load factor until reaching the limit of 3.8.

## 12.5 Conclusions

Fig. 12.4 has shown the flight envelope of the business jet at the cruise altitude of *43000 ft* with *MTOW* and considering the effects of gusts. From this figure it can be concluded that the business jet should not fly below the normal stall speed  $V_S = 62 [m/s]$ , as in this range it would not be able to lift its own maximum possible weight in any case. Moreover,  $V_C$  has become a determining and important speed. On the one hand, the allowed load factor decreases above it and that

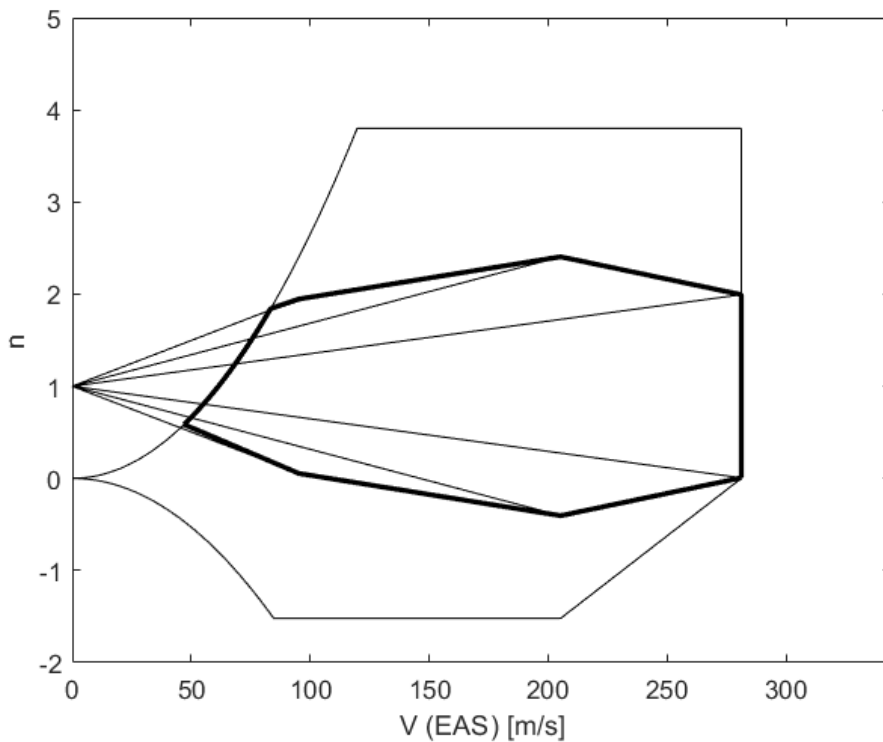


FIGURE 12.4: Combined flight envelope considering gusts effects at the cruise altitude with *MTOW*.

would be hazardous when performing extreme manoeuvres. On the other hand,  $V_C$  gives the aircraft the maximum manoeuvrability ( $n = 2.41$ ), supporting then its maximum allowed load factor of  $n = 3.8$  in case there is a positive vertical gust of its maximum intensity: *31 fps* for this speed at the cruise altitude of *43000 ft*. Having said so, the normal operation range will go from  $V_S = 62$  [*m/s*] to  $V_C = 205$  [*m/s*]. The minimum speed with almost the maximum manoeuvrability is achieved at  $V_B = 95$  [*m/s*], reaching a load factor of  $n = 1.95$ . From  $V_B$ , the load factor slightly increases with  $V$  until the maximum value is achieved at  $V_C$ ,  $n = 2.41$ . From  $V_C$  to  $V_D = 281$  [*m/s*], the load factor decreases until reaching  $n = 1.99$  at the latest speed, although  $V_C$  should not be exceeded in order to avoid undesired structural damage. Negative load factors have been almost cut due to gusts effects, although this fact is not critical as the business jet is not intended to operate with negative lift coefficients.

# Chapter 13

## Conclusions

After having reached the final point of this deliverable, it is important to state the main conclusions that come from it. The main decisions taken along the present paper have been synthesized in order to give a global idea for the results, challenges and future of this preliminary design of a Very Light Business Jet.

On the early stages of the project the requirements of the aircraft's performance were established taking into account factors, such as efficiency and passengers preferences. So that the following demands were stated: operating range of 2000 [km], 0,69 Mach cruising speed, service ceiling at 43000 [ft], 800 [m] runway length for take-off and landing and cabin's capacity for six passengers. It can be stated at the end of this preliminary design stage that all the requirements have been fulfilled, so that the initial objectives of this preliminary design have been achieved:

- Thanks to the reduced SFC of the JT15D-1B engine elected ( $0.55[\text{lb}/\text{lb} \cdot \text{h}]$ ), the operating range of 2000 [km] is achieved with a high percentage of the Maximum Payload. The cruise will take place at a service ceiling of 43000 [ft] and with a cruise Mach of  $M = 0.69$ .
- The plane is capable of landing and taking-off from airports with a runway length of 800 [m]. It is achieved thanks to the  $\Delta Cl$  given by the flaps, which is sized by considering the present regulations on  $V_{stall}$ , established on FAR-23 and depending on the landing field length. Moreover, the bucket target thrust reversal technology helps to decelerate the plane, reducing the braking

force to be done by spoilers and disc-brakes placed on the wheels, although a more detailed analysis on braking devices may be carried out in a more detailed design stage.

- The cabin of this very light business jet has been designed by taking into account that six passengers may travel comfortably inside it. Furthermore, as a differential value, the ceiling height inside the cabin has been fixed at 1.80 [m].

The main decisions regarding the preliminary design resulted in a very light business jet with a tapered low-wing configuration, T-tail, rear mounted podded engines and tricycle undercarriage. The main values of the design of the plane are summarized in Tab. 13.1. It is important to state that the total length of the plane does not consider the nose of the fuselage.

TABLE 13.1: Main parameters determined during the preliminary design stage of the Very Light Business Jet.

<b>MTOW</b>	5572 kg	<b>Range</b>	2000 km
<b>OEW</b>	3495 kg	<b>Ceiling</b>	43000 ft
<b>Capacity</b>	6 pax + 2 pilots	<b>Landing run</b>	800 m
<b>Wing surface</b>	18,2 $m^2$	<b>GC margin</b>	12,8-23,8%
<b>Span</b>	13 m	<b>Flap Type</b>	Fowler
<b>Length</b>	12.5 m	<b>Airfoil</b>	NACA 23012
<b>Power plant</b>	2 x Pratt & Whitney JT15D-1B	<b>MAC</b>	1.41 m

The airplane's wing design began with an study of the optimal aspect ratio which minimized drag. After an iterative process, the necessity of enlarging the span was observed as it couldn't reach optimal conditions (notice that the new surface still complies with Design Point limitations). The optimum  $C_L$  for this configuration is 0.52, and the minimum required is  $C_{Lmin} = 0.53$  for  $\alpha = 3.5^\circ$ , enabling the aircraft to fly at conditions close to the optimum.

The design of the tail allowed to perform an static stability analysis with fixed sticks, obtaining a margin of 1.4m of the CoG in the x-axis. In addition, the aircraft is statically stable, as the neutral point is found in a rearward position in

respect with for all the operating conditions.

With regard to the propulsion system, a rear fuselage mounted configurations with podded engines has been selected. The engines are located vertically between the wing and the empennage to avoid interference, and some nacelles modifications has been introduced to improve boundary layer behaviour. Finally, it has also been considered the use of the bucket target as the thrust reversal technology.

As this report includes only the preliminary design of the very light business jet, there is still much associated uncertainty on its conclusions. However, it is considered that with an uncertainty of less than 10% the results obtained are sufficiently valid. It is from this preliminary design that the potential customer of the project could decide whether it is viable or not, which would stop the design process or move on to a next phase.

The next stage of the design would include a more detailed design phase, focusing specially on those items which are critical for the viability of the project and the fulfillment of the requirements. Such are, for instance, the thrust reversal and the braking force to apply on the disc brakes in order to efficiently decelerate the plane when landing, a larger CFD analysis to be carried on the wing design to increase the global efficiency of the plane during cruise or the definition of the landing-gear configuration taking into account LCN values.



## Annexes



# Appendix A

## Trapezoidal and Simpson's Rule equations

### A.1 Trapezoidal Rule

The Trapezoidal Rule [23] is a first order integrative method which approximates the region under a curve as a trapezoid, solving the integral by calculating the area of the trapezoid as it can be seen at Fig. A.1. By enlarging the number of discretization  $n$ , related to the step  $\Delta x$  as the Eq. (A.2) specifies, a major number of trapezoids define the area below the curve improving the discretization error associated.

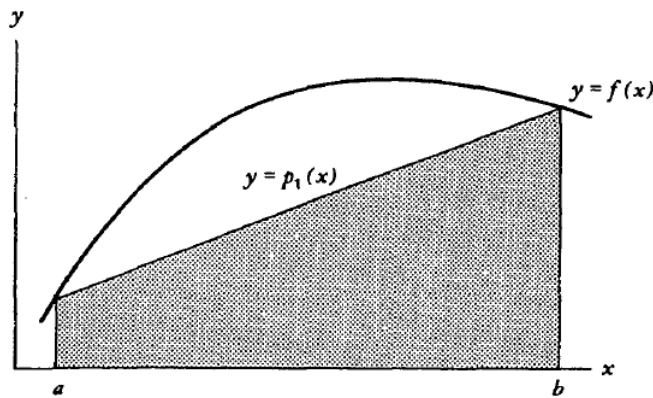


FIGURE A.1: Trapezoidal Rule representation [23]

The Trapezoidal Rule can be expressed as:

$$\int_{x_0}^{x_0 + \Delta x} f(x) dx = \frac{1}{2}(f(x_0) + f(x_0 + \Delta x))\Delta x \quad (\text{A.1})$$

In order to simplify the notation, and assuming that a regular discretization is used,  $\Delta x$  can be expressed as:

$$\Delta x = \frac{b - a}{n} \quad (\text{A.2})$$

Where  $b$  is the final integration limit,  $a$  is the starting integration limit and  $n$  the number of discretization of the domain. The Trapezoidal Rule error can be expressed as:

$$|E_n(S)| \leq \max |f''(x)| \frac{(b - a)^3}{12n^2} \quad (\text{A.3})$$

## A.2 Simpsons Rule

Simpsons rule [23] is a second order integrative method that approximates the solution using a quadratic interpolating polynomial  $p_2(f)$  (Fig. A.2). For this reason it's not known if the result is an overestimate or an underestimate, but its precision is greater than a first order integrative method as the Trapezoidal Rule [91].

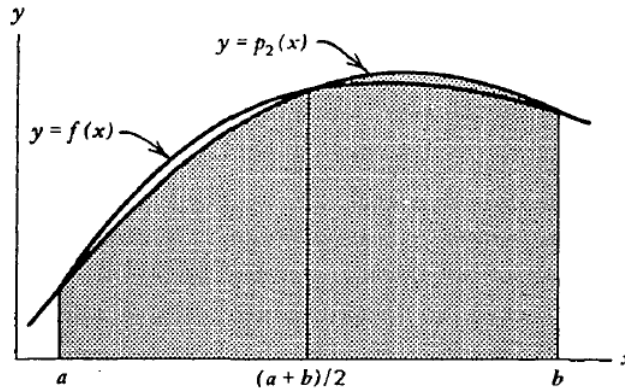


FIGURE A.2: Simpson's Rule representation [23].

Given a function  $y = f(x)$ , The Simpson's Rule is defined by :

$$\int_{x_0}^{x_1} f(x)dx \approx \frac{\Delta x}{3}(f(x_0)+4f(x_0+\Delta x)+24f(x_0+2\Delta x)+\cdots+44f(x_0+(n-1)\Delta x)+f(x_1)) \quad (\text{A.4})$$

As it has specified at Sec. A.1, the simplification Eq. (A.2) could also be applied assuming that a regular discretization is used. Its absolute error expression , with an order of  $\Delta x^5$ , is defined below:

$$| E_n(S) | \leq \max | f^{IV}(x) | \frac{(b-a)^5}{180n^4} \quad (\text{A.5})$$



## Appendix B

### Fuselage drawing

4

3

2

1

F

F

E

A

D

D

C

C

B

B

A

A

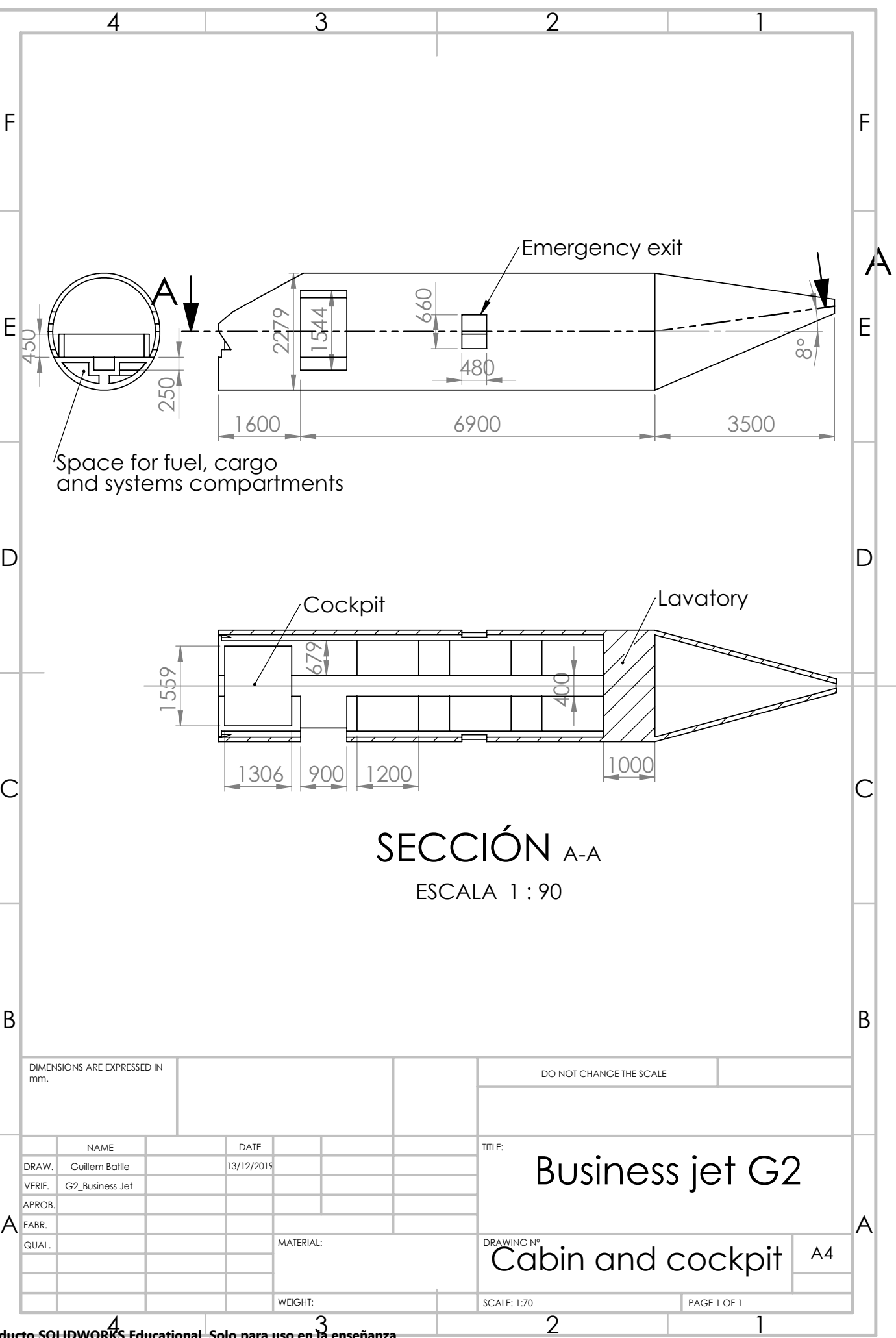
4

3

2

1

Producto SOLIDWORKS Educational. Solo para uso en la enseñanza.



# Appendix C

## Wing geometric iteration results

### C.1 Sweep and dihedral analysis

TABLE C.1: Maximum  $C_L/C_D$  and optimal  $C_L$  for  $\Lambda[^\circ] = 5, 10, 15$  and  $\Gamma[^\circ] = 2, 4, 6$

---

Wing_tapered_s0.63_d0_t0				
y(m)	chord(m)	Offset (m)	Dihedral (°)	Twist (°)
0	1.60	0	0	0
6	1.20	0.63	0	0
Alfa=5°		CL/CD=29,460	CL=0.508	

---

Wing_tapered_s1.16_d0_t0				
y(m)	chord(m)	Offset (m)	Dihedral (°)	Twist (°)
0	1.60	0	0	0
6	1.20	1.16	0	0
Alfa=5,25°		CL/CD=29,330	CL=0.525	

---

Wing_tapered_s1.71_d0_t0				
y(m)	chord(m)	Offset (m)	Dihedral (°)	Twist (°)
0	1.60	0	0	0
6	1.20	1.71	0	0

Disseny d'Avions APPENDIX C. WING GEOMETRIC ITERATION RESULTS

Alfa=5,25° CL/CD=29,173 CL=0.518 Sweep=15.02

Wing\_tapered\_s0.63\_d2\_t0

y(m)	chord(m)	Offset (m)	Dihedral (°)	Twist (°)
0	1.60	0	2	0
6	1.20	0.63	0	0

Alfa=5° CL/CD=29,447 CL=0.507

Wing\_tapered\_s1.16\_d2\_t0

y(m)	chord(m)	Offset (m)	Dihedral (°)	Twist (°)
0	1.60	0	2	0
6	1.20	1.16	0	0

Alfa=5,25° CL/CD=29,321 CL=0.524

Wing\_tapered\_s1.71\_d2\_t0

y(m)	chord(m)	Offset (m)	Dihedral (°)	Twist (°)
0	1.60	0	2	0
6	1.20	1.71	0	0

Alfa=5,25° CL/CD=29,163 CL=0.518

Wing\_tapered\_s0.63\_d4\_t0

y(m)	chord(m)	Offset (m)	Dihedral (°)	Twist (°)
0	1.60	0	4	0
6	1.20	0.63	0	0

Alfa=5° CL/CD=29,403 CL=0.507

Wing\_tapered\_s1.16\_d4\_t0

y(m)	chord(m)	Offset (m)	Dihedral (°)	Twist (°)
0	1.60	0	4	0
6	1.20	1.16	0	0

Alfa=5,25° CL/CD=29,285 CL=0.524

Wing\_tapered\_s1.71\_d4\_t0

y(m)	chord(m)	Offset (m)	Dihedral (°)	Twist (°)
0	1.60	0	0	0
6	1.20	1.71	0	0
Alfa=5,25	CL/CD=29,126	CL=0.517	Sweep=15.02	

Wing\_tapered\_s0.63\_d6\_t0

y(m)	chord(m)	Offset (m)	Dihedral (°)	Twist (°)
0	1.60	0	6	0
6	1.20	0.63	0	0
Alfa=5,25°	CL/CD=29,330	CL=0.526		

Wing\_tapered\_s1.16\_d6\_t0

y(m)	chord(m)	Offset (m)	Dihedral (°)	Twist (°)
0	1.60	0	6	0
6	1.20	1.16	0	0
Alfa=5,25°	CL/CD=29,222	CL=0.523	Sweep=10.02	

Wing\_tapered\_s1.71\_d6\_t0

y(m)	chord(m)	Offset (m)	Dihedral (°)	Twist (°)
0	1.60	0	2	0
6	1.20	1.71	0	0
Alfa=5,25°	CL/CD=29,061	CL=0.516	Sweep=15.02	

## C.2 Twist analysis

TABLE C.2: Maximum  $C_L/C_D$  and optimal  $C_L$  for  $\Lambda[^\circ] = 5, 10, 15$  and  $\Gamma[^\circ] = 2, 4, 6$ 

s0.63_d2_t2				
y(m)	chord(m)	Offset (m)	Dihedral (°)	Twist (°)
0	1.6	0	2	0
6	1.2	0.63	0	2
Alfa=4.5°		CL/CD=28,68	CL=0.531	
s0.63_d2_t4				
y(m)	chord(m)	Offset (m)	Dihedral (°)	Twist (°)
0	1.6	0	2	0
6	1.2	0.63	0	4
Alfa=5°		CL/CD=29,46	CL=0.508	
s0.63_d2_t6				
y(m)	chord(m)	Offset (m)	Dihedral (°)	Twist (°)
0	1.6	0	2	0
6	1.2	0.63	0	6
Alfa=5°		CL/CD=29,46	CL=0.508	

## Appendix D

### Xflr5 software error analysis

In order to obtain the aerodynamic parameters of the wing and to perform an stability analysis the xflr5 software has been used. Previously to its application, the software needs to be analyzed to ensure that its error is acceptable for the design stage of the project. Along these lines, experimental data of the polar curve for NACA23012 airfoil has been compared with the results of the simulations.

The software studied uses a value called  $N_{crit}$  in order to estimate the transition between laminar and turbulent boundary layer. It has been observed that the error presented by this software increases with this parameter. For that, low values have to be used. It has been decided to study the case  $N_{crit} = 2$ .

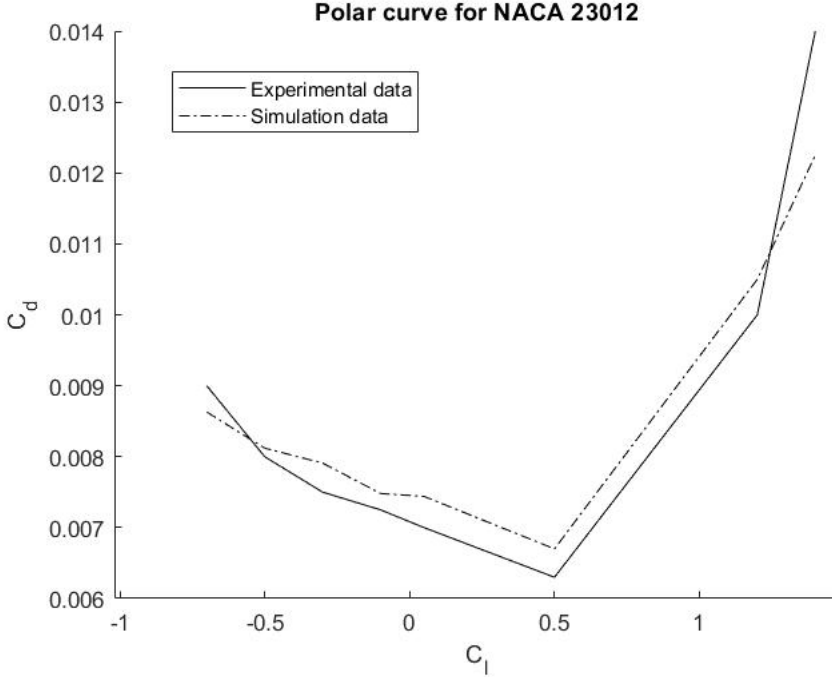


FIGURE D.1: Experimental and simulated polar curves ( $N_{crit} = 2$ ) for NACA 23012 [24]

In Fig. D.1 polar curves obtained experimentally and by simulation are shown. As it can be seen in the figure, the two curves are not equal which means that simulation data incurs in an error that needs to be analyzed. In Tab. D.1 both experimental and simulation data are shown as well as the error between them.

$C_l$	$C_d^{exp}$	$C_d^{sim}$	error
-0,7	0,009	0,00863	0,041
-0,5	0,008	0,00812	0,015
-0,3	0,0075	0,00791	0,055
-0,1	0,00725	0,00748	0,032
0,05	0,007	0,00744	0,063
0,5	0,0063	0,0067	0,063
1,2	0,01	0,0105	0,050
1,4	0,014	0,01225	0,125

TABLE D.1: Experimental and simulation data for NACA23012

As it can be seen in Tab. D.1, the maximum error occurs at  $C_l = 1,4$  and takes a value of 12,5%. Taking into account the preliminary stage of the project, the

simulations carried out would need to be performed again with a more accurate software further on the design development. In the end, considering the available tools to perform the project and its preliminary nature, it has been decided that an error of 12,5% is viable to use the software.



# Appendix E

## MATLAB Code

### E.1 Weight initial estimation

```
1 % This function calculates all weight parameters of an
2 % aircarft using
3 % different approximations to be specified throughout the
4 % script:
5 % MTOW, OEW, FW, MPL, MTOW/LTOW
6
7 %% Inputs
8
9 loadConstants; % Load different constants
10
11 Ma = Ma_ref; % Mach number at cruise phase
12 Num_engine = 2; % Number of engines
13 Wengine = Num_engine*200; % Engines weight
14
15 %% Ascending parameters
16 v_climb = 12.7*3.6; %km/s
17 v_avanc_climb = 130*3.6; %km/h
```

```

18 altitude      = Altitud*(1/3.28084)/1000; %ft to meter to
   km

19

20 % Mission parameters

21 range_mission = 2000;                      %km
22 v_cruise       = Ma*a0*f_Theta_sqrt(Altitud)*3.6; %km/h
23 Range_alternate = 200;                      %km
24 t_seguretat    = 5/60;                      %hours

25

26 % Excel results importation

27 filename = 'Mass_Private_Jet_3.xlsx';
28 sheet    = 1;
29 xlRange  = 'T22:U22';
30 data_coef = xlsread(filename,sheet,xlRange);
31 oew_mtow  = data_coef(1);
32 fw_mtow   = data_coef(2);

33

34 %% PL estimation

35

36 n_pax      = 6;      % Maximum number of passengers
37 n_crew      = 1;      % Number of crew with max. passengers
38 weight_pax  = 91.13; % Estimated weight per passenger [kg]
39 weight_crew = 77;    % Estimated weight per crew member [kg]
   ]
40 baggage     = 13;    % Estimated baggage weight [kg]

41

42 PL      = n_pax*(weight_pax+baggage);    % Total passengers
   weight [kg]
43 WCREW = n_crew*(weight_crew+baggage); % Total crew weight [
   kg]

44

45 %% MPL estimation

46

47 rho_merc   = 997;    % kg/m^3
48 rho_equipaje = baggage*1.2/(34.5*54*23e-6); % kg/m^3

```

```

49 kbd           = 0.35;
50 sb            = 147773e-6;                                % Cargo hold
   cross surface [m^2]
51 lbodega       = 7;                                    % Cargo hold
   lenght [m]
52 Vb            = sb*lbodega ;                         % Cargo hold
   volume [m^3]
53
54 %% Torenbeek estimation equation
55 MPL = PL+WCREW+rho_merc*(kbd*Vb-(n_pax+n_crew)*baggage/
   rho_equipaje);
56
57 %% First MTOW approximation
58
59 %% Definition of initial parameters for the loop
60 error          = 1;
61 n              = 1;
62 tolerancia     = 0.05;
63
64
65 %% MTOW initial value using Torenbeek reference:
66 MTOW_min = (PL-PL*0.1)/(1-oew_mtow-fw_mtow);
67
68 %% OEW calculation
69
70 %% Fuselage geometry for Torenbeek's graph calculation (p
   .147)
71
72 bf             = 2.278;                                % Height of fuselage. Not
   considering the lower part
73 hf             = 2.174;                                % Width of fuselage
74 lf             = (max(bf,hf)*Sr;                   % Lenght of fuselage
75 valor_x        = lf*(bf+hf)/2;
76 delta_we       = 130.5*valor_x-1110; % By choosing two different
   points of the graph Fig 5-3

```

```

77
78 % Roskman constants (Source: p.47, tab. 2.15 )
79 A = 0.2678;
80 B = 0.9979;
81 correct_rosk = 0.4; %Roskam's correction factor
82
83 %% Loop to find the MTOW
84
85 while error > tolerancia
86
87 n = n+1; % iterations counter
88
89 % OEW calculation using Torenbeek:
90 OEW(1) = 0.2*MTOW_min+500+delta_we+Wengine;
91
92 % OEW using Snorri Gudmundsson:
93 OEW(2) = MTOW_min*oew_mtow;
94
95 % OEW using Roskam:
96 OEW(3) = correct_rosk*(10^(A)*MTOW_min^(B));
97
98 % SECOND METHODOLOGY
99 OEW_MTOW_2 = 0.5371+0.0066*log(MTOW_min); %p.148 Snorri ,
100 but for turboprop.
101
102 % Initial approach of FW calculation
103 FW(2) = fw_mtow*MTOW_min;
104
105 % Weight ratios for each flight phase
106 w_phases = [0.990;0.995;0.995;0.980;0;0;0.990;0;0.992];
107
108 w1 = w_phases(1)*MTOW_min; % Engines start and warm up
109 w2 = w_phases(2)*w1; % Taxi
110 w3 = w_phases(3)*w2; % Take-off

```



```

136 MTOW_min = MTOW; % MTOW calculated value for future
137 iteration
138 if MTOW > 5.5e3
139     break
140 end
141
142 end
143
144 % FW recalculation
145 MTOW_def = MTOW;
146
147 w1 = w_phases(1)*MTOW_def;
148 w2 = w_phases(2)*w1;
149 w3 = w_phases(3)*w2;
150 w4 = funct_FW(range_climb,w3,v_avanc_climb,0.8,13);
151 w5 = funct_FW(range_mission+v_cruise*t_seguretat-
152 range_climb,w4,v_cruise,0.75,11);
153 w6 = w5*exp(-E_ltr*c_j_ltr/L_D_ltr);
154 w7 = w_phases(7)*w6;
155 w_res = w7*exp(-E_ltr*c_j_ltr/(0.95*L_D_ltr));
156 w8 = funct_FW(Range_alternate,w_res,128,0.9*conv_cj,10);
157 w9 = w_phases(9)*w8;
158
159 % Final weights
160 FW(3) = MTOW_def-w9;
161 OEW_def = MTOW_def-FW(3)-PL-WCREW;
162 FW_total = FW(3);
163 Wi_cruise = w4;
164 Wf_cruise = w5;
165 ratio_mtow_ltow = w8/MTOW;
166
167 end
168

```

---

<sub>169</sub> % AUTHOR'S NOTES:  
<sub>170</sub> % –Note that the iteration depends on Roskam's proposed  
 methodology by using  
<sub>171</sub> %Torenbeek's OEW approach  
<sub>172</sub> % The aim of the program is to be able to compare all the  
 results together  
<sub>173</sub> %and to decide which is better to estimate the weight of  
 the Jet Plane  
<sub>174</sub> % Some values may be reviewed for an accurate approximation  
 , specially those  
<sub>175</sub> %related to the velocity .

## E.2 Breguet Analysis

### E.2.1 Trapezoidal Rule function

<sub>1</sub> %This function calculates the range using the Trapezoidal  
 Rule with a given  
<sub>2</sub> %initial weight , final weight , the number of discretization  
 and the Breguet  
<sub>3</sub> %Equation  
<sub>4</sub>  
<sub>5</sub> **function** [R\_t] = Trapezi(a,b,n,f)  
<sub>6</sub>  
<sub>7</sub> h=(b-a)/n;  
<sub>8</sub> s=0.5\*(f(a)+f(b));  
<sub>9</sub> **for** i=1:n-1  
<sub>10</sub>     s=s+f(a+i\*h);  
<sub>11</sub> **end**  
<sub>12</sub> R\_t = h\*s; %Range using the Trapezoidal Rule  
<sub>13</sub> **end**

### E.2.2 Simpson's Rule function

```

1 %This function calculates the range using the Simpson's
2   Rule with a given
3 %initial weight, final weight, the number of discretization
4   and the Breguet
5 %Equation
6
7 function [R_s] = Simpsons(a,b,n,f)
8
9 h=(b-a)/n;
10 s=f(a)+f(b);
11 for i=1:2:n-1
12     s=s+4*f(a+i*h);
13 end
14 for i=2:2:n-2
15     s=s+2*f(a+i*h);
16 end
17 R_s=h/3*s; %Range using the Simpson's Rule
18
19 end

```

### E.2.3 Relative error script

```

1 clear all;
2 clc;
3 addpath(' ./ functions ')
4
5 loadConstants;
6 n=10;
7 a=Massa_i;
8 b=Massa_f;
9 Alt=Altitud*0.3048;
10 efic=11;
11 Ma=0.69;
12

```

```

13 f=@(W) -a0*f_Theta_sqrt(Alt)*efic*(Ma_ref^(beta_ct))*(Ma
14 ^^(1-beta_ct))/(g*c_j_ref*W);
15 %% Trapezi
16 f2=@(W) -2*a0*f_Theta_sqrt(Alt)*efic*(Ma_ref^(beta_ct))*(Ma
17 ^^(1-beta_ct))/(g*c_j_ref*W^3);
18 for i=1:1:n
19     y_max=0;
20     W=linspace(a,b,i);
21     for j=1:1:i
22         y=f2(W(1,j));
23         if abs(y)>y_max
24             y_max=abs(y);
25         end
26     end
27     error_t(1,i)=y_max*(b-a)^3/(12*i^2);
28 end
29 error_t=abs(error_t);
30 R_t = Trapezi(a,b,5000,f);
31 R_t_km=R_t/1000;
32 %% Simpson
33
34 f4=@(W) -24*a0*f_Theta_sqrt(Alt)*efic*(Ma_ref^(beta_ct))*(Ma
35 ^^(1-beta_ct))/(g*c_j_ref*W^5);
36 for i=1:1:n
37     y_max=0;
38     W=linspace(a,b,i);
39     for j=1:1:i
40         y=f4(W(1,j));
41         if abs(y)>y_max
42             y_max=abs(y);
43         end
44     end
45     error_s(1,i)=y_max*(b-a)^5/(180*i^4);

```

```

45 end
46 error_s=abs(error_s);
47 R_s = Simpsons(a,b,5000,f);
48 R_s_km=R_s/1000;
49 error_rel_s=error_s/R_s;
50 k_tfs_km = R_s_km/log(a/b);

51

52 %% Plotting

53

54 figure;
55 semilogy(error_rel_t,'-k');
56 hold on;
57 semilogy(error_rel_s,'-k');
58 legend('Trapezoidal Rule','Simpsons Rule')
59 xlabel('Number of discretization')
60 ylabel('Relative error')
61 grid on;
62 xlim([1 n])
63 hold off

```

### E.3 Payload-Range diagram

```

1 % This function outputs two plots: one with the range for a
   given weight
2 % configuration, and the other the maximum payload for a
   given range. This
3 % function depends on the different aircraft weights (MTOW,
   OEW, MZFW...)
4 % and the cruise conditions.

5
6 function [Range, Weight_t] = payload_range(MPL, OEW, MTOW,
   MFW, Ma, Alt, efic)
7
8 %% Initial inputs and vectors creation

```

```

9
10 [~,~,RF_max] = funct_weight_PLrange(OEW,MPL,10); % Reserve
   fuel when maximum payload
11 TF = MTOW-OEW-MPL-RF_max; % Trip
   fuel with MPL and MTOW
12 PL_min = MTOW-MFW-OEW; % Maximum
   payload with MFW and MTOW
13
14 % Subdivisions for each part of the diagram
15 a = 5;
16 b = 10;
17 c = 5;
18 n = a+b+c; % Total of weight configuration for creating
   the ddiagram
19
20 % Weight increases
21 TF_sub = TF/(a-1); % Trip fuel increase for the
   first part
22 PL_sub1 = (MPL-PL_min)/b; % Payload decrease for the
   second part
23 PL_sub2 = (PL_min)/c; % Payload decrease for the
   third part
24
25 % Vectors creation
26 Weight_t = 1:n; % Total weight
27 Weight_pl = 1:n; % Payload weight
28 Weight_fw = 1:n; % Fuel weight
29 Weight_OEW = 1:n; % OEW
30 Weight_PL = 1:n; % PL
31 Weight_RF = 1:n; % RF
32 Range = 1:n; % Range
33
34 % Initial weight configuration definition
35 Weight_t(1) = OEW+MPL+RF_max;
36 Weight_pl(1) = MPL;

```

```

37 Weight_fw(1) = 0;
38
39 %% Loop for different weight configurations
40
41 for i = 2:1:a
42     Weight_pl(i) = Weight_pl(i-1);
43     Weight_fw(i) = Weight_fw(i-1)+TF_sub;
44     Weight_t(i) = Weight_t(1)+Weight_fw(i);
45 end
46
47 for i = a+1:1:a+b
48     Weight_pl(i) = Weight_pl(i-1)-PL_sub1;
49     Weight_fw(i) = Weight_fw(i-1)+abs(Weight_pl(i)-
50         Weight_pl(i-1));
51     Weight_t(i) = Weight_t(i-1);
52 end
53 for i = a+b+1:1:n
54     Weight_pl(i) = Weight_pl(i-1)-PL_sub2;
55     Weight_fw(i) = Weight_fw(i-1);
56     Weight_t(i) = Weight_t(i-1)-PL_sub2;
57 end
58
59 for i = 1:1:n
60     [W_i, W_f, RF] = funct_weight_PLrange(OEW, Weight_pl(i),
61         Weight_fw(i));
62     [~, Range(i)] = Breguet_singleMaAlt(Ma, Alt, efic, W_i,
63         W_f);
64     Weight_OEW(i) = OEW;
65     Weight_PL(i) = OEW+Weight_pl(i);
66     Weight_RF(i) = Weight_PL(i)+RF;
67 end
68
69 %% Plotting

```

```

69 figure ;
70 plot (Range, Weight_t, '-k', ...
71 Range, Weight_OEW, '—k', ...
72 Range, Weight_PL, ':k', ...
73 Range, Weight_RF, '-.k')
74 ylim ([0,MTOW+500])
75 xlim ([0,Range(n)+100])
76 xlabel ('Range [km]')
77 grid on
78
79 figure ;
80 plot (Range, Weight_pl, '-k'); grid on;
81 xlim ([0,Range(n)+100])
82 xlabel ('Range [km]')
83 ylabel ('Payload [kg]')
84
85 end

```

## E.4 Design Point matching graph

```

1 %% CRUISE
2 z_ft=43000; %[ft] Cruise altitude as a performance
   requirement
3 z=z_ft*0.3048; %[m] Flight altitude 13100 m
4 z_11=11000; %[m]
5 T_11=216.6; %K sea level average temperature
6 g_0=9.81; %[m/s^2]
7 R=287; %[m^2/s^2K]
8 density_11=0.363; %[kg/m^3] air density at 11000 meters
9 density_0=1.225; %[kg/m^3] air density at sea level
10 density=density_11*exp((g_0/(R*T_11))*(z_11-z)) %[kg/m^3]
   at cruise altitude
11
12 V=205; %[m/s] based on average cruise velocity

```

```

13 CD0=0.02; % Statistic from literature
14 A=9.2; %Based on average of similar jets and statistic from
           literature
15 e=0.85; %Oswald efficiency factor based on literature
16 q=0.5*density*V^2; % [Pa] Dynamic pressure
17 f_3=0.89; %Relation between Wcr/W_TO
18
19 weight_surface=0:5:600;
20 thrust_weight_1=(1/9.8)*(density_0/density)*f_3.*((q./(
           weight_surface*f_3)).*(CD0+((weight_surface.*f_3).^2/((q
           )^2*pi*A*e))) );
21
22 %% TAKE OFF DISTANCE
23 S_tofl=800; %[m] Take Off Field Lenght
24 Cl_max_TO=1.9; %CL maximum take-off based on statistic from
           literature
25 sigma=1; %Relation between air density in take off altitude
           vs sea level air density
26 kto=13.3; %[m^3/kg] Take off Statistic Factor
27
28 weight_surface=0:5:600;
29 thrust_weight_2=kto*(1/9.8)*(weight_surface/(sigma*
           Cl_max_TO*S_tofl));
30
31 %% LANDING DISTANCE
32 Cl_max_L=2.6;
33 S_lfl=800; %[m] Landing distance
34 f=0.76; % Weight ratio (Wl/Wto) between landing and take
           off
35 kl=0.5*density_0*(1/(0.507*9.81)); % [kg/m^3] Landing
           statistic factor
36
37 weight_surface=kl*(1/f)*sigma*Cl_max_L*S_lfl;
38

```

```

39 %% CLIMB RATE DURING SECOND SEGMENT WITH CRITICAL ENGINE
40 FAILURE
41 Ne=2; % Number of engines that operate
42 f_1=1; %Relation between T_to_1e/T_2_1e
43 f_2=0.9801; %Relation between W_2/W_TO
44 E=8.8; %Eficiency CL/CD at 2nd regime configuration from
45 literature
46
47 thrust_weight_3=(Ne/(Ne-1))*f_1*f_2*((1/E)+gamma);
48
49 %% PLOTS
50 fig = figure;
51 leftColor = [0 0 0];
52 rightColor = [0 0 0];
53 set(fig, 'defaultAxesColorOrder',[leftColor; rightColor]);
54 yyaxis left;
55 plot(weight_surface,thrust_weight_1,'k-','LineWidth',2)
56 axis([0 500 0 1.4])
57 title('Design point');
58 xlabel('m_{TO}/ S_{W} [kg/m^{2}]');
59 ylabel('T_{TO}/ W_{TO}');
60 grid on;
61 grid minor;
62 hold on;
63 plot(weight_surface,thrust_weight_2,'k:','LineWidth',2)
64 hold on;
65 xline(weight_surface,'k-.' , 'LineWidth',2);
66 yline(thrust_weight_3,'k—' , 'LineWidth',2);
67 legend('Cruise', 'Take-off Distance', 'Landing distance', 'Climb rate 2nd Reg. OEI');
68
69 %% ENGINES
70 yyaxis right;

```

```

71 axis ([0 500 0 1.4])
72 yline(19580/(5572*9.81) , 'k-' , 'LineWidth' ,0.2)
73 yline(24440/(5572*9.81) , 'k-' , 'LineWidth' ,0.2)
74 yline(26240/(5572*9.81) , 'k-' , 'LineWidth' ,0.2)
75 yline(14360/(5572*9.81) , 'k-' , 'LineWidth' ,0.2)
76 yline(12000/(5572*9.81) , 'k-' , 'LineWidth' ,0.2)

```

## E.5 Flap Sizing Method

```

1 clear all
2 clc
3 %% INITIAL DATA
4 ML=4235; %Landing mass [kg]
5 g=9.81; %Gravitation acceleration [m/s^2]
6 rho=1.225; %Air density a Sea Level [kg/m^3]
7 S_w=18.2; %Wing surface [m^2]
8 b=25*3.281; %Wing span [b]
9 b_if=2.2*3.281; %Flap span location ratio
10 taper=0.75; %Taper ratio
11 sweep=4.66*(2*pi/360); %Wing sweep angle [rad]
12 t_c=0.12; %Thickness ratio of the airfoil
13 sL=2625; %Landing Field Length [ft]
14
15 %% INITIAL CALCULATIONS
16 Vs_kt=sqrt(sL/0.5136); %Stall velocity [kt]
17 Vs=Vs_kt*0.5144; %Stall velocity [m/s]
18
19 CL_max=1.27; %Clean configuration (obtained from wing
    simulation)
20 CL_max_L=(2*ML*g)/(rho*Vs^2*S_w); %Lift coefficient Landing
    configuration
21 KA=(1-0.08*((cos(sweep))^2))*(cos(sweep))^0.75; %Sweep
    correction parameter
22

```

```

23 %% INITIAL VALUES
24 cf_c=[0.10 0.15 0.20 0.25 0.30 0.40 0.50]; %Flap chord
25 ratio
26 C1_defl=[2.6 3.2 3.7 4.2 4.5 5.2 5.7]; %C_l_delta_l (see
27 figure 7.12)
28 alpha_f=[0.22 0.25 0.32 0.4 0.42 0.5 0.55]; %alpha_d_f (see
29 figure 7.16)
30 K_prima=[0.565 0.535 0.510 0.485 0.465 0.445 0.425]; %K' (
31 see figure 7.13)
32
33 K_plain_split=[0.95 0.9 0.83 0.75 0.65 0.5 0.4]; %K (see
34 figure 7.14)
35 K_single_slotted=[0.99 0.97 0.96 0.93 0.85 0.6 0.45]; %K (
36 see figure 7.14)
37
38 %% SOLVER
39 affirmation=0;
40
41 %while affirmation==1
42
43 for i=1:1:7 %Chord
44     for j=1:1:7 %Span
45         bf(i,j)=b*bf_b(j);
46         ni=b_if/b;
47         no(i,j)=(bf(i,j)+ni)/b;
48         Sf_Sw(i,j)=((no(i,j)-ni)*(2-(1-taper)*(ni+no(i,j))))/
49         (1+taper);

```

```

49         end
50     end
51
52
53     for i=1:1:7 %Plain Flap chord
54         for j=1:1:7 %Span
55             delta_cl_max_L_plain(i,j)=Cl_defl(i).*%
56             deflection(1)*K_prima(i)*K_plain_split(i)%
57             ;
58             delta_CL_max_L_calc_p(i,j)=%
59             delta_cl_max_L_plain(i,j).*KA*Sf_Sw(i,j)%
60             ;
61         end
62     end
63
64
65     for i=1:1:7 %Single Slotted Flap chord
66         for j=1:1:7 %Span
67             C_c=1+2*(z_c)*tan(deflection(2)/2);
68             delta_cl_max_L_slotted(i,j)=1.8*pi*(1+0.8*(t_c)%
69             )*C_c*alpha_f(i)*deflection(2)*%
70             K_single_slotted(i);
71             delta_CL_max_L_calc_s(i,j)=%
72             delta_cl_max_L_slotted(i,j).*KA*Sf_Sw(i,j)%
73             ;
74         end
75     end
76
77
78     for i=1:1:7 %Fowler Flap chord
79         for j=1:1:7 %Span
80             a(i,j)=(1+cf_c(i));
81             delta_cl_max_L_fowler(i,j)=1.8*pi*(1+0.8*(t_c))%
82             *a(i,j)*alpha_f(i)*deflection(3)*K_fowler(i)%
83             ;
84             delta_CL_max_L_calc_f(i,j)=%
85             delta_cl_max_L_fowler(i,j).*KA*Sf_Sw(i,j)%
86             ;
87         end
88     end

```

```

74      end

75

76      figure(1) %Plain flap
77      plot(cf_c,delta_CL_max_L_calc_p(:, :) )
78      xlabel(" c_f/c", 'Interpreter', 'tex')
79      ylabel(" \Delta_{C_{Lmax}}{L}", 'Interpreter', 'tex')
80      hleg = legend('0.55', '0.60', '0.65', '0.70', '0.75', '0.80', '0.85');
81      htitle = get(hleg, 'Title');
82      set(htitle, 'String', 'Flap span ratio (bf/b)')
83      title('Plain Flap')
84      yline(delta_CL_max_L_sup)

85

86      figure(2)%Single Slotted flap
87      plot(cf_c,delta_CL_max_L_calc_s(:, :) )
88      xlabel(" c_f/c", 'Interpreter', 'tex')
89      ylabel(" \Delta_{C_{Lmax}}{L}", 'Interpreter', 'tex')
90      hleg = legend('0.55', '0.60', '0.65', '0.70', '0.75', '0.80', '0.85');
91      htitle = get(hleg, 'Title');
92      set(htitle, 'String', 'Flap span ratio (bf/b)')
93      title('Single Slotted Flap')
94      yline(delta_CL_max_L_sup)

95

96      figure(3)%Fowler flap
97      plot(cf_c,delta_CL_max_L_calc_f(:, :) )
98      xlabel(" c_f/c", 'Interpreter', 'tex')
99      ylabel(" \Delta_{C_{Lmax}}{L}", 'Interpreter', 'tex')
100     hleg = legend('0.55', '0.60', '0.65', '0.70', '0.75', '0.80', '0.85');
101     htitle = get(hleg, 'Title');
102     set(htitle, 'String', 'Flap span ratio (bf/b)')

```

```

103     title( 'Fowler Flap' )
104     yline( delta_CL_max_L_sup )

```

## E.6 LG disposition loop

```

1 % This function all LG parameters relevant in a
  preliminary
2 % design, as well as the wheel loads and the LCN
3
4 function [LG_height, track, NLG_pos, MLG_pos, contador] =
  LG (b, dihedral, sweep, A, Xcg_for_MTOW, Xcg_aft_MTOW,
  es)
5 %% Inputs:
6 % b          = wingspan      [m]
7 % dihedral   = dihedral angle [deg]
8 % sweep      = sweep angle   [deg]
9 % A          = Aspect Ratio
10 % a         = Distance between the Xac and CDG_for [m].+
  value. TBD
11 a          = Xcg_for_MTOW; % EXAMPLE. TO BE REPLACED
12 % h_cg      = height of the CDG
13 ny         = 0.5;
14 k_sg       = 1/2;
15
16 cdg_envelope = abs(Xcg_for_MTOW-Xcg_aft_MTOW); % Distance
  between the extreme positions of the CDG
17 y          = a+cdg_envelope; % Distance
  between the Xac and CDG_aft [m]
18
19 % Approximation for guard angle considering no slats (
  Torenbeek, page 351)
20 guard = 7*(1+3/A); % [deg]
21

```

```

22 pitch_TD = guard; % [deg] pitch angle when touchdown (
    Supposed the same as guard angle, assumption based on
    Torenbeek page 353)

23
24 delta = 0.001;      % Acceptable difference on the MLG
    position

25
26 Track_loop = false;

27
28 % Supposed value for the distance between wheels
29 t_sup = 2; % [m]

30
31 contador = 1;

32
33 %% Beginning of the loop for the track calculation

34
35 while Track_loop == false

36
37
38 %% MLG location

39
40 % Wheels height due to the 8 deg restriction. 10% of margin
    applied for

41 % downward movement of wing tip (Torenbeek, page 350)
42 LG_height = (b-t_sup)/2*(tand(8)-tand(dihedral)+tand(guard)
    *tand(sweep))*1.1; % [m]

43
44 % MLG distance after the maximum aft possible CDG position
    (distance

45 % between last possible CDG and MLG)
46 lm = (LG_height+es)*tand(pitch_TD);
47 lm = 1.1*lm; % Margin of 10%
48
49 MLG_pos = y+lm;
50

```

---

```

51 % -----NLG LOCATION-----
52
53 % Distances measured from the Xac
54 ln1 = (lm+cdg_envelope)*0.92/0.08 - a;
55 ln2 = lm*0.85/0.15 - y;
56
57 NLG_pos = (ln1+ln2)/2; % NLG at the mid point between
58 % NLG_aft and NLG_for.
59 %
60
61 h_cg = LG_height+1; % CDG height is 1m above the LG
62
63 % Radius determination
64 r = ny * h_cg * (1+4*k_sg*es*h_cg/(t_sup^2));
65
66 % Distances between NLG and CDGs
67 x = NLG_pos + a; % Distance between the extrem
68 % forward position of the CDG and the NLG
69
70 % Track claculation
71 angle = asin(r/x);
72 track = 2*tan(angle)*(ln+lm);
73 track = 1.2*track;
74
75 %% Track verification
76
77 if abs(track-t_sup) > delta
78     t_sup = track;
79     contador = contador + 1;
80 else
81     Track_loop = true;
82 end

```

---

```

83
84 end
85
86
87 end

```

## E.7 Flight envelopes

```

1 function [Vs1, Va, Vd, Vf, Vs1_neg, Vs_flap, Vd_h] =
  manoeuvres(MTOW, Sw, Cn_max, Cn_max_TO, Ma_c, c_aero,
  CL_alpha)

2
3 %% Inputs
4
5 loadConstants;
6 g           = 9.81;
7 rho         = 1.225;    % Air density at sea level
8 a0          = 343;      % Speed of sound at sea level
9 n_max_flaps = 2;
10 n_min      = -1.52;
11 n_max      = 3.8;    % From class slides for small aircraft
12 i           = 80;

13
14 %% Airspeeds calculation without flaps
15
16 stall_factor = 0.5*rho*Sw*Cn_max/(MTOW*g);

17
18 % Relevant airspeeds
19 %Vc = sqrt((2*MTOW*g)/(rho*Sw*Cn_cr)); % Cruise speed at
  sea level with MTOW and Cn_cr
20 Vd      = 1.37*Ma_c*a0;                      % Vd according to
  C 23.335 b)
21 Vs1    = sqrt(1/stall_factor);                % Stall airspeed
  for n=1

```

```

22 Va_f = sqrt(n_max/stall_factor); % Stall airspeed
    for n_max
23 Va = Vs1*sqrt(n_max);
24
25 % Vectors for the plot
26 V1 = linspace(0, Va_f, i); % Vector for airspeed
    from 0 to Va
27 n1 = stall_factor*V1.^2;
28
29 %% Flap curve
30
31 stall_factor_TO = 0.5*rho*Sw*Cn_max_TO/(MTOW*g);
32
33 % Relevant airspeeds
34 Vs_flap = sqrt(1/stall_factor_TO); % Stall speed
    with flaps
35 Vf1 = sqrt(n_max_flaps/stall_factor_TO); % Stall
    airspeed with flaps for n_max_flaps
36 Vf = max(1.8*Vs_flap, 1.4*Vs1); % Maximum
    airspeed with flaps;
37
38 % Vectors for the plot
39 V2 = linspace(0, Vf1, i);
40 n2 = stall_factor_TO*V2.^2;
41
42 %% Negative curve
43
44 neg_factor = 0.5*rho*Sw*Cn_max*(-0.8)/(MTOW*g);
45
46 % Relevant airspeeds
47 Vs1_neg = sqrt(n_min/neg_factor); % Stall airspeed for
    minimum factor (negative)
48
49 % Vectors for the plot
50 V_neg = linspace(0, Vs1_neg, i);

```

```

51 n_neg = neg_factor*V_neg.^2;
52
53 %% Full vectors creation (SL)
54
55 delta = 0.01;
56
57 % Curve without flaps
58 n_noFlaps = [n1, n_max, n_max, 0];
59 V_noFlaps = [V1, Va_f+delta, Vd, Vd+delta];
60
61 % Curve with flaps
62 n_flaps = [n2, n_max_flaps, n_max_flaps];
63 V_flaps = [V2, Vf1+delta, Vf];
64
65 % Negative curve
66 n_inv = [n_neg, n_min, n_min, 0];
67 V_inv = [V_neg, Vs1_neg+delta, Ma_c*a0, Vd];
68
69 %% Manoeuvre diagram plotting (SL)
70
71 figure;
72 plot (V_noFlaps, n_noFlaps, '-k', 'LineWidth', 2); hold on;
73 plot (V_flaps, n_flaps, '-k', 'LineWidth', 2)
74 plot (V_inv, n_inv, '-k', 'LineWidth', 2)
75 xlabel ('V (EAS) [m/s]')
76 ylabel ('n')
77 xlim ([0 Vd+20])
78 ylim ([-2 5])
79
80 %% Full vectors creation (43000 ft)
81
82 Vd_h = 1.37*Ma_c*a0*f_Theta_sqrt(43000);
83
84 % Curve without flaps
85 n_noFlaps_h = [n1, n_max, n_max, 0];

```

```

86 V_noFlaps_h = [V1, Va_f+delta, Vd_h, Vd_h+delta];
87
88 % Curve with flaps
89 n_flaps_h = [n2, n_max_flaps, n_max_flaps];
90 V_flaps_h = [V2, Vf1+delta, Vf];
91
92 % Negative curve
93 n_inv_h = [n_neg, n_min, n_min, 0];
94 V_inv_h = [V_neg, Vs1_neg+delta, Ma_c*a0*f_Theta_sqrt
95 (43000), Vd_h];
96
97 %% Manoeuvre diagram plotting (43000 ft)
98 figure;
99 plot (V_noFlaps_h, n_noFlaps_h, '-k', 'LineWidth', 2); hold on
100 ;
101 plot (V_flaps_h, n_flaps_h, '-k', 'LineWidth', 2)
102 plot (V_inv_h, n_inv_h, '-k', 'LineWidth', 2)
103 xlabel ('V (EAS) [m/s]')
104 ylabel ('n')
105 xlim ([0 Vd+20])
106 ylim ([-2 5])
107
108 %% Gust diagram
109 % Inputs
110 Vc = Ma_c*a0*f_Theta_sqrt(43000);
111 rho_h = 0.245; % [kg/m^3] Air density at 43000 ft
112
113 Ud_D = 4.88; % [m/s] = 16 ft/s
114 Ud_C = 9.45; % [m/s] = 31 ft/s
115 Ud_B = 13.72; % [m/s] = 45 ft/s
116
117 mu_g = 2*(MTOW/Sw)/(rho_h*c_aero*CL_alpha*g); % aeroplane
118 mass ratio CS23.337 c)

```

```

118 kg = 0.88*mu_g/(5.3+mu_g); % gust
      alleviation factor

119
120 %% Gusts lines creation

121
122 n_D = 1+kg*(0.5*rho*Vd_h*Ud_D*CL_alpha*Sw)/(MTOW*g);
123 n_C = 1+kg*(0.5*rho*Vc*Ud_C*CL_alpha*Sw)/(MTOW*g);

124
125 Vb_1 = Vs1*sqrt(n_C);
126 Vb_2 = Va_f; % TO BE CHANGED
127 Vb = min(Vb_1, Vb_2);
128 Vb = 88; % Manually introduced

129
130 n_B = 1+kg*(0.5*rho*Vb*Ud_B*CL_alpha*Sw)/(MTOW*g);
131 n_C_neg = 1-kg*(0.5*rho*Vc*Ud_C*CL_alpha*Sw)/(MTOW*g);
132 n_B_neg = 1-kg*(0.5*rho*Vb*Ud_B*CL_alpha*Sw)/(MTOW*g);
133 n_D_neg = 1-kg*(0.5*rho*Vd_h*Ud_D*CL_alpha*Sw)/(MTOW*g);

134
135 n_D1 = [1, n_D];
136 n_D2 = [1, n_D_neg];
137 V_D = [0, Vd_h];
138 n_C1 = [1, n_C];
139 n_C2 = [1, n_C_neg];
140 V_C = [0, Vc];
141 n_B1 = [1, n_B];
142 n_B2 = [1, n_B_neg];
143 V_B = [0, Vb];

144
145 %% Gusts plotting

146
147 figure;
148 plot (V_noFlaps_h, n_noFlaps_h, '-k', 'LineWidth', 2); hold on
;
149 plot (V_inv_h, n_inv_h, '-k', 'LineWidth', 2)

```

```

150 plot (V_D,n_D1, '-k', V_D, n_D2, '-k', V_C,n_C1, '-k', V_C,
151 n_C2, '-k', V_B,n_B1, '-k', V_B,n_B2, '-k')
152 xlabel ( 'V (EAS) [m/s] ')
153 ylabel ( 'n' )
154 xlim ([0 Vd+20])
155 ylim ([-2 5])
156
157 %% Diagram vectors considering gusts
158
159
160 m = (n_B-1)/Vb; % Slope of gust line for Vb
161 gust_b = @(V) m*V+1; % Gust line for Vb
162 gust_b_neg = @(V) -m*V+1; % Gust line for -Vb
163
164 boolean_j = false;
165 boolean_i = false;
166
167 for z = 1:1:i
168     if n1(z) >= gust_b_neg(V1(z)) && boolean_j == false
169         pos_j = z;
170         boolean_j = true;
171     elseif n1(z) >= gust_b(V1(z)) && boolean_i == false
172         pos_i = z;
173         boolean_i = true;
174     elseif boolean_j == true && boolean_i == true
175         break;
176     end
177 end
178
179
180 n2 = min(n_B, n_max);
181 n3 = min(n_C, n_max);
182 n4 = min(n_D, n_max);
183 if n_D_neg > 0

```

```

184     n5 = n_D_neg;
185 else
186     n5 = 0;
187 end
188 n6 = max(n_C_neg, n_min);
189 n7 = max(n_B_neg, n_min);
190
191 n_curve12 = n1(pos_j:pos_i);
192 V_curve12 = V1(pos_j:pos_i);
193
194 n_gust_pos = [n_curve12, n3, n4, n5];
195 V_gust_pos = [V_curve12, Vc, Vd_h, Vd_h+delta];
196 n_gust_neg = [n1(pos_j), n7, n6, n5];
197 V_gust_neg = [V1(pos_j), Vb, Vc, Vd_h+delta];
198
199 figure;
200 plot (V_noFlaps_h, n_noFlaps_h, '-k'); hold on;
201 plot (V_inv_h, n_inv_h, '-k')
202 plot (V_D,n_D1, '-k', V_D, n_D2, '-k', V_C,n_C1, '-k', V_C,
203     n_C2, '-k', V_B,n_B1, '-k', V_B,n_B2, '-k')
204 plot (V_gust_pos, n_gust_pos, '-k', 'LineWidth', 2);
205 plot (V_gust_neg, n_gust_neg, '-k', 'LineWidth', 2)
206 xlabel ('V (EAS) [m/s]')
207 ylabel ('n')
208  xlim ([0 Vd+20])
209  ylim ([-2 5])
210 end

```

## E.8 Plate 2D

```

1 % HEAT TRANSFER STUDY IN A 2D PLATE
2 % In this script the main objective is to develop a code
   for

```

```

3 % discretize 1 different materials. 2D plate , permanent
4 regime , with
5
6 clear all ;
7 clc ;
8 close all ;
9
10 %% DATA
11
12 %Physical
13 hg=50; %Heat transfer coefficient [W/K m^2]
14 Tg=20; %External/ambient temperature [ C ]
15 k_1=20; %Conductivity [W/m K]
16 %qv=1e3; %Internal heat sources [W/m^2]
17 qv=0;
18 Lx=1; %Width
19 Ly=1; %Height
20 W=1; %Thickness
21
22
23 %Numerical
24 N=100; %Number of control volumes in x direction
25 M=100; %Number of control volumes in y direction
26 T_i=25; %Initial temperature for solver
27 d=1e-8; %Delta: precision for the solver
28
29 %% PREVIOUS CALCULATIONS
30 delta_x=Lx/N;
31 delta_y=Ly/M;
32 S_x=delta_x*W;
33 S_y=delta_y*W;
34 V_p=delta_x*delta_y*W;
35
36 a=[0 Lx Lx 0 0];

```

```

37 b=[0 0 Ly Ly 0];
38
39 %Distribution of the nodes
40 node(1,1,1)=0;
41 node(1,1,2)=0;
42 node(M+2,1,1)=0;
43 node(M+2,1,2)=Ly;
44 node(M+2,N+2,1)=Lx;
45 node(M+2,N+2,2)=Ly;
46 node(1,N+2,1)=Lx;
47 node(1,N+2,2)=0;
48
49 for j=2:1:N+1
50     node(1,j,1)=delta_x*(j-2)+delta_x/2;
51     node(1,j,2)=0;
52 end
53
54 for j=2:1:N+1
55     node(N+2,j,1)=delta_x*(j-2)+delta_x/2;
56     node(N+2,j,2)=Ly;
57 end
58
59 for i=2:1:M+1
60     node(i,1,1)=0;
61     node(i,1,2)=delta_y*(i-2)+delta_y/2;
62 end
63 for i=2:1:M+1
64     node(i,M+2,1)=Lx;
65     node(i,M+2,2)=delta_y*(i-2)+delta_y/2;
66 end
67
68 for i=2:1:M+1
69     for j=2:1:N+1
70         node(i,j,1)=(j-2)*delta_x+(delta_x/2);
71         node(i,j,2)=(i-2)*delta_y+(delta_y/2);

```

```
72         end
73 end
74
75 for j=1:1:N+2
76     for i=1:1:M+2
77         k(j, i)=k_1;
78     end
79 end
80
81 f1=figure(1)
82 plot(node(:,:,1), node(:,:,2), 'k.')
83
84
85 %% INITAL MAP OF TEMPERATURES
86 for i=1:1:M+2
87     for j=1:1:N+2
88         Ts(i, j)=T_i;
89     end
90 end
91
92 %% DISCRETIZATION COEFFICIENTS
93
94 ae(1,1)=0;
95 aw(1,1)=0;
96 an(1,1)=0;
97 as(1,1)=0;
98 ap(1,1)=0;
99 bp(1,1)=0;
100
101 ae(N+2,1)=0;
102 aw(N+2,1)=0;
103 an(N+2,1)=0;
104 as(N+2,1)=0;
105 ap(N+2,1)=0;
106 bp(N+2,1)=0;
```

```

107
108 ae (N+2,M+2)=0;
109 aw (N+2,M+2)=0;
110 an (N+2,M+2)=0;
111 as (N+2,M+2)=0;
112 ap (N+2,M+2)=0;
113 bp (N+2,M+2)=0;

114
115 ae (1,M+2)=0;
116 aw (1,M+2)=0;
117 an (1,M+2)=0;
118 as (1,M+2)=0;
119 ap (1,M+2)=0;
120 bp (1,M+2)=0;

121
122 %Left wall
123 for i=2:1:M+1
124     ae(i,1)=k(i,1)*S_y/(delta_x/2);
125     aw(i,1)=0;
126     an(i,1)=0;
127     as(i,1)=0;
128     ap(i,1)=ae(i,1)+hg*S_y;
129     bp(i,1)=hg*Tg*S_y;
130 end

131
132 %Right wall
133 for i=2:1:M+1
134     ae(i,N+2)=0;
135     aw(i,N+2)=k(i,N+1)*S_y/(delta_x/2);
136     an(i,N+2)=0;
137     as(i,N+2)=0;
138     ap(i,N+2)=aw(i,M+2)+hg*S_y;
139     bp(i,N+2)=hg*Tg*S_y;
140 end

```

141

```

142 %Upper wall
143 for j=2:1:N+1
144     ae(1,j)=0;
145     aw(1,j)=0;
146     an(1,j)=0;
147     as(1,j)=k(2,j)*S_x/(delta_y/2);
148     ap(1,j)=as(1,j)+hg*S_x;
149     bp(1,j)=hg*Tg*S_x;
150 end
151
152 %Lower wall
153 for j=2:1:N+1
154     ae(M+2,j)=0;
155     aw(M+2,j)=0;
156     an(M+2,j)=(k(N+1,1)*S_x)/(delta_y/2);
157     as(M+2,j)=0;
158     ap(M+2,j)=an(M+2,j)+hg*S_x;
159     bp(M+2,j)=hg*Tg*S_x;
160 end
161
162 for i=2:1:M+1
163     for j=2:1:N+1
164         ae(i,j)=(k(i,j)*S_y)/delta_x;
165         aw(i,j)=(k(i,j-1)*S_y)/delta_x;
166         an(i,j)=(k(i-1,j)*S_x)/delta_y;
167         as(i,j)=(k(i,j)*S_x)/delta_y;
168         ap(i,j)=ae(i,j)+aw(i,j)+an(i,j)+as(i,j);
169         bp(i,j)=qv*V_p;
170     end
171 end
172
173 %% GAUSS-SEIDEL
174 afirmation=0;
175 iteracions=0;
176

```

```

177 while affirmation==0
178     T(1,1)=(Ts(2,1)+Ts(1,2))/2; %NW
179     T(M+2,1)=(Ts(M+1,1)+Ts(M+2,2))/2; %SW
180     T(M+2,N+2)=(Ts(M+2,N+1)+Ts(M+1,N+2))/2; %SE
181     T(1,N+2)=(Ts(1,N+1)+Ts(2,N+2))/2; %NE
182
183     for i=2:1:M+1 %Left wall
184         T(i,1)=(ae(i,1)*Ts(i,2)+bp(i,1))/ap(i,1);
185     end
186
187     for j=2:1:N+1 %Upper wall
188         T(1,j)=(as(1,j)*Ts(2,j)+bp(1,j))/ap(1,j);
189     end
190
191     for i=2:1:M+1
192         for j=2:1:N+1
193             T(i,j)=(ae(i,j)*Ts(i,j+1)+aw(i,j)*T(i,j-1)+an(i,j)*T(i-1,j)+as(i,j)*Ts(i+1,j)+bp(i,j))/ap(i,j);
194         end
195     end
196
197     for i=2:1:M+1 %Right wall
198         T(i,N+2)=(aw(i,N+2)*T(i,N+1)+an(i,N+2)*T(i-1,N+2)+as(i,N+2)*Ts(i+1,N+2)+bp(i,N+2))/ap(i,N+2);
199     end
200
201     for j=2:1:N+1 %Lower wall
202         T(M+2,j)=(aw(M+2,j)*T(M+2,j-1)+ae(M+2,j)*Ts(M+2,j+1)+an(M+2,j)*T(M+1,j)+bp(M+2,j))/ap(M+2,j);
203     end
204
205     maxdifference=0;
206
207     for i=1:1:M+2

```

```
208     for j=1:1:N+2
209         pre1(i,j)=abs(Ts(i,j)-T(i,j));
210
211         if (pre1(i,j)>maxdifference)
212             maxdifference=pre1(i,j);
213         end
214
215         Ts(i,j)=T(i,j);
216     end
217
218
219     if (maxdifference<d)
220         affirmation=1;
221     else
222         affirmation=0;
223     end
224
225     iteracions=iteracions+1;
226 end
227
228
229 %% PLOT TEMPERATURES VISUALIZATION
230 f2=figure(2)
231 Z=T;
232 surf(z)
233 view(2)
234 imagesc(z)
235 colormap jet
236 c=colorbar;
237 c.Label.String = 'Temperature in C '
238 xlabel('X nodes');
239 ylabel('Y nodes');
240 title('Temperatures map. Case 6');
241 axis equal;
242
```

```

243 %% HEAT FLUXES VERIFICATION
244 Qconv1=0;
245 Qconv2=0;
246 Qconv3=0;
247 Qconv4=0;
248 Qv=0;
249
250 for i=2:1:M+1
251     Qconv1=Qconv1+((Tg-T(i,1))*hg*S_y);
252 end
253
254 for i=2:1:M+1
255     Qconv2=Qconv2+((Tg-T(i,N+2))*hg*S_y);
256 end
257
258 for j=2:1:N+1
259     Qconv3=Qconv3+((T(1,j)-Tg)*hg*S_x);
260 end
261
262 for j=2:1:N+1
263     Qconv4=Qconv4+((T(M+2,j)-Tg)*hg*S_x);
264 end
265
266 for i=2:1:M+1
267     for j=2:1:N+1
268         Qv=Qv+qv*V_p;
269     end
270 end
271
272 Qtot=Qconv1+Qconv2+Qv

```



# Bibliography

- [1] Sadraey, M. H., Aircraft design: A systems engineering approach. John Wiley & Sons, 2012.
- [2] Aviation, G., “Quarterly shipments and billings.” <https://gama.aero/facts-and-statistics/quarterly-shipments-and-billings/>. [Accessed on 24/10/2019].
- [3] Roskam, J., Airplane design. DARcorporation, 1985.
- [4] Commons, W., “De havilland canada dhc-8.” [https://commons.wikimedia.org/wiki/De\\_Havilland\\_Canada\\_DHC-8](https://commons.wikimedia.org/wiki/De_Havilland_Canada_DHC-8), Sept. 2019. [Accessed on 19/10/2019].
- [5] Stackexchange, A., “What are the advantages or disadvantages of a mid wing design?” <https://aviation.stackexchange.com/questions/24973/what-are-the-advantages-or-disadvantages-of-a-mid-wing-design>, Feb. 2016. [Accessed on 19/10/2019].
- [6] Torenbeek, E., Synthesis of subsonic airplane design: an introduction to the preliminary design of subsonic general aviation and transport aircraft, with emphasis on layout, aerodynamic design, propulsion and performance. Springer Science & Business Media, 1982.
- [7] Corporation, C. D., “Cirrus official website. cirrus vision jet.” <https://cirrusaircraft.com/aircraft/vision-jet/>, 2019. [Accessed on 17/10/2019].
- [8] Wikipedia, t. f. e., “Conventional landing gear.” [http://www.wikiwand.com/en/Conventional\\_landing\\_gear](http://www.wikiwand.com/en/Conventional_landing_gear). [Accessed on 04/10/2019].

- [9] Wikipedia, t. f. e., “Tricycle landing gear.” [https://en.wikipedia.org/wiki/Tricycle\\_landing\\_gear](https://en.wikipedia.org/wiki/Tricycle_landing_gear). [Accessed on 04/10/2019].
- [10] Mangalgiri, P., “Composite materials for aerospace application,” Bulletin Material Science, vol. 22, no. 3, pp. 657–664, 1999.
- [11] Mrazova, M., “Advanced composite materials of the future in aerospace industry,” Incas Bulletin, vol. 5, pp. 139–150, 2013. DOI: [10.13111/2066-8201.2013.5.3.14](https://doi.org/10.13111/2066-8201.2013.5.3.14).
- [12] Sparling, G. A. J., “Preliminary sizing – matching chart.” <http://www.aerospacengineering.net/preliminary-sizing-matching-chart/>. [Accessed on 24/10/2019].
- [13] Gudmundsson, S., General aviation aircraft design: Applied Methods and Procedures. Butterworth-Heinemann Editors, 2013.
- [14] Carmen López Sánchez, Diego Sánchez Franco, R. C. M., “Hurricane-cs: Control surfaces and high lift devices modeling and sizing program,” 31st Congress of the International Council of the Aeronautical Sciences, 2018.
- [15] Zaccai, D., Design Framework for Trailing-Edge High-Lift Systems. PhD thesis, Faculty of Aerospace Engineering. Delft University of Technology, 2014.
- [16] Scholz, D., Aircraft Design. Lecture Notes. Hamburg University of Applied Sciences, 2015.
- [17] Hall, C. A. and Crichton, D., “Engine and installation configurations for a silent aircraft,” tech. rep., Cambridge University Engineering Department, 2015.
- [18] Siddiqui, M. A. and Haq, M. S., “Review of thrust reverser mechanism used in turbofan jet engine aircraft,” International Journal of Engineering Research and Technology, 2013. Department of Mechanical Engineering, University Polytechnic, Integral University, India.
- [19] Coburn, B., Wu, Z., and Weaver, P., “Buckling analysis of stiffened variable angle tow panels,” Composite Structures, vol. 111, p. 259–270, 05 2014.

- [20] Han, T.-S., Ural, A., Chen, C.-S., Zehnder, A., Ingraffea, A., and Billington, S., “Delamination buckling and propagation analysis of honeycomb panels using a cohesive element approach,” *International Journal of Fracture*, vol. 115, pp. 101–123, 05 2002.
- [21] Willden, K., M. S. G. C. B. T., “Composite fuselage crown panel manufacturing technology,” *NASA Technical Reports Server*, September 1992.
- [22] Fujino, M., “Design and development of the hondajet,” *Journal of Aircraft*, vol. 42, no. 3, 2005.
- [23] Moakes, A. J. and Wilkes, M. V., *A Short Introduction to Numerical Analysis*, vol. 51. The Mathematical Gazette, 1967.
- [24] Ira H. Abbott, Albert E. von Doenhoff, L. S. S., “Summary of airfoil data,” no. 824.
- [25] Price, C. A. E. and Intl, W., “Business and Comercial Airplanes,” *B and C Jets*, no. May, pp. 94–103, 2015.
- [26] Textron Aviation Inc, E., “EASA IM.A 502 TC for Cessna Citation Mustang 525,” *Type Certificate Data Sheet*, no. June, pp. 1–10, 2018.
- [27] “Business jets specification and performance data.” [https://aviationweek.com/site-files/aviationweek.com/files/uploads/2015/05/Business%20Airplane%20Tables\\_May\\_2015\\_revised.pdf](https://aviationweek.com/site-files/aviationweek.com/files/uploads/2015/05/Business%20Airplane%20Tables_May_2015_revised.pdf), 2015. [Accessed on 24/10/2019].
- [28] “Citation mustang specifications.” [https://web.archive.org/web/20160527164647/http://cessna.txtav.com/en/citation/mustang#\\_model-specs](https://web.archive.org/web/20160527164647/http://cessna.txtav.com/en/citation/mustang#_model-specs), 2016. [Accessed on 24/10/2019].
- [29] Embraer, E., “IM.A 157 TC for Embraer Phenom 100,” *Type Certificate Data Sheet*, no. 7, pp. 1–9, 2017.
- [30] “Hondajet specifications.” <https://www.hondajet.com/hondajet/specifications>, 2019. [Accessed on 24/10/2019].
- [31] Honda Aircraft, E., “IM.A 352 TC for HondaJet HA-520,” *Type Certificate Data Sheet*, no. December, pp. 1–10, 2018.

- [32] Eclipse Aerospace Inc., E., “IM.A 171 TC for ECLIPSE EA500,” Type Certificate Data Sheet, no. April, pp. 1–18, 2016.
- [33] Syberjet, “Sj30.” [www.syberjet.com/sj30](http://www.syberjet.com/sj30). [Accessed on 02/10/2019].
- [34] “Adam aircraft a700 specs and description.” <http://jetav.com/adam-aircraft-a700-specs-and-description/>, 2018. [Accessed on 24/10/2019].
- [35] Textron Aviation Inc, E., “EASA IM.A 078 TC for Citation 525M2,” Type Certificate Data Sheet, no. 13, pp. 1–48, 2019.
- [36] GlobalAir, “Citation jet 525.” <https://www.globalair.com/aircraft-for-sale/Specifications?specid=192>. [Accessed on 02/10/2019].
- [37] “Lear 24/25 study guide.” <http://aircabaviation.com/pilots-corner/lear-24-25/>, 2015. [Accessed on 24/10/2019].
- [38] Bombardier Aviation Inc, F., “FAA-A10CE TC for Learjet24,” Type Certificate Data Sheet, pp. 10–14, 2011.
- [39] Anyelo Andrés Pulido Gonzalez, M. F. L., Diseño conceptual, preliminar y análisis en CFD de un avión jet ultra ligero. PhD thesis, Facultad de Ingeniería y ciencias básicas, Fundación universitaria Los Libertadores, 2019.
- [40] Raymer, D. P., Aircraft Design A Conceptual Approach. Wright-Patterson Air Force Base, Ohio, 1989.
- [41] EASA, “Certification Specifications for Normal-Category Aeroplanes,” CS-23, no. Amendment 5, pp. 1–33, 2017.
- [42] “High Flying Bathrooms | PrivateFly Blog.” <https://blog.privatefly.com/us/high-flying-bathrooms>, October 2019. [Accessed on 09/10/2019].
- [43] Engel I& Volkers Aviation, “Aircraft categories.” <https://www.engelvoelkers.com/en-lu/aviation/aircraft-categories/>. [Accessed on 08/10/2019].
- [44] Young, A., Manager, G., and Sale, A., “Business aviation market update report,” AMSTAT. In Inventories Between, p. 7, 2012.

- [45] Aviation Broker, “Light jets.” <https://www.aviation-broker.com/es/aviones/light-jets.html>. [Accessed on 08/10/2019].
- [46] “Embraer phenom 100.” <https://www.aircharteradvisors.com/embraer-phenom-100/>. [Accessed on 24/10/2019].
- [47] “Cessna aircraft citation m2.” <https://www.africair.com/aircraft/cessna-citation-m2/>, 2019. [Accessed on 24/10/2019].
- [48] Roland, J., “What’s the average weight for men?” <https://www.healthline.com/health/mens-health/average-weight-for-men>. [Accessed on 26/10/2019].
- [49] WorldData.info, “Body size by country.” <https://www.worlddata.info/average-bodyheight.php>. [Accessed on 26/10/2019].
- [50] van der Broek-Serle, Z. B. F., “Survey on standard weights of passengers and baggage,” tech. rep., NEA, 2009.
- [51] EASA, “AMC and GM to CS-23,” AMC, no. Issue 2, pp. 1–52, 2017.
- [52] Embraer, “Embraer: Phenom 100ev.” <https://executive.embraer.com/global/en/phenom-100ev>. [Accessed on 25/10/2019].
- [53] Sadraey, M. H., “Fuselage design,” Aerospace Series, pp. 341–411, 2006.
- [54] Defence, T., “The airbus a400m atlas – part 2 (what is so good about it anyway).” <https://www.thinkdefence.co.uk/2012/09/the-airbus-a400m-atlas-part-2-what-is-so-good-about-it-anyway/>, Sept. 2012. [Accessed on 19/10/2019].
- [55] Davies, A., “Airbus proves its huge new warplane doesn’t need a paved runway.” <https://www.businessinsider.com/photo-airbus-a400m-2013-9?IR=T>, September 2013. [Accessed on 19/10/2019].
- [56] Franchini, S. and García, Ó. L., Introducción a la ingeniería aeroespacial. Escuela Técnica Superior de Ingenieros Aeronáuticos, Universidad Politécnica de Madrid, 2008.
- [57] Lloyd R. Jenkinson, Paul Simpkin, D. R., Civil Jet Aircraft Design. Aiaa Education Series, AIAA (American Institute of Aeronautics & Ast, 1999.

- [58] Aerospaceweb, “Aircraft landing gear layout.” <http://www.aerospaceweb.org/question/design/q0200.shtml>. [Accessed on 10/10/2019].
- [59] Gudmundsson, S., “Chapter 15 - aircraft drag analysis,” in General Aviation Aircraft Design (Gudmundsson, S., ed.), pp. 661 – 760, Boston: Butterworth-Heinemann, 2014.
- [60] Ibon Serrano, Roberto Osés, B. C. M. L. M. C. d. T. S. F. S. F., “Materiales metálicos de uso frecuente en aeronáutica: aleaciones ligeras al-li.” <https://www.interempresas.net/MetalMecanica/Articulos/101138-Materiales-metalicos-de-uso-frecuente-en-aeronautica-aleaciones-ligeras-Al.html>. [Accessed on 24/10/2019].
- [61] Materials, A., “Aluminum 2090 alloy (uns a92090).” <https://www.azom.com/article.aspx?ArticleID=8715>. [Accessed on 24/10/2019].
- [62] Materials, A., “Aluminum 8090 alloy (uns a89090).” <https://www.azom.com/article.aspx?ArticleID=8789>. [Accessed on 24/10/2019].
- [63] Composites, T. A., “Tc2751 product data sheet.” [https://www.toraytac.com/media/870a26cd-0cf4-49f7-bda7-af4815cf28b2/uLPXEQ/TAC/Documents/Data\\_sheets/Thermoset/UD20tapes20and20prepregs/TC275-1\\_Epoxy\\_PDS.pdf](https://www.toraytac.com/media/870a26cd-0cf4-49f7-bda7-af4815cf28b2/uLPXEQ/TAC/Documents/Data_sheets/Thermoset/UD20tapes20and20prepregs/TC275-1_Epoxy_PDS.pdf). [Accessed on 24/10/2019].
- [64] Composites, T. A., “Tc2751e product data sheet.” [https://www.toraytac.com/media/11af92b1-a9bd-4d3b-a5f2-00f3184179e8/9Uj0hg/TAC/Documents/Data\\_sheets/Thermoset/UD20tapes20and20prepregs/TC275-1E\\_Epoxy\\_PDS.pdf](https://www.toraytac.com/media/11af92b1-a9bd-4d3b-a5f2-00f3184179e8/9Uj0hg/TAC/Documents/Data_sheets/Thermoset/UD20tapes20and20prepregs/TC275-1E_Epoxy_PDS.pdf). [Accessed on 24/10/2019].
- [65] Got'e, I. V., “List of Frequently Used EASA Abbreviations,” Time of Troubles, pp. xv–xvi, 2019.
- [66] Bombardier Aviation Inc, F., “FAA-A10CE TC for Learjet24,” Type Certificate Data Sheet, no. May, pp. 1–39, 2012.
- [67] “What is the difference between 'commercial operation' and 'commercial air transport (cat) operation'?:” May 2019.

- [68] EU, “Common Technical Requirements and Administrative Procedures Applicable to Commercial Transportation by Aeroplane,” Official Journal of the European Union, vol. 2005, no. No 859/2008, 2008.
- [69] Yoon, S. and Jameson, A., “Lower-upper symmetric-gauss-seidel method for the euler and navier-stokes equations,” AIAA journal, vol. 26, no. 9, pp. 1025–1026, 1988.
- [70] GlobalAir, “Eclipse aerospace total eclipse 500.” <https://www.globalair.com/aircraft-for-sale/Specifications?specid=888>. [Accessed on 02/10/2019].
- [71] TopSpeed, “2006-2010 cessna citation mustang.” <https://www.topspeed.com/aviation/aviation-reviews/cessna/2006-2010-cessna-citation-mustang-ar83930.html>. [Accessed on 02/10/2019].
- [72] GlobalAir, “Embraer phenom 100.” <https://www.globalair.com/aircraft-for-sale/Specifications?specid=719>. [Accessed on 02/10/2019].
- [73] Anderson, J. D., Aircraft performance and design /. WCB/McGraw-Hill, 1999.
- [74] P&W, E., “EASA IM.E 077 TC for Pratt & Whitney JT15D,” Type Certificate Data Sheet, no. September, pp. 1–8, 2006.
- [75] “Notice of Proposed Amendment 2016-06 ( C ) Fuel planning and management,” 2016.
- [76] Coma, M., “UPC-Airplane Design, Theory Class Notes.” Imparted during course 2018-2019 Q1.
- [77] AirbusLTD, “Beluga – for outsized cargo transport.” <https://www.airbus.com/aircraft/freighter/beluga.html>, May 2017. [Accessed on 09/10/2019].
- [78] Berger, M., Geometry revealed: a Jacob’s ladder to modern higher geometry. Springer Science & Business Media, 2010.

- [79] Anderson Jr, J. D., Fundamentals of aerodynamics. Tata McGraw-Hill Education, 1985.
- [80] “Stall detection.” <https://sourceforge.net/p/xflr5/discussion/679396/thread/2d9c38ce/>, April 2015.
- [81] Anderson, J. D., Introduction to flight, vol. 199. McGraw-Hill Boston, 2005.
- [82] Tulapurkara, G., “Airplane design (aerodynamics chapter 5).” [https://nptel.ac.in/content/storage2/courses/101106035/028\\_Chapter%205\\_L21%20\\_\(04-10-2013\).pdf](https://nptel.ac.in/content/storage2/courses/101106035/028_Chapter%205_L21%20_(04-10-2013).pdf).
- [83] Hoak, D., USAF Stability and Control Datcom. McDonnell Douglas Corporation, 2nd ed., 1960.
- [84] “Empennage general design.” <https://aerospaceengineeringblog.com/thrust-reversal/>. [Accessed on 12/12/2019].
- [85] Ira H. Abbott, A. E. V. D., Theory of Wing Sections, Including a Summary of Airfoil Data. Dover Publications, Inc, 1959.
- [86] Tierno, M. A., Cortés, M., and Márquez, C., Mecánica del vuelo. Escuela Técnica Superior de Ingenieros Aeronáuticos, Universidad Politécnica de Madrid, 2009.
- [87] Daniel Wise, Avery Leonard, K. Z., “Aiaa design competition proposal light business jet family design,” 2016. Georgia Institute of Technology.
- [88] “Thrust reversal.” <https://aerospaceengineeringblog.com/thrust-reversal/>, 2012. [Accessed on 2/12/2019].
- [89] of Transportation Federal Aviation Administration Standards Division, U. D., Airframe and Powerplant - MECHANICS AIRFRAME HANDBOOK. U.S. Goverment Printing Office, 1972.
- [90] Matsui, N. and Sato, K., “Research work of the all-composite fuselage,” July 2003. 14th International Conference on Composite Materials.
- [91] Sparling, G. A. J., “node6 @ www.math.pitt.edu.” <http://www.math.pitt.edu/{}sparling/23021/23022numapprox2/node6.html>. [Accessed on 11/10/2019].